USE OF RATE TRANSIENT ANALYSIS TO ENHANCE

THE WELL PERFORMANCE OF A MATURE GAS FIELD

A Thesis

by

BASAYIR HUSSAIN MOHSIN AL-LAWATI

Submitted to the Office of Graduate and Professional Studies of
Texas A&M University
in partial fulfillment of the requirements for the degree of

MASTER OF SCIENCE

Chair of Committee,	Thomas A. Blasingame
Committee Members,	Maria A. Barrufet
	Hadi Nasrabadi
Head of Department,	A. Daniel Hill

May 2017

Major Subject: Petroleum Engineering

ABSTRACT

The BHA gas field plays a significant role in Oman's gas production. However, production forecasts and reserves estimation in this gas condensate field have shown considerable uncertainty due to the formation complexity and the relatively low permeability (1-5 md). Mismatches between the observed reservoir performance and deterministic performance predictions have resulted in continuous revision of the booked reserves for this field. To address these reserves revisions, we deployed modern time-rate analysis and time-pressure-rate analysis techniques to improve the analysis and interpretation of the reservoir performance data, and thus better constrain the estimated ultimate recovery (EUR) results for the BHA field.

Microsoft® Excel® is used to perform "time-rate" or "decline curve" analysis (DCA) on a selected group of fourteen wells. These wells were chosen based on the continuity of the production data (some wells do not have continuously measured pressures). We follow the industry-standard practice for wells in unconventional reservoirs, where the EUR is estimated at 30 years from the forecasted production trend. Specifically, we estimate reserves using both the Modified Hyperbolic (MH) and Power Law Exponential (PLE) methods.

In addition to "time-rate" analysis, we also perform "time-rate-pressure" analysis or "rate transient analysis" (RTA) on these same fourteen well cases using the commercial software package Topaze (Kappa Engineering). In the RTA workflow, we first utilize the diagnostic plots to estimate model parameters and then perform a simulation history match using the anazlytical solution for a vertical well with a finite- or infinite-conductivity vertical fracture. Using the history-matched reservoir model, we then generate a forecast of at least 30 years and we use the cumulative production at 30 years as a proxy for EUR for comparison with DCA methods.

We tabulate the 30-year EUR values from DCA and RTA, as well as the model parameters used to obtain these forecasts. We provide simplified correlations of EUR results and model parameters for the DCA and estimates of reservoir properties obtained from RTA. The overall goal of this work is to demonstrate the applicability of these methods to improve our confidence in the estimated reserves for the BHA field.

DEDICATION

To my parents, for their unconditional love.

ACKNOWLEDGMENTS

I would like to express my gratitude to…

My committee chair, Dr. Thomas Blasingame, for his guidance, his kindness, his patience, and his relentless demand for perfection.

Dr. Barrufet and Dr. Nasrabadi for their time, support, and service as my committee members.

My PDO mentor Mohamed Al-Salhi for his unyielding support.

The project manager Cornelis (Kees) Veeken for his time and commitment to this project.

My family and friends for their love, their care, and their unwavering support.

Finally, my beloved Oman, for sponsoring my education thus far.

CONTRIBUTORS AND FUNDING SOURCES

Contributors

This work was supported by a thesis committee consisting of Professor Thomas A Blasingame [advisor] and Assistant Professor Hadi Nasrabadi of the Department of Petroleum Engineering and Professor Maria A. Barrufet of the Department of Chemical Engineering.

The data analyzed in this work was supplied by an operating company in the Sultanate of Oman. The work was analyzed by the student with the support of the advisor and project manager from the operating company.

Funding Sources

The graduate study was sponsored by a scholarship from The Government of Oman.

TABLE OF CONTENTS

Page

LIST OF FIGURES

LIST OF TABLES

INTRODUCTION

1.1 Objectives

The main objectives of this work are to use "time-rate" (or "decline curve") analysis (DCA) and "time-rate-pressure" analysis (or "rate transient analysis") (RTA) to provide the following:

- an understanding of the reservoir potential of the BHA field.
- a comparison of reserves estimates from "time-rate" and "time-rate-pressure" methods.
- a correlation of reserves and reservoir property estimates.

1.2 Statement of the Problem

1.2.1 Time-Rate Analysis

Traditionally, the estimation of reserves in low-permeability reservoirs has been performed using "time-rate" analysis (or DCA) first summarized by Arps (1945). The DCA methods are preferred due to their ease of use. These are simple, empirical parametric relationships for rate solely as a function of time (*i.e.*, no reservoir properties are considered). Historically, the most popular DCA model is that of the "hyperbolic" relation derived from a purely mathematical standpoint, the base definition of which is:

$$\frac{d}{dt}\left[\frac{q}{dq/dt}\right] = -b \quad \text{.....(1)}$$

Integrating Eq. 1 as shown in (Blasingame and Rushing 2005), the hyperbolic time-rate relation is given by:

$$q = \frac{q_i}{[1 + bD_i t]^{1/b}} \quad \text{(hyperbolic decline relation) .....(2)}$$

Where:

q_i = Initial flowrate, volume/time.

D_i = Hyperbolic decline constant, 1/time.

b = Hyperbolic decline exponent, dimensionless

Depending on the value of this exponent, the equations are classified as exponential (b=0), hyperbolic (0<b<1), and harmonic (b=1), where the exponential and harmonic relations are given by:

$$q = q_i \exp[-D_i t] \quad \text{([}b\text{=0] exponential decline relation) .....(3)}$$

$$q = \frac{q_i}{1 + D_i t} \quad \text{([}b\text{=1] harmonic decline relation) .....(4)}$$

It is important to note that the traditional acceptable range for the hyperbolic decline exponent is 0<b<1, which is taken from the assumption of boundary-dominated flow. However, for unconventional reservoirs

it is not uncommon to observe extended periods of transient "linear flow" behavior, for which the rate is proportional to the square root of time.

The genesis of this observed linear flow behavior is the solution for flow in a vertically fractured well decline, which is given by:

$$q = c\,\frac{1}{\sqrt{t}} \qquad \left[c = \frac{1}{8.128494}\,(p_i - p_{wf})\,\frac{1}{B}\sqrt{\frac{\phi c_t}{\mu}}\,A_{xf}\,\sqrt{k} \right] \qquad \text{.....(5)}$$

Substitution of the b=2 into Eq. 2, yields:

$$q = \frac{q_i}{[1 + 2D_i t]^{1/2}} \text{ as } t \text{ becomes "large, "} q \rightarrow \frac{q_i}{\sqrt{2D_i}}\,\frac{1}{\sqrt{t}} \qquad \text{.....(6)}$$

Modern time-rate analysis techniques — specifically, the modified hyperbolic (MH) and the power-law exponential (PLE) models — have been proposed for use in matching early transient flow periods (Seshadri and Mattar 2010). First introduced by Robertson (1988), the modified hyperbolic relation uses the hyperbolic decline to match early transient periods, where the decline exponent (b) can be greater than 1 and then transitions to exponential decline, during boundary-dominated flow.

$$q(t) = \left\{ \begin{array}{ll} q_{i,\text{hyp}}\,\dfrac{1}{[1 + bD_i t]^{1/b}} & (t < t_{\lim}) \\ q_{\lim}\,\exp[\,-D_{\lim}\,(t - t_{\lim})] & (t > t_{\lim}) \end{array} \right\} \text{ where } \begin{array}{l} q_{\lim} = q_{i,\text{hyp}}\left[\dfrac{D_{\lim}}{D_i}\right]^{(1/b)} \\ t_{\lim} = \dfrac{1}{bD_i}\left[\left[\dfrac{q_{i,\text{hyp}}}{q_{\lim}}\right]^{b} - 1\right] \end{array} \qquad \text{.....(7)}$$

The power-law exponential (PLE) used by Ilk et al. (2008) to address low-permeability reservoirs, was developed by modifying the exponential decline.

$$q(t) = \hat{q}_i \exp[\,-D_\infty t - \hat{D}_i t^n\,] \qquad \text{.....(8)}$$

1.2.2 Time-Rate-Pressure Analysis (or Rate Transient Analysis (RTA))

In contrast to "time-rate" analysis, "time-pressure-rate" analysis (or RTA) incorporates pressure into the diagnostics and analysis methods, and as such, requires a reservoir model (analytical, numerical, or hybrid). It should be noted that these RTA methods are rigorously based in theory, and they are valid for any/all flow regimes (transient flow, transition flow, and boundary-dominated flow regimes), provided that these regimes are accurately represented in the prescribed reservoir model.

RTA methods are used estimate reservoir properties (*e.g.*, skin factor, fracture half-length, formation permeability, etc.) and reservoir volume (assuming the existence of boundary-dominated flow behavior). Our approach will be to predict EUR using the prescribed reservoir model by forecasting production

performance to 30 years (our proxy for EUR). We will propose at least one and as many as three pressure extrapolation schemes for the rate forecast (*i.e.*, extrapolation of the last known pressure and extrapolation of at least one pressure profile extending from the last known pressure to the assumed abandonment pressure of 200 psia).

1.2.3 Data Acquisition/Preparation

In order to perform the work required in this thesis, the following data are required:

- PVT (phase behavior) data (laboratory fluid reports)
- Well completion data (completion/stimulation data, well tubulars, etc.)
- Operations data (compressor timing, well work-overs, etc.)
- Reservoir data (petrophysical data, reservoir thickness, geologic features, etc.)
- Production data (flowrate and pressure historical data)

Once acquired, all of the data are checked and cross-checked to the extent possible. In this study it was quite difficult to verify operations data (*i.e.*, many cases exhibited features in the production data that appear to be related to workover or other types of well operations, but such records were not available). Production data are filtered and checked for inconsistencies. Due to absence of bottomhole pressure gauges, bottomhole pressure calculations are conducted and validated with measured initial pressures (from pressure surveys taken during the initial completion phase).

1.2.4 Analysis Inventory — Production Analysis Plots

The following diagnostic plots are used to diagnose and analyze production data on a per well basis:

- q_g and p_{wf} versus t — *orientation plot*
- $\log(q_g)$ and p_{wf} versus t — *orientation plot*
- $\log(q_g)$ and $\log(G_p)$ versus $\log(t)$ — *orientation plot*
- $\log(q_g/\Delta m(p))$, $\log(q_g/\Delta m(p))_{i,,}$ and $\log(q_g/\Delta m(p))_{id}$ versus $\log(G_p/q_g)$ — *time-rate-pressure analysis*
- $\log(\Delta m(p)/q_g)_{id}$ and $\log(\Delta m(p)/q_g)$ versus $\log(G_p/q_g)$ — *time-rate-pressure analysis*
- $\log(q_g)$, p_{wf} and $\log(G_p)$ versus t — *history match presentation plot*
- $\log(q_g)$ versus t — *time-rate and time-rate-pressure presentation plot*
- $\log(q_g)$ versus $\log(t)$ — *time-rate and time-rate-pressure presentation plot*
- q_g versus G_p — *history match presentation plot*
- $\log(q_g)$ versus G_p — *history match presentation plot*
- p_{wf} versus t — *orientation plot*
- p_{wf} versus G_p — *orientation plot*

LITERATURE REVIEW

This chapter summarizes the development of decline curve analysis beginning with time-rate analysis, followed by modern time-rate analysis, and finally time-rate-pressure-time analysis. We then present an overview of the BHA Field, including a reservoir description and well completion information.

2.1 Time-Rate Analysis

Decline Curve Analysis (DCA) is a general methodology that traditionally uses flowrate and time data to predict the production performance of a well and estimate its reserves. The early works of Anderson and Arnold (1908), Lewis and Beal (1918), Cutler (1924), Johnson and Bollens (1928), and others led to the major developments of Arps DCA in 1944. DCA methods are based on a "hyperbolic" relation and enable forecasts to be obtained graphically through straight-line extrapolations of actual production data using semilog rate vs. time plots in the exponential case and semilog rate vs. cumulative production plots for the harmonic case. It is in the linearity and minimal data requirement that the Arps DCA is most frequently used and sometimes even misused. Empirical Arps DCA assumes the following:

1. Production must be in the boundary-dominated flow period.
2. Production must occur under stabilized flow conditions, meaning constant bottomhole pressures.
3. Unchanging reservoir boundaries (fixed volume).
4. Constant permeability and skin factor

A major development in DCA occurred when Fetkovich (1980) introduced type-curve matching, a method by which plots are constructed for a given reservoir using solutions to flow equations. Production data plotted on a log-log plot can be simply matched to theoretical solutions. Using Arps hyperbolic relationship, Fetkovich graphed the decline curves for *b* values ranging between 0-1, in 0.1 increments for a *Di* of 1. Fetkovich noticed that at very small times, the curves overlap and become indistinguishable. As a result, Fetkovich combined the analytical constant-pressure infinite and finite solutions for early time with Arps empirical decline curve correlations on a log-log plot to not only predict production data, but also reservoir properties. This led in the development of modern DCA. Carter (1985) further expanded type-curve matching for the gas phase — however, a fundamental constraint remained; the well is assumed to be produced at a constant bottomhole flowing pressure.

2.2 Modern Time-Rate Analysis

Extended transient linear flow periods have become more prevalent with increased development of low-permeability formations. Traditional Arps time-rate relations are unable to appropriately model these periods, since these equations assume boundary-dominated flow. Modification to the time-rate analysis method has been evolving since Gentry and McCray (1978) examined rock and fluid property effects on the constants of Arps decline curve equations. Contrary to the prior belief that the decline exponent (b) must be constrained between 0 and 1 (1945) they concluded from their numerical simulation study that reservoir heterogeneity can produce b values greater than one. Maley (1985) analyzed fractured tight gas wells, concluding that these wells or wells that exhibit linear flow can also have decline exponents that exceed one.

Robertson (1988) noticed that though the Arp's exponential and hyperbolic equations are most widely used, neither is truly representative of actual production rates. The hyperbolic function is commonly applied to the early stages of production followed by an exponential tail. He therefore proposed a piecewise function that allowed for application to different flow regimes where the decline constant is initially hyperbolic until a set D_{limit} value, after which D is not allowed to decline and the equation switches to exponential decline.

Despite the widespread use of the modified hyperbolic, which is widely accepted for $b<1$, Seshadri and Mattar (2010) examined its applicability when $b>1$ to fit the transient linear flow period for production data in low permeability reservoirs. In addition, they compared this method to the power-law exponential relationship introduced by Ilk et al. (2008). The "power law loss ratio" or power-law exponential (PLE) relationship was introduced to specifically address tight gas or shale gas wells. His equation is a modification of the Arps exponential decline function and is derived from the observed behavior that the D-parameter exhibits: a decaying power-law behavior and a constant behavior at large times. It has flexibility to model the different flow regimes (transient, transition, and boundary-dominated flow), but ultimately turns into exponential decline later and is presented below:

$$q(t) = \hat{q}_i \exp[\ -D_\infty t - \hat{D}_i t^n] \quad \text{.....(9)}$$

Where:

n = Time exponent (between 0 and 1), dimensionless.

$\hat{q}_i$ = Initial rate, volume/time.

D_∞ = Decline constant at infinite time, 1/time

$\hat{D}_i$ = Instantaneous decline rate for the PLE model, 1/(time)^n

We find that the t^n term dominates at small times to account for transient and transition flow regimes experienced by both fractured and unfractured reservoirs, while the $D\infty$ term dominates at large times. This

results in high initial production rates that become smaller with time as is the case with tight gas wells. The $D\infty$ term serves to provide a lower limit on the decline, to avoid overestimation

From their comparison of the MH and PLE methods, Seshadri and Mattar (2010) concluded that the EUR forecast results obtained from both methods are relevant and comparable. They found, however, that the MH method is easier to model than PLE because the PLE requires tuning of four parameters to model production data and any change in one parameters requires modification of the other parameters to achieve a good fit.

2.3 Time-Rate-Pressure

Time-rate-pressure or rate-transient analysis (RTA), a further advancement of modern decline curve analysis, enables estimation of reservoir properties, similar to pressure transient analysis (PTA). The advantage of using RTA for this purpose is associated with the cost reduction of closing in the well for extended periods while the pressure builds up, specifically in low permeability reservoirs, where extended transient-phase periods are required for the well to reach boundary conditions.

The advancement in RTA started with efforts by Blasingame and Lee (1986) to determine reservoir characteristics from variable rate production. Unlike the method suggested by Earlougher (1972), which was able to account for variable rate, this method does not require average reservoir pressure determination, meaning that the well does not need be shut in. The main assumption in the Blasingame and Lee method was that any additional transient effects that resulted from variable flow are negligible when compared to the overall effect of the reservoir boundary. Therefore, unless the rate change is significant and the transient effects dominate, their solution is acceptable for a single-phase liquid flow in a bounded reservoir using a constant rate solution.

Blasingame, Johnston, and Lee (1989) presented a significant improvement in type curves. By integrating the pressure drop function, rather than differentiating it, noisy data is mitigated, providing a more unique type curve match. Blasingame, McCray, and Lee (1991) introduced a solution for the variable rate/variable pressure system through a superposition function, capturing rate changes. This constant pressure function is derived from the constant rate function, utilizing the fact that the cumulative production for both is equivalent. This method not only captures large variations in production rates and even shut-ins, but also provides good approximation during the transient flow phase.

Palacio and Blasingame (1993) presented a simplified and non-iterative type-curve analysis method by plotting the flowrate, flowrate integral, and flowrate integral–derivative functions versus material balance time on a log-log scale. This method employs a material-balance equation combined with the pseudosteady-state flow equation to accurately estimate reservoir properties and reserves for single-phase flow. A major

advancement in this method is in its ability to account for not only liquids, but also gases through use of the concepts of pseudo-time defined by Fraim and Wattenbarger (1987) and pseudo-pressures defined by Al-Hussainy, Ramey, and Crawford (1966). Doublet et al. (1994) introduced a method that estimates reservoir properties and in-place volumes for production data not constrained to constant rates or bottomhole pressures. Agarwal et al. (1999)developed a new set of production type curves using concepts derived from pressure transient analysis for vertical wells of finite and infinite conductivity fractures. Sureshjani and Gerami (2011) developed a new equation fit for gas and gas condensate reservoirs. He concluded that ignoring relative permeability dependency on velocity still provides for acceptable estimates on in-place volumes.

Ilk et al. (2010) provided a review of the tools available to diagnose and assess a reservoir, the challenges and pitfalls pertinent to production analysis, and guidance for best practices. Due to non-uniqueness in estimating well and reservoir properties using production analysis in unconventional reservoirs, Ilk et al. (2011) suggested the need to couple production analysis with other techniques. They demonstrate a workflow consisting of production data diagnostics, production data analysis, and production forecast to evaluate well performance of a reservoir. Ilk et al. (2011) used parametric correlations to integrate rate-time analysis and model-based production analysis to wells in four fields (shale and tight gas reservoirs). Ilk et al. (2011) concluded that formation permeability and fracture half-length are well correlated with parameters of time-rate relations, provided a large number of wells and high quality of data are available.

2.4 Field Overview

BHA is the largest gas producing field in Oman. The field was discovered in 1991 with the drilling of BHA-27. The field has undergone considerable study beginning with the first Field Development Plan (FDP) in 1994 followed by FDP updates in 1996, 2000, 2005, and 2010. An ongoing FDP update is currently underway. The field is divided by faults into three blocks: Main, Graben, and South. BHA Main (**Fig. 1**), referred to as the BHA field, was first produced in 1999 and is the focus of this study.

2.5 Reservoir Description

The BHA field covers an area of 46,879 acres (or 197 km^2). It is anticlinal in structure and is oriented in the SW-NE direction. The reservoir has a fluvial depositional environment, with reservoir properties improving in the northern direction. Reservoir fluids are accumulated in two producing reservoirs: rich gas condensate in Barik and lean gas in the Miqrat. Until 2001, production was solely from the Barik reservoir, after which commingled production was introduced. Wells producing exclusively from the Barik reservoir are examined in this study. The initial reservoir pressure is 7,440 psia (or 51,300 kPa) and the dewpoint pressure is 6,080 psia (or 41,955 kPa). The reservoir temperature is 278 °F (or 137 °C). The porosity ranges

between 1-12% and the permeability between 0.001-20 md. The condensate gas-oil ratio ranges between 115-130 $m^3/10^6Sm^3$.

2.6 Well Completions

Wells in this field are drilled vertically and are then fractured to enhance productivity of the low permeability reservoir formation. The field is currently produced under depletion drive. Proactive preventative measures are taken in order to minimize effects of liquid loading due to the significantly high dewpoint pressure. Liquid loading occurs in gas condensate wells producing at low rates, when the reservoir is below the dewpoint. Once the production reaches a critical rate, liquid accumulates and the well eventually stops producing. A number of production enhancement techniques have been implemented in the BHA field and others are planned. One of these, intermittent production, is a means of preventing liquid build-up around the wellbore by shutting in wells once liquid loading occurs and reopening the well to "flush" the liquids out of the well and the near-well region. As the reservoir pressure continues to decrease, more liquid is formed, and thus longer shut-in periods are required. Another means of preventing liquid loading from occurring is through use of surface compression. Surface compressors lower surface pressures, enhancing lift of produced fluids to surface by lowering the tubing performance curve. Similarly, installation of insert tubing velocity strings also lowers the tubing performance curves.

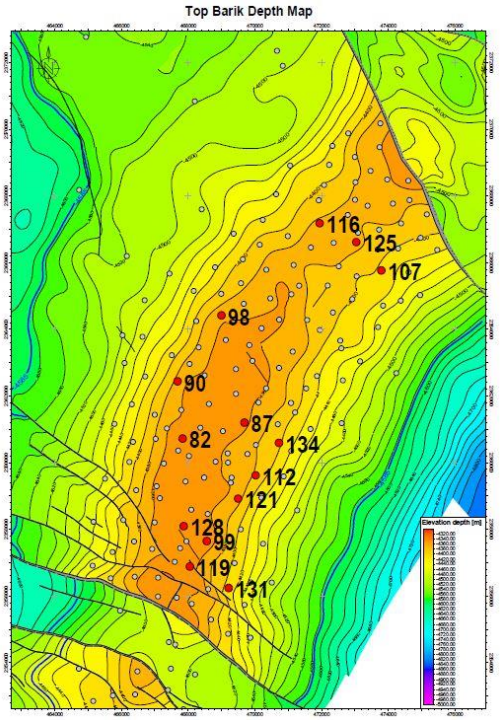

Fig. 1 — Map of BHA Field (Oman).

ANALYSIS OF WELL PERFORMANCE

This chapter describes the data preparation and interval selection process for both the decline curve analysis (DCA) and rate transient analysis (RTA) methods. It also includes an analysis for each of the three example cases used in this study with supporting figures. The same approach was applied to the remaining 11 wells, as shown in Appendices A and B.

3.1 Time-Rate Analysis (or DCA)

We used two modern techniques of "time-rate" or "decline curve" analysis (DCA) to historically match the time-rate data and used the match to obtain the EUR from a 30-year forecast. We used Microsoft® Excel® to perform the time-rate analysis using the two models chosen in this work — i.e., the "Modified Hyperbolic" and "Power Law Exponential" DCA models.

We analyzed 14 well cases in this work from a total of 30 wells provided by the company. The selected wells had continuous and available data for production and pressure. Cases in which pressures were reported after more than one year of production were eliminated and not considered in the study. Wells with frequent and extended shut-in periods were also removed from this study

After selecting the 14 well cases, we began our "time-rate" analysis by filtering and preparing the data. Production data was filtered by eliminating early-time rates that were not representative of the well's true production behavior. During these periods production rates were either well above or below the expected production performance. Although these rates were eliminated from the well performance analysis, these flowrates and associated cumulative productions were incorporated in the calculation of the 30-year EUR.

3.2 Time-Rate-Pressure Production Analysis (Rate Transient Analysis (RTA))

"Time-rate-pressure" analysis or "rate transient analysis" (RTA) was used in this work to both history-match and generate a forecast used to calculate the 30-year EUR for each case. We analyzed 14 well cases using the commercial software package Topaze (Kappa Engineering). The required data included laboratory fluid property reports, well completion data, reservoir data, production data, and operational information. While we need bottomhole pressures for RTA, only surface pressures were recorded in the field. We used the commercial software package Prosper by Petroleum Experts to calculate bottomhole pressures. We believe that although the calculated bottomhole pressures are representative, one of the limitations in using this program is in its inability to accurately predict pressures at very low production rates and hence pressures at low production rates were not used.

After all required information is input, we edit production data. Due to the significant noise present in both pressure and production data, only minimal and essential data editing was done, specifically for the flowrate

data. A given production data point was only eliminated if it was significantly higher than the overall trend. In such a case, we attributed that point as an allocation error and removed it from the dataset. We emphasize that this was done a few times and on an exception basis. Next, we review the pressure data. We observed that due to limitations of Prosper (the pressure calculation software produced by Petroleum Experts), at very low flowrates the calculated pressures do not fit the trend of the pressure data and in many cases exceeded the initial reservoir pressure. Therefore, we judiciously eliminated these data while maintaining the general trend of the calculated pressures.

Next, we select the interval for analysis by analyzing the early time production data. Similar to the case of time-rate analysis, we analyzed the period in which reported flowrates are representative of the reservoir behavior. Accurate selection of this period impacts the shape of the auxiliary plots at early material balance times.

Wells in the BHA field are vertical and hydraulically-fractured. We therefore used diagnostic plots to estimate model parameters for a vertical well with either a finite or infinite conductivity. We changed different reservoir properties (*e.g.*, skin factor, fracture half-length, formation permeability, etc.) and reservoir volume (assuming the existence of boundary-dominated flow behavior) to achieve a match in both the auxiliary plots and the rate history plots. We used time-dependent skin effects to match periods that are difficult to match, where we assume that the time-dependent skin effects account for localized errors in pressure. Finally, we used the matched RTA model to forecast the production performance to calculate the 30-year EUR. We created three pressure extrapolation schemes for the flowrate forecasts. A detailed well analysis is presented in the field example case (BHA Well 087).

3.3 Discussion of DCA and RTA Results

This section presents three well analyses to demonstrate the use of Time-Rate (or DCA) and Time-Rate-Pressure Analysis (or RTA) used in this study. We provide both the analysis and supporting plots used to diagnose each well reviewed in this section. The first well analysis provides detailed explanations, while the following two cases are summarized for comparison. The remaining eleven wells (for a total of 14 wells) are presented in **APPENDIX A**.

3.3.1 Field Example — BHA Well 87

We selected BHA Well 087 to demonstrate our detailed analysis and interpretation methodology for wells in the BHA gas field. Our initial well analysis begins by evaluating the production history plot **(Fig. 2**), which presents the gas flowrate (red symbols) and the calculated bottomhole pressure (blue symbols) data as a function of time. In **Fig. 3** we present the same functions, but now the gas flowrate (red symbols) is presented on a logarithmic scale.

BHA Well 087 has been on production for 16 years, and we note that the flowing pressure data are only available starting the second year of production. Despite repeated enquiries to the operating company, it appears that the pressure data are not completely synchronous with the flowrate data, and there are several cases where pressures only become available 3-4 years into production (such cases were not selected for this work). To be clear, we only consider data analysis for periods where both flowrates and pressures are reported.

In addition, gas flowrates are allocated monthly. The operator informed us of irregularities in allocations, but we believe, based on our work to date, that the flowrate data are relevant for both time-rate and time-rate-pressure analysis methods. The surface pressures are reported daily, and we believe that these pressure data are relevant and representative. The differences in rate and pressure frequencies are not ideal, but these differences are fairly typical for production data analysis performed in practice.

In **Fig. 4**, we plot the gas flowrates and cumulative gas production versus time on a log-log scale. This is an "orientation plot". Specifically, our goal is to observe specific flow regimes; and we note that we have placed a half-slope trend on this plot to indicate possible transient linear flow behavior (≈400-2,100 days). It appears that boundary-dominated flow occurs at about 2,100-3,000 days, although such a conclusion is speculative due to the erratic nature of the flowrate data.

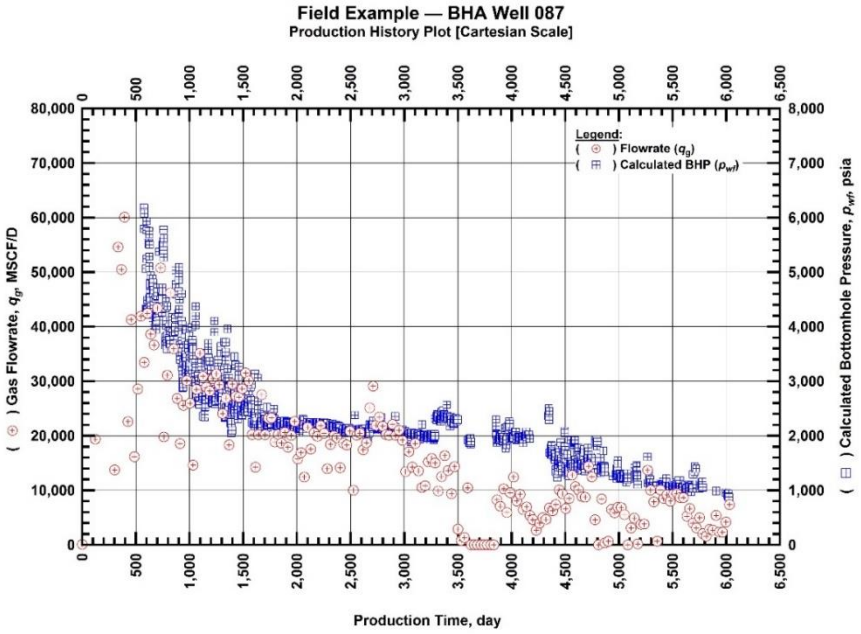

Fig. 2 — Cartesian plot for BHA Well 087 — Production history plot of calculated bottomhole pressures and gas flowrates as a function of production time.

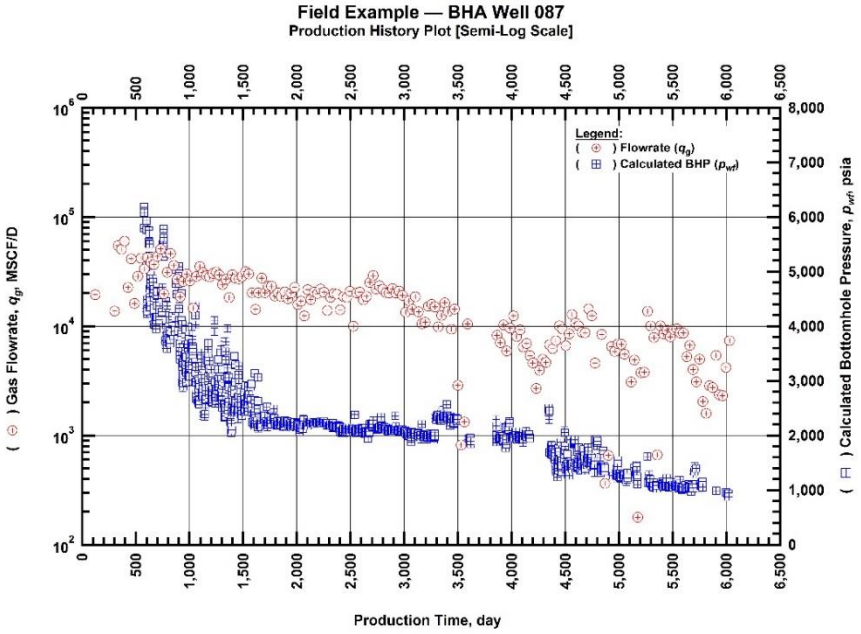

Fig. 3 — Semilog plot for BHA Well 087 — Production history plot of calculated bottomhole pressures and gas flowrates as a function of production time.

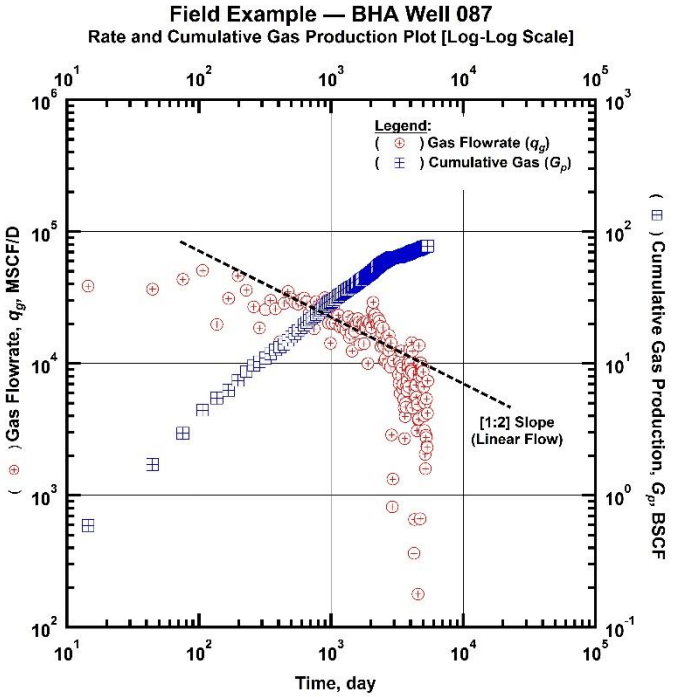

Fig. 4 — Log-Log plot for BHA Well 087 — Gas flowrate and cumulative gas production as a function of production time.

The wells in the BHA gas field are hydraulically fractured to enable economic production in this low-permeability reservoir. Hydraulically fractured wells present characteristic flow regimes based on the "conductivity" of the created vertical fractures. The typical cases observed in practice are:

- *Uniform flux fracture*: Uniform reservoir production per unit length of fracture. Characterized by 1:2 slope on a log-log plot for higher values of time (essentially formation linear flow).
- *Infinite-conductivity fracture*: Dimensionless fracture conductivity >100 (Lee 1996). Characterized by 1:2 slope on a log-log plot (*"formation linear flow"*). (**Fig. 5)**
- *Finite-conductivity fracture*: Dimensionless fracture conductivity <10 (Lee 1996). Characterized by 1:4 slope on a log-log plot (*"bilinear flow"*). (Fig. 5)

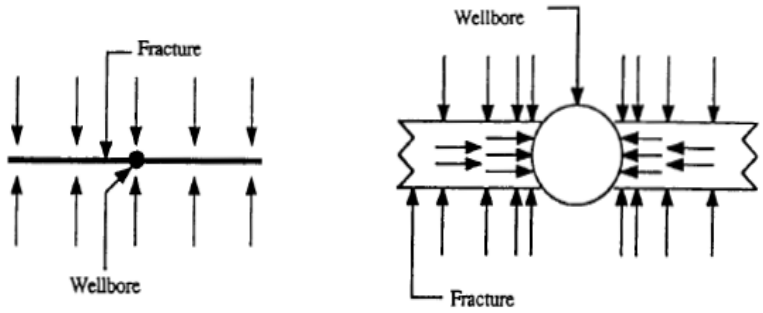

Fig. 5 — Schematic of formation-linear flow (left) and formation-bilinear flow (right) (Lee 1996).

For rate transient analysis (RTA), the use of "diagnostic plots" such as the "Log-Log" and "Blasingame" plots provides meaningful insight about the behavior of a well. The Log-Log plot consists of flowrate-normalized pressure-drop ($\Delta m(p)/q_g$) "integral" and the "integral derivative" functions plotted as against the material balance time function. We used cumulative gas production divided by gas flowrate to approximate the gas material balance time function, which is perfectly acceptable as we are using this for "diagnostics," not rigorous "analysis". We use these functions for visualizing the behavior of the production data. The analysis is performed by history matching the prescribed reservoir model to the production data functions.

The RTA methodology provides for analysis to be performed on both transient flow and boundary-dominated data. On the "Log-Log" plot, transient flow data are typically represented by a gently increasing trend (certain transient flow regimes have unique straight-line trends — *e.g.*, linear flow behavior has a 1:2 slope trend). For boundary-dominated flow a 1:1 slope trend occurs at late times. The application of material balance time is particularly useful because this approach provides a constant-rate equivalent for variable flowrate/variable pressure drop data independent of the reservoir properties. (Palacio and Blasingame 1993).

In **Fig. 6** we provide a schematic of the "Log-Log" plot (specifically the "integral derivative" function) where the different regimes can be observed. In **Fig. 7,** we present the "Log-Log" plot for BHA Well 087, both the ($\Delta m(p)/q_g$) "integral" and the "integral derivative" data functions are shown (as symbols), as well as the model match (black lines). For the material balance time period of approximately 200-4,000 days, the ($\Delta m(p)/q_g$) "integral" function suggests a 1:2 slope trend, which is indicative of an infinite conductivity vertical fracture. For the material balance time period > 4,000 hours an approximate 1:1 slope trend is observed, which confirms boundary-dominated flow behavior.

Similar to the "Log-Log" plot, the "Blasingame" plot uses ($q_g/\Delta m(p)$) functions versus G_p/q_g as alternate means of presenting and diagnosing data. In **Fig. 8** we provide a schematic Blasingame plot which uses the rate "integral derivative" function to highlight various flow regimes. For reference, the "Blasingame" plot presents a (negative) unit slope during boundary-dominated flow. Transient flow features observed on the "Blasingame" plot depend on the nature of the prescribed reservoir model(s).

In **Fig. 9** we present the "Blasingame" plot constructed for BHA Well 087 where all of the ($q_g/\Delta m(p)$) functions are plotted versus G_p/q_g. The "Blasingame" plot is somewhat more susceptible to data noise. Although the rate function ($q_g/\Delta m(p)$) is typically less affected, the integral and integral derivative functions are often significantly affected by data noise. There are schemes to edit spurious data, but such schemes are not used in this work. As shown in **Fig. 9**, the ($q_g/\Delta m(p)$) data function (red symbols) is fairly well-behaved, but the auxiliary functions are affected. The model match is actually quite good for the ($q_g/\Delta m(p)$) function. And as noted, the auxiliary functions could be improved with judicious editing of the ($q_g/\Delta m(p)$) data function (red symbols). For this work, we use the "Blasingame" plot as a check for the match of the data and model functions, and to validate certain flow regimes (*e.g.*, linear flow and boundary-dominated flow).

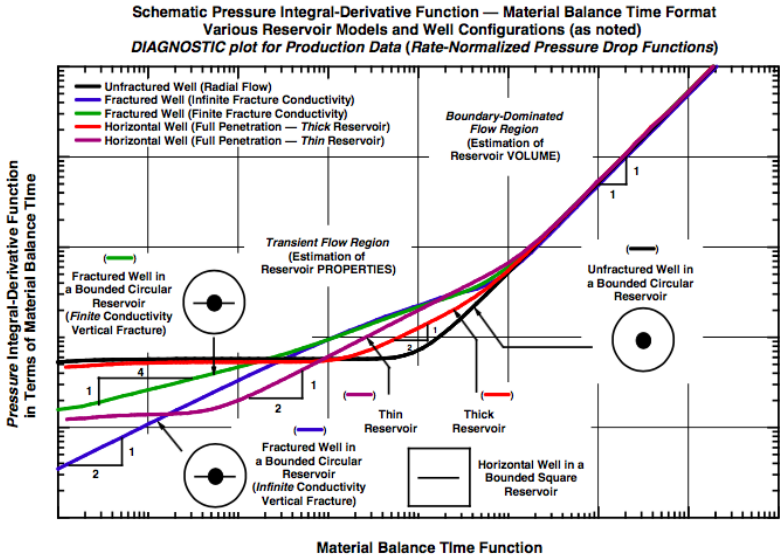

Fig. 6 — "Log-Log plot" schematic pressure drop integral-derivation functions, Ilk et al. (2010)

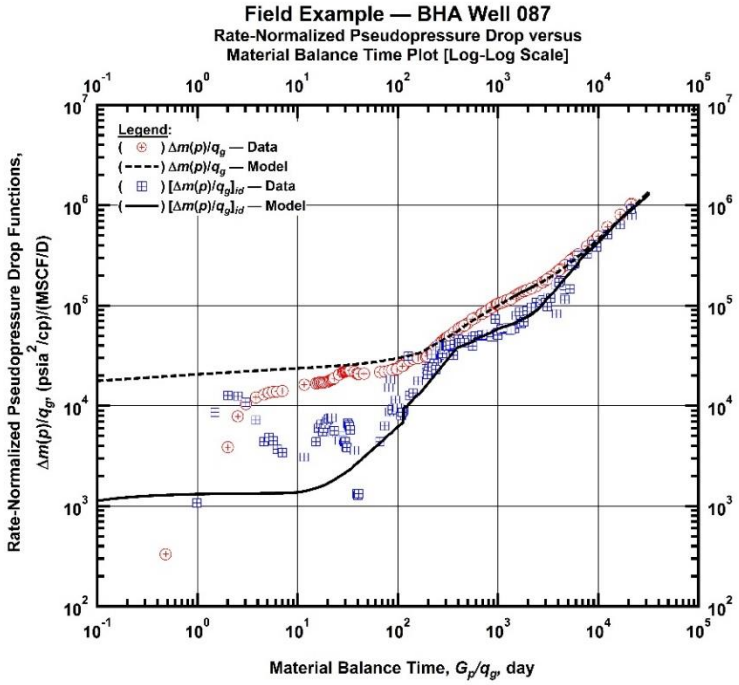

Fig. 7 — Log-Log plot for BHA Well 087 — Rate-normalized pseudopressure drop versus material balance time ("Log-Log Plot").

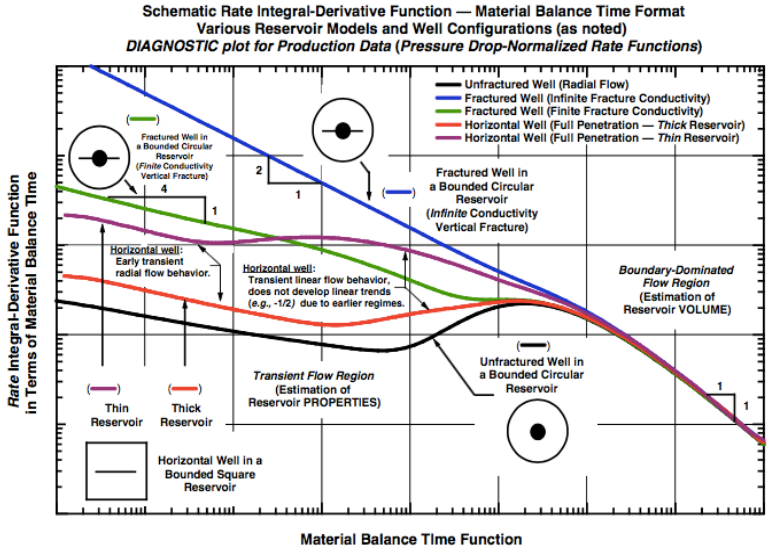

Fig. 8 — "Blasingame plot" schematic rate integral-derivation functions, Ilk et al. (2010)

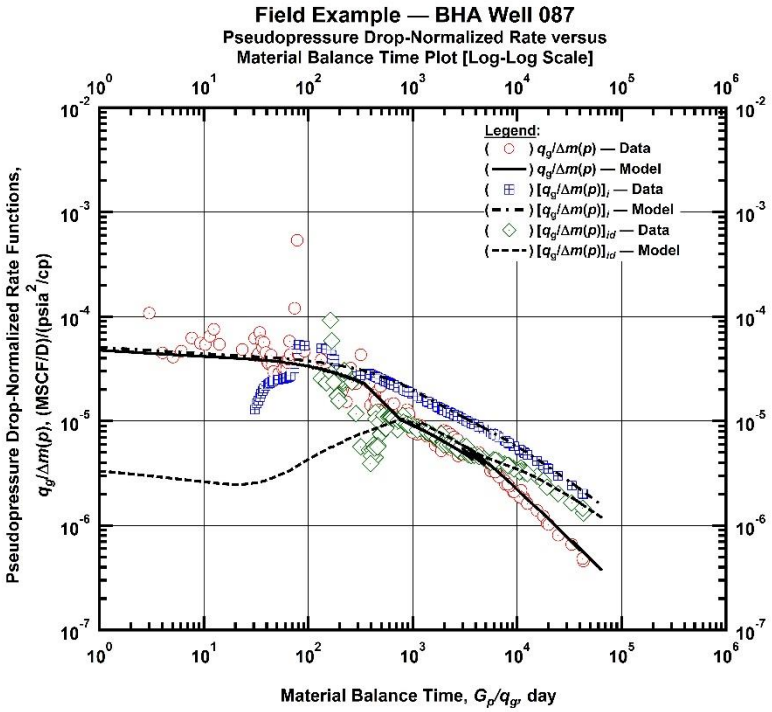

Fig. 9 — Log-Log plot for BHA Well 087 — Pseudopressure drop-normalized rate function versus material balance time ("Blasingame plot").

In **Fig. 10** we present the gas flowrate, flowing bottomhole pressure, and cumulative gas production data (symbols) along with the model match for this case generated using an analytical solution in the Topaze software (Kappa Engineering). Visually, the selected model provides an excellent match with each of the functions. The late time pressure data match (>4,000 days) is somewhat erratic, but roughly coincides with the flowing bottomhole pressure data. It is important to note that there are several periods during the performance history in which well interventions and surface constraints affect well performance, and we note that a "time-dependent" skin effect was required to achieve the match shown in **Fig. 10.**

In **Fig. 11** we present gas flowrate versus cumulative gas production data (symbols) on a Cartesian scale along with the associated history match for this case (blue line). As with the match shown in **Fig. 10**, this match is also very good considering the issues of data frequency, data noise, and undocumented well intervention work. We must also credit the "time-dependent" skin effect for the quality of the history match shown in **Fig. 11.**

We require a 30-year production forecast from both the "time-rate" (DCA) and "time-pressure-rate" (RTA) analyses, and as such, we present the extrapolation results for the DCA and RTA matches in **Fig. 12** (gas flowrate versus time on a semilog scale). We note that for this case we used three scenarios to extrapolate the pressure for the RTA model in order to generate 30-year performance forecasts:

Scenario 1: Extrapolated a single flowing bottomhole pressure (p_{wf}) of 2600 psia.
Scenario 2: Extrapolated a p_{wf} reduction every year, taking p_{wf} from 900 to 200 psia.
Scenario 3: Extrapolated a p_{wf} reduction every 5 years, taking p_{wf} from 900 to 200 psia.

From **Fig. 12** we note that the rate extrapolations for the RTA match (using three pressure extrapolation scenarios) are all considerably higher than the two rate extrapolations generated using DCA methods (specifically the modified hyperbolic (MH) and power-law exponential (PLE) time-rate models). As a point of reference, the power-law exponential model tends to be more conservative than the modified hyperbolic model, and based on the trends in **Fig. 12** we can comment that both of these models appear relevant, but they also appear quite conservative compared to the rate extrapolations (forecasts) generated using the history-matched RTA model.

To complement **Fig. 12**, we provide **Fig 13,** which is a log-log rendering of the functions shown in **Fig. 12**. **Fig. 13** provides a somewhat stronger indication that BHA Well 087 is significantly influenced by depletion at late times and that the estimated ultimate recoveries (EUR) predicted by the time-rate and time-rate-pressure forecasts are reasonable and relevant.

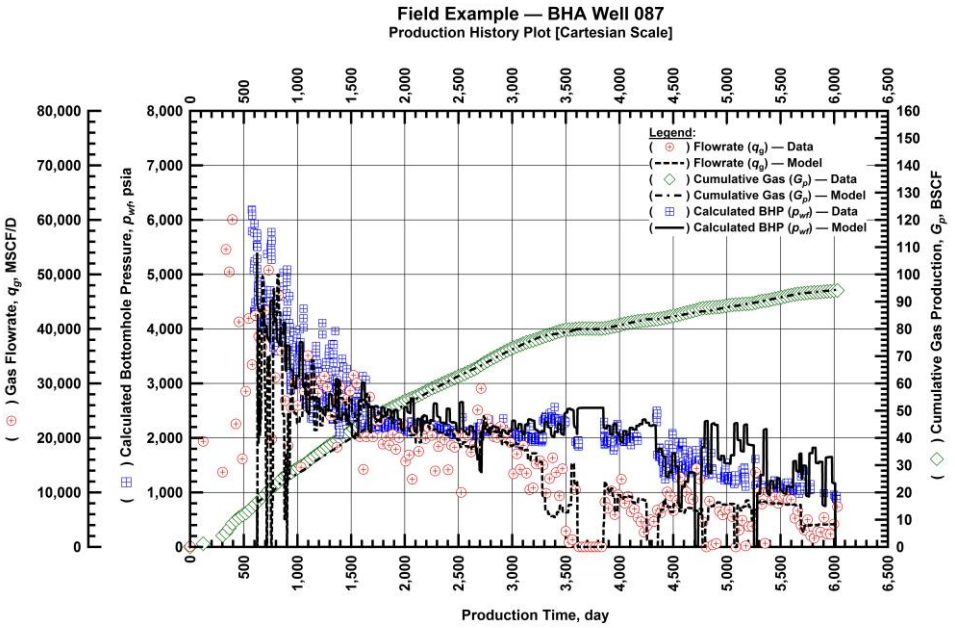

Fig. 10 — Cartesian plot for BHA Well 087 — production history and RTA history-match (gas flowrate, calculated bottomhole pressure, and cumulative gas production versus production time).

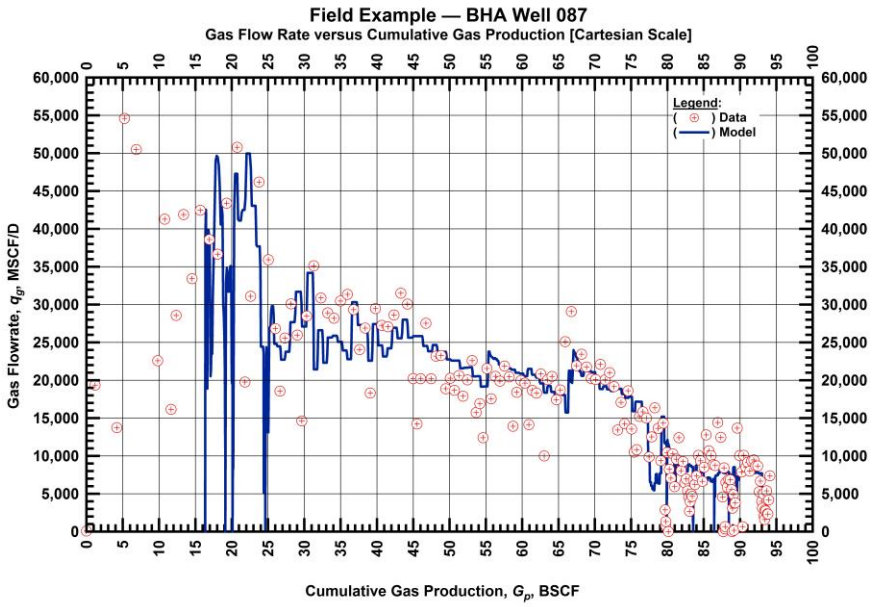

Fig. 11 — Cartesian plot for BHA Well 087 — historical and history-matched gas flowrate versus cumulative gas production.

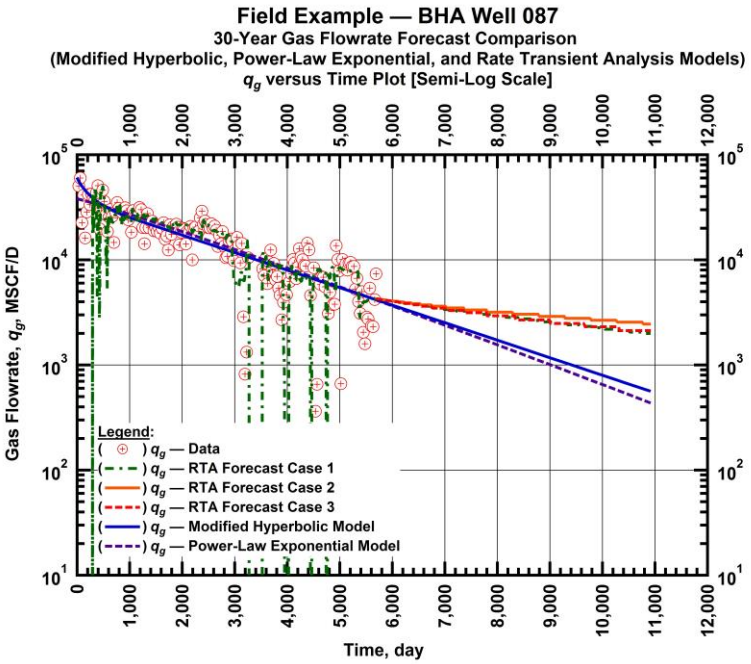

Fig. 12 — Semilog plot for BHA Well 087 — Gas flowrate versus time for various RTA forecast cases (1, 2, 3) and Modified Hyperbolic and Power-Law Exponentialtime-rate models.

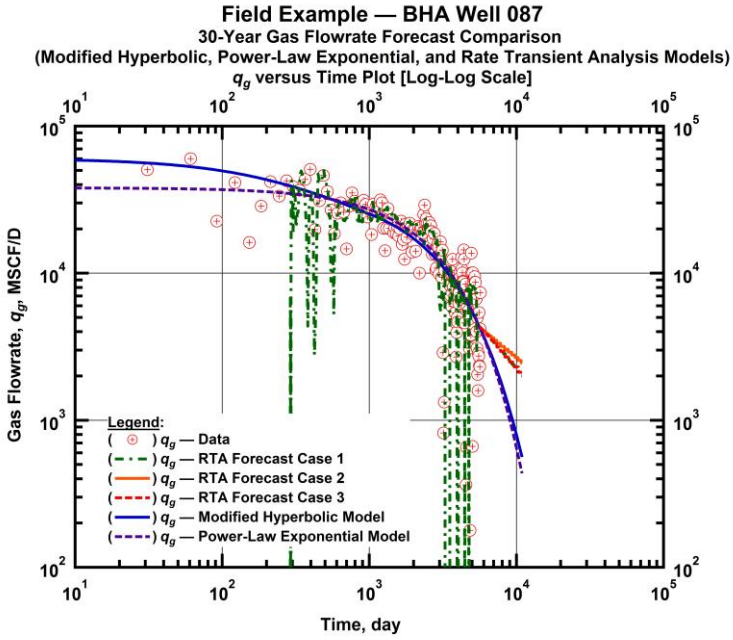

Fig. 13 — Log-Log plot for BHA Well 087 — Gas flowrate versus time for various RTA forecast cases (1, 2, 3) and Modified Hyperbolic and Power-Law Exponential time-rate models.

In **Fig. 14** we present the historical flowing bottomhole pressure plotted versus time, along with the pressure extrapolation scenarios used with the RTA model to generate the required 30-year forecast. Although there is "path-dependency", the rate extrapolations will eventually achieve the same recovery for a given abandonment pressure. In **Fig. 15** we present the pressure history and extrapolation scenarios versus cumulative gas production instead of time for a visualization of this behavior.

In **Fig. 16** we present the gas flowrate versus cumulative gas production data along with the history-matched extrapolated results generated from the RTA (analytical) model. These are the same results presented in **Fig. 12** and **Fig. 13**, only now presented against cumulative gas production to highlight the late-time depletion behavior. The most aggressive depletion occurs for the constant p_{wf} extrapolation (i.e., p_{wf} = 2600 psia). The other two scenarios show there is a "path-dependency" (as would be expected), but since both scenarios are taken to the abandonment pressure of 200 psia, the total gas recovery for each scenario is the same.

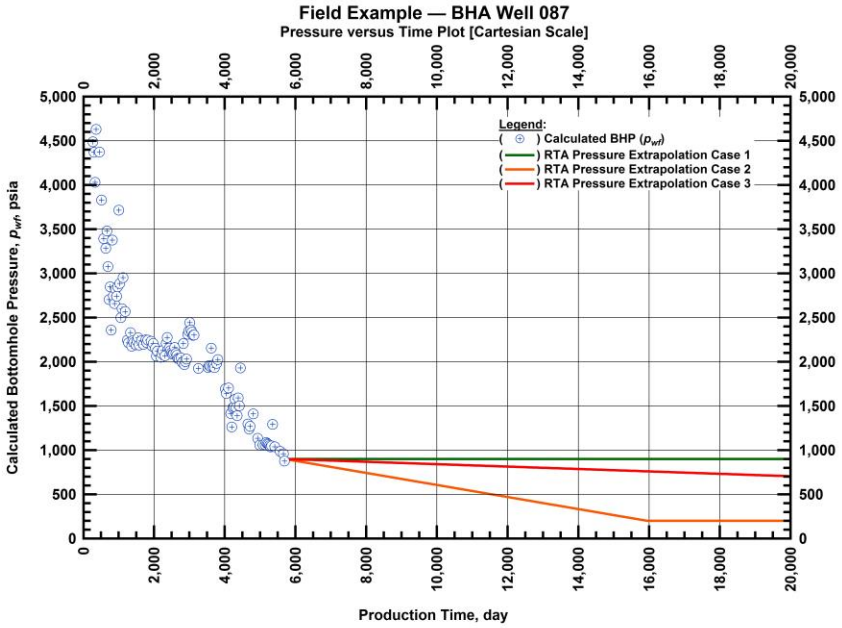

Fig. 14 — Cartesian plot for BHA Well 087 — historical and extrapolated bottomhole flowing pressures versus time (these pressure extrapolation scenarios are used for the RTA model).

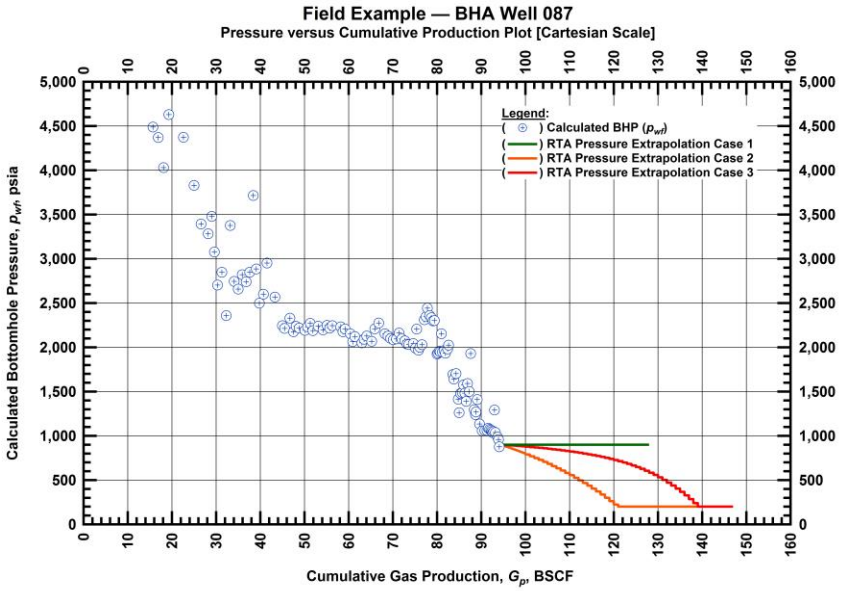

Fig. 15 — Cartesian plot for BHA Well 087 — historical and extrapolated bottomhole flowing pressures versus cumulative gas production (these pressure extrapolation scenarios are used for the RTA model).

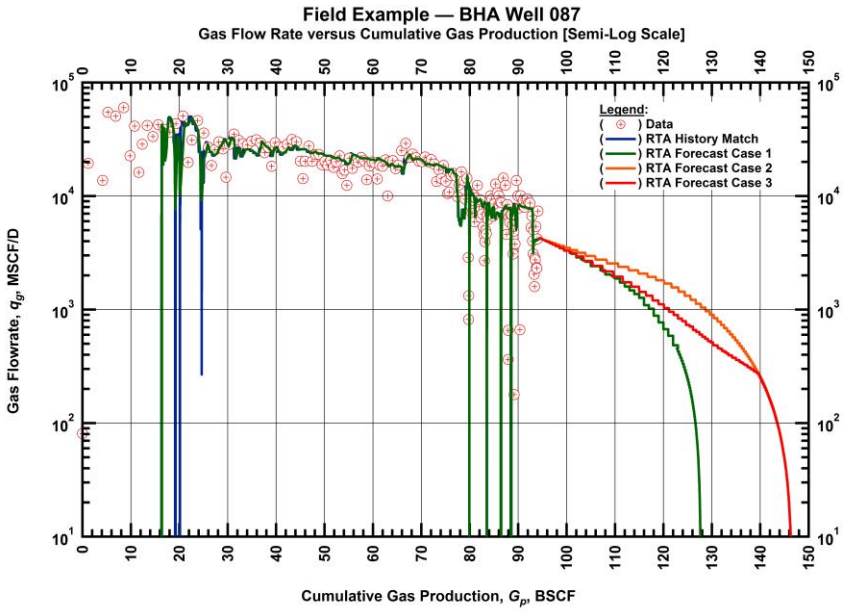

Fig. 16 — Semilog plot for BHA Well 087 — historical, history-matched, and forecasted gas flowrate versus cumulative gas production (various pressure extrapolation scenarios are prescribed (in time) for the RTA model).

3.3.2 Field Example — BHA Well 082

The analysis for BHA Well 082 begins by reviewing the production history plot **(Fig. 17** and **Fig 18)**. BHA Well 082 has been producing for more than 15 years and we note that due to practices in the field, the flowing surface pressures (which are converted to bottomhole pressures) are only available after the first year of production. Pressure and production data have been filtered due to the erratic nature of the data beginning 2008 (approximately 3000 days) and we believe that this behavior could be attributed to liquid loading. Observing the possible "linear flow" trend exhibited by the flowrate data in **Fig. 19** (i.e., the imposed straight-line trend), we speculate that transient linear flow behavior exists between ≈150-2,000 days.

Figs. 20-21 are used for "rate transient analysis" (or RTA) to identify the relevant reservoir model (in this case a vertical well with a single vertical fracture of high conductivity) and to present the match of the model against the data trends. A good model match occurs during late times (which is somewhat expected as this behavior is driven by reservoir volume). However; the match at early times is not particularly good, we believe in most part due to data noise. Specific to the "Blasingame" plot **(Fig. 21),** we note considerable instability in the raw productivity index (red circle symbols), which leads to very poor performance of the auxiliary functions (i.e., the "rate integral" function (blue symbols) and the "rate-integral derivative" function (green symbols)). Our interpretation from **Figs. 20-21** is that boundary-dominated flow is fully developed at ≈2,000 days material balance time.

In **Fig. 22** we present the traditional "history match" plot of rate, cumulative production, and pressure as functions of time, and in **Fig. 23** we present the gas flowrate versus cumulative production match as a further validation. An excellent model match is achieved. These matches required the use of "time-dependent skin" in order to capture the behavior exhibited during certain production periods. As an example, production rates declined significantly at ≈1,900 days and time-dependent skin was used to match this sudden decline in production rates, with no corresponding changes in pressures.

Figs. 24-25 present the Log-Log and semilog plots (respectively) for comparing the rate extrapolations generated from each of the two models. There are three RTA model extrapolations, each based on the assumption of an extrapolated pressure history (**Figs. 26-27)**. In this case (BHA Well 082) the RTA predictions are consistently higher than the DCA extrapolations, with PLE being most conservative model (which is expected). The RTA model extrapolations are higher than the DCA results for several reasons, but we suspect that the dominant reason is that the RTA model captures the compressibility of the gas in its calculations, which provides more energy and a higher flowrate extrapolation than a simple time-rate extrapolation which has no intrinsic capability to model the behavior of the fluid properties. As a final comparison, we present the RTA extrapolations on a semilog "rate-cumulative" plot in **Fig. 28**.

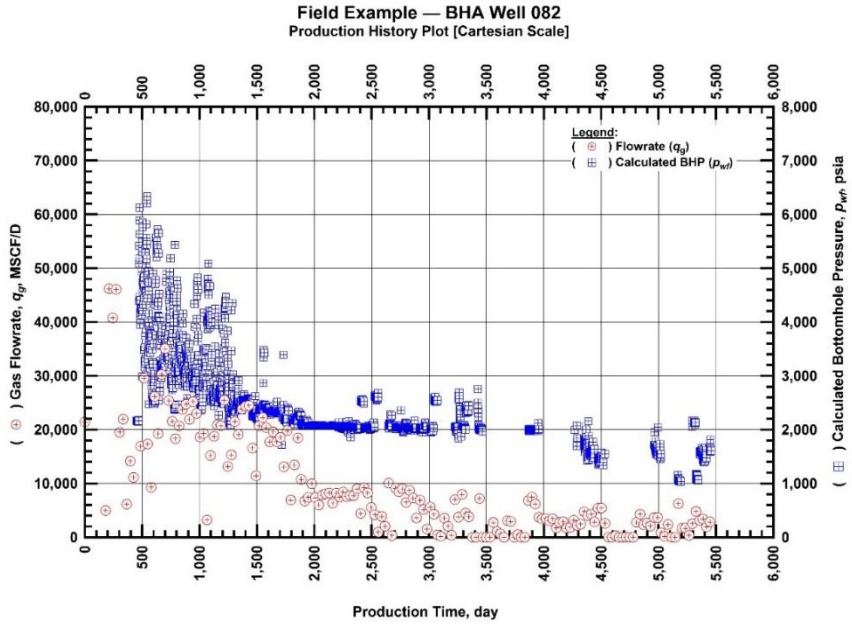

Fig. 17 — Cartesian plot for BHA Well 082 — Production history plot of calculated bottomhole pressures and gas flowrates as a function of production time.

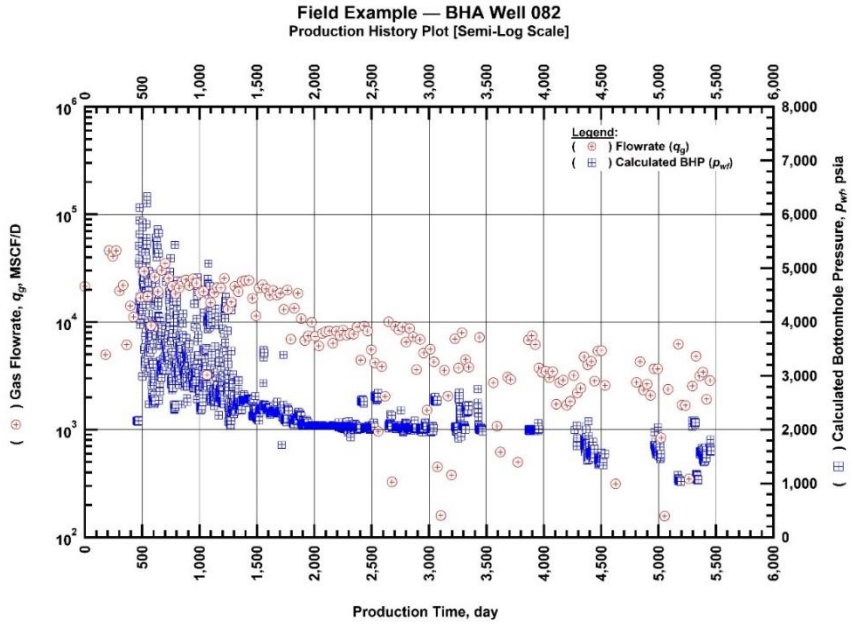

Fig. 18 — Semilog plot for BHA Well 082 — Production history plot of calculated bottomhole pressures and gas flowrates as a function of production time.

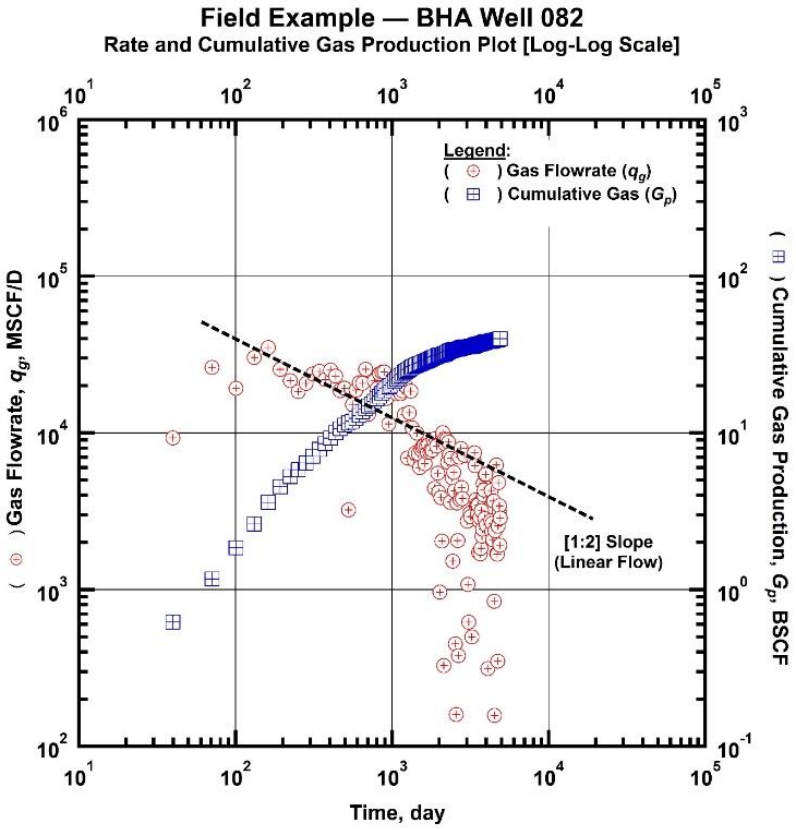

Fig. 19 — Log-Log plot for BHA Well 082 — Gas flowrate and cumulative gas production as a function of production time.

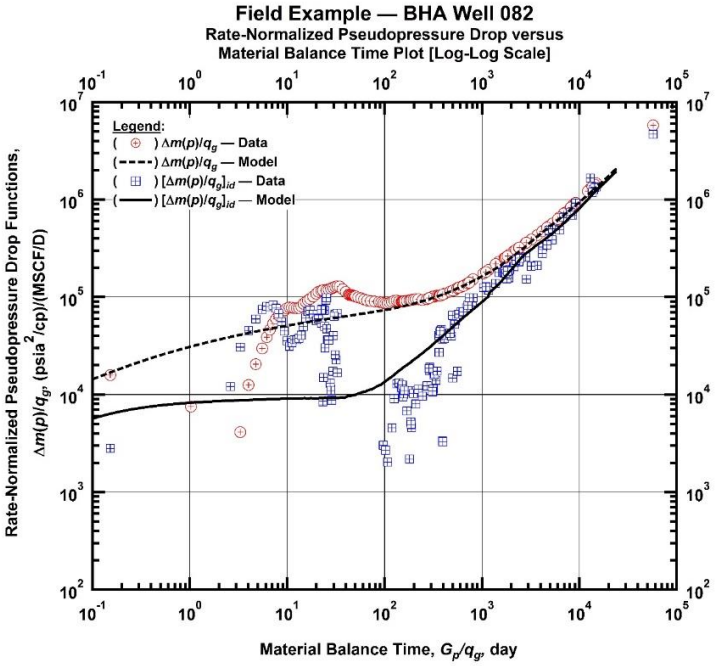

Fig. 20 — Log-Log plot for BHA Well 082 — Rate-normalized pseudopressure drop versus material balance time ("Log-Log Plot").

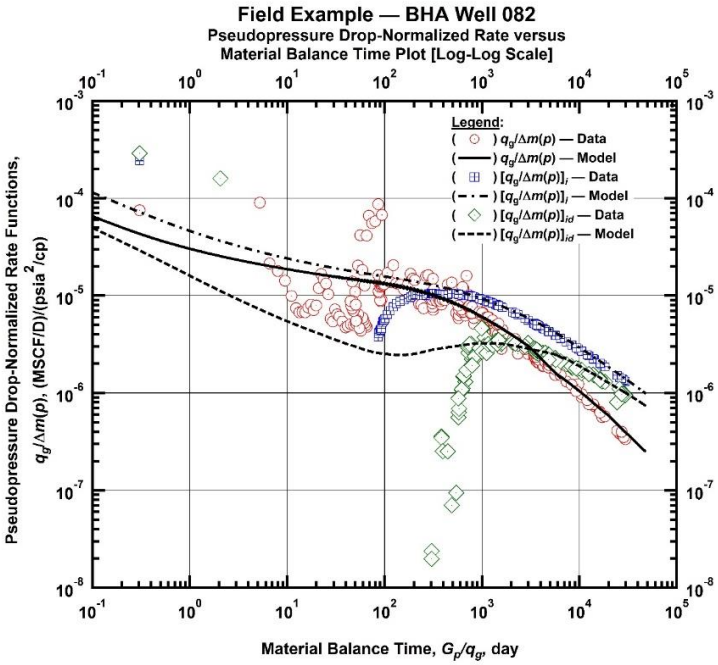

Fig. 21 — Log-Log plot for BHA Well 082 — Pseudopressure drop-normalized rate function versus material balance time ("Blasingame plot").

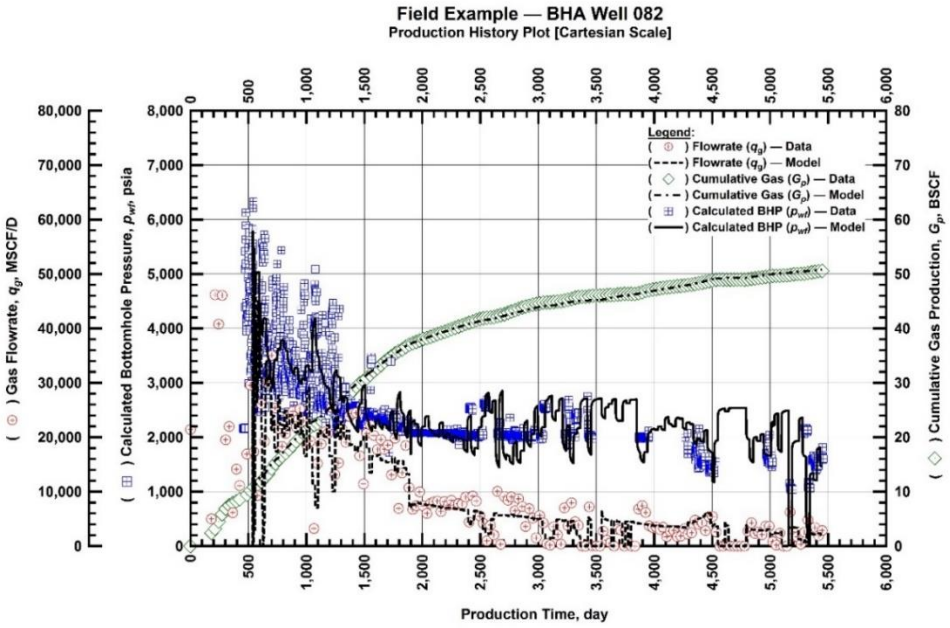

Fig. 22 — Cartesian plot for BHA Well 082 — production history and RTA history-match gas flowrate, calculated bottomhole pressure, and cumulative gas production production time).

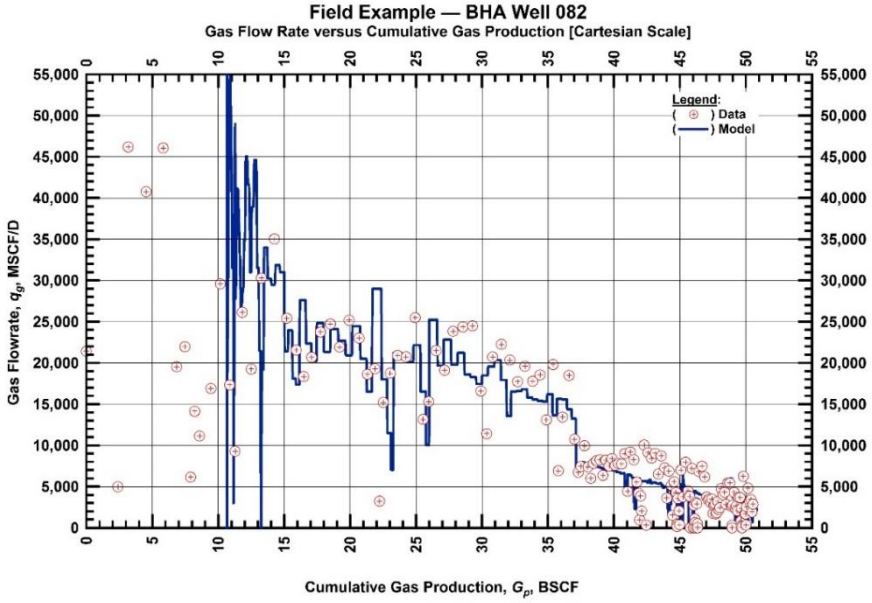

Fig. 23 — Cartesian plot for BHA Well 082 — historical and history-matched gas flowrate versus cumulative gas production.

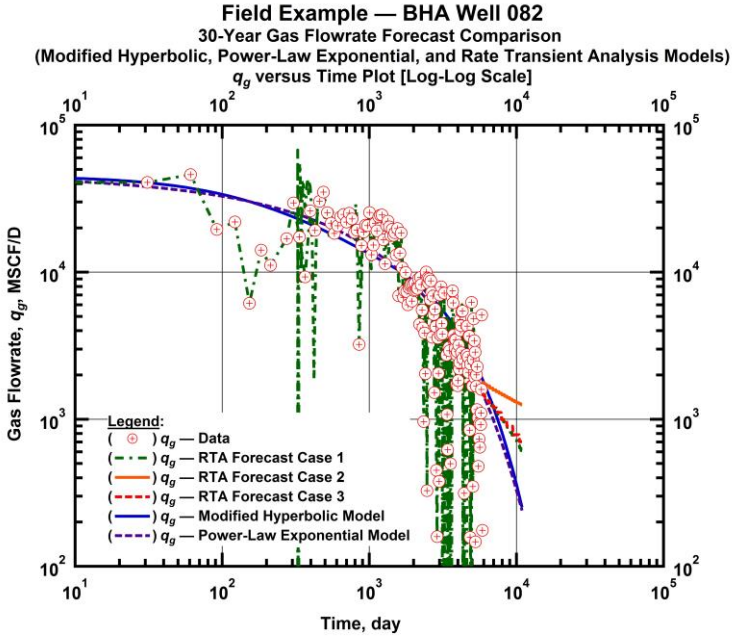

Fig. 24 — Log-Log plot for BHA Well 082 — Gas flowrate versus time for various RTA forecast cases (1, 2, 3) and Modified Hyperbolic and Power-Law Exponential time-rate models.

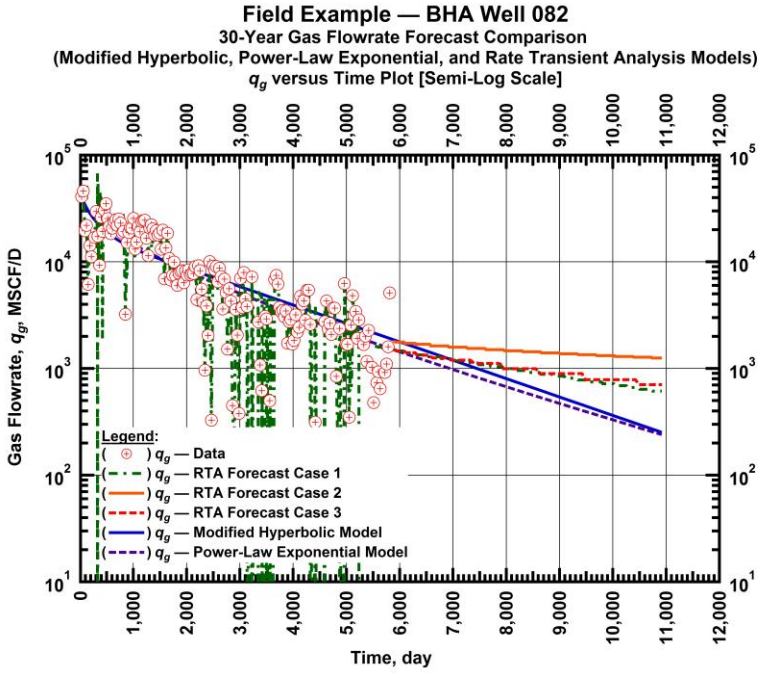

Fig. 25 — Semilog plot for BHA Well 082 — Gas flowrate versus time for various RTA forecast cases (1, 2, 3) and Modified Hyperbolic and Power-Law Exponential time-rate models.

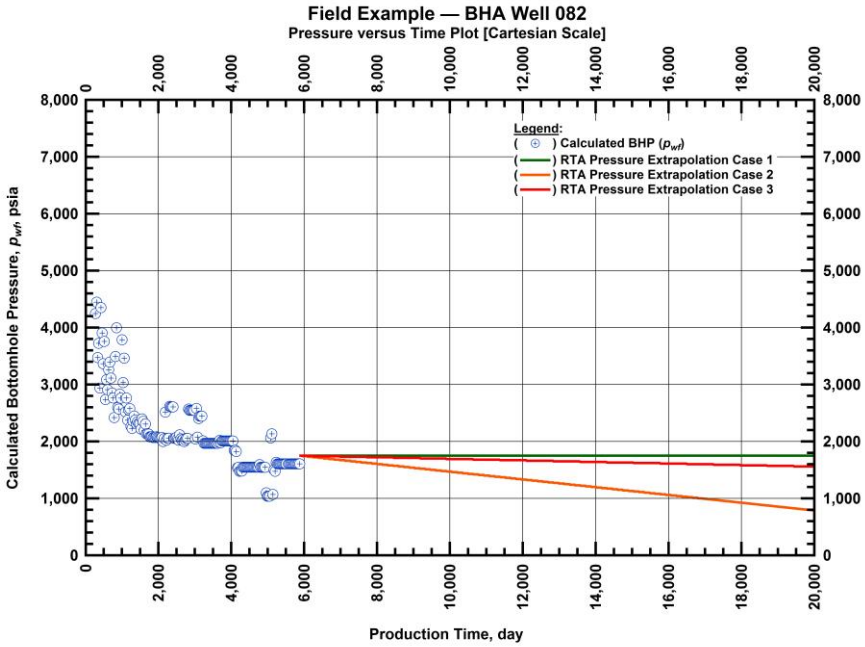

Fig. 26 — Cartesian plot for BHA Well 082 — historical and extrapolated bottomhole pressures versus time (these pressure extrapolation scenarios are used for RTA model).

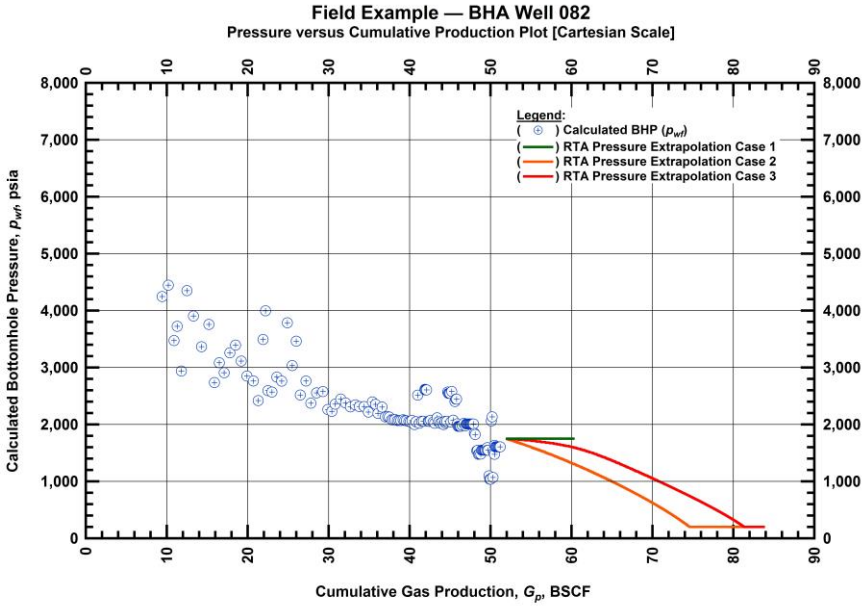

Fig. 27 — Cartesian plot for BHA Well 082 — historical and extrapolated bottomhole flowing pressures versus cumulative gas production (these pressure extrapolation scenarios used for the RTA model).

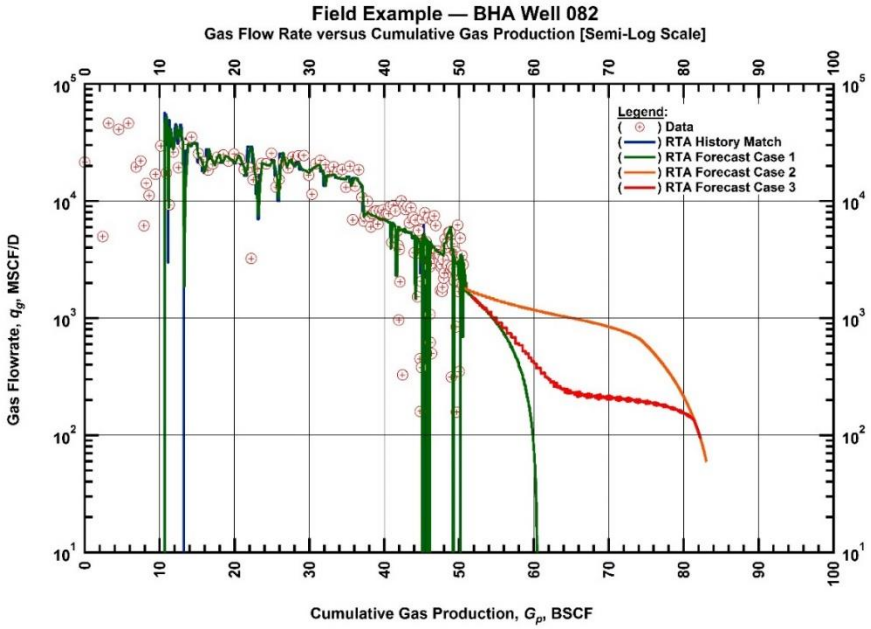

Fig. 28 — Semilog plot for BHA Well 082 — historical, history-matched, and forecasted gas flowrate versus cumulative gas production (various pressure extrapolation scenarios are prescribed (in time) for the RTA model).

3.3.3 Field Example — BHA Well 112

The initial analysis for BHA Well 112 begins by plotting the gas flowrates and calculated bottomhole pressures as a function of time on both Cartesian and semilog scales (**Figs. 29-30).** In reviewing these plots, we observe that the well has been producing for more than 16 years. The pressure data (blue symbols) is initially noisy, but becomes more consistent during the remainder of the production period. However; between 1,000-3,700 days, the surface pressure appears to be producing against a set choke pressure, resulting in a constant calculated bottomhole pressure of approximately 2,000 psia. At ≈3,700 days (or mid-2010) first-stage compression was installed and resulted in a slight increase in gas flowrates. After the addition of second- and third-stage compression (at 4,800 and 5,700 days, respectively), the gas flowrate production of BHA Well 112 stabilized and continued to produce at a low declining rate. In **Fig. 31** we observe a possible "linear flow" trend exhibited by the flowrate data and speculate that transient linear flow behavior exists between ≈300-4,000 days.

We use the "diagnostic plots", "Log-Log" plot (**Fig. 32**) and the "Blasingame" plot (**Fig. 33**), for RTA to determine different flow regimes. The model fit is obtained by adjusting the reservoir properties and reservoir volume, where for the case of BHA Well 112, we chose a vertical well with a single vertical fracture of high conductivity. A good model match is achieved during late times. Based on these plots, we believe that boundary-dominated flow is fully developed at 800 days material balance time.

In **Fig**. **34**, we observe that an excellent model match is achieved in the production history plot. Due to the erratic behavior of early time data, the analysis begins after ≈200 days of production. A good overall pressure match is achieved until ≈3,700 days, where calculated bottomhole pressures decreased from ≈2,100-1,700 psia after the installation of the first-stage surface compressor. During this period, we note that despite the use of "time-dependent skin", the model suggests that these flowrates should produce a smaller pressure drop than those recorded, resulting in a slight pressure mismatch during this period. In **Fig**. **35**, we confirm that in general there is an excellent match in the "rate-cumulative" plot.

Figs. 36-37 present the three rate extrapolations generated from the RTA models and the rate extrapolations generated from the two DCA models (i.e., the modified hyperbolic (MH) and the power-law exponential (PLE)). Each of the three RTA model extrapolations is based on the assumption of an extrapolated pressure history, where these pressure histories are presented in **Figs. 38-39**. We note that in this case (BHA Well 112), the RTA predictions are comparable to the DCA extrapolations, with PLE being the most conservative model.

As a final comparison, we present the RTA extrapolations on a semilog "rate-cumulative" plot in **Fig. 40**. Decreasing the intake pressure in the RTA cases from a constant 1,150 psia to the assumed abandonment pressure of 200 psia predicts a 19 % increase in production.

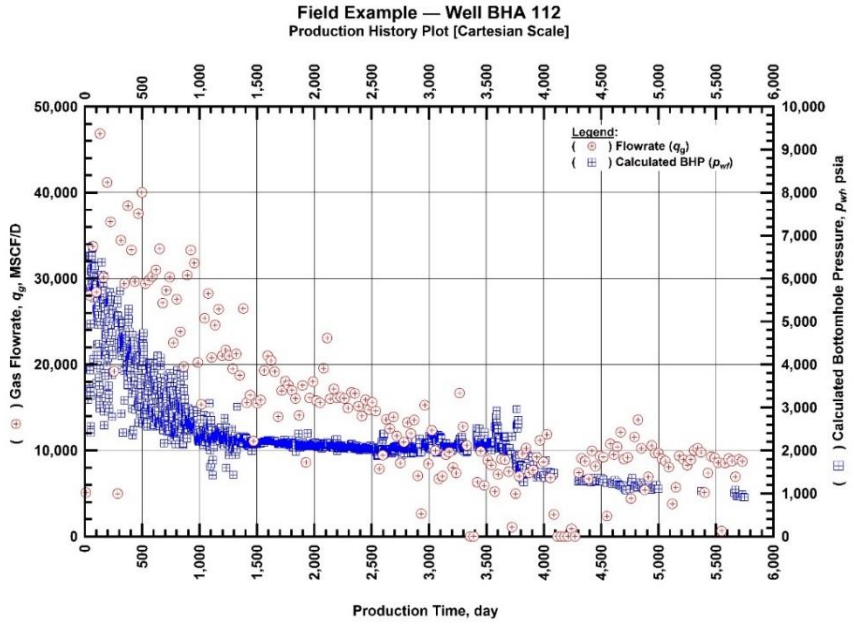

Fig. 29 — Cartesian plot for well BHA 112 — Production history plot of calculated bottomhole pressures and gas flowrates as a function of production time.

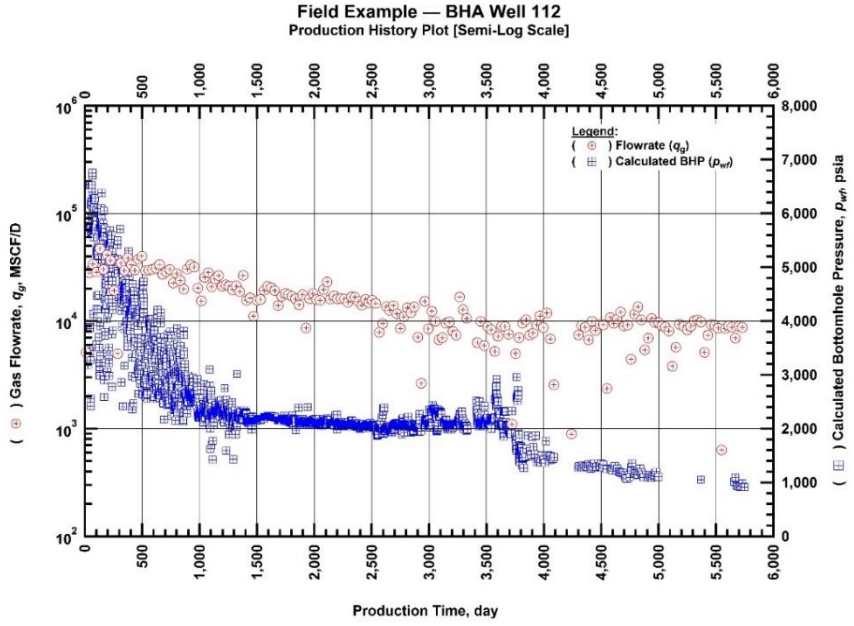

Fig. 30 — Semilog plot for well BHA 112 — Production history plot of calculated bottomhole pressures and gas flowrates as a function of production time.

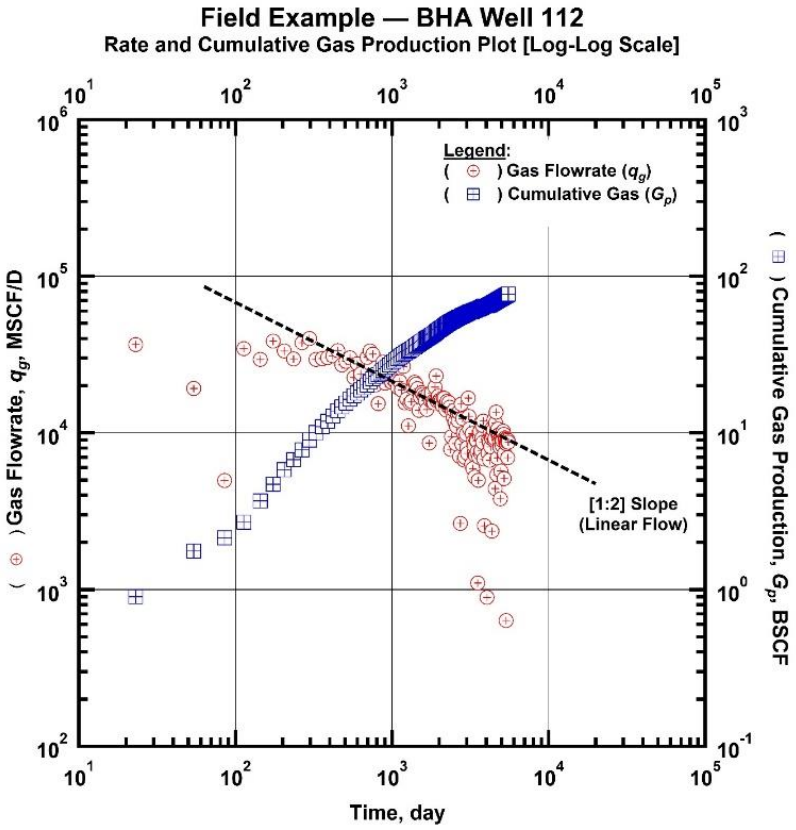

Fig. 31 — Log-Log plot for well BHA 112 — Gas flowrate and cumulative gas production as a function of production time.

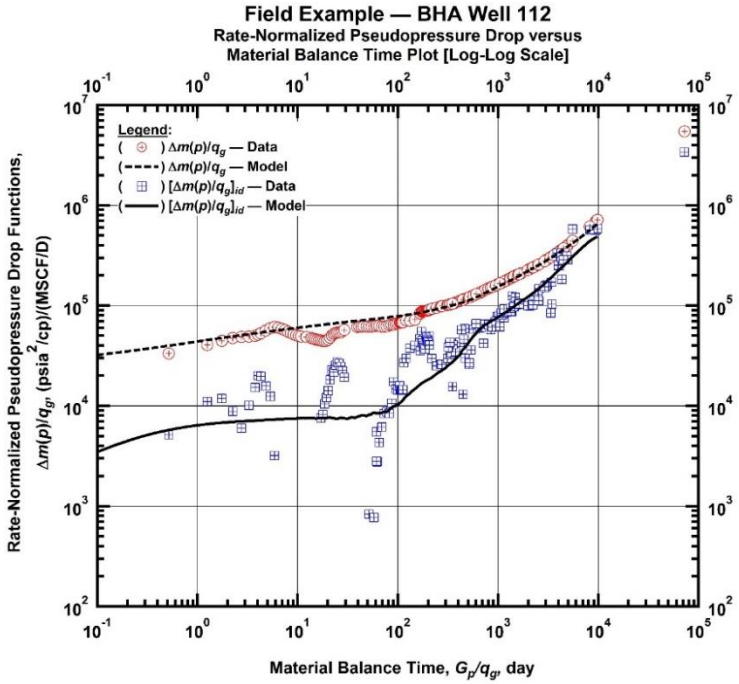

Fig. 32 — Log-Log plot for well BHA 112 — Rate-normalized pseudopressure drop versus material balance time ("Log-Log Plot").

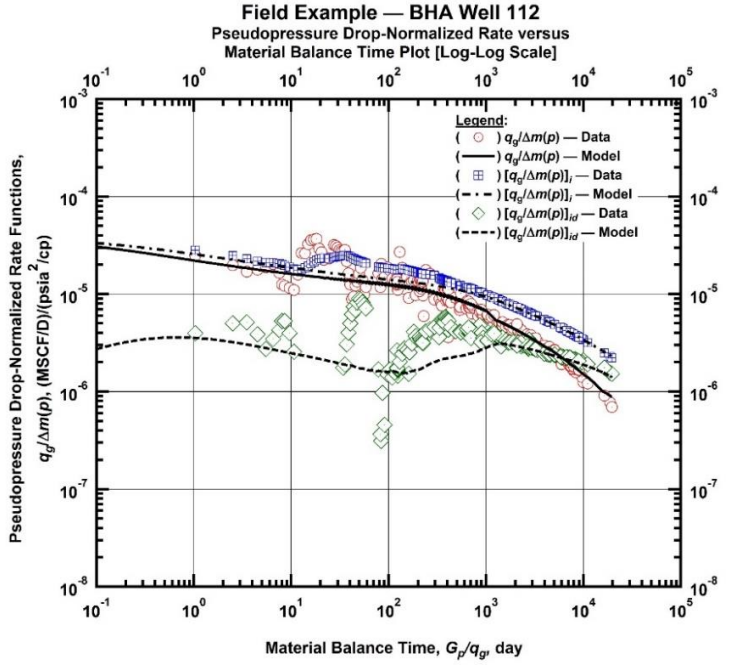

Fig. 33 — Log-Log plot for well BHA 112 — Pseudopressure drop-normalized rate function versus material balance time ("Blasingame plot").

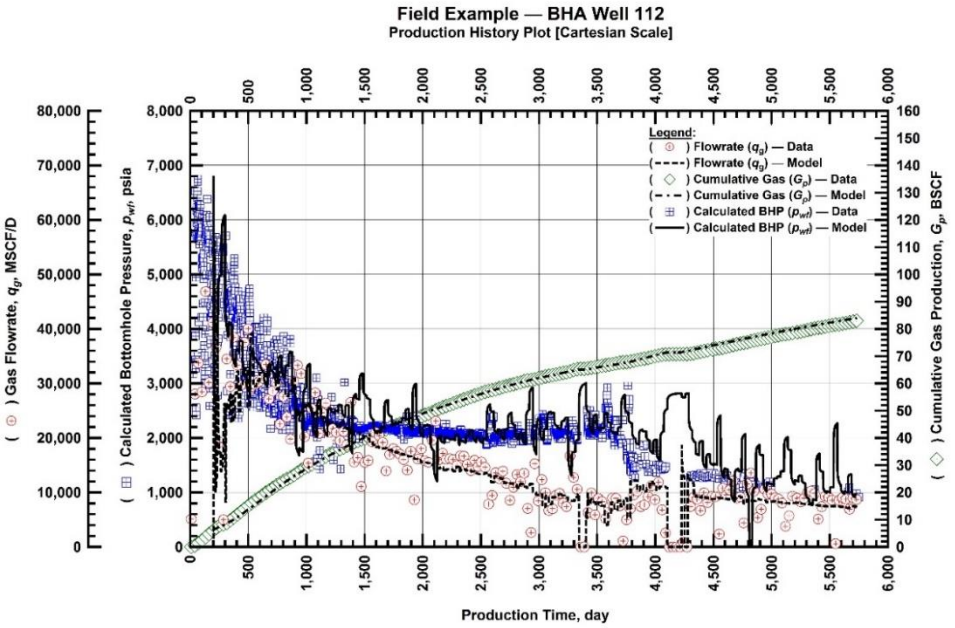

Fig. 34 — Cartesian plot for well BHA 112 — production history and RTA history-match (gas flowrate, calculated bottomhole pressure, and cumulative gas production versus production time).

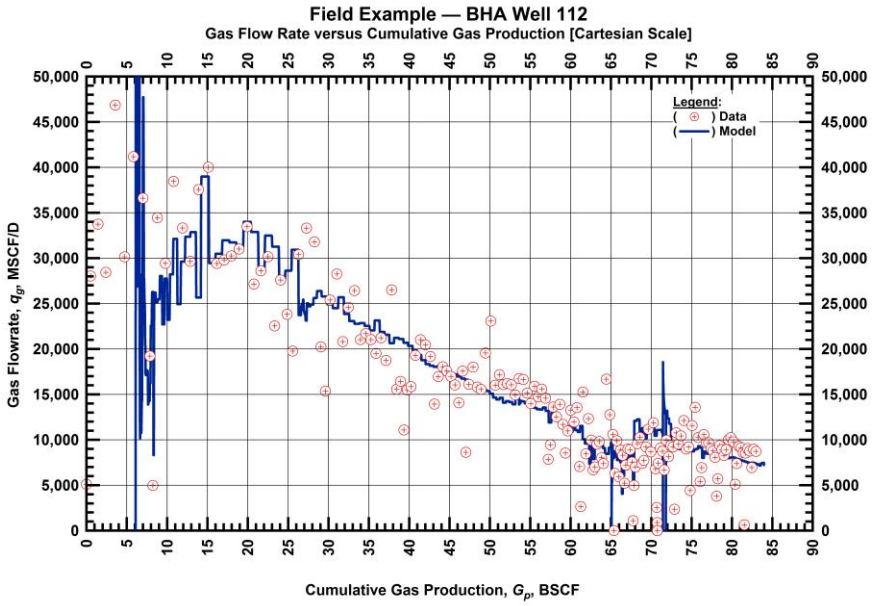

Fig. 35 — Cartesian plot for well BHA 112 — historical and history-matched gas flowrate versus cumulative gas production.

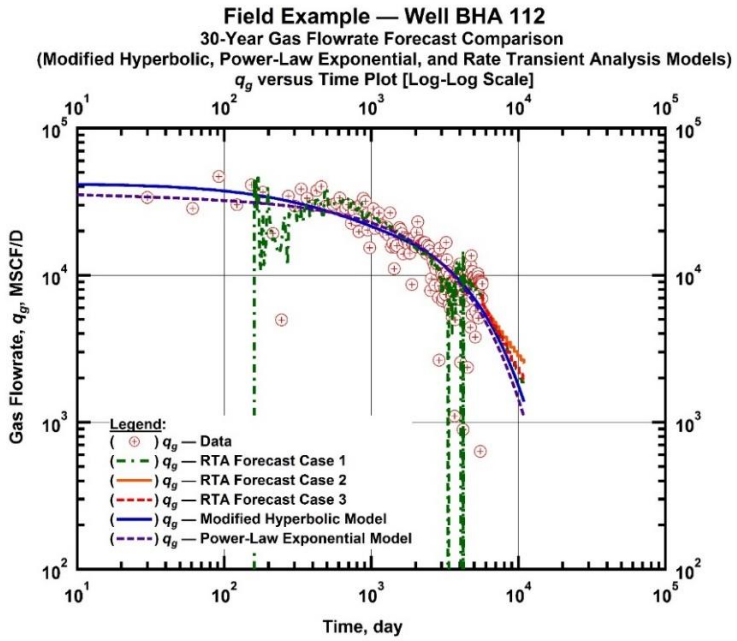

Fig. 36 — Log-Log plot for well BHA 112 — Gas flowrate versus time for various RTA forecast cases (1, 2, 3) and Modified Hyperbolic and Power-Law Exponential time-rate models.

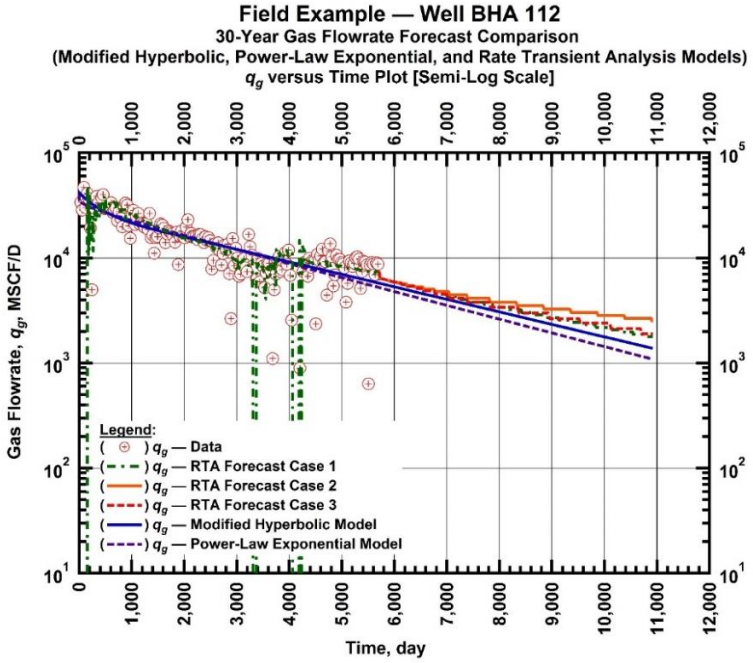

Fig. 37 — Semilog plot for well BHA 112 — Gas flowrate versus time for various RTA forecast cases (1, 2, 3) and Modified Hyperbolic and Power-Law Exponential time-rate models.

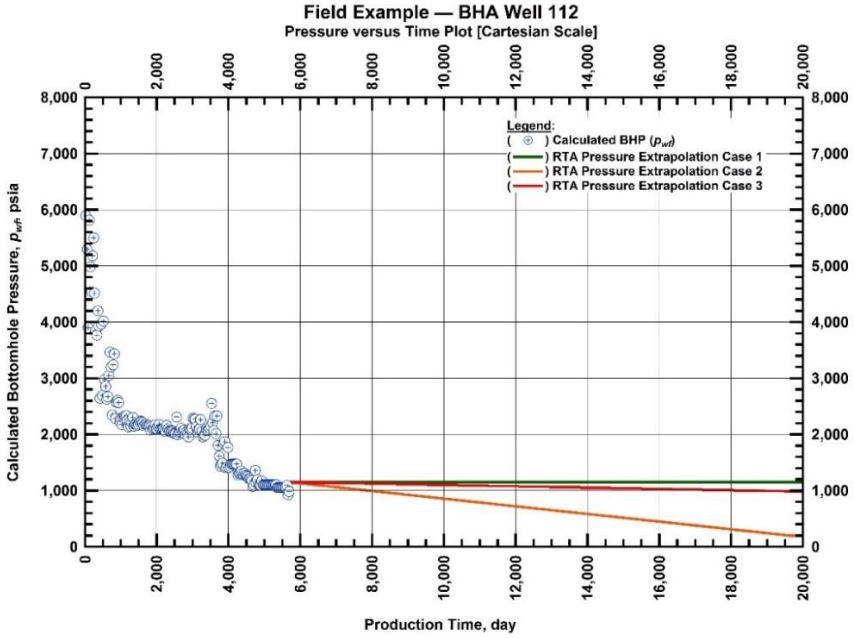

Fig. 38 — Cartesian plot for well BHA 112 — historical and extrapolated bottomhole flowing pressures versus time (these pressure extrapolation scenarios are used for the RTA model).

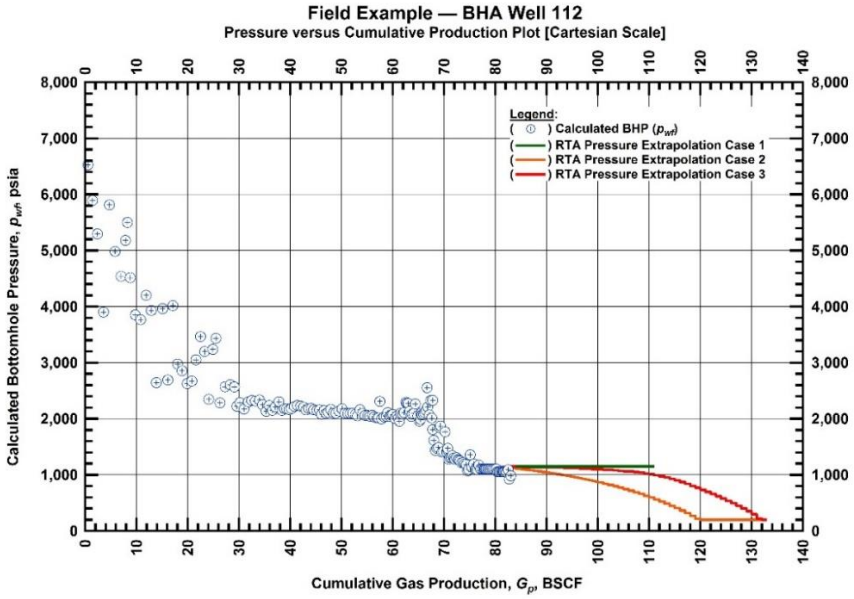

Fig. 39 — Cartesian plot for well BHA 112 — historical and extrapolated bottomhole flowing pressures versus cumulative gas production (these pressure extrapolation scenarios are used for the RTA model).

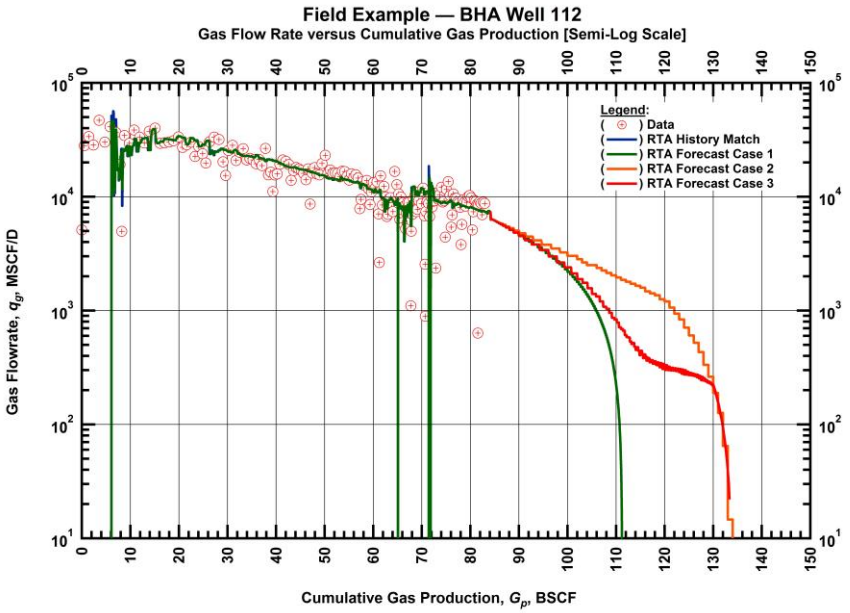

Fig. 40 — Semilog plot for well BHA 112 — historical, history-matched, and forecasted gas flowrate versus cumulative gas production (various pressure extrapolation scenarios are prescribed (in time) for the RTA model).

INTEGRATION OF RESULTS

This chapter describes the results obtained from performing modern time-rate analysis (DCA) and model-based production analysis (RTA), in addition to presenting existing results from production transient analysis (PTA) in sections 4.1-4.3. We then develop correlation plots for each of the DCA and RTA results separately in sections 4.4 and 4.5. Finally, in section 4.6, we attempt to integrate the DCA and RTA results to attain a correlation between the parameters from the time-rate relations and the well/reservoir properties estimated from RTA analysis.

4.1 Results from Time-Rate Analysis (DCA)

Error! Reference source not found. presents the parameters that were used to match the production history rates using the Modified Hyperbolic DCA relation (MH). In reviewing these parameters, we find that with the exception of BHA Wells 119 and 131, we were able to match the historical production rates using decline exponent values (b) exceeding one. Values of b greater than one are generally used to match the extended transient linear flow periods observed in low-permeability reservoirs. When examining the location of BHA Wells 119 and 131, in which we used b values slightly lower than 1, we find that they are geologically located adjacent to each other in the southernmost part of the field, where the fluvial channels are well developed and better reservoir properties are reported.

The range of b values observed for the remaining twelve wells is between 1.02 and 1.85, where the 1.02 decline exponent corresponds to BHA Well 99, immediately north of BHA Well 121. We can see that for the cases of BHA Wells 119 and 131 that the value of D_e is lower than other wells, meaning that these wells switch to exponential decline at higher declines much earlier than the rest of the wells, suggesting that boundary-dominated flow (BDF) may also be observed earlier.

Table 1 — Match parameters from Modified Hyperbolic DCA method.

Field Example	q_i (MSCF/D)	D_i (D^{-1})	b	D_e
82	45000	0.0036	1.55	15
87	60000	0.0023	1.80	12
90	39500	0.0025	1.65	14
98	43000	0.0012	1.50	17
99	70000	0.0015	1.02	11
103	55579	0.0025	1.26	14
112	42000	0.0013	1.80	10
116	56000	0.0085	1.75	10
119	67200	0.0010	0.95	9
121	49500	0.0031	1.60	18
125	36000	0.0010	1.40	29
128	45500	0.0014	1.85	15
131	38000	0.0020	0.88	5
134	38000	0.0025	1.30	16

In **Table 2** we present the parameters used to match the historical production rates using the Power-Law Exponential DCA relation (PLE). In reviewing these parameters we note that the time exponent, n, ranges between 0 and 1. In line with our observation of the MH data, we note that the D_∞ term is notably smaller in the case of BHA Wells 119 and 131 and n values are relatively close to 1, indicating good reservoir properties, and that the well decline becomes exponential (since decline becomes exponential when D_∞=0 and n=1). Seshadri (2010) states that as n approaches 0, the power law begins high and becomes lower over time, much like the behavior of tight reservoirs.

Table 2 — Match parameters obtained using power-law exponential DCA method. .

Field Example	$\hat{q}_i$ (MSCF/D)	n	$\hat{D}$	D_∞
82	46500	0.4550	0.04	0.000230
87	39019	0.1200	0.03	0.000349
90	40696	0.1000	0.25	0.000410
98	43000	0.0010	0.10	0.000521
99	70000	0.1200	0.17	0.000380
103	55579	0.1932	0.15	0.000409
112	43000	0.1200	0.15	0.000295
116	55000	0.3020	0.16	0.000164
119	61500	0.7350	0.0028	0.000090
121	55000	0.1000	0.30	0.000515
125	45000	0.1450	0.10	0.000810
128	65000	0.1000	0.31	0.000400
131	48000	0.3800	0.10	0.000040
134	40000	0.0450	0.45	0.000450

Next, we tabulate the calculated 30-year Estimated Ultimate Recovery (EUR) for both the MH and PLE time-rate relations, in addition to percent difference between them (**Table 3**). We note that the difference between the two methods is less than 4%, with the MH relation having slightly higher EUR, while PLE tends to be more conservative.

Table 3 — 30-year EUR values from the MH and PLE DCA methods and the absolute difference between them.

Field Example	Power-Law Exponential (MSCF)	Modified Hyperbolic (MSCF)	Percent Difference (%)
82	55.02	56.60	2.87
87	106.60	108.50	1.78
90	61.21	61.36	0.25
98	78.04	78.92	1.12
99	129.15	129.25	0.08
103	72.17	72.63	0.64
112	97.18	100.33	3.24
116	60.33	60.39	0.10
119	154.39	155.25	0.56
121	60.98	61.27	0.48
125	44.82	45.41	1.31
128	110.61	110.88	0.25
131	52.18	54.16	3.79
134	47.46	47.67	0.44

4.2 Results from Time-Rate-Pressure Analysis (RTA)

In **Table 4** we summarize the well/reservoir parameters that were obtained when performing time-rate-pressure analysis (or RTA). We highlight that while *kh* values range between 171 and 513 md-ft, estimated *kh* for BHA Well 87 is significantly higher as a result of both high permeability and net thickness. The fracture half-length (x_f) is between 52 and 139 ft. The gas initially in place (STGIIP) is between 88 and 185 BSCF. We note that *s* reported is the first skin value used to match the historical production period.

Table 5 summarizes EUR values predicted by forecasting the production performance to 30 years using RTA. As we previously mentioned we have three cases, each corresponding to a different pressure extrapolation:

Case 1: Extrapolated a single flowing bottomhole pressure (p_{wf}).

Case 2: Extrapolated a p_{wf} reduction every year to a p_{wf} of 200 psia.

Case 3: Extrapolated a p_{wf} reduction every 5 years p_{wf} to 200 psia.

In each case, the pressure extrapolation used is that of the last known pressure. We find that Case 1 yields a lower 30-year EUR prediction than Cases 2 and 3, where the p_{wf}.is reduced to 200 psia. The difference between Cases 2 and 3 results from path dependency to reach the final pressure. Since Case 2 declines yearly, production is accelerated, while Case 3 takes a longer time to achieve the same production. Furthermore, the difference between 30-year EUR values would be magnified in wells that produce for short time periods. Regarding wells in the BHA field, these differences are reduced due to the fact that in most cases there is around 10-15 years of production associated with the calculation of the 30-year EUR for each well.

Table 4 — Match well/reservoir parameters obtained from time-rate-pressure analysis (or RTA).

Field Example	kh (md-ft)	k (md)	x_f (ft)	STGIIP (BSCF)	Re (ft)	P_i (psia)	$1+s$
82	171	0.38	60	88.3	1820	5800	1.0
87	1190	2.98	55	153	2700	5400	6.0
90	198	0.497	85	118	2400	5134	3.7
98	365	0.917	90	115	2390	5000	3.9
99	400	2.8	139	172	4940	3648	1.0
103	270	0.675	65	119	2180	5288	3.0
112	210	0.521	100	140	2370	6813	2.5
116	210	0.653	70	86	2330	5400	2.7
119	513	1.2	80	211	2990	6135	1.6
121	280	0.71	90	94.8	1420	5500	3.4
125	340	0.965	52	82.8	2000	5400	3.0
128	192	0.429	81	185	2430	5521	1.5
131	215	0.657	90	70.8	1950	4900	1.9
134	171	0.4	80	88.5	2000	4600	2.3

Table 5 — 30-year EUR volumes from three different pressure extrapolations and percent deference between them.

Field Example	Case 1 (MSCF)	Case 2 (MSCF)	Case 3 (MSCF)	Difference Between Cases 1 and 2 (%)	Difference Between Cases 1 and 3 (%)
82	56.69	58.34	56.83	2.91	0.25
87	109.00	110.00	108.95	0.92	-0.05
90	64.97	65.32	65.00	0.54	0.03
98	83.04	86.35	83.48	3.99	0.53
99	136.03	140.49	136.70	3.28	0.49
103	87.55	91.41	88.34	4.41	0.90
112	102.11	104.39	102.35	2.24	0.23
116	61.56	63.49	61.78	3.14	0.36
119	164.03	168.60	165.37	2.79	0.81
121	65.71	67.63	66.20	2.92	0.74
125	46.09	53.12	47.30	15.27	2.63
128	120.07	120.92	120.06	0.71	-0.01
131	50.57	53.89	51.09	6.56	1.03
134	50.79	51.48	50.85	1.35	0.12

4.3 Results from Existing Pressure Transient Analysis (PTA)

In **Table 6** we present the match parameters provided by the company for pressure transient analysis (PTA) conducted during the early production periods for each of the following wells. The PTA was performed shortly after the drilling of each well and show negative skin values, indicative of fracturing or stimulation. In addition, the model used for each of these wells is for that of finite conductivity fractures.

Table 6 — Match parameters obtained from existing pressure transient analysis.

Field Example	Date	*kh* (md-ft)	Skin	WBS (bbl/psia)
82	1998	48.6	-3.13	0.063
87	1998	70.3	-3.61	0.0825
98	1999	53.1	-4.6	0.08
98	2000	38.2	-4.65	0.325
99	1999	154	-4.9	0.084
116	1999	105	-5.7	0.596
125	1999	117	-4.9	0.0893
128	2000	136	-5.14	0.0713

4.4 Correlation of Time-Rate Analysis (DCA) Results

In **Fig 41** we provide a correlation plot for the 30-year EUR forecast obtained using the MH relation as a function of EUR from the PLE relation (data provided in **Table 3**). We find that although EUR values are very similar, PLE tends to be slightly more conservative.

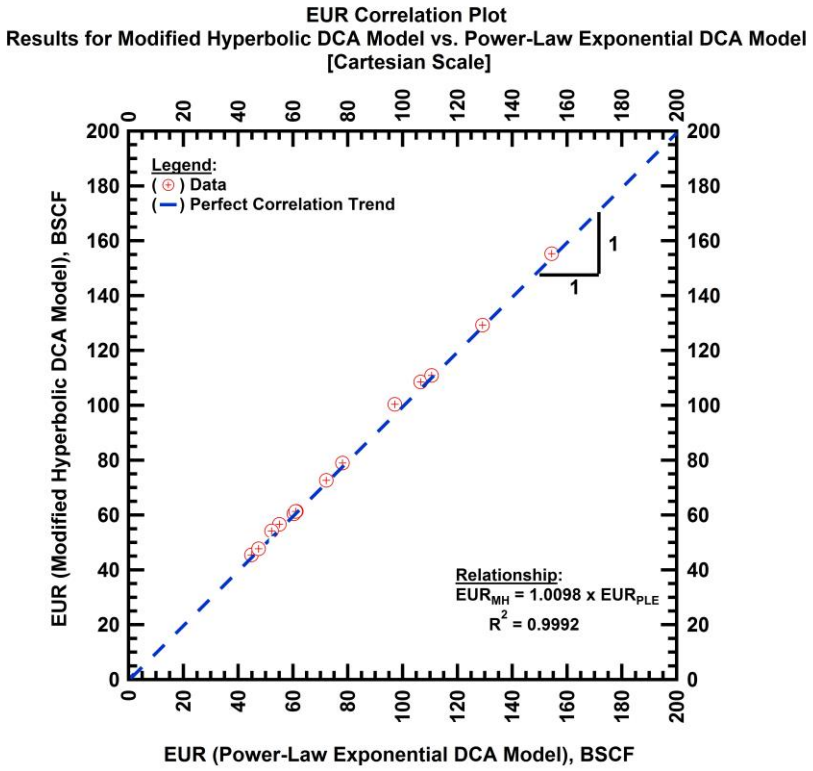

Fig. 41 — EUR correlation plot for the modified hyperbolic DCA model versus power-law exponential DCA model.

4.5 Correlation of Time-Rate-Pressure Analysis (RTA) Results

This section contains correlation plots for the 30-year EUR values obtained from the three different pressure extrapolations. In reviewing the EUR from Case 1 versus Case 2 cross-plot (**Fig. 42**), we note that while the data lies very close to the perfect correlation trend, Case 2 predicts slightly higher reserves since this case assumes decreasing p_{wf} , while Case 1 assumes constant $p_{wf.}$ We next examine **Fig. 43** where we find that this case yielded improved R^2 values of around 0.999 from the 0.997 in **Fig. 42**. In **Fig. 44**, we note that when comparing Cases 2 and 3, we find that Case 2 predicts higher EUR values due to its yearly decreasing trend than Case 3, in which the pressure decreases every 5 years. .

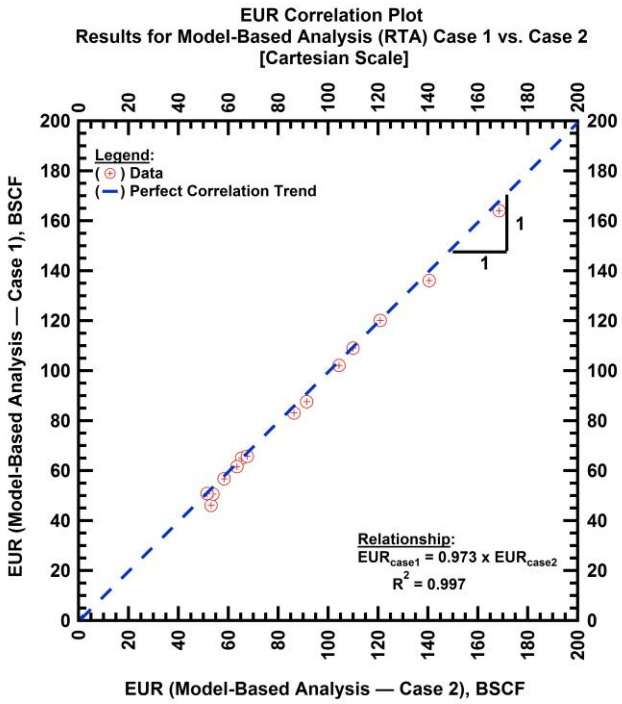

Fig. 42 — EUR correlation plot for the model-based analysis of Case 1 versus Case 2.

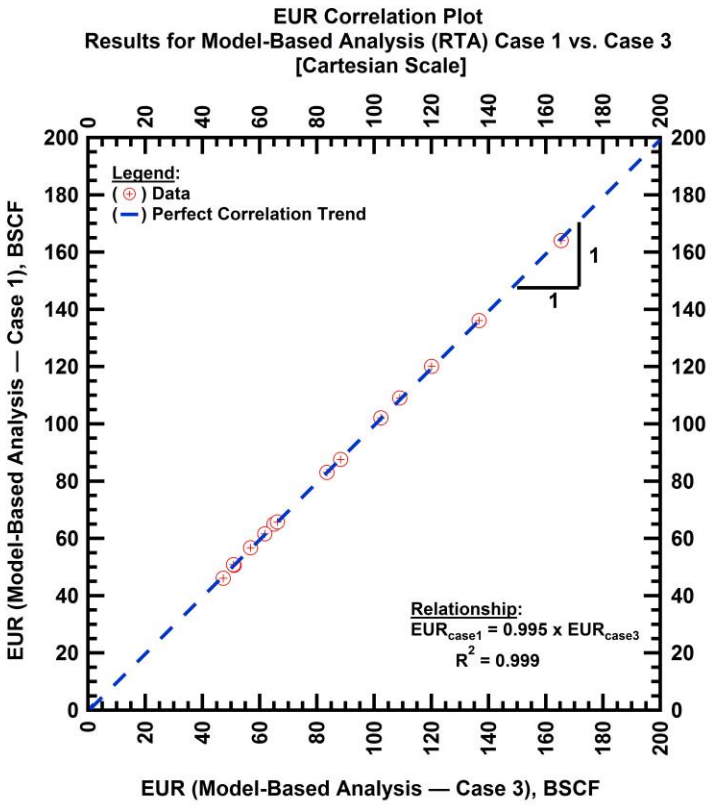

Fig. 43 — EUR correlation plot for the model-based analysis of Case 1 versus Case 3.

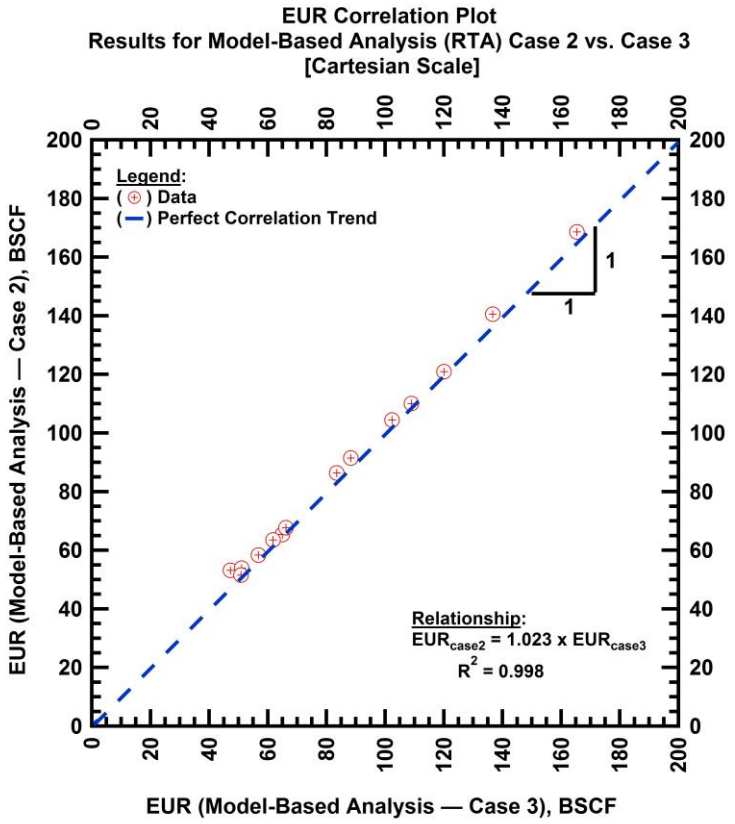

Fig. 44 — EUR correlation plot for the model-based analysis of Case 2 versus Case 3.

In **Fig. 45** we create a cross-plot of Gas Initially in Place (STGIIP) calculated from well/reservoir properties versus STGIIP obtained from model-based analysis. We obtain a fairly good match between the data and the perfect correlation trend from the parametric relationship presented in the figure.

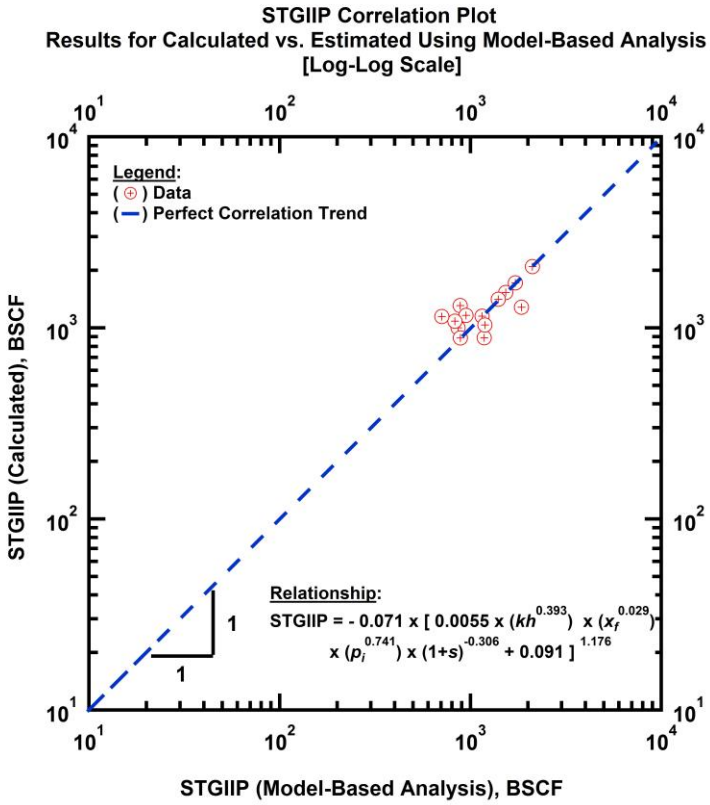

Fig. 45 — STGIIP calcualated versus STGIIP estimated from RTA.

4.6 Correlation of DCA and RTA Results

The purpose of this section is to develop parametric correlations between parameters of time-rate (DCA) relation and well/reservoir properties obtained from model-based analysis (RTA). Specifically we look for a relationship between the MH time-rate parameters: b, q_i, and D_i and the PLE time-rate relation parameters: $\hat{q}_i$, $\hat{D}_i$, and n with properties estimated using RTA (STGIIP, x_f, and kh). We believe that for wells of similar completions in the same reservoir, there should be a relationship between their well/reservoir properties and flow parameters. We attempt to integrate these results for the 14 wells analyzed in this work.

We begin by reviewing the 30-year EUR values obtained from the MH and model-based analysis Case 1 methods. In **Fig. 46** we note that similar results are estimated at low EUR values; wells predicting higher EUR values tend to be slightly underestimated using the MH method. This is observed from the slope of the trendline, which is less than 0.950, stating that on average RTA estimates are around 5% higher. We highlight that Case 1 refers to the pressure extrapolation scenario that consists of constant pressure as determined by the last believed flowing pressure experienced by the well. As such, this is the most conservative case, resulting in the lowest EUR values as compared to Cases 2 and 3, which correspond to pressure profiles that assume yearly (in Case 2) or every five years (in Case 3) reduction in abandonment pressures to a final flowing pressure of 200 psia.

We note that a very similar trend is observed when comparing PLE and RTA Case 1 in **Fig. 47**, since DCA 30-year estimations of EUR values from the MH and PLE methods are very similar. The trendline slope is 0.941, which is slightly less than that obtained in the MH case, since PLE is a little more conservative as compared to MH.

However, when comparing Case 2 to the DCA methods, we find a larger difference between the EUR results. This is attributed to the fact that recovery varies depending on the development plan of the field. Given p_{wf} decreases yearly, as is the scenario in Case 2, gas production can be accelerated resulting in path dependency to the same ultimate cumulative production than Case 3, where longer time is needed result in the same EUR

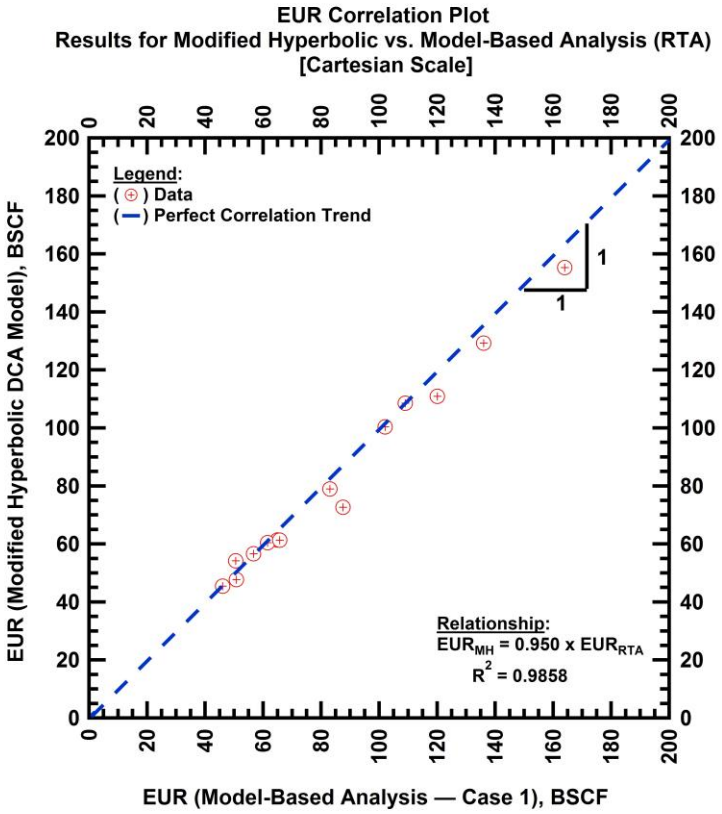

Fig. 46 — EUR correlation plot for the modified hyperbolic versus model-based analysis (RTA).

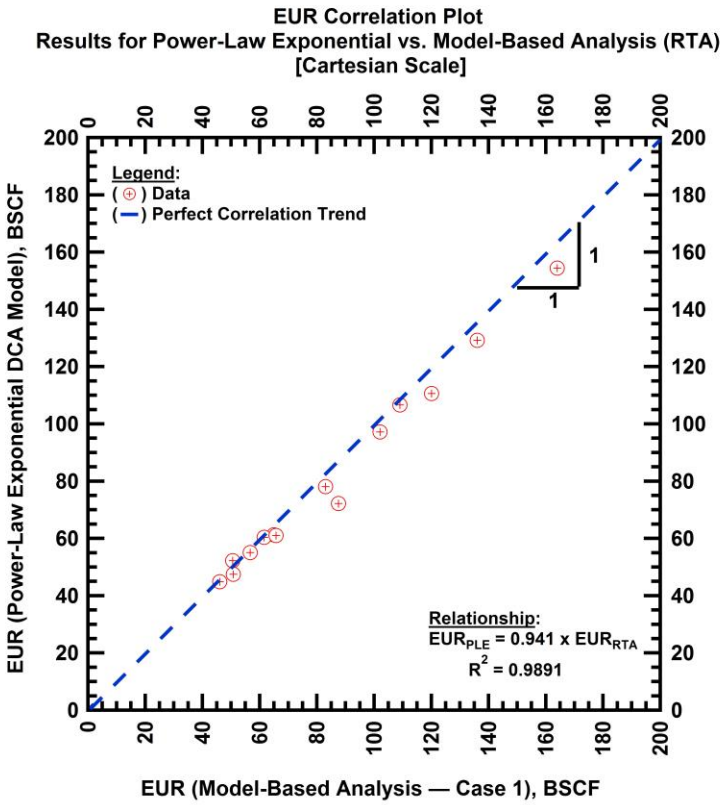

Fig. 47 — EUR correlation plot for the Power-Law Exponential DCA model versus Model-Based Analysis (RTA).

Next, we examine the MH time-rate relation with the results obtained from RTA (**Fig. 48**). We use solver in Microsoft Excel to minimize the difference between Gas Initially in Place (STGIIP) estimated from RTA and values modeled using parameters obtained from MH. We apply non-linear regression for different types of equations and present the best scenario in this section. **APPENDIX C** contains the cross-plots as well as the regression variables used for the other scenarios. We believe that the relationships we develop are relevant and can be applied to other well with similar completions producing from the Barik reservoir of the BHA field.

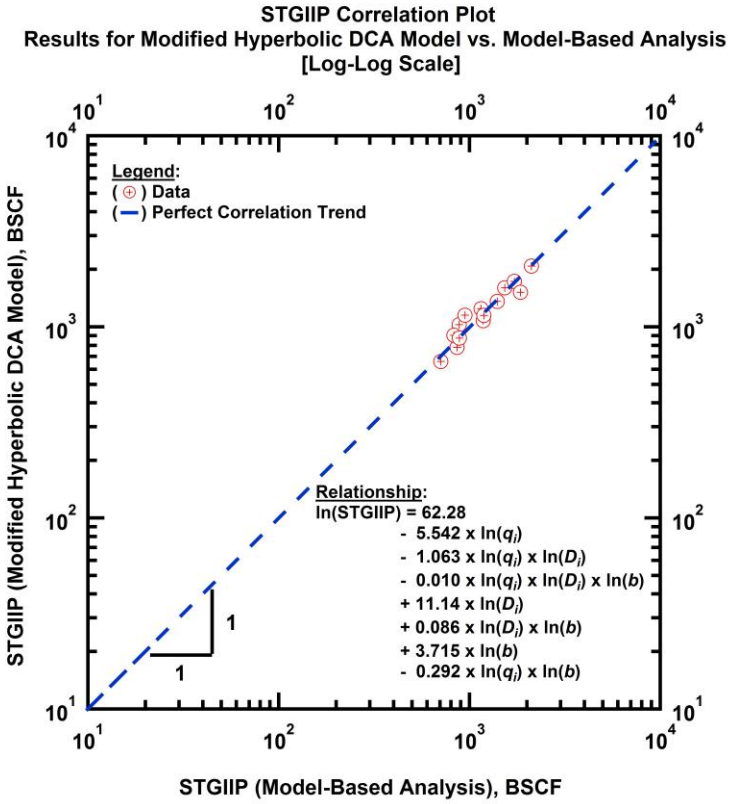

Fig. 48 — Correlation plot comparing STGIIP calculated using the Modified Hyperbolic DCA model parameters versus STGIIP estimated using Model-Based Analysis (RTA).

We next develop a correlation for *kh*. Using non-linear regression we obtain a relationship between *kh* and the q_i, D_i, and *b* parameters (Fig. 49). A very good match is achieved between data and the perfect correlation trend.

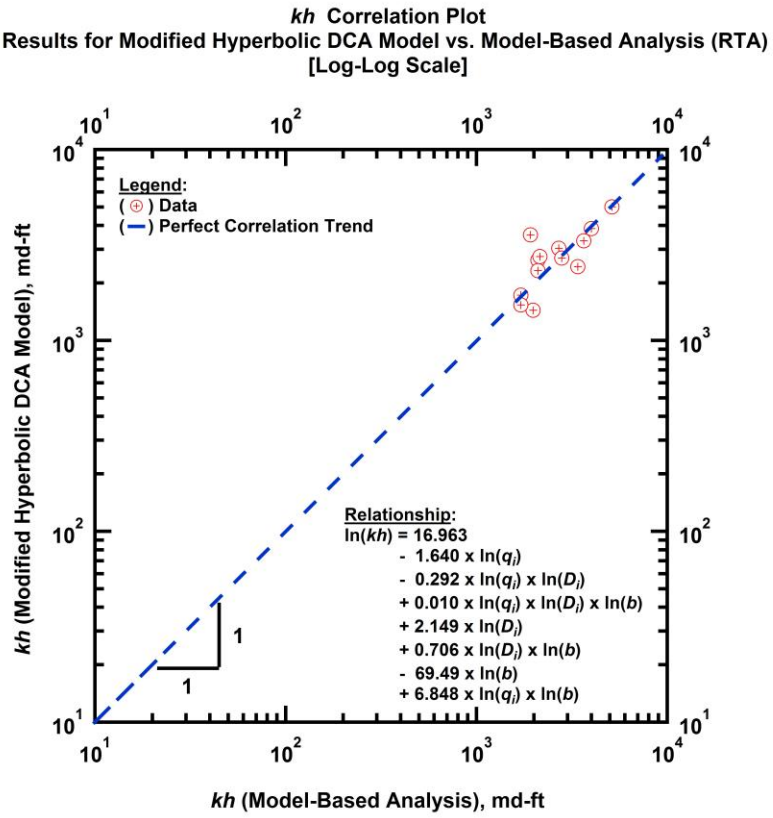

Fig. 49 — Correlation plot comparing *kh* calculated using the Modified Hyperbolic DCA model parameters versus *kh* estimated using Model-Based Analysis (RTA).

Finally, we present the best relationship obtained for the fracture half-length (x_f) in **Fig. 50**. Here we find that the same type of relationship produces the best match between the data and the perfect correlation trend. However, we notice here that although most of the data lies near or on the trendline, there is one point that corresponds to BHA Well 103, which was removed when performing the regression.

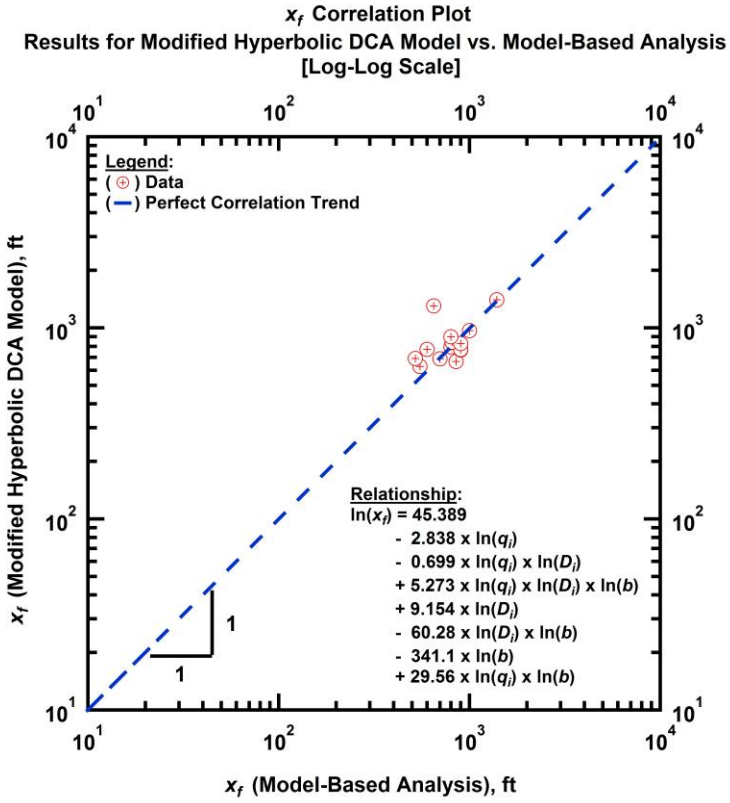

Fig. 50 — Correlation plot comparing x_f calculated using the Modified Hyperbolic DCA model parameters versus x_f estimated using Model-Based Analysis (RTA).

We next develop correlation plots for the PLE parameters ($\hat{q}_i$, $\hat{D}_i$, and n). In **Fig. 51** we present a relationship for the best case scenario match between the data and the perfect correlation trend. We note that while most of the data falls on the trendline, there are a few data points that have a parallel trend above the line.

In **Fig. 52** we develop a relationship for the x_f parameters and find that we were able to obtain a very good match using a power-law relationship with an added constant. Finally, in **Fig. 53** we obtain a relationship for x_f and with the exception of an outlier, most of the data fits the perfect correlation trend well.

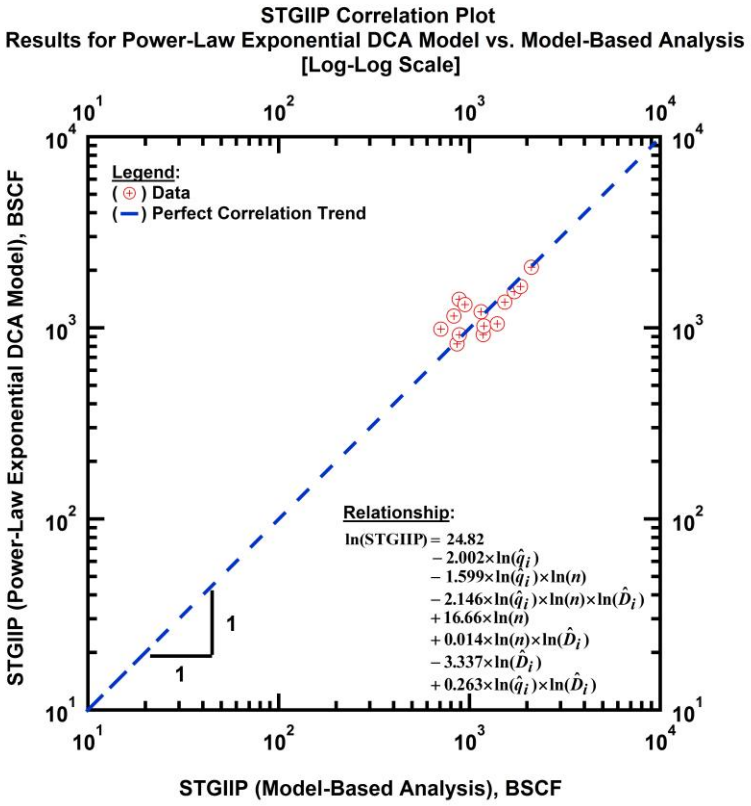

Fig. 51 — Correlation plot comparing STGIIP calculated using the Power-Law Exponential DCA model parameters versus STGIIP estimated using Model-Based Analysis (RTA).

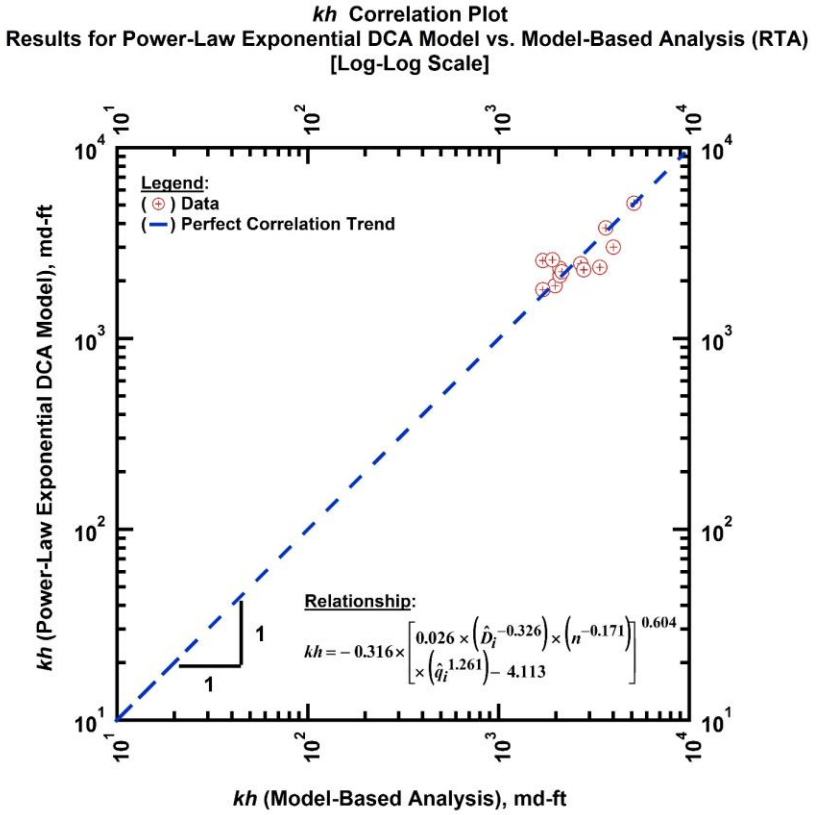

Fig. 52 — Correlation plot comparing *kh* calculated using the Power-Law Exponential DCA model parameters versus *kh* estimated using Model-Based Analysis (RTA).

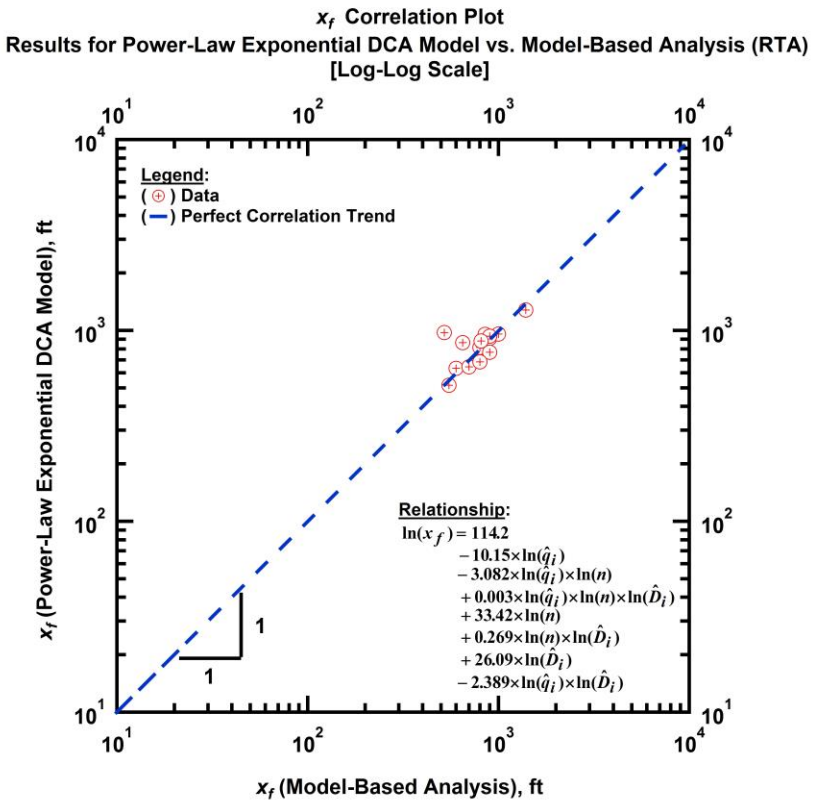

Fig. 53 — Correlation plot comparing x_f calculated using the Power-Law Exponential DCA model parameters versus x_f estimated using Model-Based Analysis (RTA).

SUMMARY, CONCLUSIONS, AND RECOMMENDATIONS FOR FUTURE WORK

5.1 Summary

In this thesis the goal is to provide a production-based reservoir characterization study for the BHA field in Oman. An operator in Oman provided data which have been made anonymous as a requirement of confidentiality. This work was conducted using commercial software and MS Excel. The work focused on the diagnostic analysis and interpretation of time-rate and time-rate-pressure data acquired from the operator. These data were quality checked for inconsistencies and diagnostic plots were created to confirm/validate the various flow regimes required for analysis.

Long-term production performance data confirm boundary-dominated flow behavior (for EUR) and the early production history data have been analyzed using "rate transient analysis" (or RTA) to estimate reservoir properties such as permeability and fracture half-length. As is the standard practice for the analysis of wells in low/ultra-low permeability reservoirs, the EUR was determined at 30-years from the production forecasts obtained from time-rate and time-pressure-rate techniques.

We created correlations of EUR results and model parameters for the DCA relations and estimates of reservoir properties obtained from RTA. Parametric correlations developed for the STGIIP, x_f, and kh parameters provide a means to attain RTA parameters using DCA relations.

5.2 Conclusions

- The data utilized for the BHA field are generally acceptable for reservoir engineering calculations.
- The time-rate analysis (i.e., the use of the modified hyperbolic and power-law exponential time-rate models) performed in this work is problematic for some cases (the data have significant scatter/noise and often exhibit features caused by production operations). However, in general, we believe that the forecasts and EUR estimates obtained from the time-rate analyses are statistically relevant.
- The time-rate-pressure analyses (i.e., rate transient analysis (or RTA)) performed in this work appears to be robust and relevant for almost all cases considered. There are several cases which require the use of the time-dependent skin model to account for changes in production operations (most likely work-overs). The results from the rate transient analyses compare well with expectations and appear to be well-correlated for the cases we have considered in this work.
- The DCA (MH and PLE) relations result in more conservative production estimates than RTA.
- From the results acquired, we believe that RTA results in more accurate estimates of reserves for low-permeability reservoirs than deterministic DCA methods.
- High production data quality and quantity yield improved development of parametric correlations.

- Parametric correlations developed for the STGIIP, x_f, and kh parameters provide a means to attain RTA parameters using DCA relations.

5.3 Recommendations for Future Work

- Diagnostic time-rate analysis methods (use of the instantaneously calculated $D(t)$ and $b(t)$ functions) should improve the interpretation of time-rate analyses. However, we acknowledge that derivative diagnostic methods would likely not perform well for most of the cases considered in this study due to data noise and operational practices.
- A "big data" approach could be considered for the cases considered in this work, specifically the correlation of production rate and pressure trends with completion metrics. Techniques such as "non-parametric" regression could be used to identify characteristic trends in the production data.
- The only pressure transient data provided were for very early times (i.e., well within the first year of production). With some of these wells approaching 20 years in age, it would be advantageous to perform formal pressure transient tests for comparison with the legacy data. For reference, we did attempt to find shut-in events where the surface pressure data could be used for pressure transient analysis, but not one single shut-in case had data with the necessary integrity/fidelity from which pressure transient analysis methods could be applied.

REFERENCES

Agarwal, R.G., Gardner, D.C., Kleinsteiber, S.W. et al. 1999. Analyzing Well Production Data Using Combined-Type-Curve and Decline-Curve Analysis Concepts. *SPE Reservoir Evaluation & Engineering* **2** (05): 478–486. SPE-57916-PA. http://dx.doi.org/10.2118/57916-PA.

Al-Hussainy, R., Ramey, H.J., Jr., Crawford, P.B. 1966. The Flow of Real Gases Through Porous Media. *Journal of Petroleum Technology* **18** (05). SPE-1243-A-PA. http://dx.doi.org/10.2118/1243-A-PA.

Arps, J.J. 1945. Analysis of Decline Curves. *Transactions of the AIME* **160** (01). SPE-945228-G. http://dx.doi.org/10.2118/945228-G.

Blasingame, T.A., Johnston, J.L., Lee, W.J. 1989. Type-Curve Analysis Using the Pressure Integral Method. SPE California Regional Meeting, Bakersfield, California, 5-7 April. SPE-18799-MS. http://dx.doi.org/10.2118/18799-MS.

Blasingame, T.A., Lee, W.J. 1986. Variable-Rate Reservoir Limits Testing. Permian Basin Oil and Gas Recovery Conference, Midland, Texas, 13-15 March. SPE-15028-MS. http://dx.doi.org/10.2118/15028-MS.

Blasingame, T.A., McCray, T.L., Lee, W.J. 1991. Decline Curve Analysis for Variable Pressure Drop/Variable Flowrate Systems. SPE Gas Technology Symposium, Houston, Texas, 22-24 January. SPE-21513-MS. http://dx.doi.org/10.2118/21513-MS.

Blasingame, T.A., Rushing, J.A. 2005. A Production-Based Method for Direct Estimation of Gas in Place and Reserves. SPE Eastern Regional Meeting, Morgantown, West Virginia, 14–16 September. SPE-98042-MS. http://dx.doi.org/10.2118/98042-MS.

Carter, R.D. 1985. Type Curves for Finite Radial and Linear Gas-Flow Systems: Constant-Terminal-Pressure Case. *Society of Petroleum Engineers Journal* **25** (05): 719-728. SPE-12917-PA. http://dx.doi.org/10.2118/12917-PA.

Doublet, L.E., Pande, P.K., McCollum, T.J. et al. 1994. Decline Curve Analysis Using Type Curves--Analysis of Oil Well Production Data Using Material Balance Time: Application to Field Cases. International Petroleum Conference and Exhibition of Mexico, Veracruz, Mexico, 10-13 October. SPE-28688-MS. http://dx.doi.org/10.2118/28688-MS.

Earlougher, R.C., Jr. 1972. Variable Flow Rate Reservoir Limit Testing. *Journal of Petroleum Technology* **24** (12). SPE-3892-PA. http://dx.doi.org/10.2118/3892-PA.

Fetkovich, M.J. 1980. Decline Curve Analysis Using Type Curves. *Journal of Petroleum Technology* **32** (06): 1065-1077. SPE-4629-PA. http://dx.doi.org/10.2118/4629-PA.

Fraim, M.L., Wattenbarger, R.A. 1987. Gas Reservoir Decline-Curve Analysis Using Type Curves With Real Gas Pseudopressure and Normalized Time. **2** (04): 671-682. SPE-14238-PA. http://dx.doi.org/10.2118/14238-PA.

Gentry, R.W., McCray, A.W. 1978. The Effect of Reservoir and Fluid Properties on Production Decline Curves. *Journal of Petroleum Technology* **30** (09): 1327-1341. SPE-6341-PA. http://dx.doi.org/10.2118/6341-PA.

Ilk, D., Anderson, D.M., Stotts, G.W.J. et al. 2010. Production Data Analysis--Challenges, Pitfalls, Diagnostics. *SPE Reservoir Evaluation & Engineering* **13** (03): 538-552. SPE-102048-PA. http://dx.doi.org/10.2118/102048-PA.

Ilk, D., Jenkins, C.D., Blasingame, T.A. 2011. Production Analysis in Unconventional Reservoirs - Diagnostics, Challenges, and Methodologies. North American Unconventional Gas Conference and Exhibition, The Woodlands, Texas, 14–16 June. SPE-144376-MS. http://dx.doi.org/10.2118/144376-MS.

Ilk, D., Rushing, J.A., Blasingame, T.A. 2011. Integration of Production Analysis and Rate-Time Analysis via Parametric Correlations -- Theoretical Considerations and Practical Applications. SPE Hydraulic Fracturing Technology Conference, The Woodlands, Texas, 24–26 January. SPE-140556-MS. http://dx.doi.org/10.2118/140556-MS.

Ilk, D., Rushing, J.A., Perego, A.D. et al. 2008. Exponential vs. Hyperbolic Decline in Tight Gas Sands: Understanding the Origin and Implications for Reserve Estimates Using Arps' Decline Curves. SPE Annual Technical Conference and Exhibition, Denver, Colorado, 21–24 September. SPE-116731-MS. http://dx.doi.org/10.2118/116731-MS.

Lee, J.W., R. 1996. *Gas Reservoir Engineering*. Richardson, TX: Society of Petroleum Engineering.

Lewis, J.O., Beal, C.H. 1918. Some New Methods for Estimating the Future Production of Oil Wells. *Transactions of the AIME* **59** (01): 492–520. SPE-918492-G. http://dx.doi.org/10.2118/918492-G.

Maley, S. 1985. The Use of Conventional Decline Curve Analysis in Tight Gas Well Applications. SPE/DOE Low Permeability Gas Reservoirs Symposium, Denver, Colorado, May 19–22. SPE-13898-MS. http://dx.doi.org/10.2118/13898-MS.

Palacio, J.C., Blasingame, T.A. 1993. Decline-Curve Analysis With Type Curves - Analysis of Gas Well Production Data. Low Permeability Reservoirs Symposium, Denver, Colorado, 26-28 April. SPE-25909-MS. http://dx.doi.org/10.2118/25909-MS.

Robertson, S. 1988. Generalized Hyperbolic Equation. SPE-18731-MS.

Seshadri, J.N., Mattar, L. 2010. Comparison of Power Law and Modified Hyperbolic Decline Methods. Canadian Unconventional Resources and International Petroleum Conference, Calgary, Alberta, Canada, 19-21 October. SPE-137320-MS. http://dx.doi.org/10.2118/137320-MS.

Sureshjani, M.H., Gerami, S. 2011. A New Model for Modern Production-Decline Analysis of Gas/Condensate Reservoirs. *Journal of Canadian Petroleum Technology* **50** (7/8): 10-23. SPE-149709-PA. http://dx.doi.org/10.2118/149709-PA.

NOMENCLATURE

Field Variables:

General:

G_p = Cumulative Gas Production, L^3 [BSCF]
$m(p)$ = Real gas pseudopressure, M/Lt [psi^2/cp]
$\Delta m(p)$ = Real gas pseudopressure drop ($m(p_i) - m(p_{wf})$), M/Lt^2 [psi^2/cp]
p = Pressure, M/Lt^2 [psia]
p_i = Initial pressure, M/Lt^2 [psia]
p_{wf} = Calculated bottomhole flowing pressure, M/Lt^2 [psia]
t = Production time, *t* [D] or [hr]
x_f = Fracture half-length, ft

Modified Hyperbolic Model:

b = Hyperbolic decline exponent, dimensionless
D_i = Hyperbolic decline constant, 1/t [1/D]
D_{lim} = Arps modified-hyperbolic model parameter, 1/t [1/D]
k = Formation permeability, md
q = *Flowrate, L^3/t [MSCF/D]*
$q_{i,exp}$ = Arps exponential model parameter, L^3/t [MSCF/D]
$q_{i,hyp}$ = Arps hyperbolic model parameter, L^3/t [MSCF/D]
q_{lim} = Arps modified-hyperbolic model parameter, L^3/t [MSCF/D]
t_{lim} = Arps modified-hyperbolic model parameter, t [D]
x_f = Fracture half-length, ft

Ilk Power-Law Exponential Model:

$\hat{D}_i$ = Ilk, et al power-law exponential model parameter, $(1/t)^n$ $[1/D]^n$
D_∞ = Ilk, et al power-law exponential model parameter, 1/t [1/D]
$\hat{q}_i$ = Ilk, et al power-law exponential model parameter, L^3/t [MSCF/D]
n = Ilk, et al power-law exponential model parameter, dimensionless

Subscripts:

g = Gas
i = Initial or integral
id = Integral-derivative

APPENDIX A
BHA FIELD EXAMPLES

This appendix presents a complete list of figures used to diagnose and analyze the wells reviewed in this study. Each series of plots provides character and insight for the production performance behavior for a given well.

Map — BHA Field

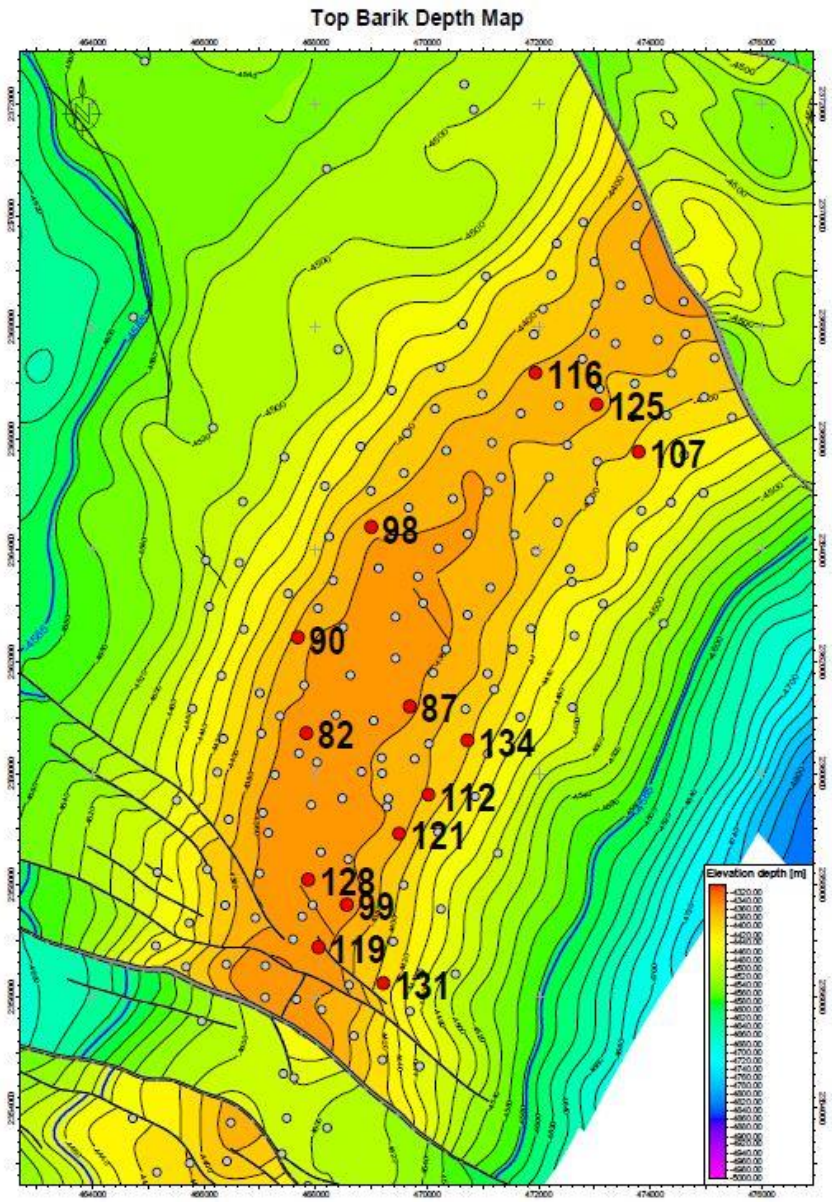

Fig. 54 — Map of BHA Field (Oman).

Field Example — BHA Well 090

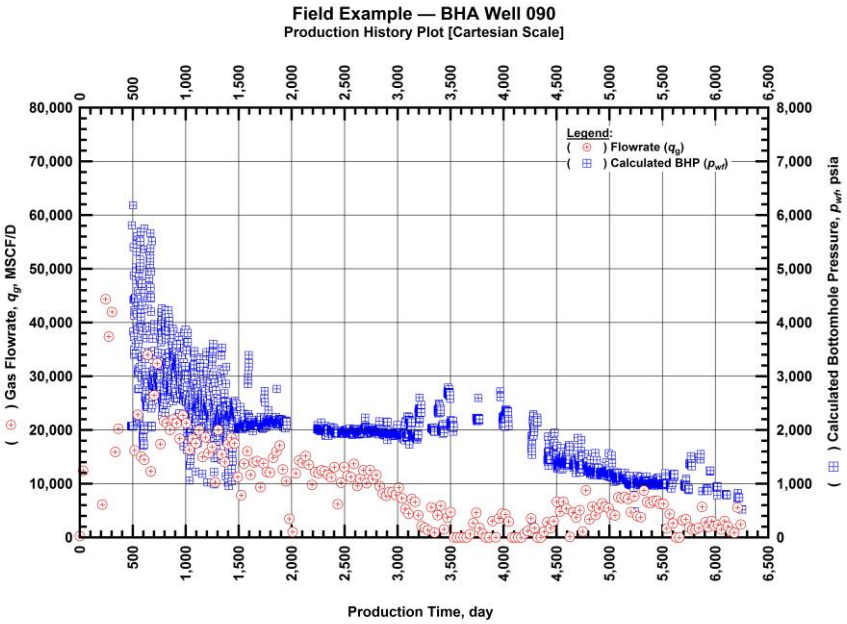

Fig. 55 — Cartesian plot for BHA Well 090 — Production history plot of calculated bottomhole pressures and gas flowrates as a function of production time.

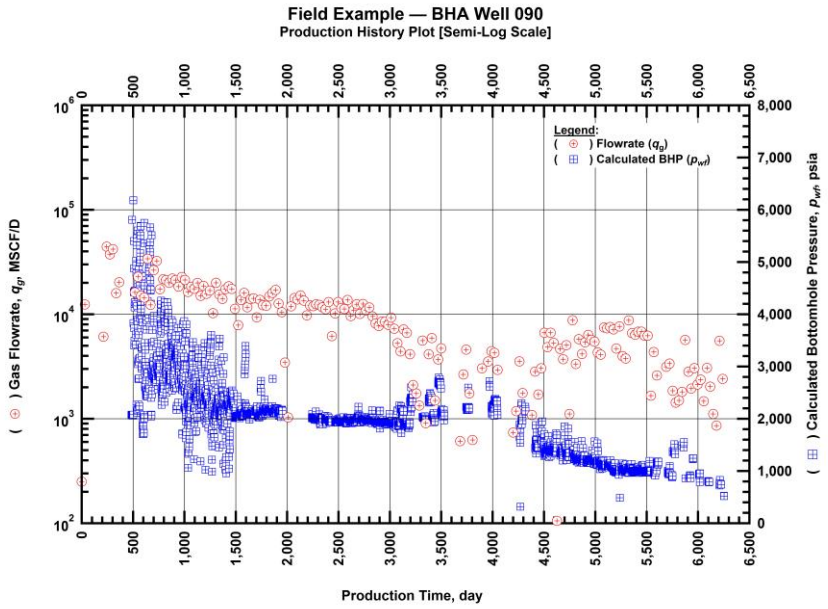

Fig. 56 — Semilog plot for BHA Well 090 — Production history plot of calculated bottomhole pressures and gas flowrates as a function of production time.

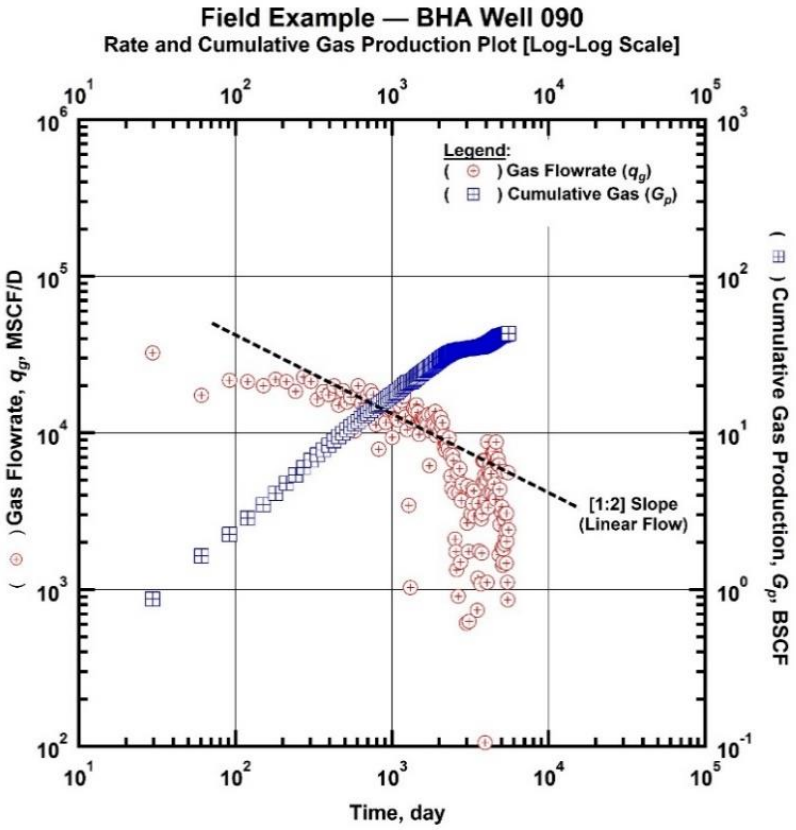

Fig. 57 — Log-Log plot for BHA Well 090 — Gas flowrate and cumulative gas production as a function of production time.

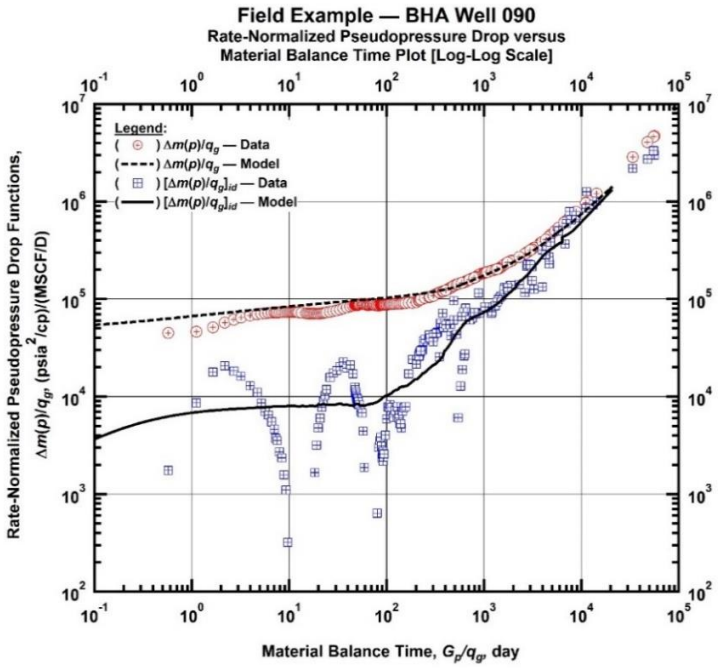

Fig. 58 — Log-Log plot for BHA Well 090 — Rate-normalized pseudopressure drop versus material balance time ("Log-Log Plot").

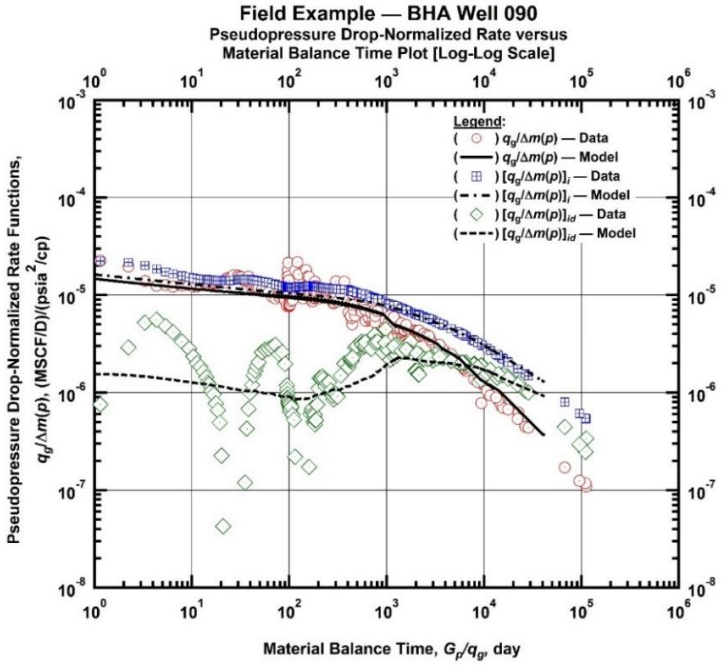

Fig. 59 — Log-Log plot for BHA Well 090 — Pseudopressure drop-normalized rate function versus material balance time ("Blasingame plot").

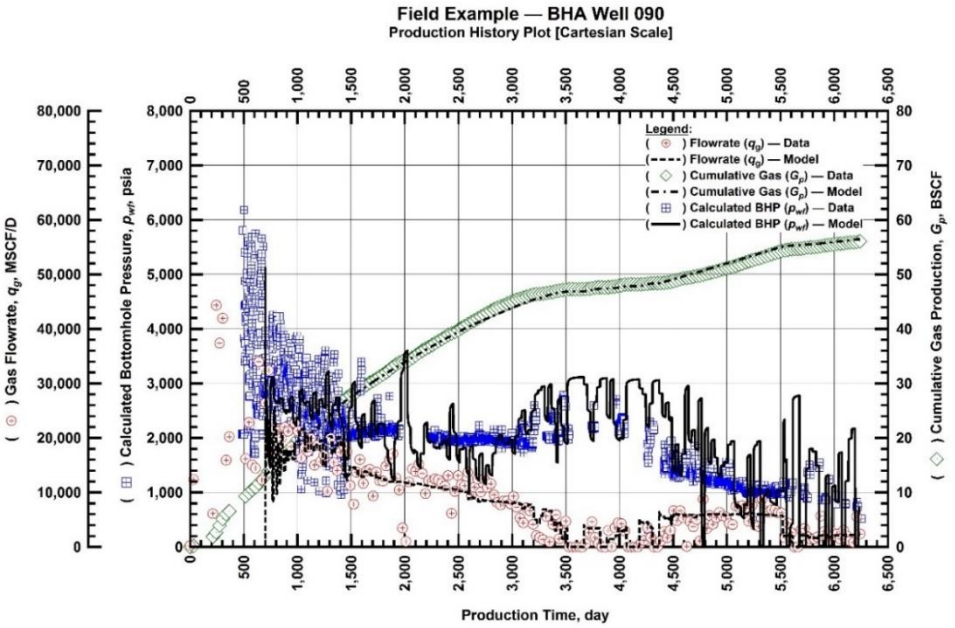

Fig. 60 — Cartesian plot for BHA Well 090 — production history and RTA history-match (gas flowrate, calculated bottomhole pressure, and cumulative gas production versus production time).

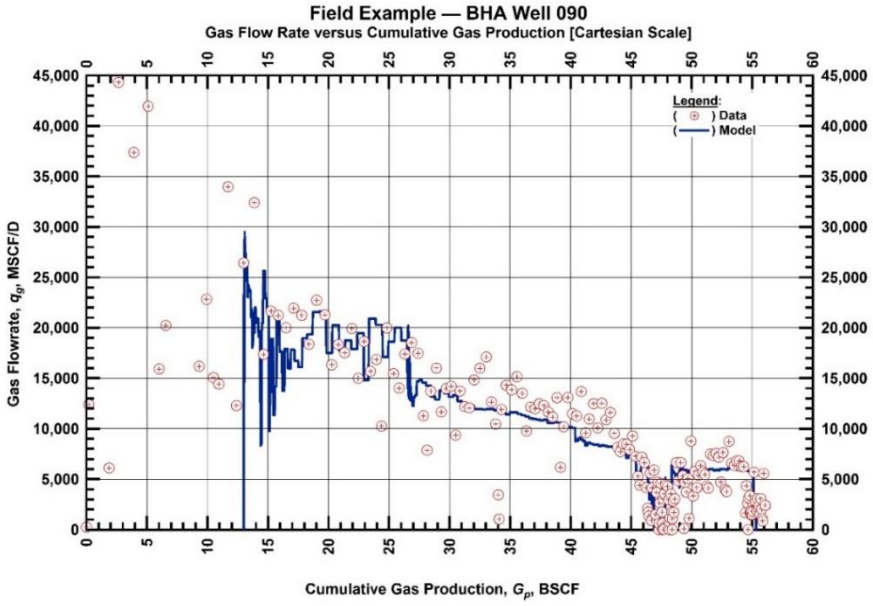

Fig. 61 — Cartesian plot for BHA Well 090 — historical and history-matched gas flowrate versus cumulative gas production.

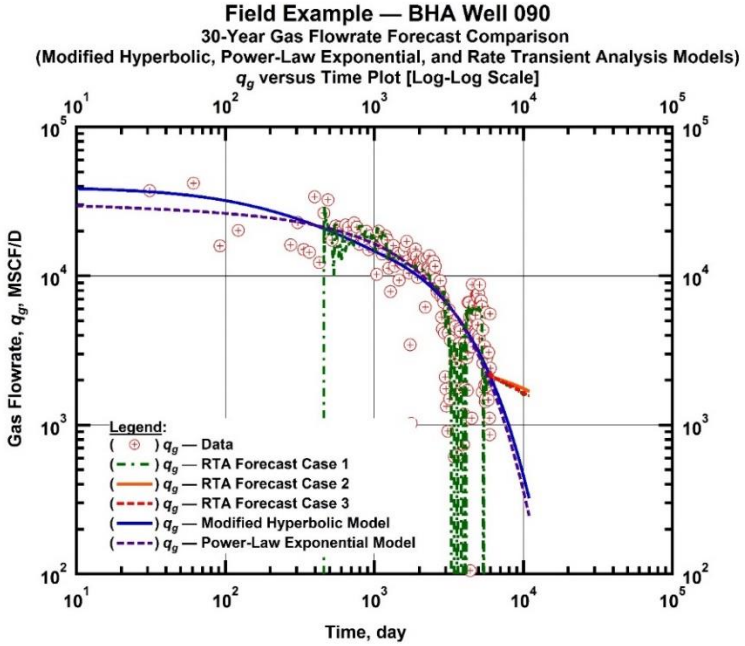

Fig. 62 — Log-Log plot for BHA Well 090 — Gas flowrate versus time for various RTA forecast cases (1, 2, 3) and Modified Hyperbolic and Power-Law Exponential time-rate models.

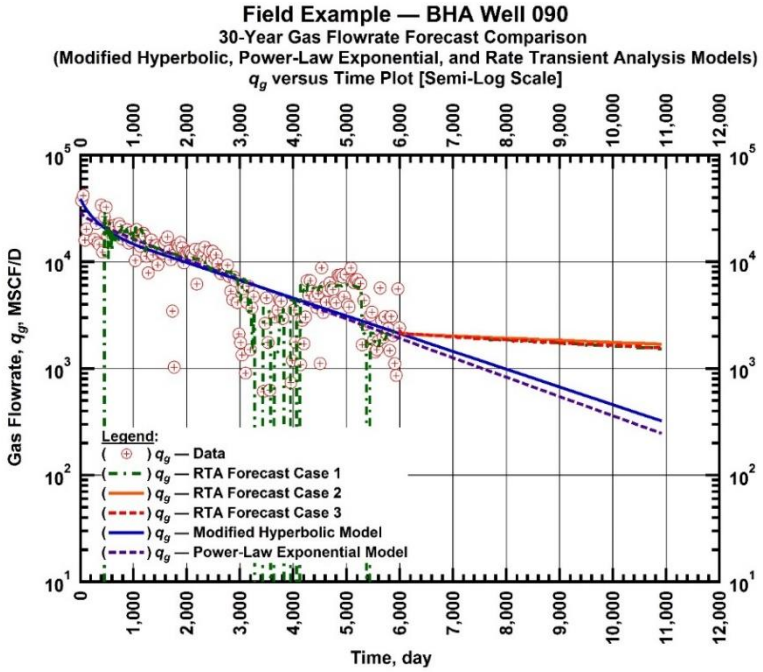

Fig. 63 — Semilog plot for BHA Well 090 — Gas flowrate versus time for various RTA forecast cases (1, 2, 3) and Modified Hyperbolic and Power-Law Exponential time-rate models.

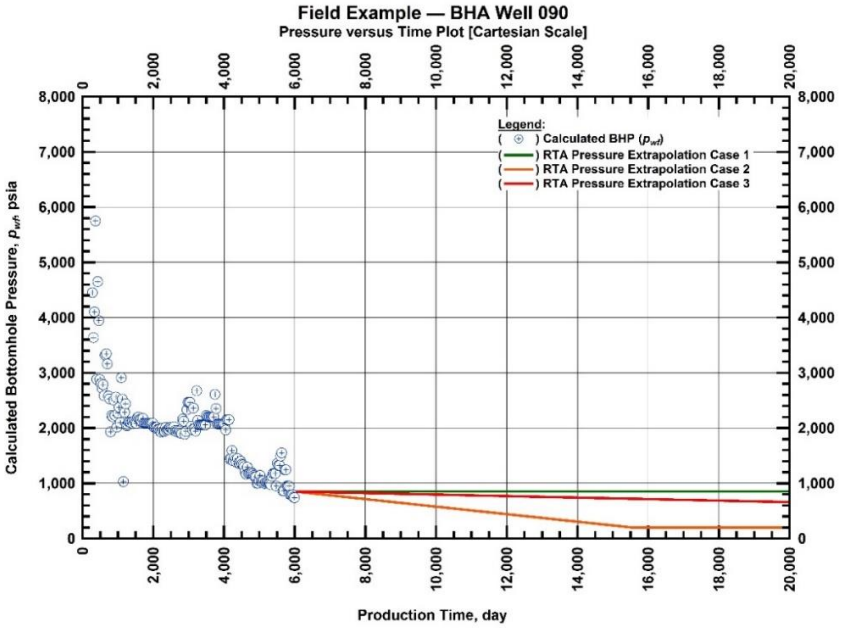

Fig. 64 — Cartesian plot for BHA Well 090 — historical and extrapolated bottomhole flowing pressures versus time (these pressure extrapolation scenarios are used for the RTA model).

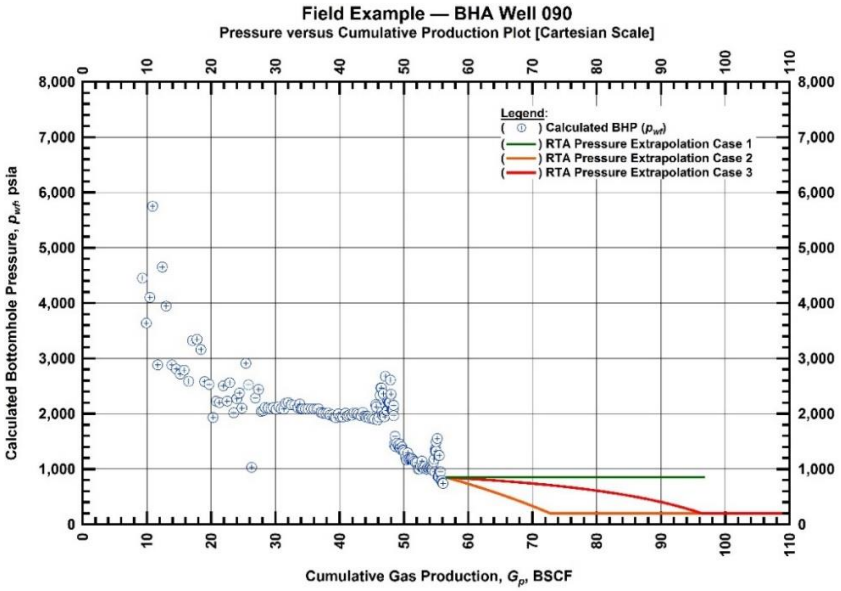

Fig. 65 — Cartesian plot for BHA Well 090 — historical and extrapolated bottomhole flowing pressures versus cumulative gas production (these pressure extrapolation scenarios are used for the RTA model).

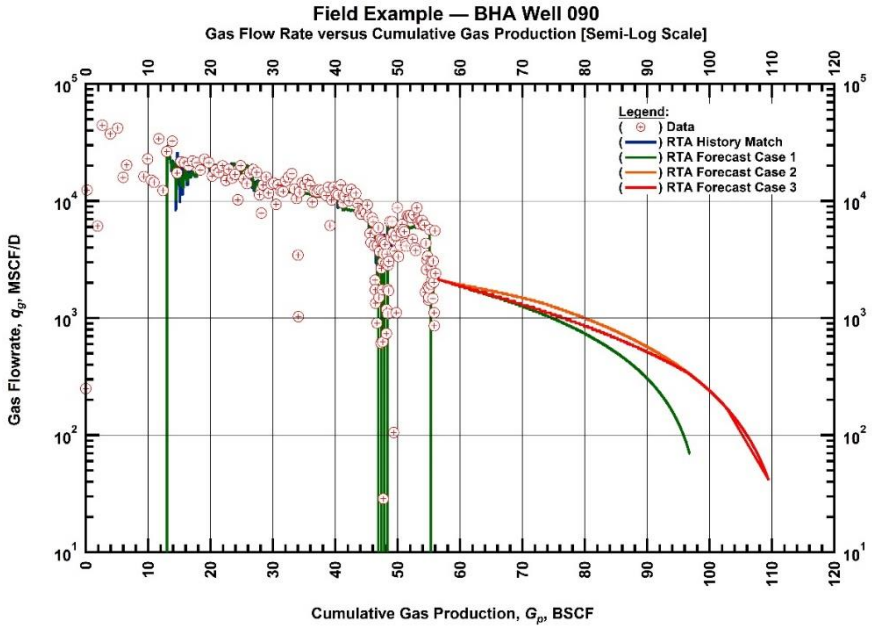

Fig. 66 — Semilog plot for BHA Well 090 — historical, history-matched, and forecasted gas flowrate versus cumulative gas production (various pressure extrapolation scenarios are prescribed (in time) for the RTA model).

Field Example — BHA Well 098

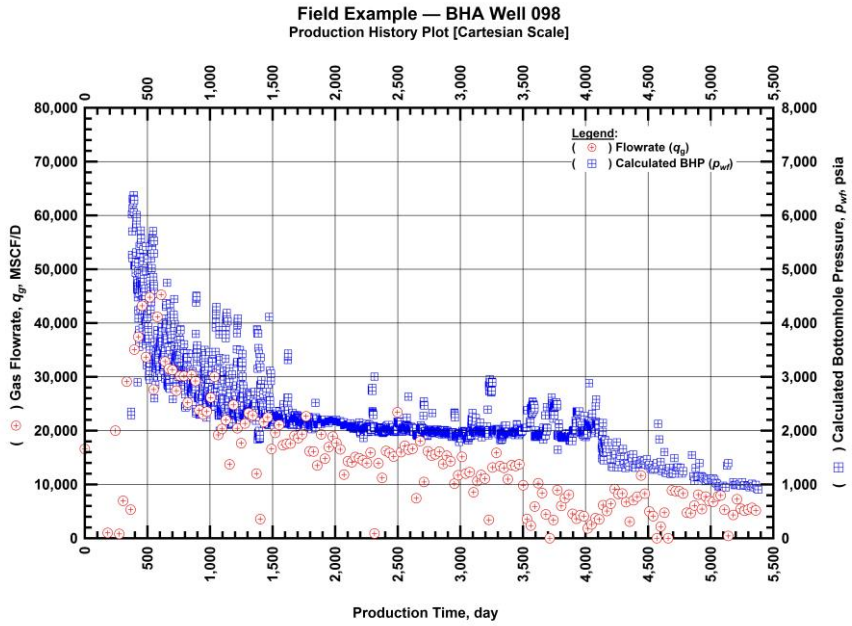

Fig. 67 — Cartesian plot for BHA Well 098 — Production history plot of calculated bottomhole pressures and gas flowrates as a function of production time.

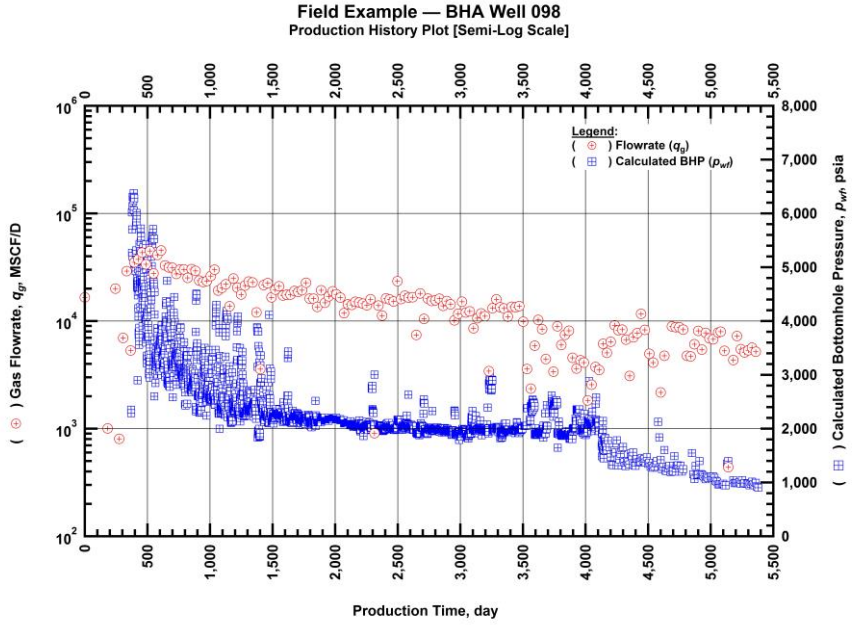

Fig. 68 — Semilog plot for BHA Well 098 — Production history plot of calculated bottomhole pressures and gas flowrates as a function of production time.

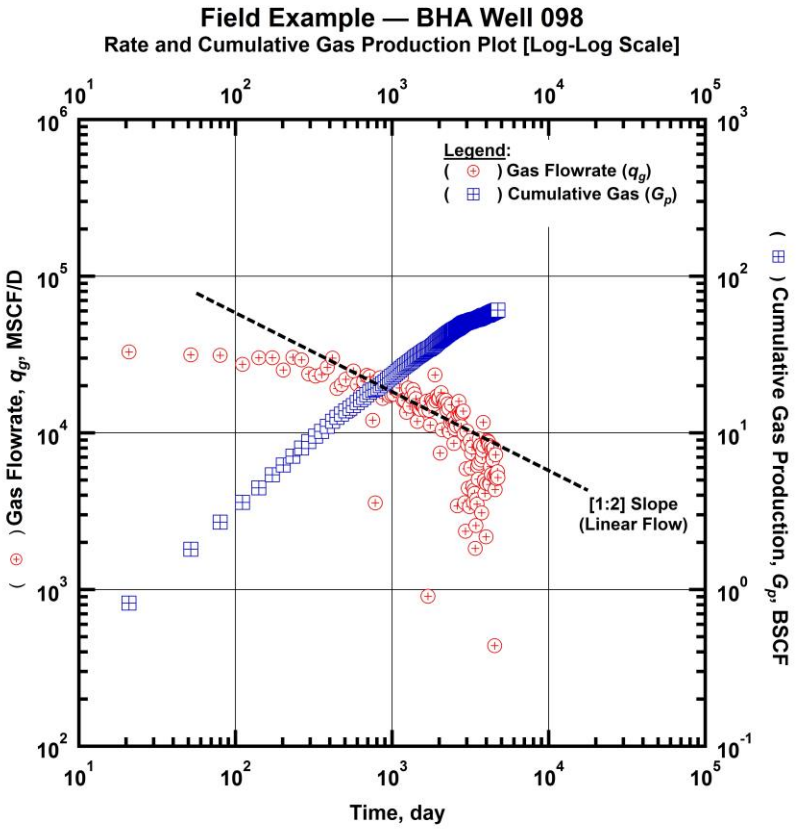

Fig. 69 — Log-Log plot for BHA Well 098 — Gas flowrate and cumulative gas production as a function of production time.

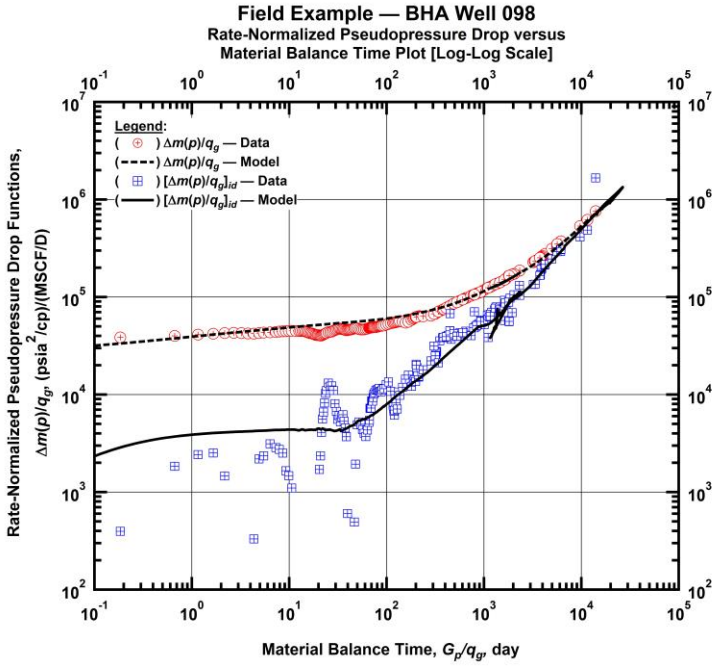

Fig. 70 — Log-Log plot for BHA Well 098 — Rate-normalized pseudopressure drop versus material balance time ("Log-Log Plot").

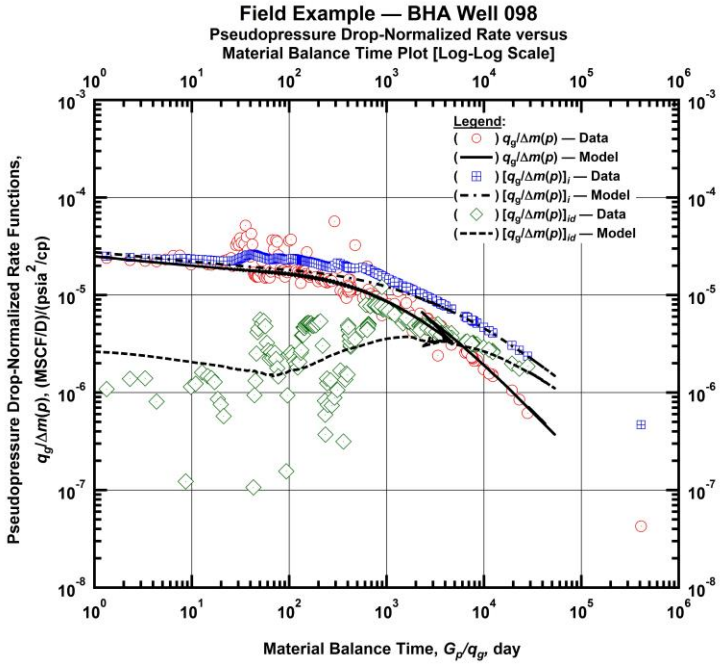

Fig. 71 — Log-Log plot for BHA Well 098 — Pseudopressure drop-normalized rate function versus material balance time ("Blasingame plot").

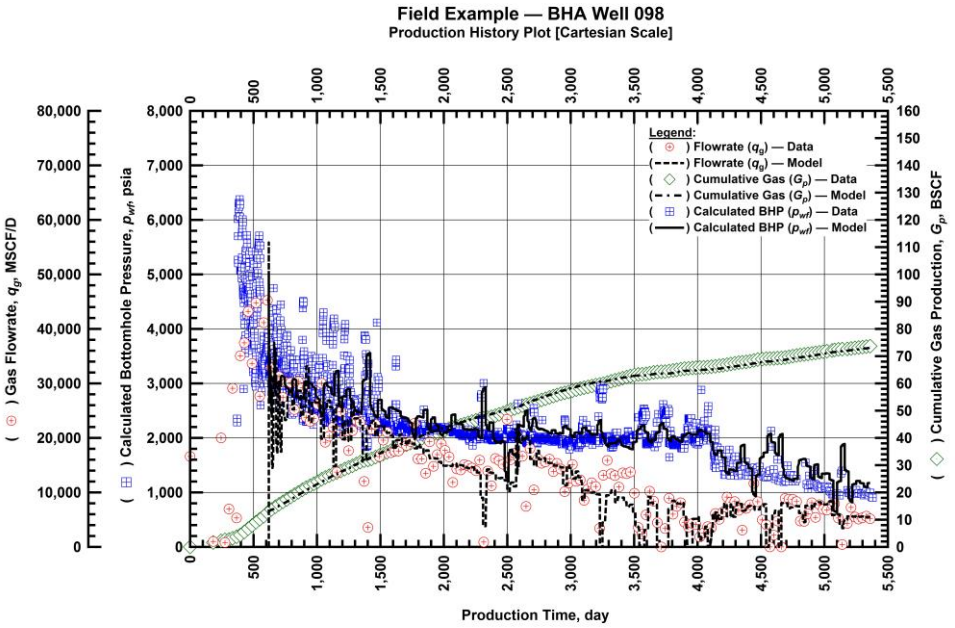

Fig. 72 — Cartesian plot for BHA Well 098 — production history and RTA history-match (gas flowrate, calculated bottomhole pressure, and cumulative gas production versus production time).

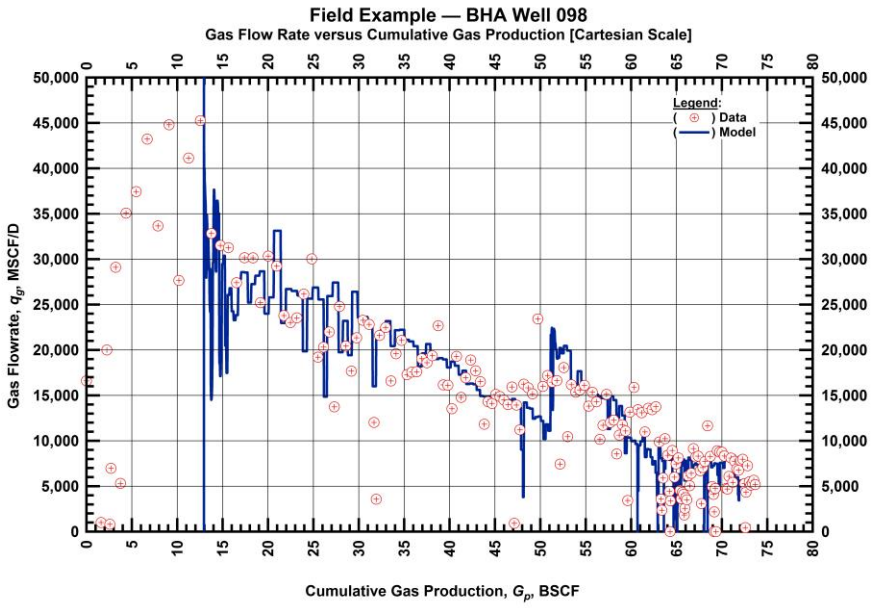

Fig. 73 — Cartesian plot for BHA Well 098 — historical and history-matched gas flowrate versus cumulative gas production.

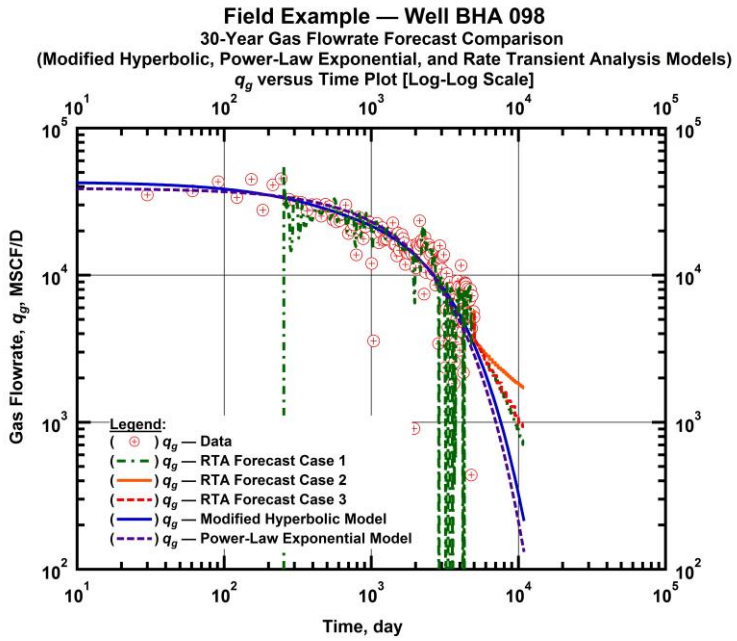

Fig. 74 — Log-Log plot for BHA Well 098 — Gas flowrate versus time for various RTA forecast cases (1, 2, 3) and Modified Hyperbolic and Power-Law Exponential time-rate models.

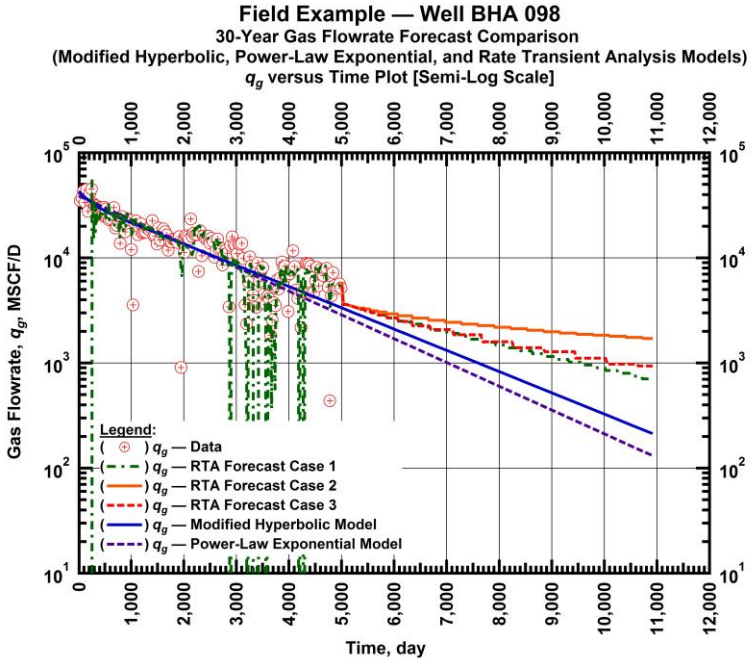

Fig. 75 — Semilog plot for BHA Well 098 — Gas flowrate versus time for various RTA forecast cases (1, 2, 3) and Modified Hyperbolic and Power-Law Exponential time-rate models.

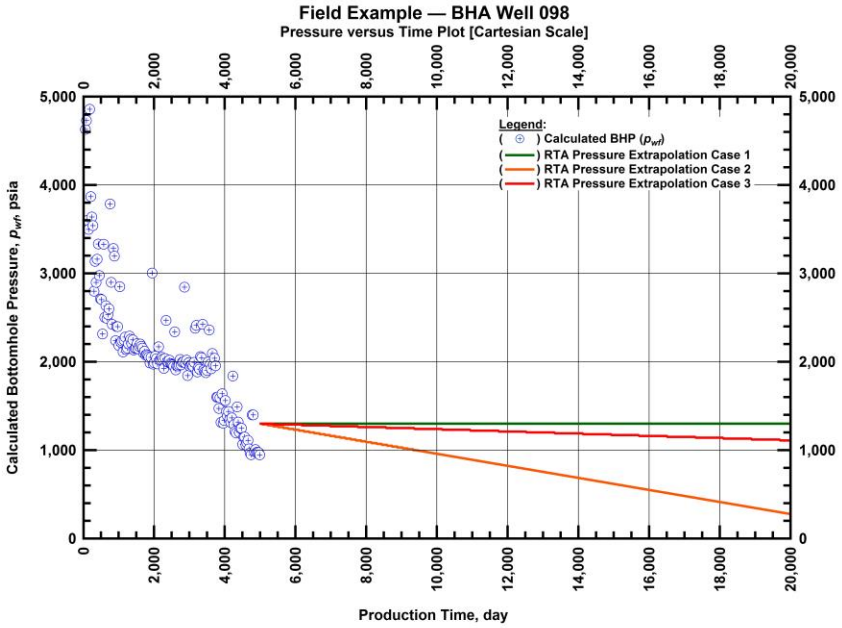

Fig. 76 — Cartesian plot for BHA Well 098 — historical and extrapolated bottomhole flowing pressures versus time (these pressure extrapolation scenarios are used for the RTA model).

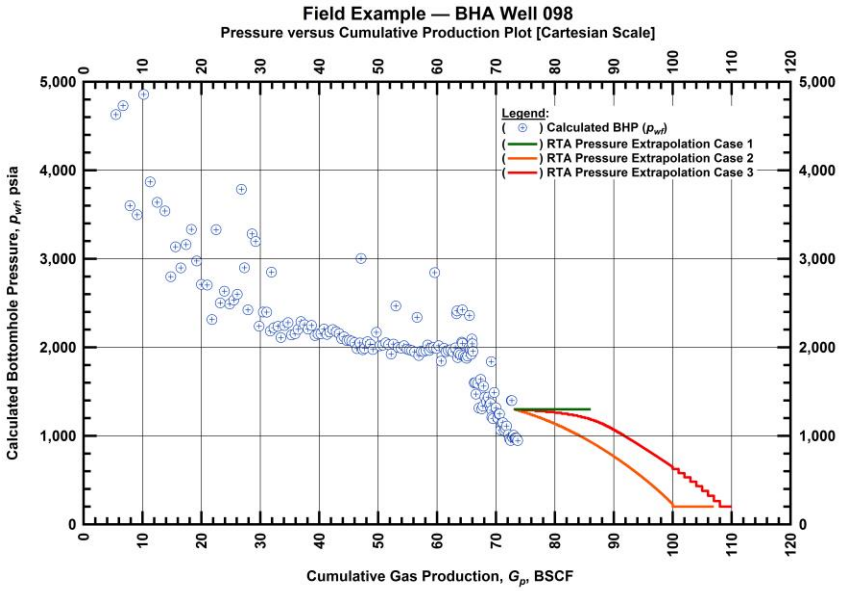

Fig. 77 — Cartesian plot for BHA Well 098 — historical and extrapolated bottomhole flowing pressures versus cumulative gas production (these pressure extrapolation scenarios are used for the RTA model).

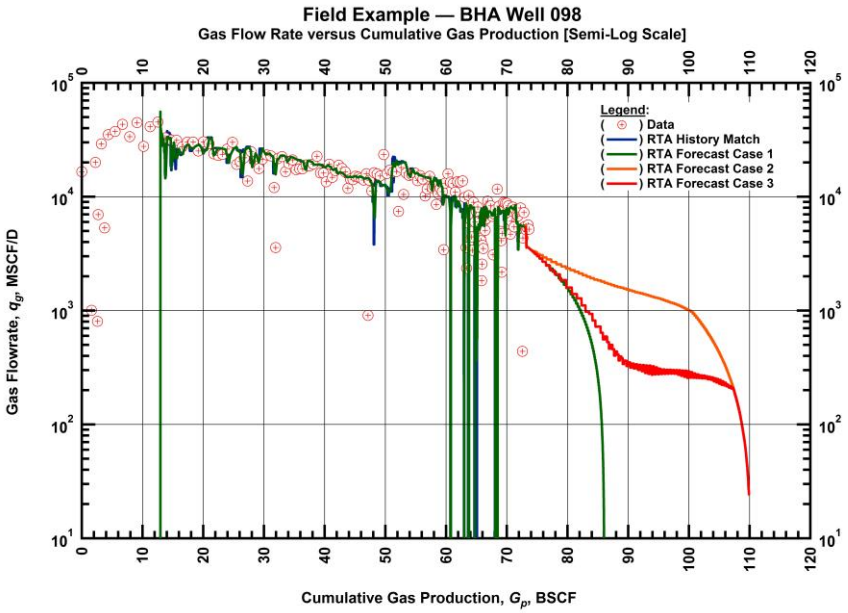

Fig. 78 — Semilog plot for BHA Well 098 — historical, history-matched, and forecasted gas flowrate versus cumulative gas production (various pressure extrapolation scenarios are prescribed (in time) for the RTA model).

Field Example — BHA Well 099

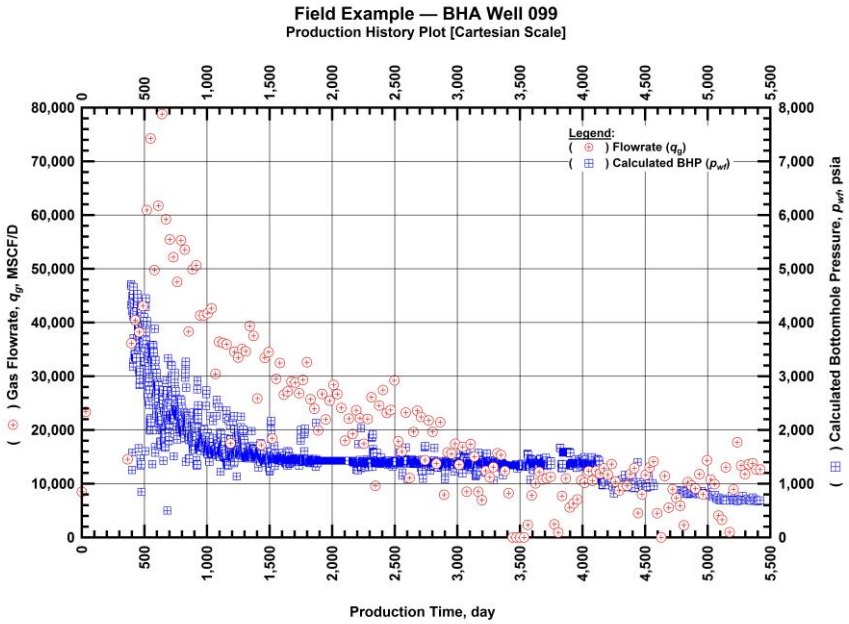

Fig. 79 — Cartesian plot for BHA Well 099 — Production history plot of calculated bottomhole pressures and gas flowrates as a function of production time.

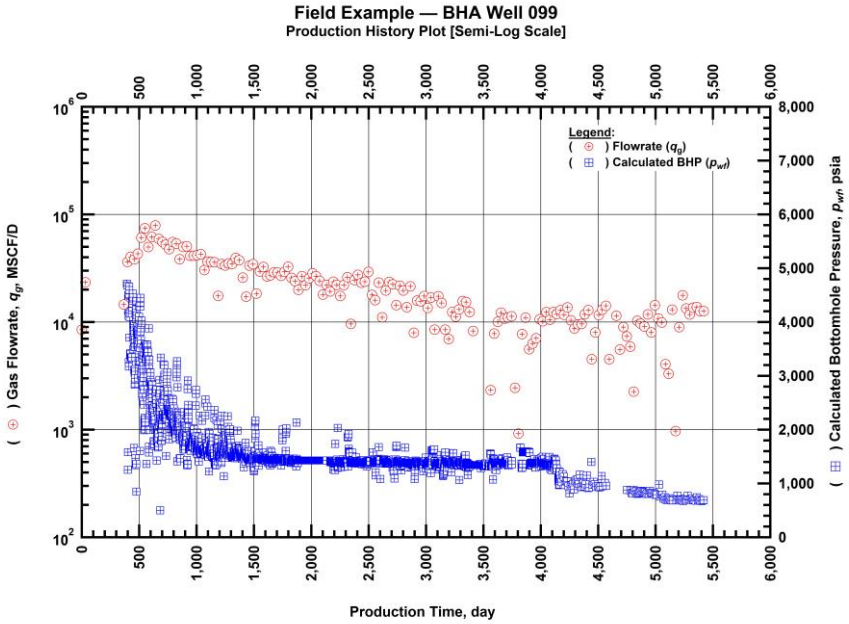

Fig. 80 — Semilog plot for BHA Well 099 — Production history plot of calculated bottomhole pressures and gas flowrates as a function of production time.

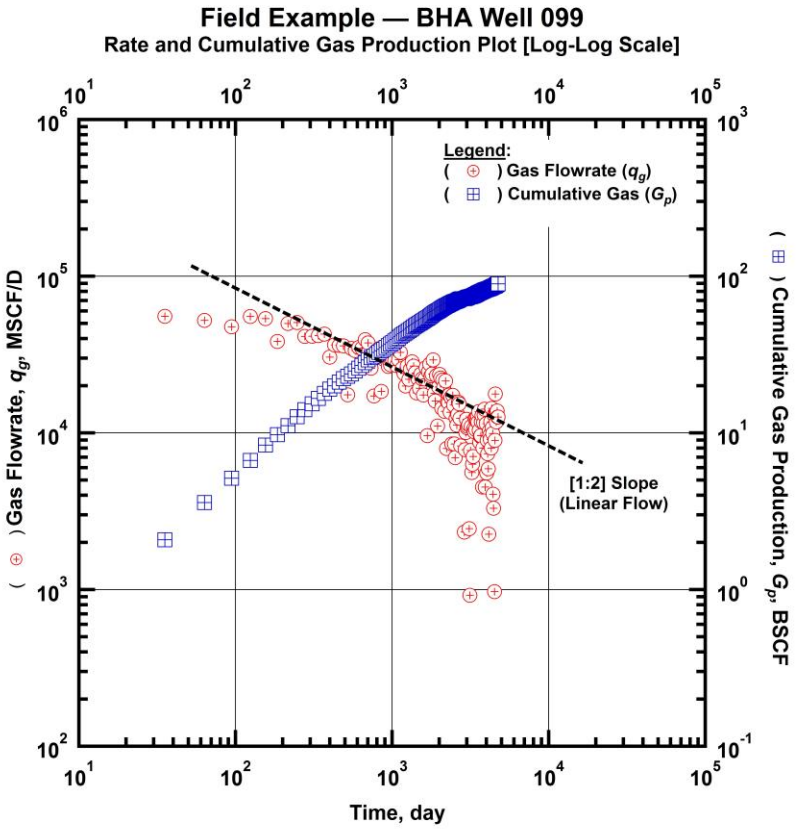

Fig. 81 — Log-Log plot for BHA Well 099 — Gas flowrate and cumulative gas production as a function of production time.

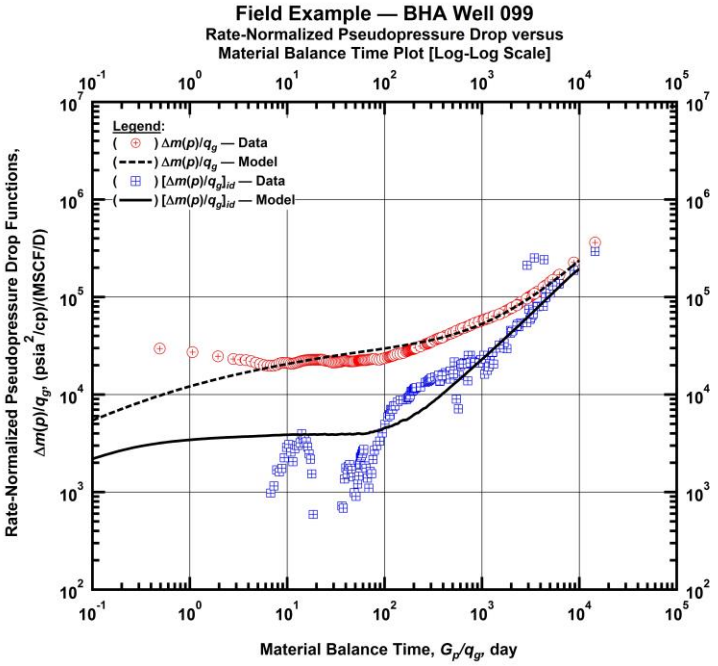

Fig. 82 — Log-Log plot for BHA Well 099 — Rate-normalized pseudopressure drop versus material balance time ("Log-Log Plot").

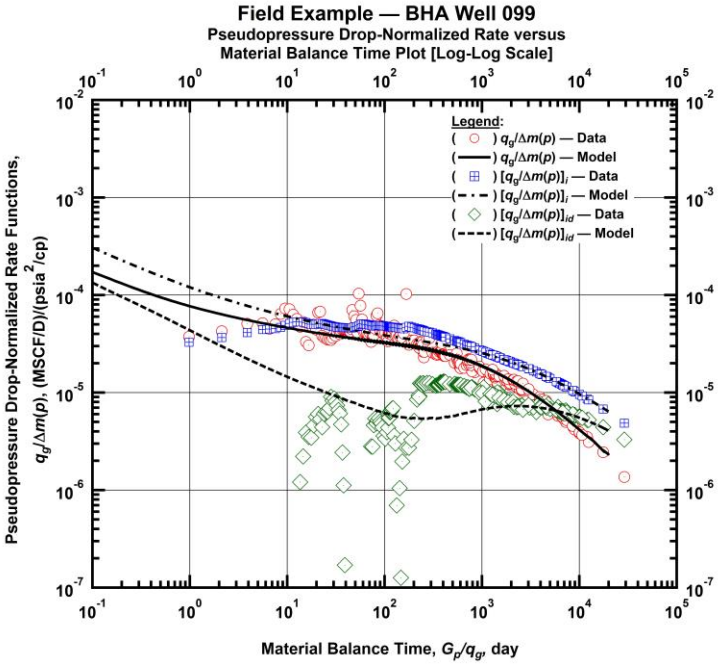

Fig. 83 — Log-Log plot for BHA Well 099 — Pseudopressure drop-normalized rate function versus material balance time ("Blasingame plot").

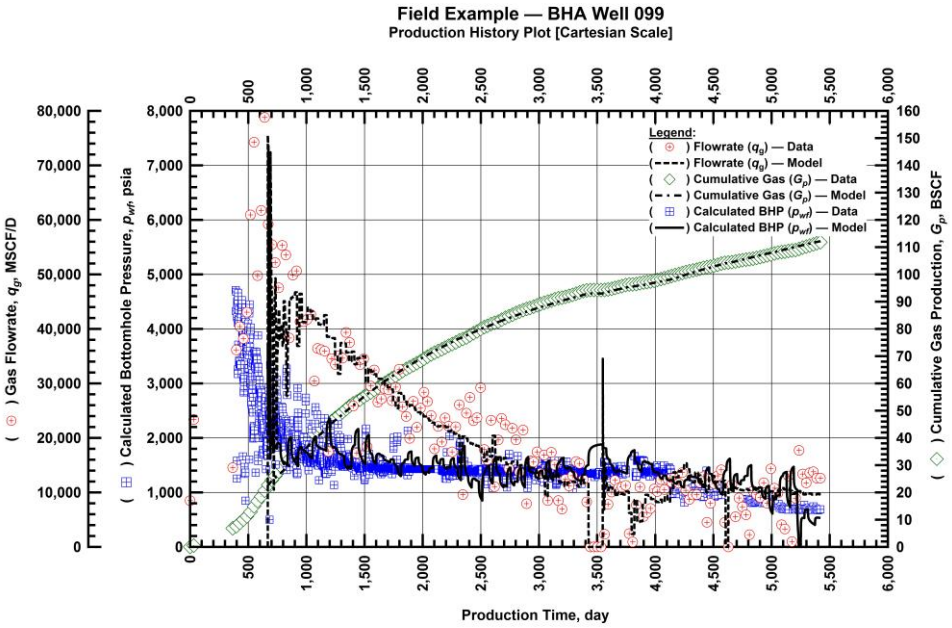

Fig. 84 — Cartesian plot for BHA Well 099 — production history and RTA history-match (gas flowrate, calculated bottomhole pressure, and cumulative gas production versus production time).

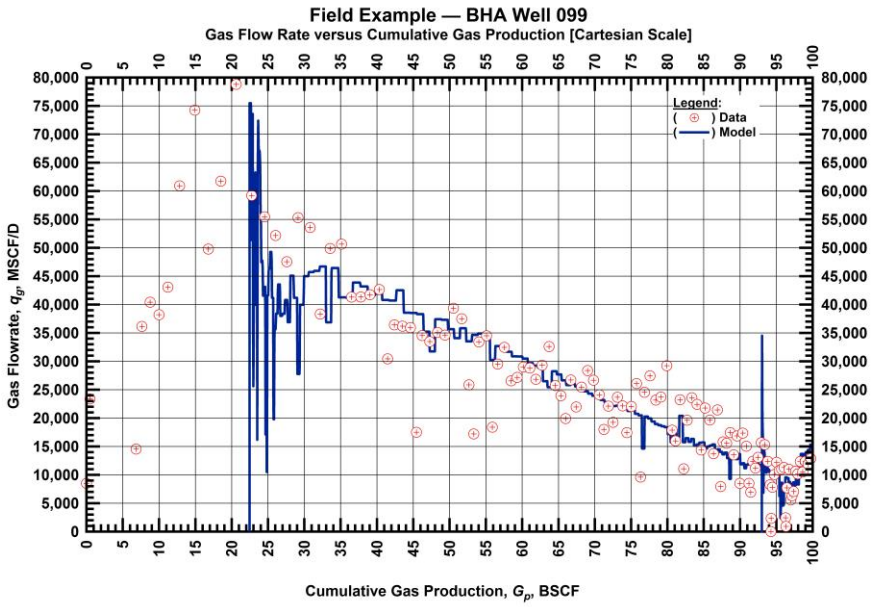

Fig. 85 — Cartesian plot for BHA Well 099 — historical and history-matched gas flowrate versus cumulative gas production.

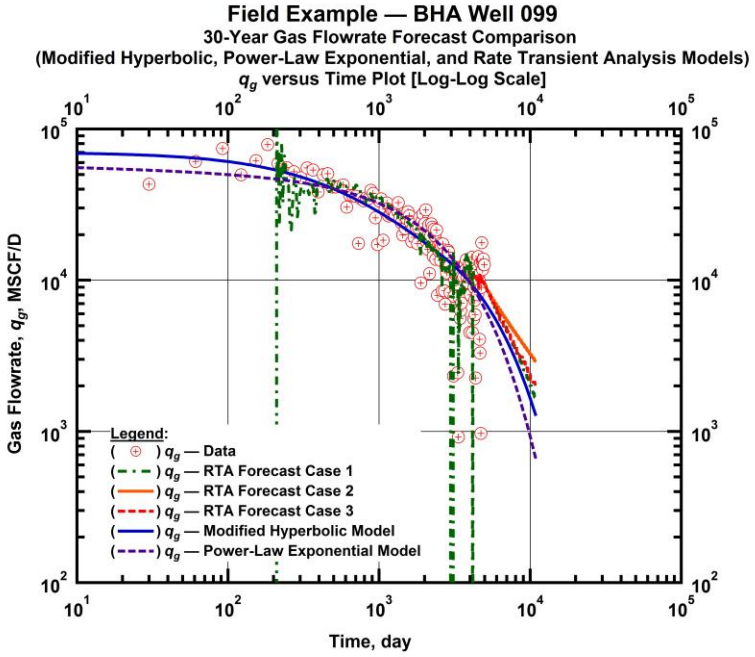

Fig. 86 — Log-Log plot for BHA Well 099 — Gas flowrate versus time for various RTA forecast cases (1, 2, 3) and Modified Hyperbolic and Power-Law Exponential time-rate models.

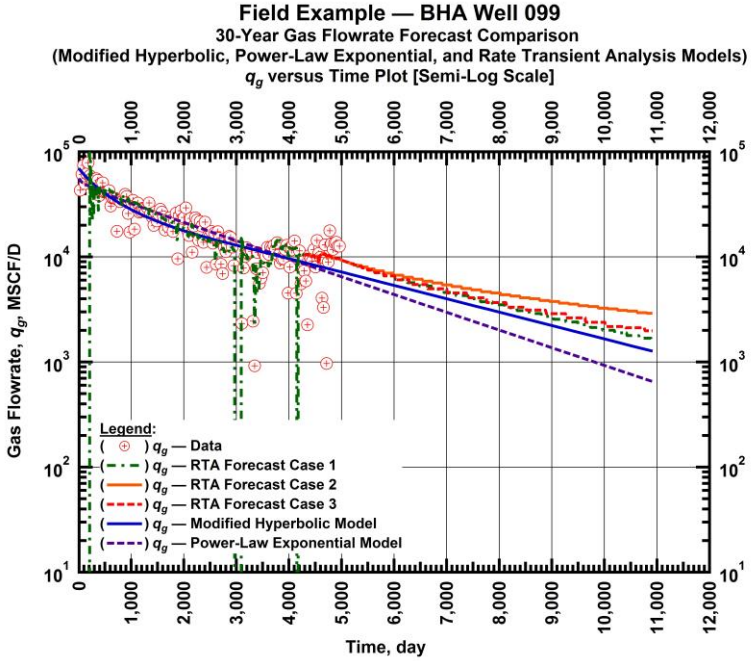

Fig. 87 — Semilog plot for BHA Well 099 — Gas flowrate versus time for various RTA forecast cases (1, 2, 3) and Modified Hyperbolic and Power-Law Exponential time-rate models.

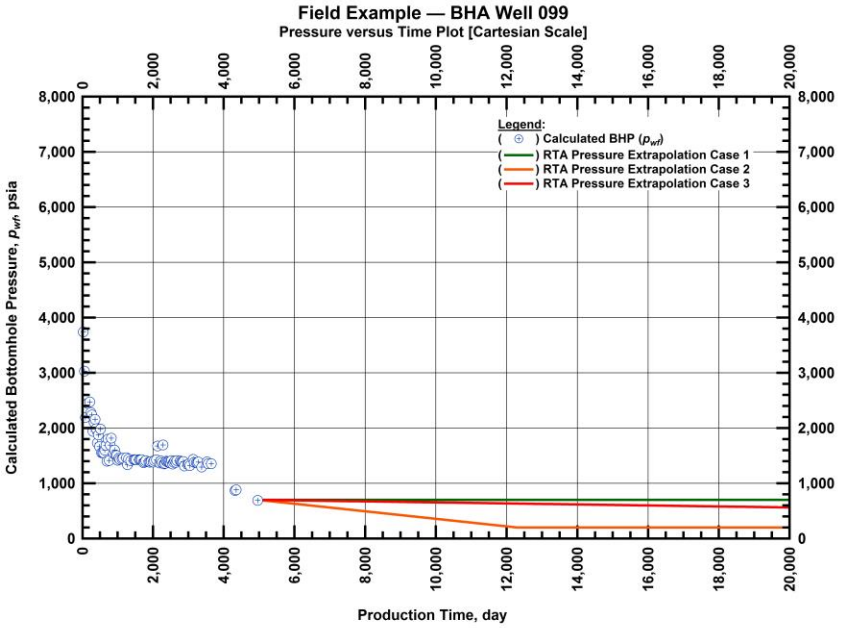

Fig. 88 — Cartesian plot for BHA Well 099 — historical and extrapolated bottomhole flowing pressures versus time (these pressure extrapolation scenarios are used for the RTA model).

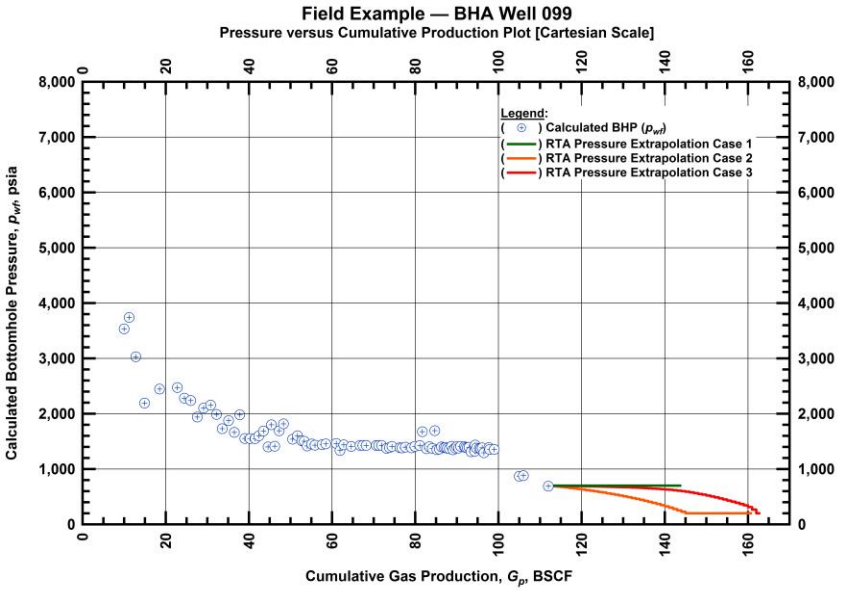

Fig. 89 — Cartesian plot for BHA Well 099 — historical and extrapolated bottomhole flowing pressures versus cumulative gas production (these pressure extrapolation scenarios are used for the RTA model).

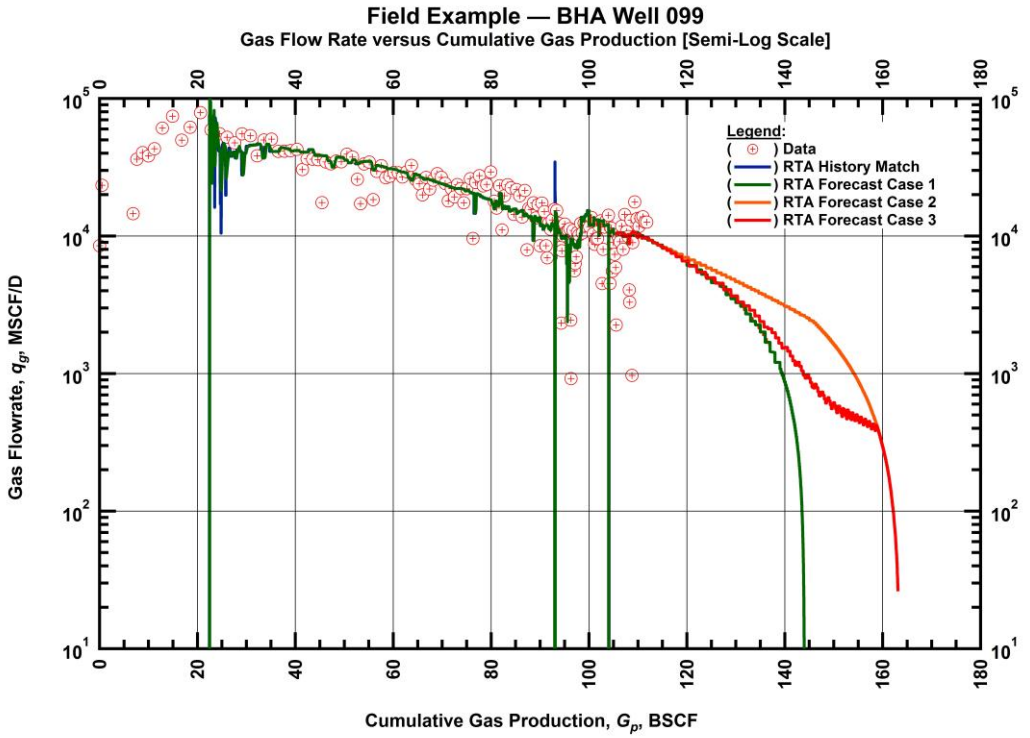

Fig. 90 — Semilog plot for BHA Well 099 — historical, history-matched, and forecasted gas flowrate versus cumulative gas production (various pressure extrapolation scenarios are prescribed (in time) for the RTA model).

Field Example — BHA Well 103

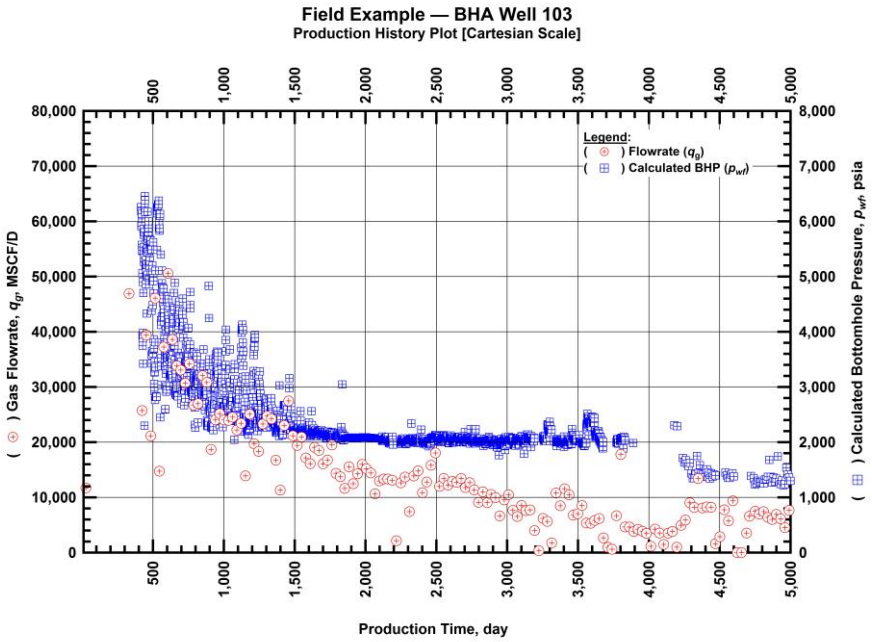

Fig. 91 — Cartesian plot for BHA Well 103 — Production history plot of calculated bottomhole pressures and gas flowrates as a function of production time.

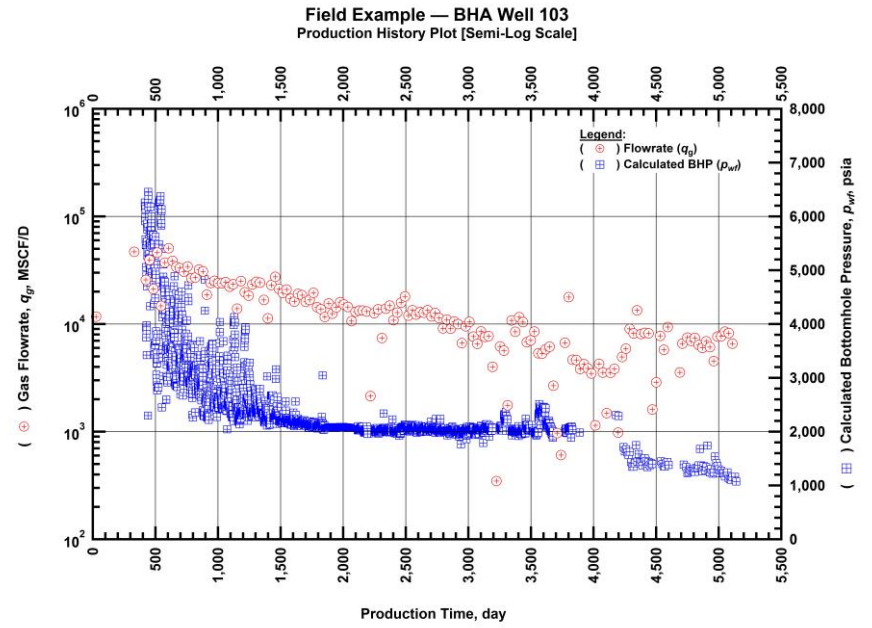

Fig. 92 — Semilog plot for BHA Well 103 — Production history plot of calculated bottomhole pressures and gas flowrates as a function of production time

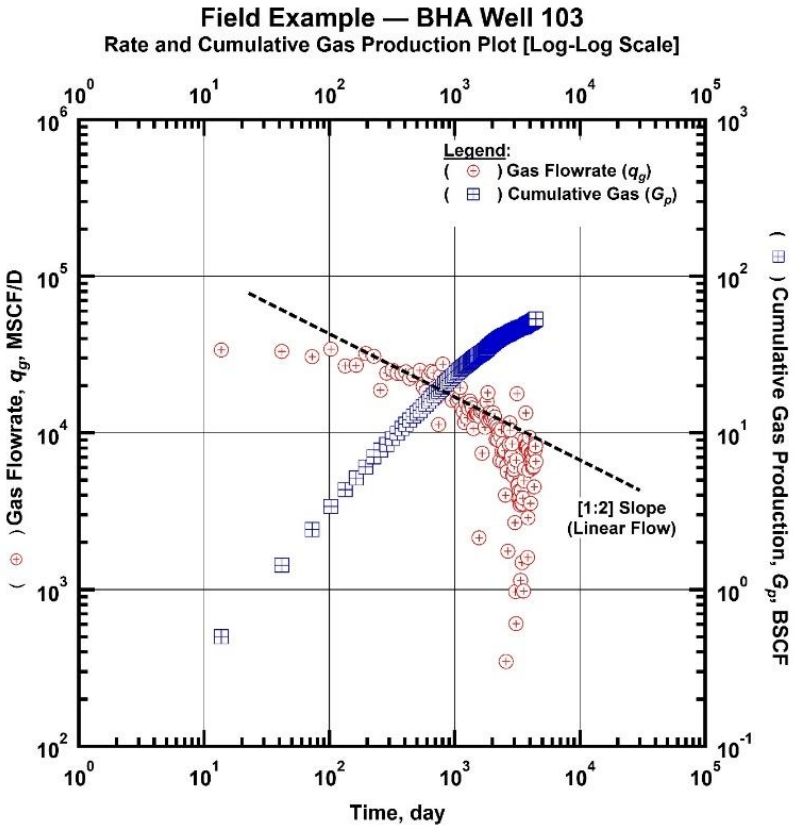

Fig. 93 — Log-Log plot for BHA Well 103 — Gas flowrate and cumulative gas production as a function of production time.

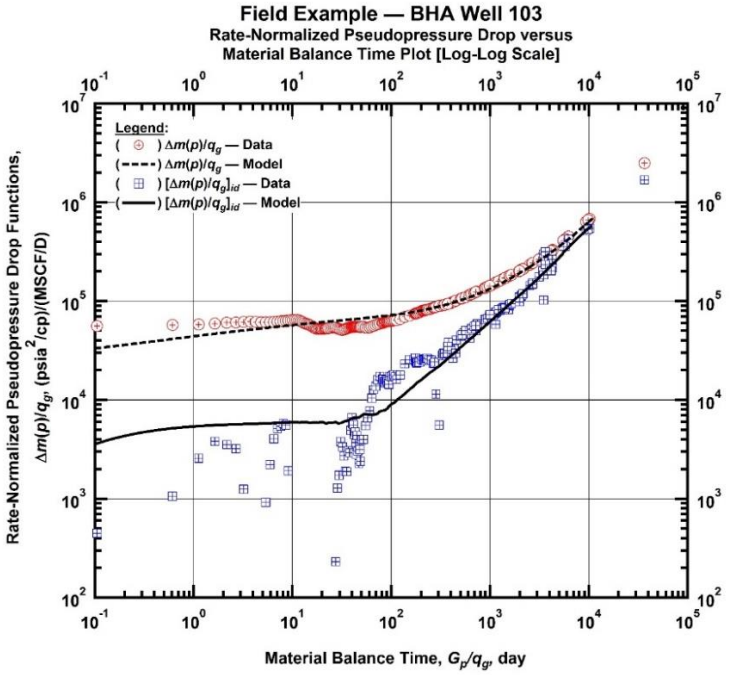

Fig. 94 — Log-Log plot for BHA Well 103 — Rate-normalized pseudopressure drop versus balance time ("Log-Log Plot").

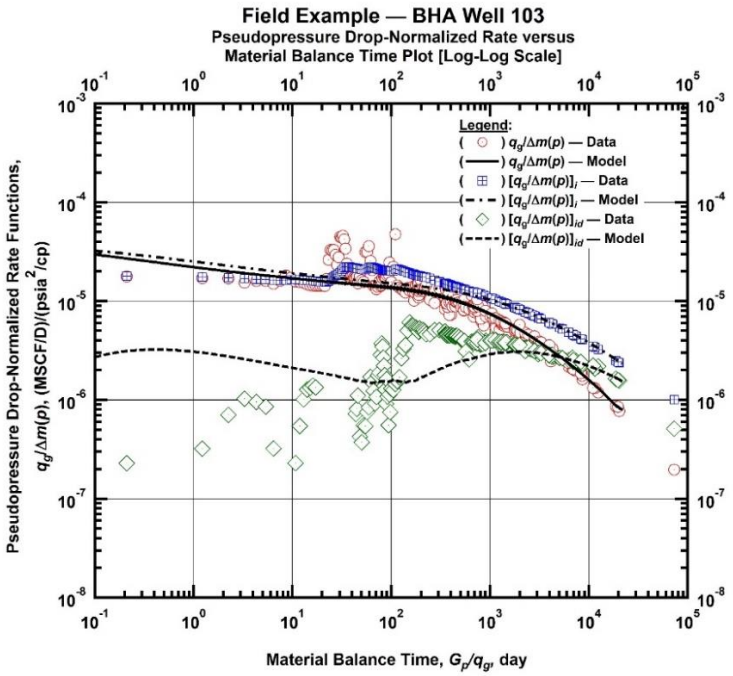

Fig. 95 — Log-Log plot for BHA Well 103 — Pseudopressure drop-normalized rate function versus material balance time ("Blasingame plot").

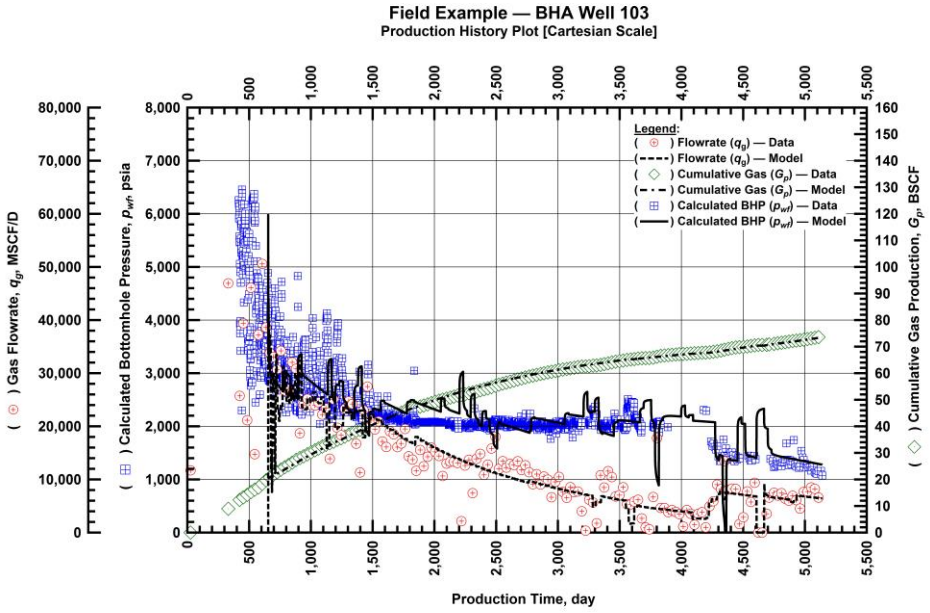

Fig. 96 — Cartesian plot for BHA Well 103 — production history and RTA history-match (gas flowrate, calculated bottomhole pressure, and cumulative gas production versus. production time).

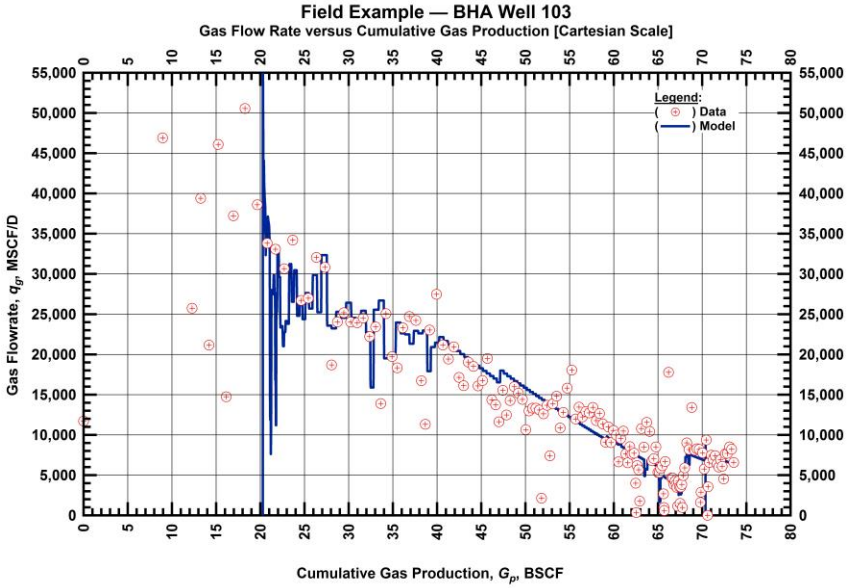

Fig. 97 — Cartesian plot for BHA Well 103 — historical and history-matched gas flowrate versus cumulative gas production.

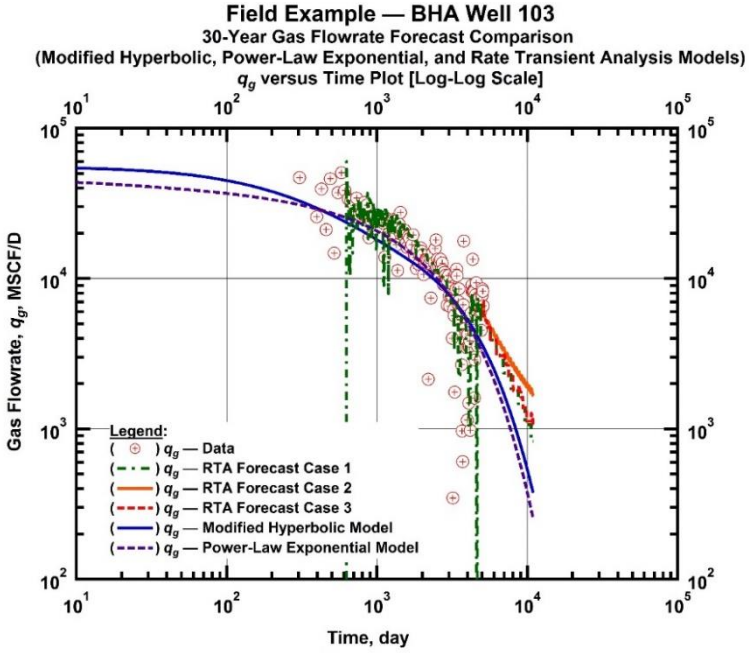

Fig. 98 — Log-Log plot for BHA Well 103 — Gas flowrate versus time for various RTA forecast cases (1, 2, 3) and Modified Hyperbolic and Power-Law Exponential time-rate models.

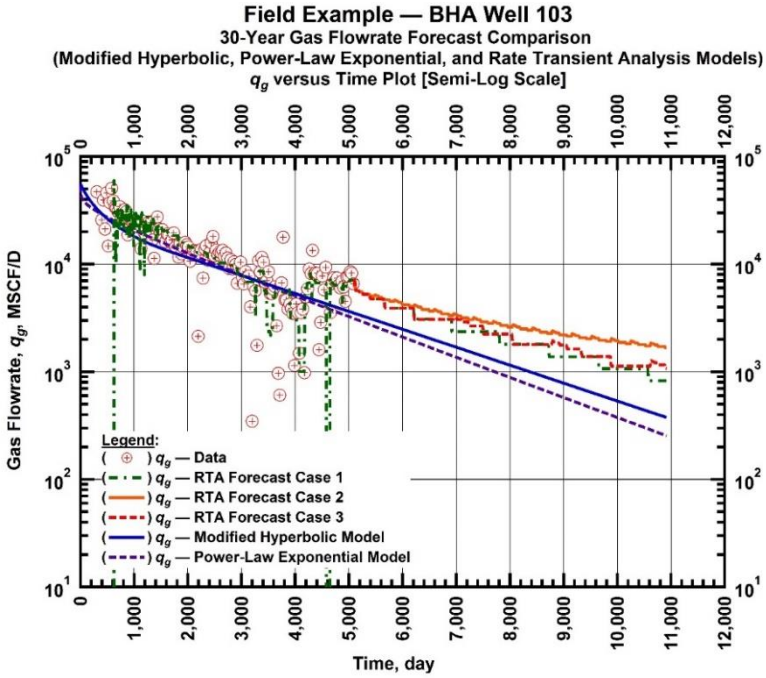

Fig. 99 — Semilog plot for BHA Well 103 — Gas flowrate versus time for various RTA forecast cases (1, 2, 3) and Modified Hyperbolic and Power-Law Exponential time-rate models.

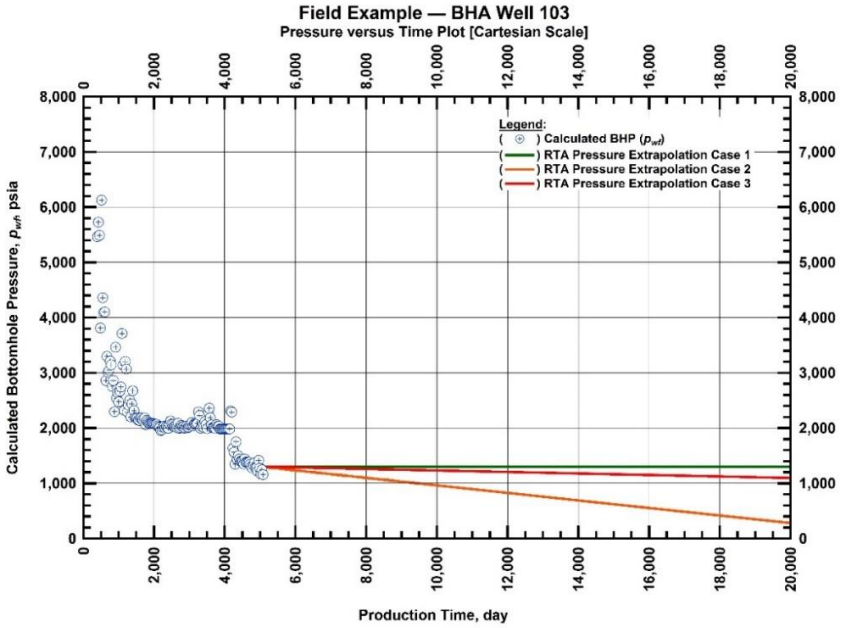

Fig. 100 — Cartesian plot for BHA Well 103 — historical and extrapolated bottomhole flowing pressures versus time (these pressure extrapolation scenarios are used for the RTA model).

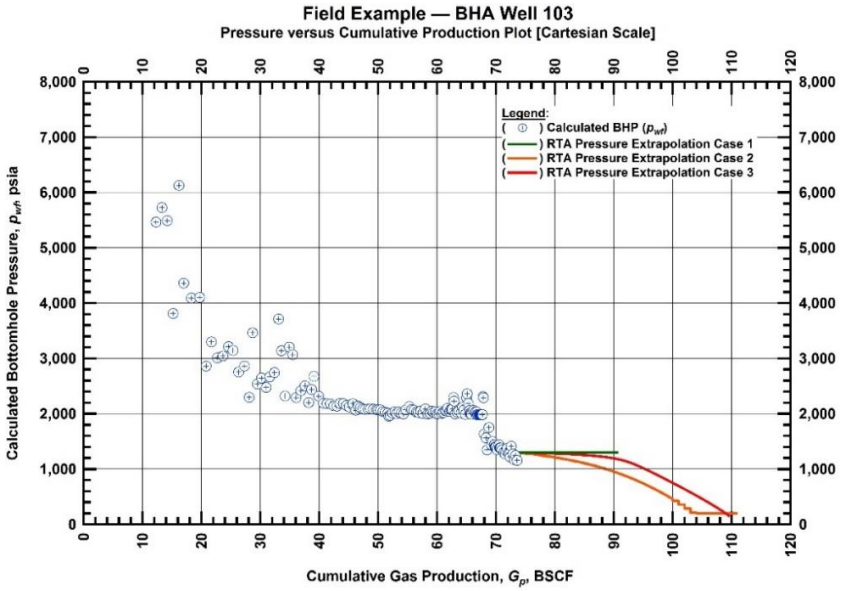

Fig. 101 — Cartesian plot for BHA Well 103 — historical and extrapolated bottomhole flowing pressures versus cumulative gas production (these pressure extrapolation scenarios are used for the RTA model).

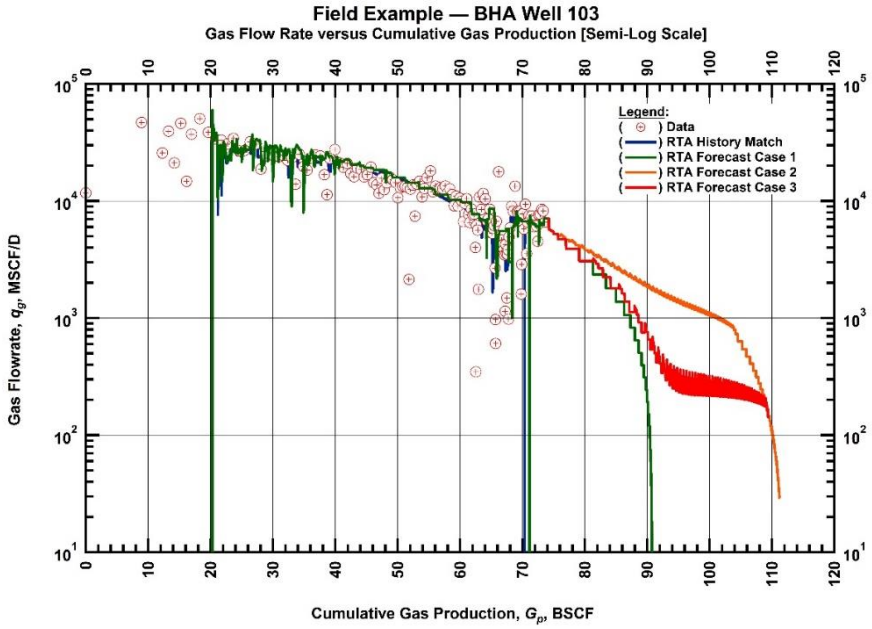

Fig. 102 — Semilog plot for BHA Well 103 — historical, history-matched, and forecasted gas flowrate versus cumulative gas production (various pressure extrapolation scenarios are prescribed (in time) for the RTA model).

Field Example — BHA Well 116

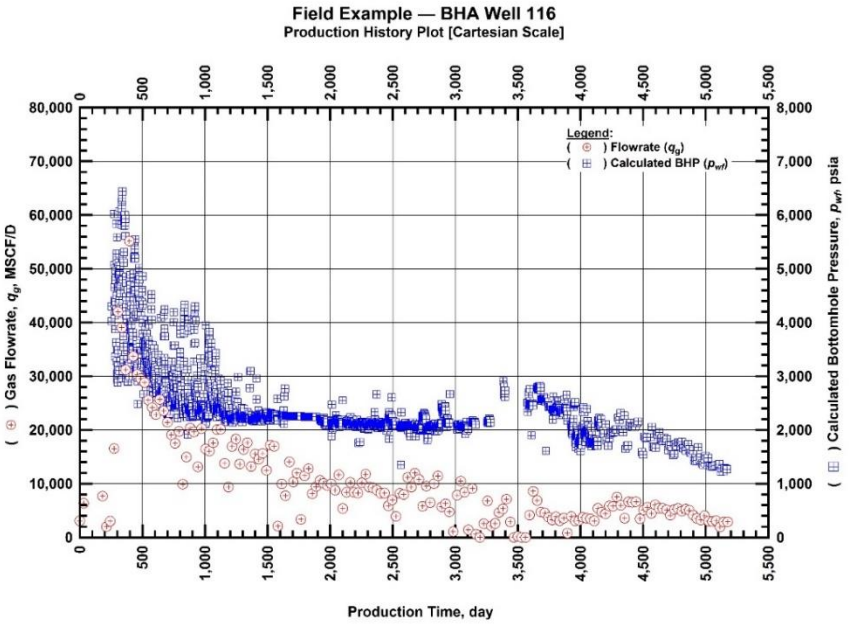

Fig. 103 — Cartesian plot for BHA Well 116 — Production history plot of calculated bottomhole pressures and gas flowrates as a function of production time.

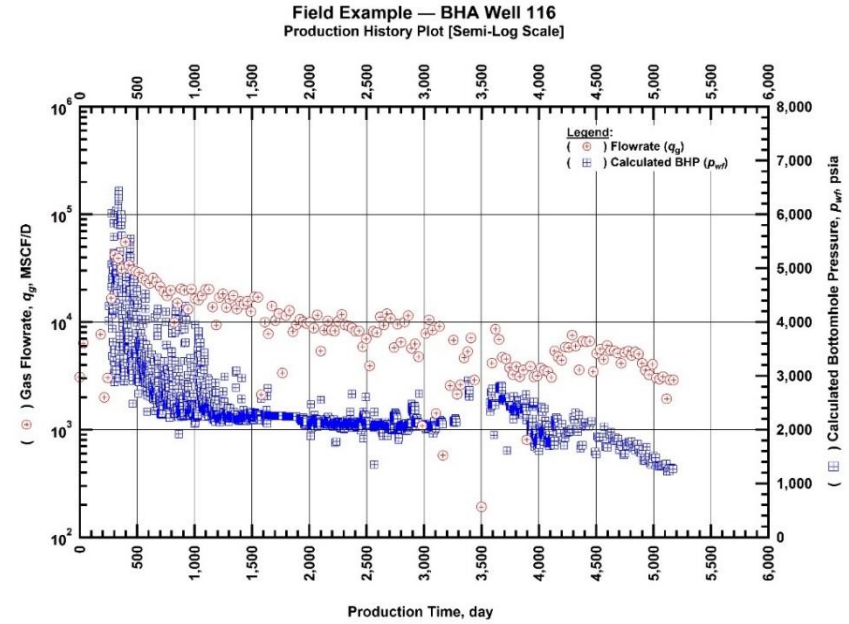

Fig. 104 — Semilog plot for BHA Well 116 — Production history plot of calculated bottomhole pressures and gas flowrates as a function of production time.

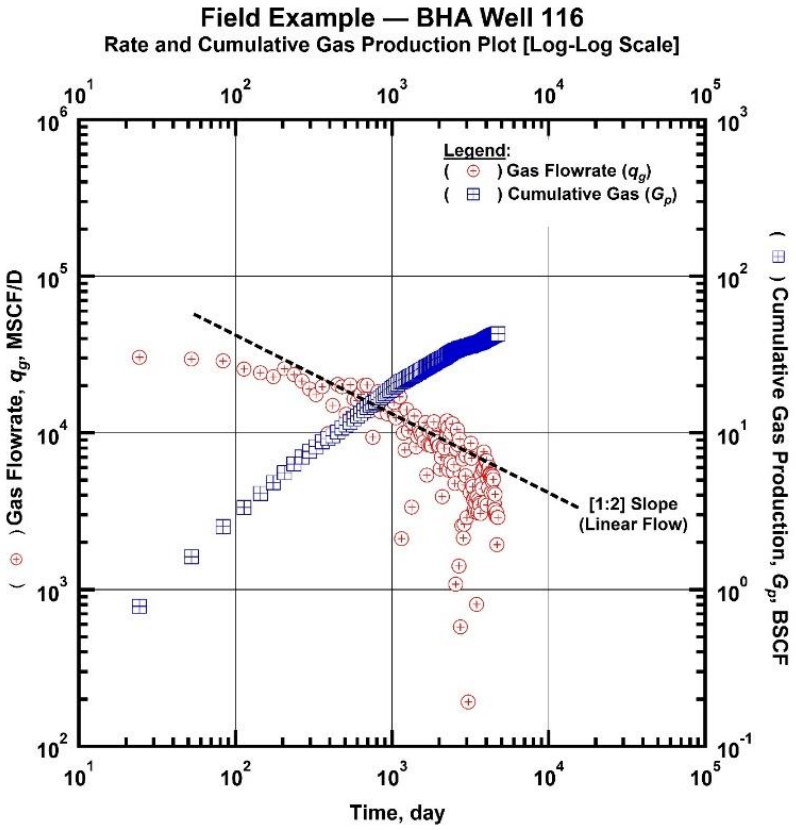

Fig. 105 — Log-Log plot for BHA Well 116 — Gas flowrate and cumulative gas production as a function of production time.

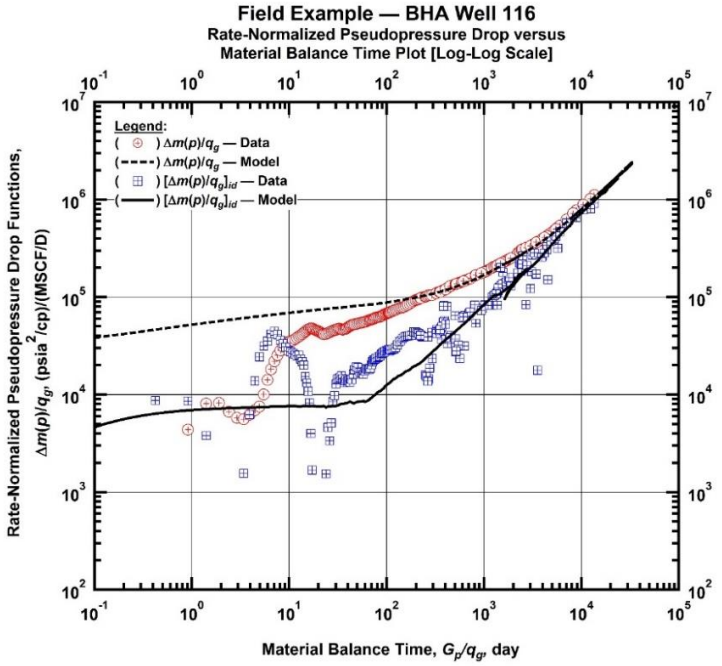

Fig. 106 — Log-Log plot for BHA Well 116 — Rate-normalized pseudopressure drop versus material balance time ("Log-Log Plot").

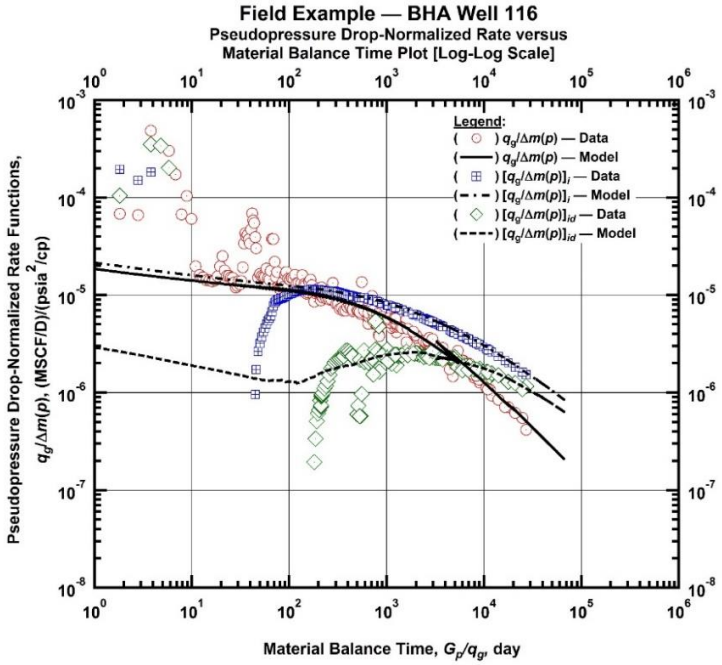

Fig. 107 — Log-Log plot for BHA Well 116 — Pseudopressure drop-normalized rate function versus material balance time ("Blasingame plot").

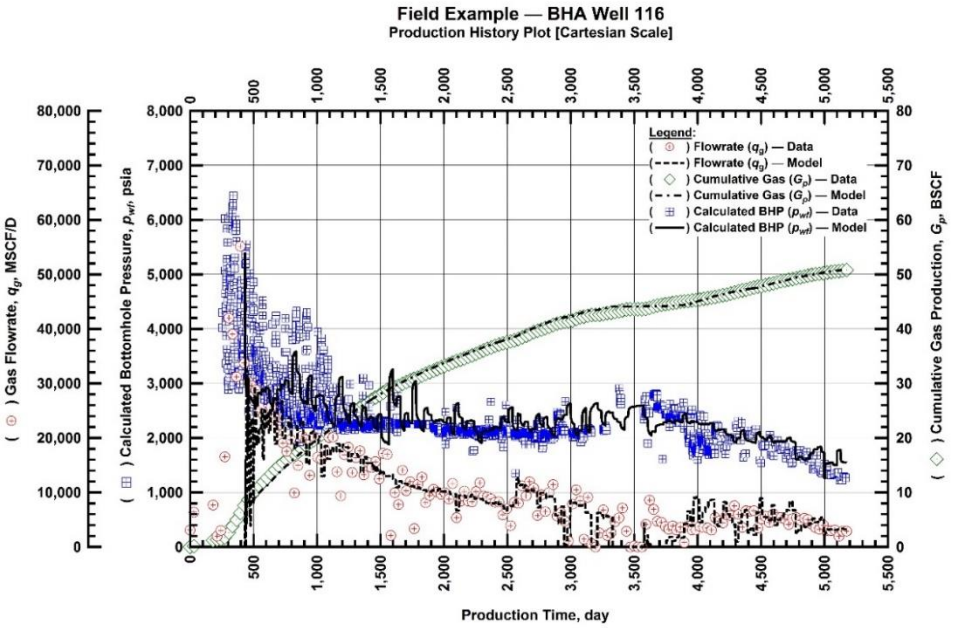

Fig. 108 — Cartesian plot for BHA Well 116 — production history and RTA history-match (gas flowrate, calculated bottomhole pressure, and cumulative gas production versus production time).

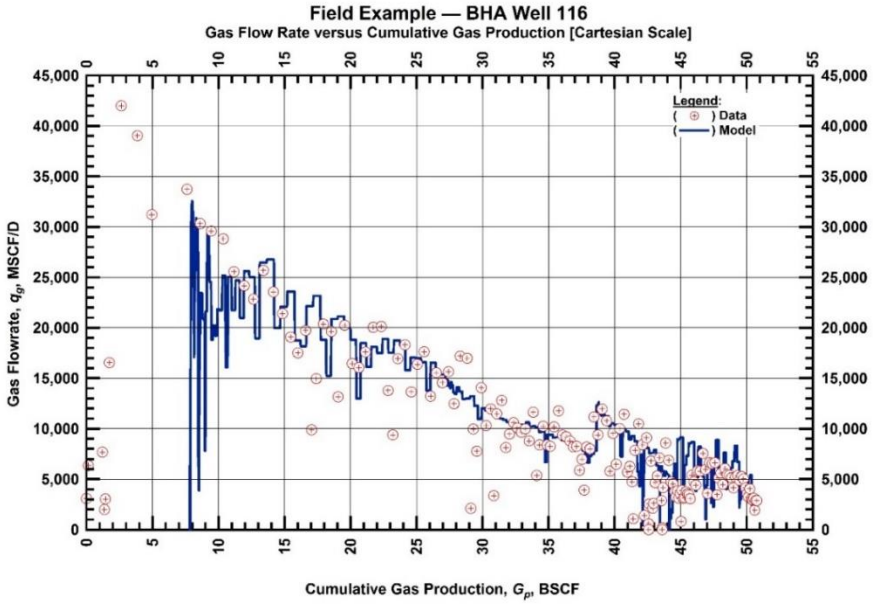

Fig. 109 — Cartesian plot for BHA Well 116 — historical and history-matched gas flowrate versus cumulative gas production.

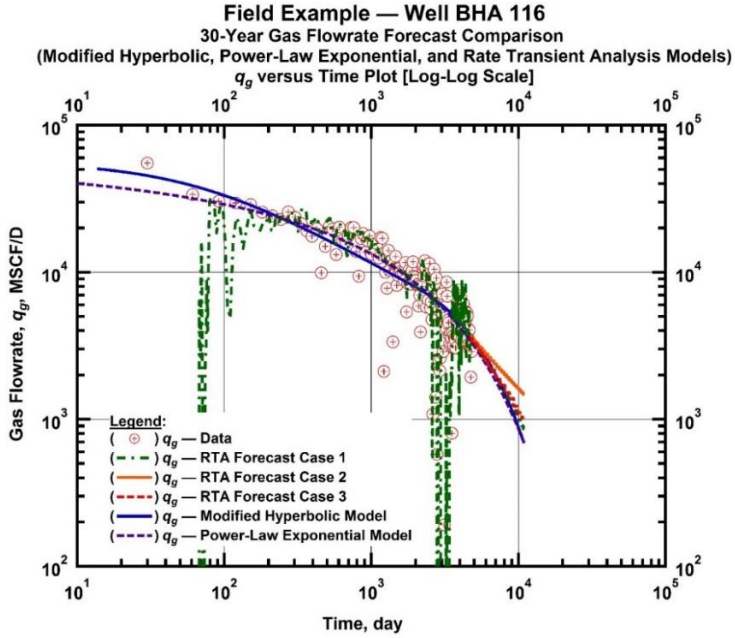

Fig. 110 — Log-Log plot for BHA Well 116 — Gas flowrate versus time for various RTA forecast cases (1, 2, 3) and Modified Hyperbolic and Power-Law Exponential time-rate models.

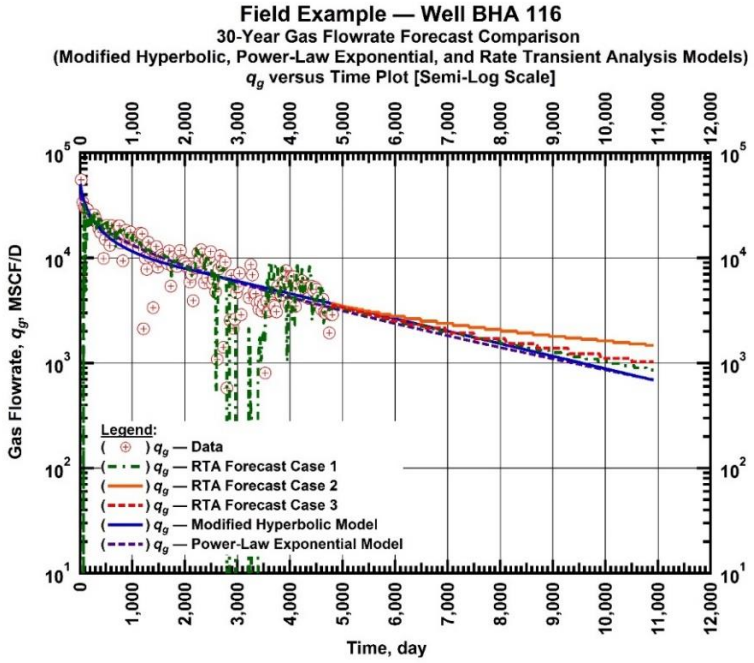

Fig. 111 — Semilog plot for BHA Well 116 — Gas flowrate versus time for various RTA forecast cases (1, 2, 3) and Modified Hyperbolic and Power-Law Exponential time-rate models.

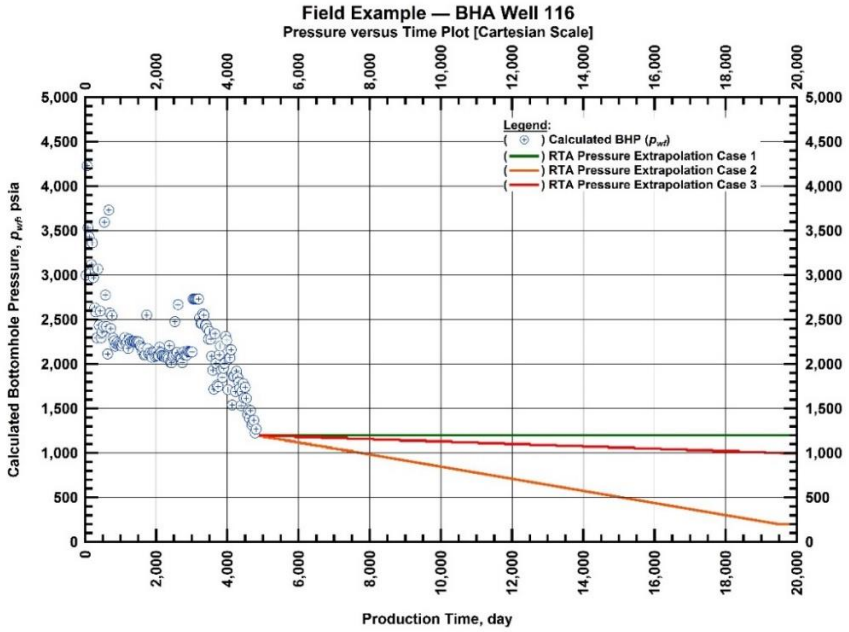

Fig. 112 — Cartesian plot for BHA Well 116 — historical and extrapolated bottomhole flowing pressures versus time (these pressure extrapolation scenarios are used for the RTA model).

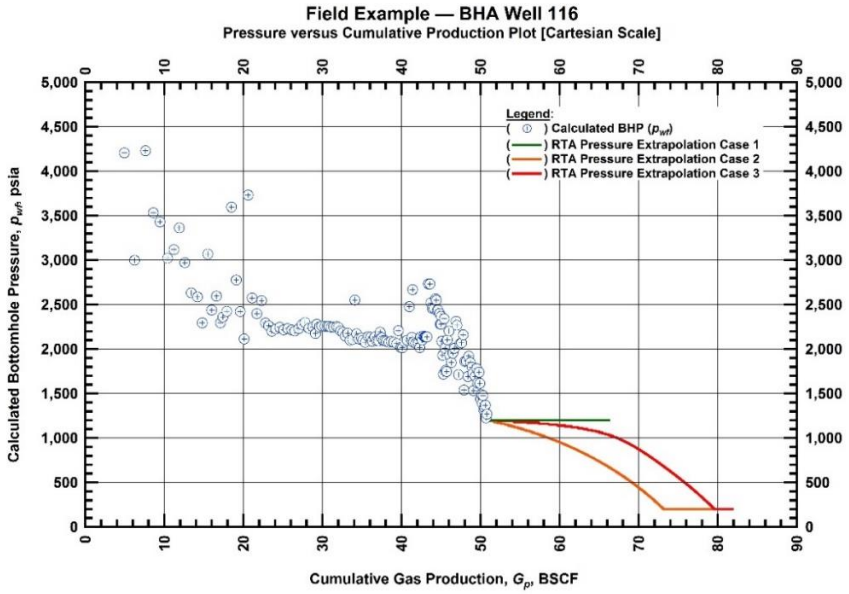

Fig. 113 — Cartesian plot for BHA Well 116 — historical and extrapolated bottomhole flowing pressures versus cumulative gas production (these pressure extrapolation scenarios are used for the RTA model).

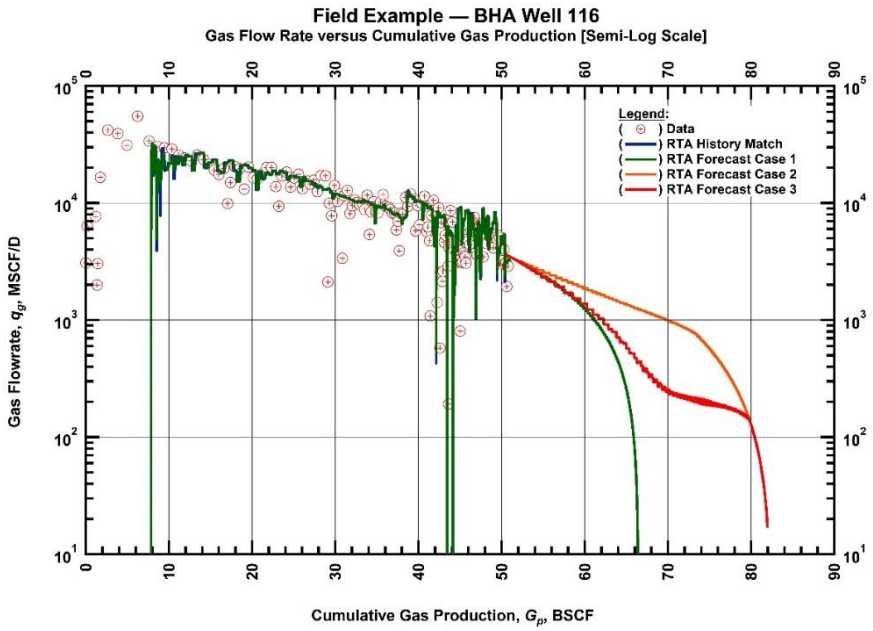

Fig. 114 — Semilog plot for BHA Well 116 — historical, history-matched, and forecasted gas flowrate versus cumulative gas production (various pressure extrapolation scenarios are prescribed (in time) for the RTA model).

Field Example — BHA Well 119

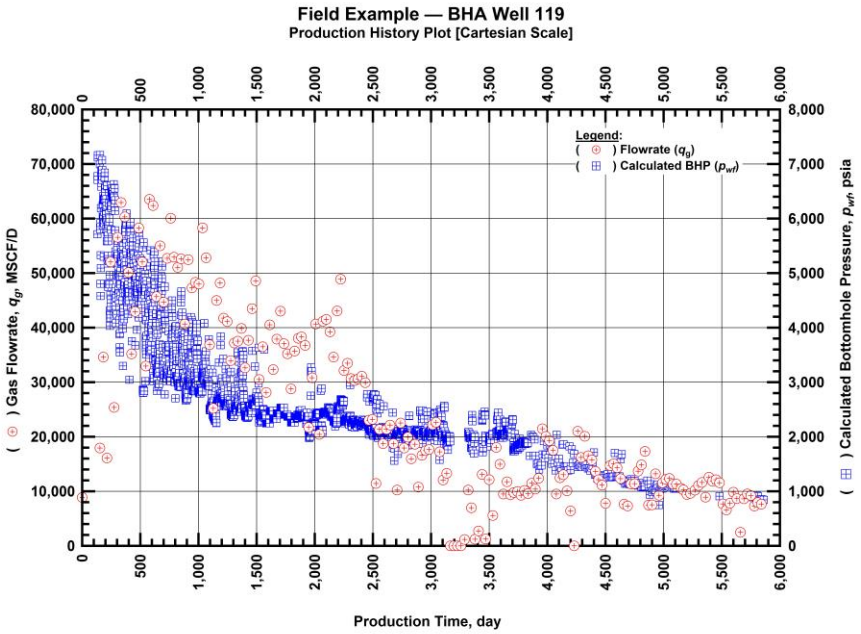

Fig. 115 — Cartesian plot for BHA Well 119 — Production history plot of calculated bottomhole pressures and gas flowrates as a function of production time.

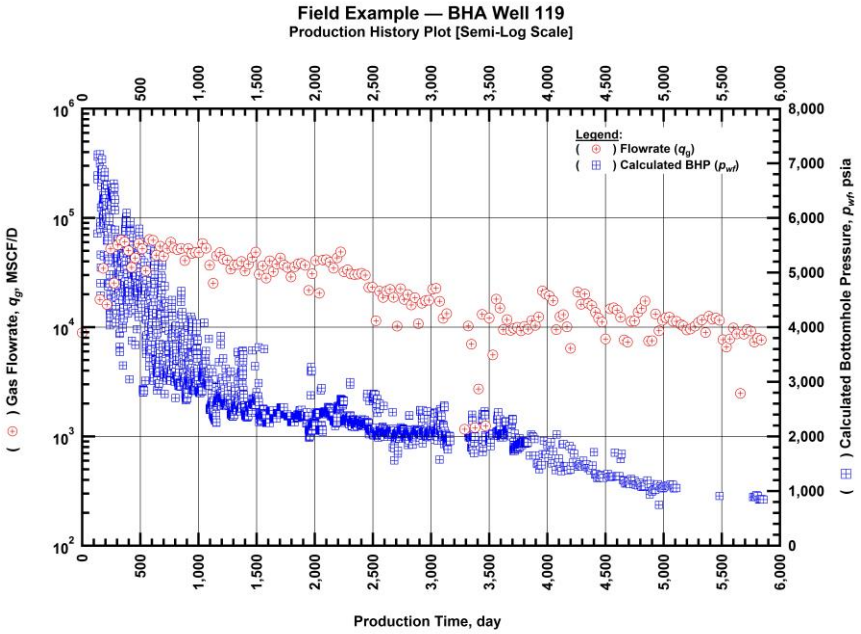

Fig. 116 — Semilog plot for BHA Well 119 — Production history plot of calculated bottomhole and gas flowrates as a function of production time.

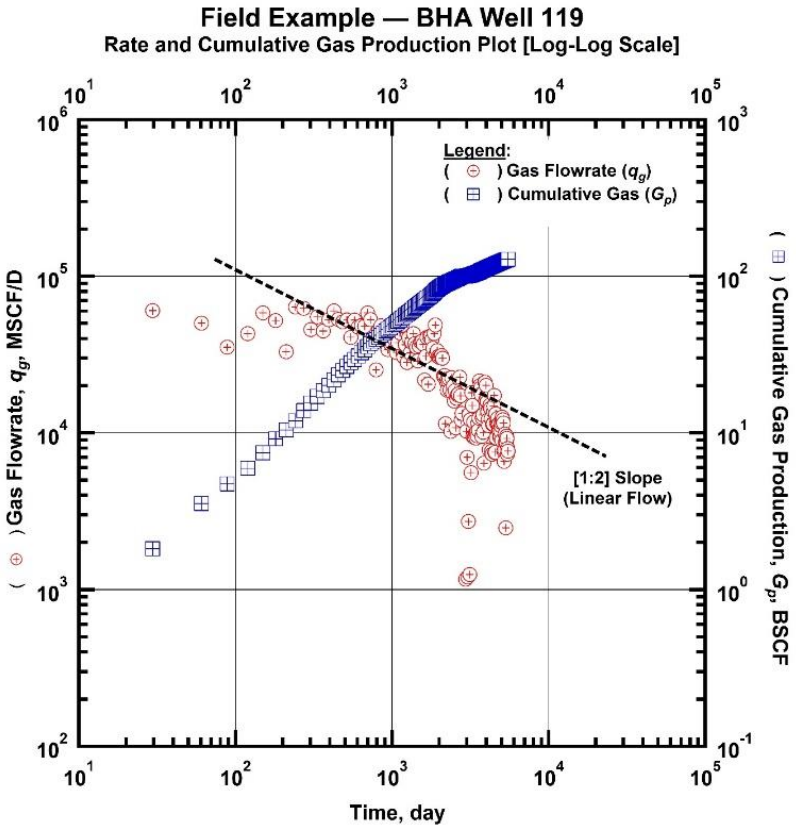

Fig. 117 — Log-Log plot for BHA Well 119 — Gas flowrate and cumulative gas production as a function of production time.

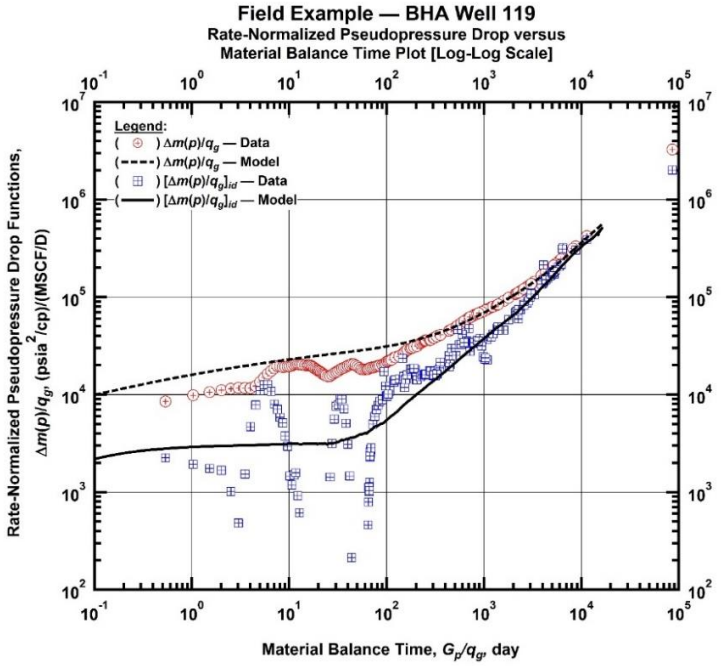

Fig. 118 — Log-Log plot for BHA Well 119 — Rate-normalized pseudopressure drop versus material balance time ("Log-Log Plot").

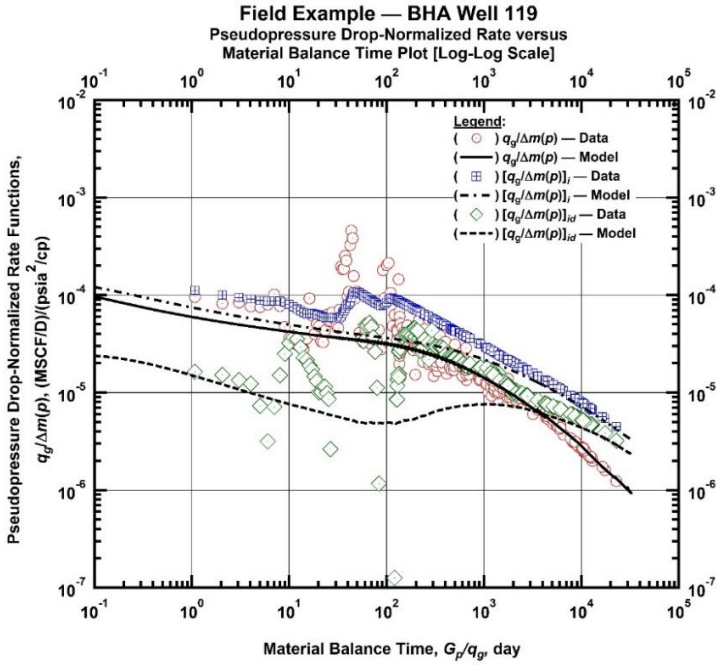

Fig. 119 — Log-Log plot for BHA Well 119 — Pseudopressure drop-normalized rate function versus material balance time ("Blasingame plot").

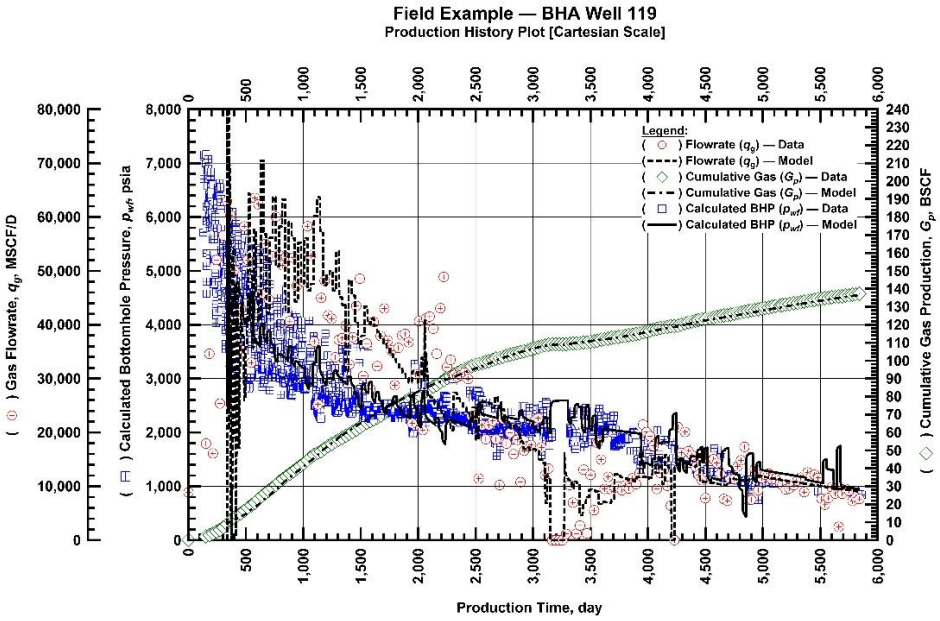

Fig. 120 — Cartesian plot for BHA Well 119 — production history and RTA history-match (gas flowrate, calculated bottomhole pressure, and cumulative gas production versus production time).

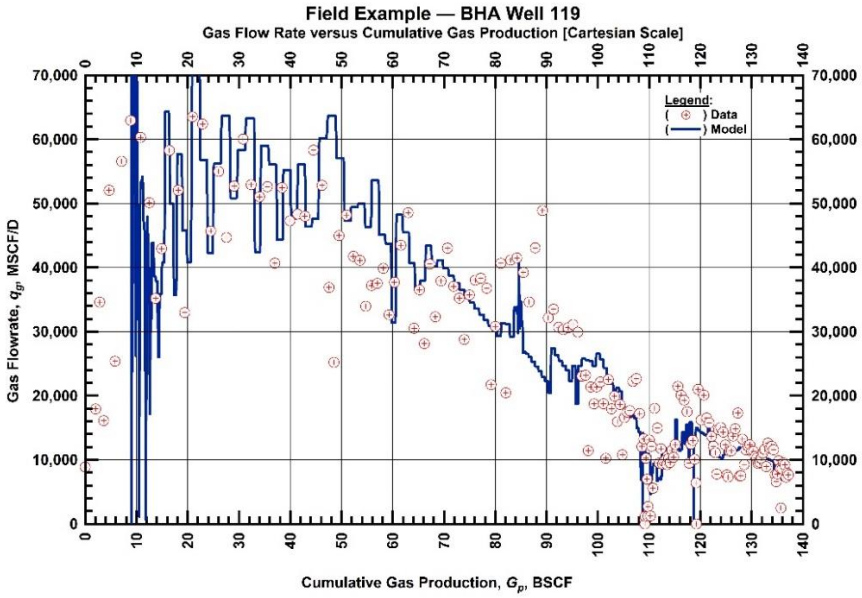

Fig. 121 — Cartesian plot for BHA Well 119 — historical and history-matched gas flowrate versus cumulative gas production.

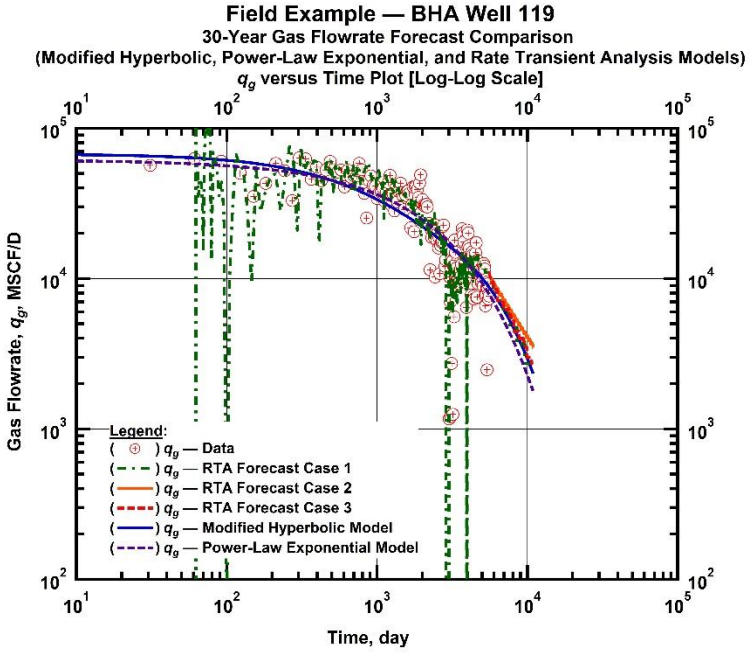

Fig. 122 — Log-Log plot for BHA Well 119 — Gas flowrate versus time for various RTA forecast cases (1, 2, 3) and Modified Hyperbolic and Power-Law Exponential time-rate models.

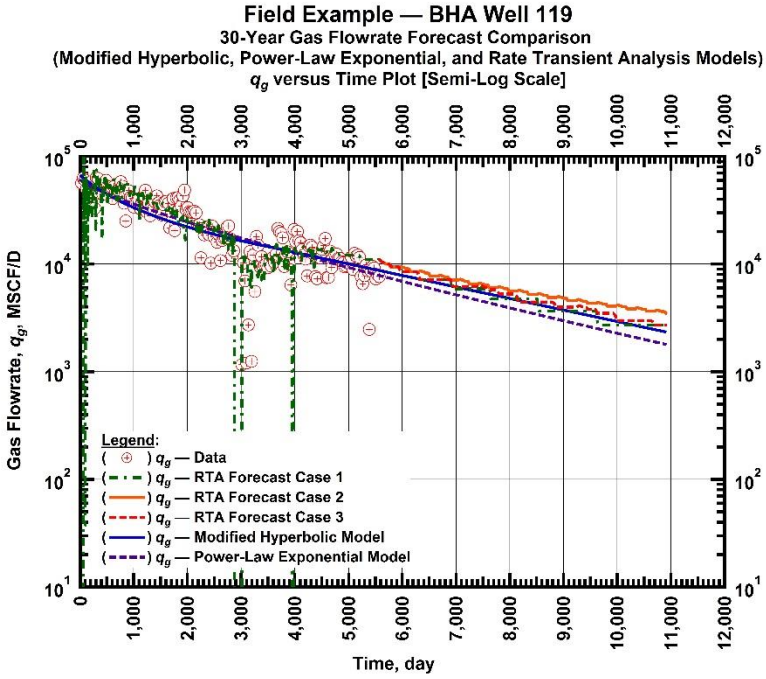

Fig. 123 — Semilog plot for BHA Well 119 — Gas flowrate versus time for various RTA forecast cases (1, 2, 3) and Modified Hyperbolic and Power-Law Exponential time-rate models.

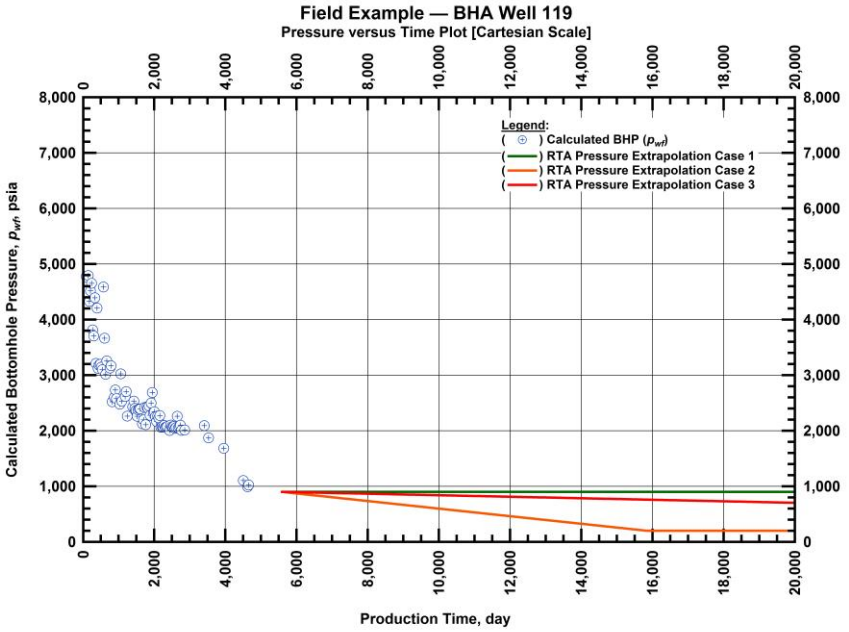

Fig. 124 — Cartesian plot for BHA Well 119 — historical and extrapolated bottomhole flowing pressures versus time (these pressure extrapolation scenarios are used for the RTA model).

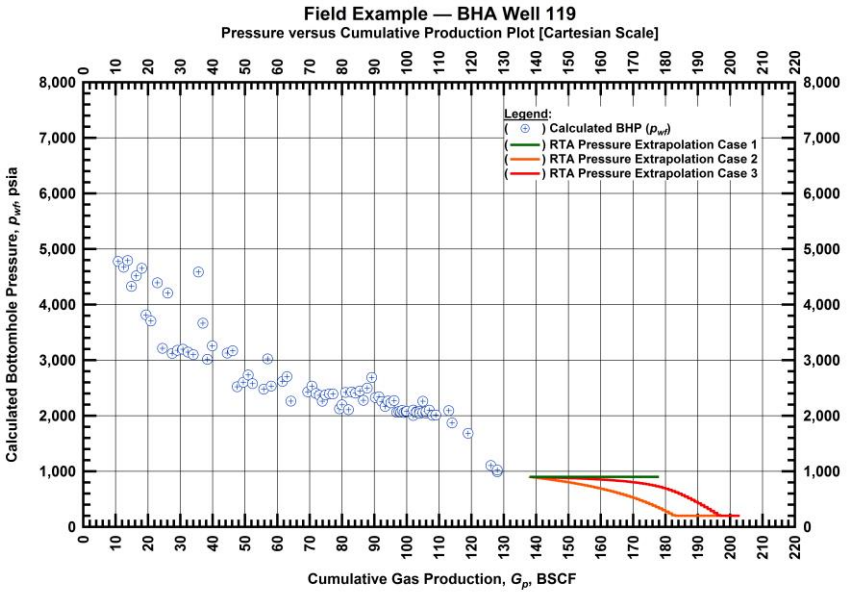

Fig. 125 — Cartesian plot for BHA Well 119 — historical and extrapolated bottomhole flowing pressures versus cumulative gas production (these pressure extrapolation scenarios are used for the RTA model).

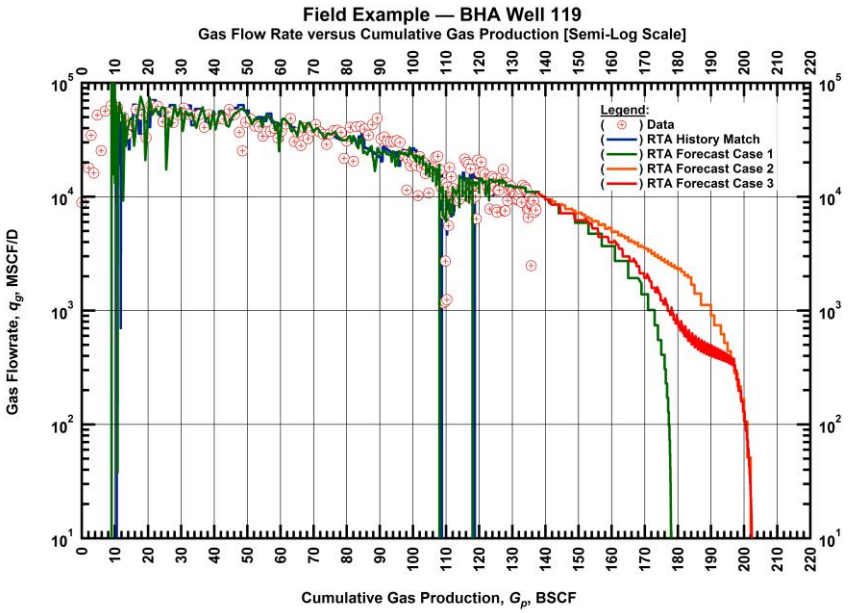

Fig. 126 — Semilog plot for BHA Well 119 — historical, history-matched, and forecasted gas flowrate versus cumulative gas production (various pressure extrapolation scenarios are prescribed (in time) for the RTA model).

Field Example — BHA Well 121

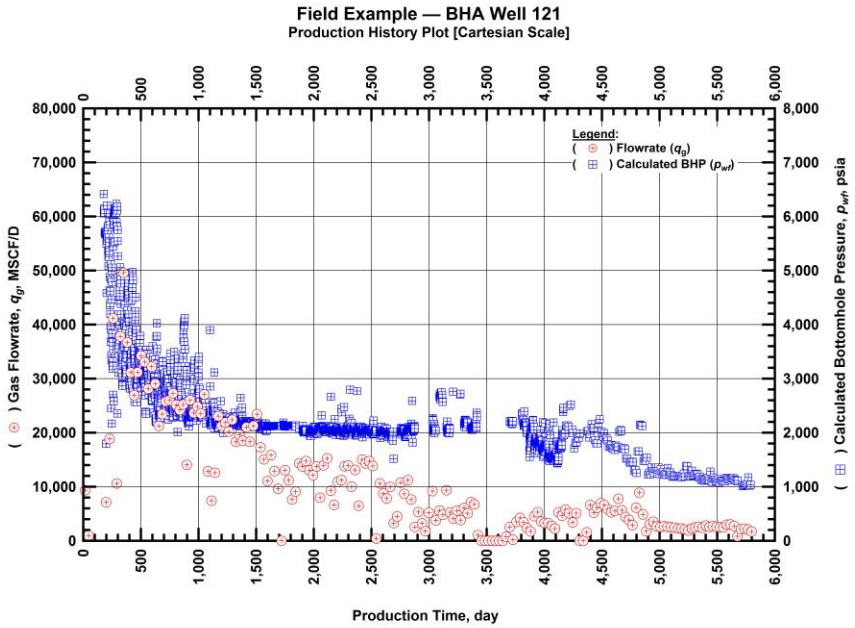

Fig. 127 — Cartesian plot for BHA Well 121 — Production history plot of calculated bottomhole pressures and gas flowrates as a function of production time.

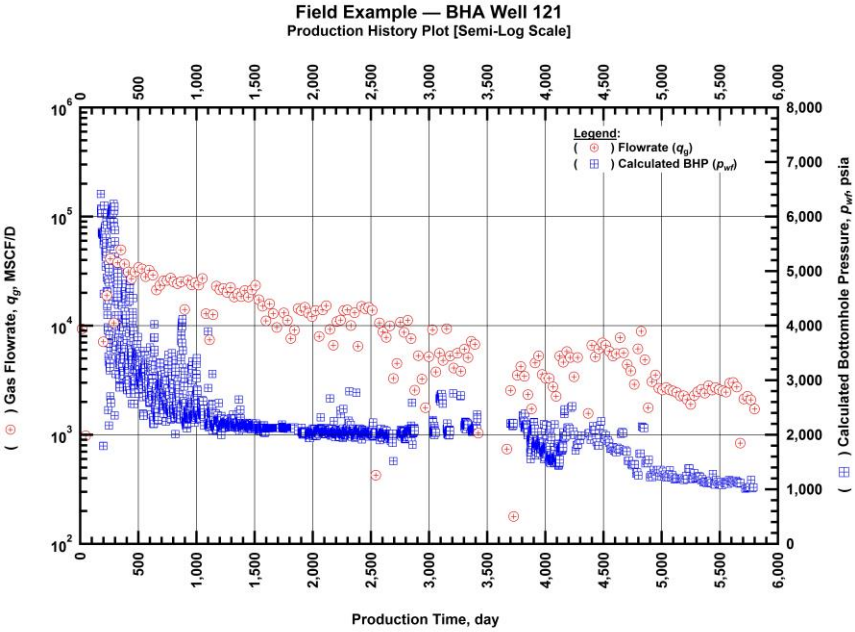

Fig. 128 — Semilog plot for BHA Well 121 — Production history plot of calculated bottomhole pressures and gas flowrates as a function of production time.

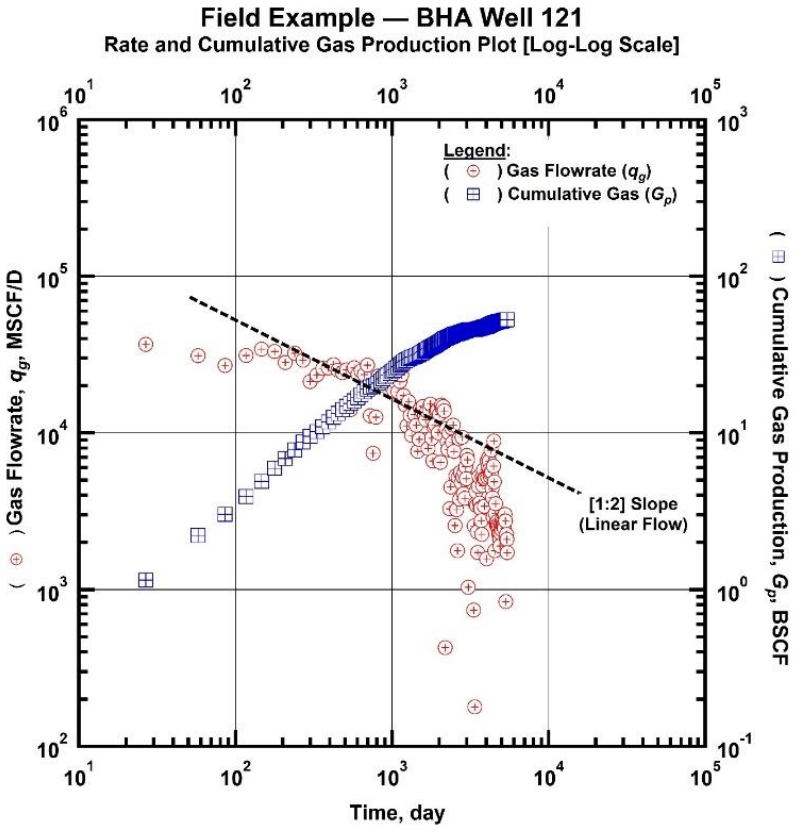

Fig. 129 — Log-Log plot for BHA Well 121 — Gas flowrate and cumulative gas production as a function of production time.

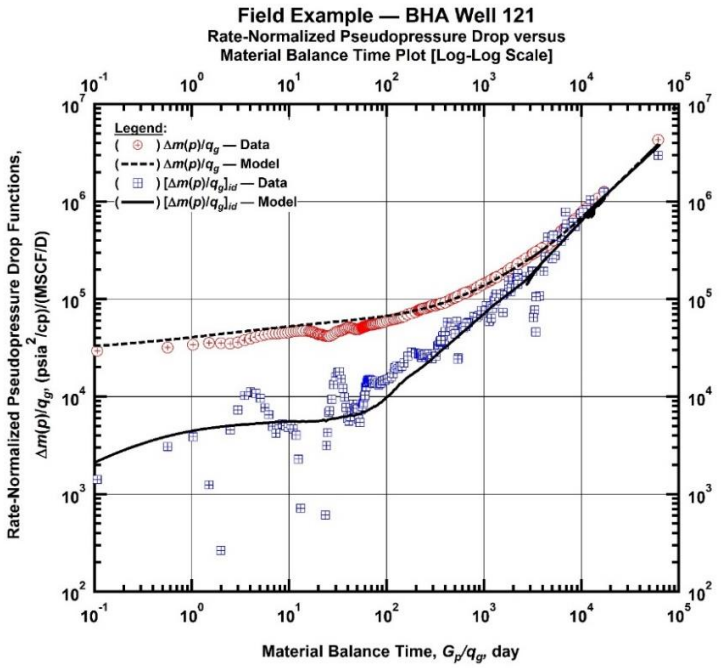

Fig. 130 — Log-Log plot for BHA Well 121 — Rate-normalized pseudopressure drop versus material balance time ("Log-Log Plot").

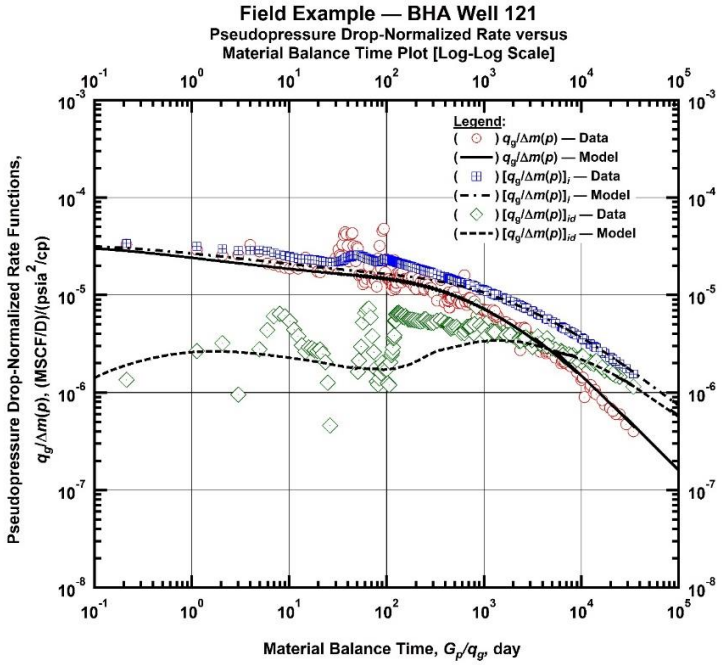

Fig. 131 — Log-Log plot for BHA Well 121 — Pseudopressure drop-normalized rate function versus material balance time ("Blasingame plot").

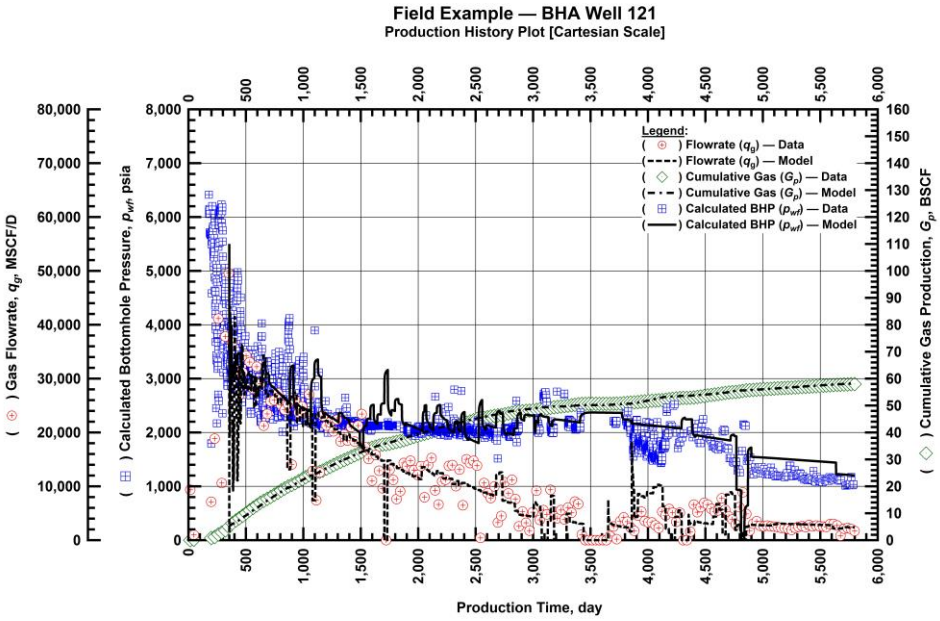

Fig. 132 — Cartesian plot for BHA Well 121 — production history and RTA history-match (gas flowrate, calculated bottomhole pressure, and cumulative gas production versus production time).

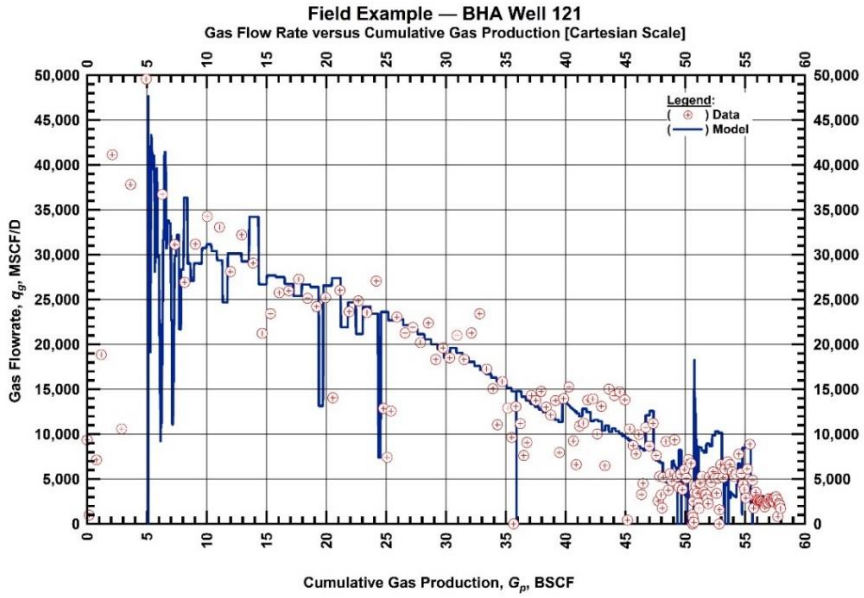

Fig. 133 — Cartesian plot for BHA Well 121 — historical and history-matched gas flowrate versus cumulative gas production.

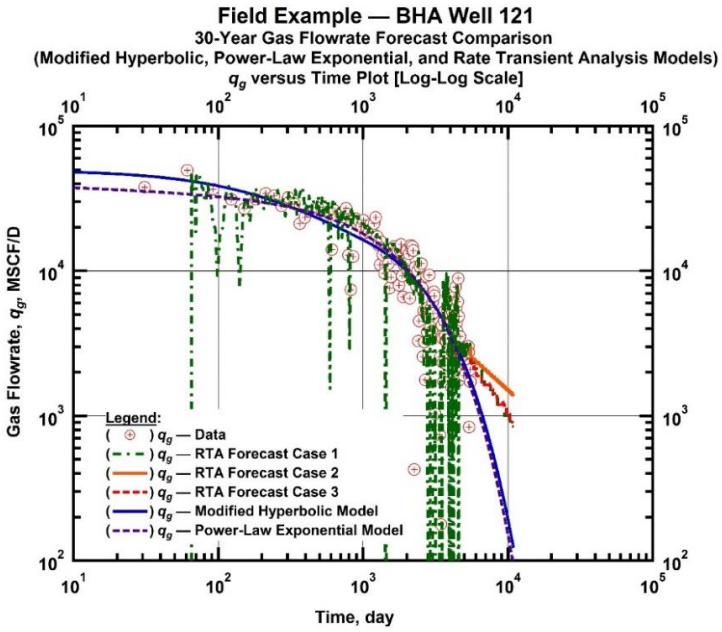

Fig. 134 — Log-Log plot for BHA Well 121 — Gas flowrate versus time for various RTA forecast cases (1, 2, 3) and Modified Hyperbolic and Power-Law Exponential time-rate models.

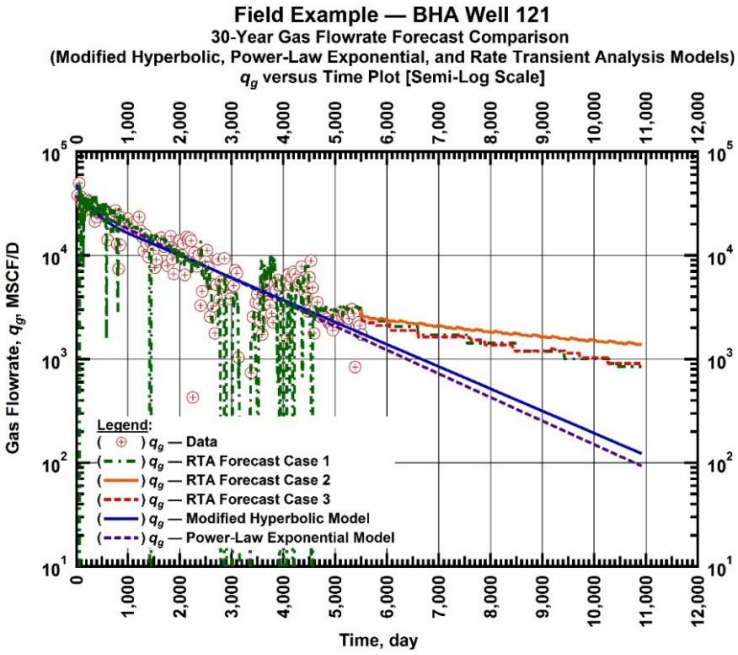

Fig. 135 — Semilog plot for BHA Well 121 — Gas flowrate versus time for various RTA forecast cases (1, 2, 3) and Modified Hyperbolic and Power-Law Exponential time-rate models.

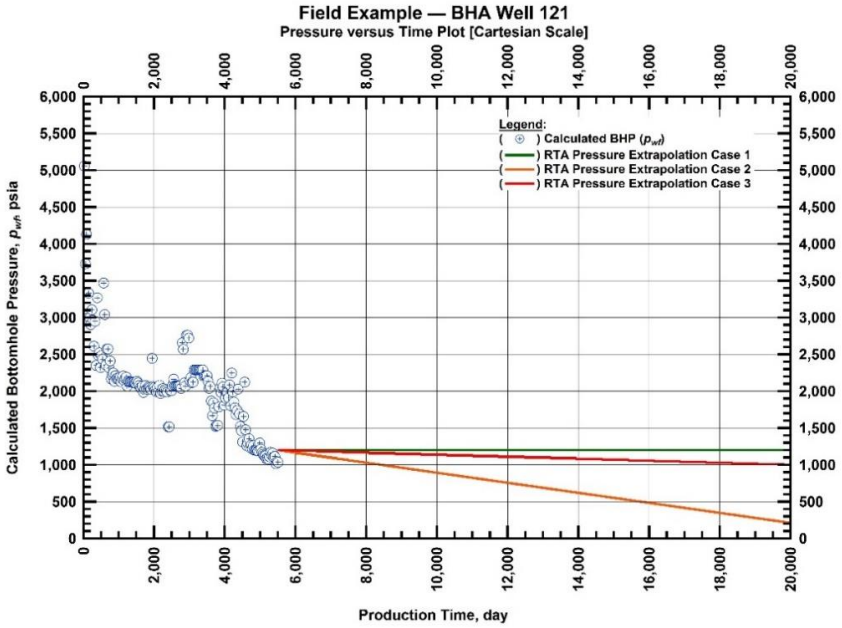

Fig. 136 — Cartesian plot for BHA Well 121 — historical and extrapolated bottomhole flowing pressures versus time (these pressure extrapolation scenarios are used for the RTA model).

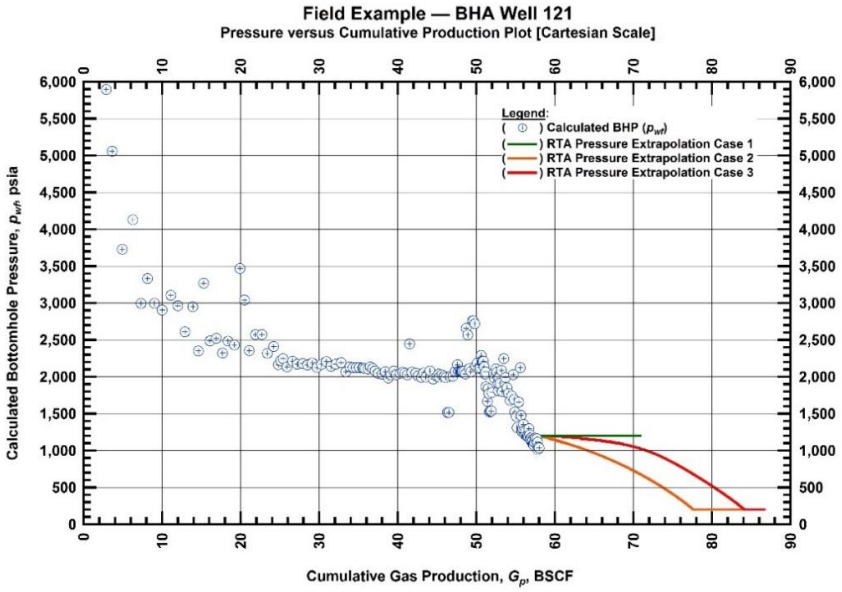

Fig. 137 — Cartesian plot for BHA Well 121 — historical and extrapolated bottomhole flowing pressures versus cumulative gas production (these pressure extrapolation scenarios are used for the RTA model).

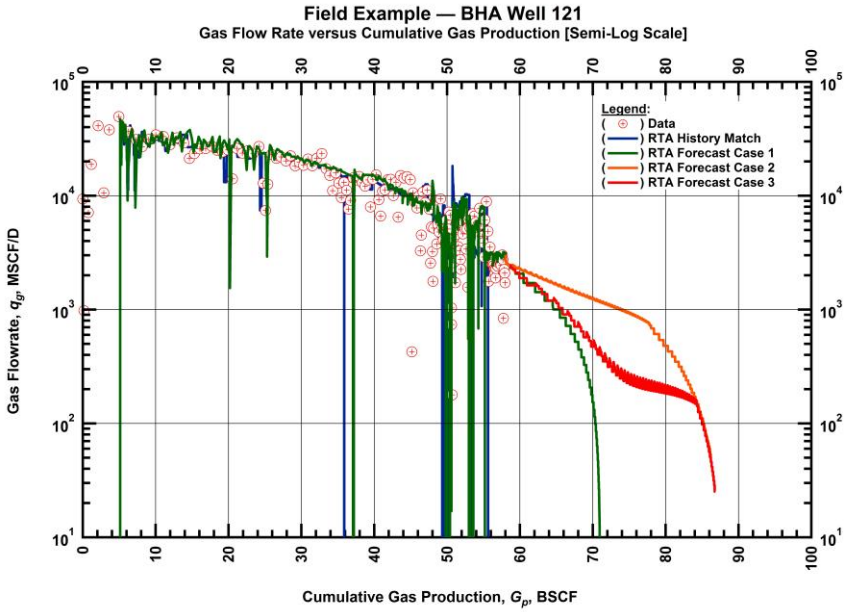

Fig. 138 — Semilog plot for BHA Well 121 — historical, history-matched, and forecasted gas flowrate versus cumulative gas production (various pressure extrapolation scenarios are prescribed (in time) for the RTA model).

Field Example — BHA Well 125

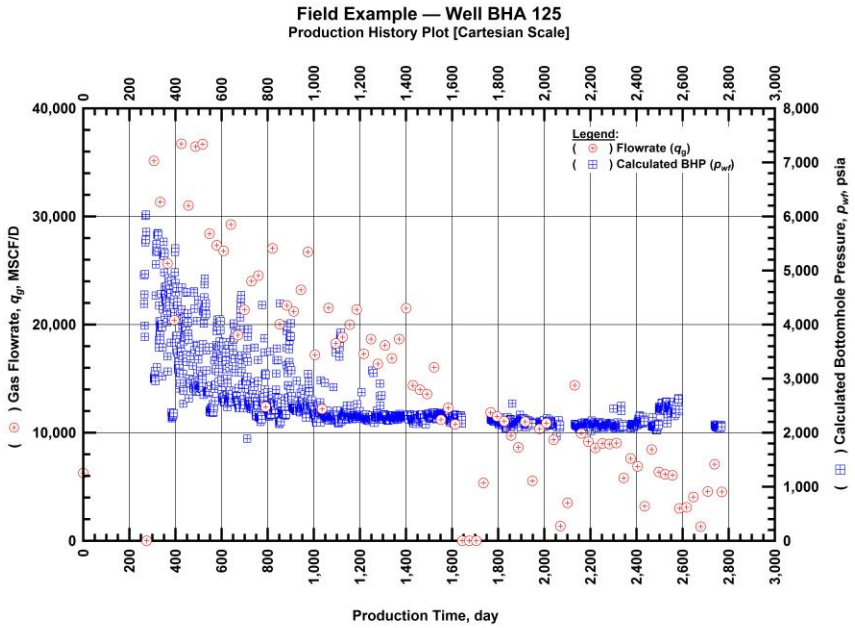

Fig. 139 — Cartesian plot for BHA Well 125 — Production history plot of calculated bottomhole pressures and gas flowrates as a function of production time.

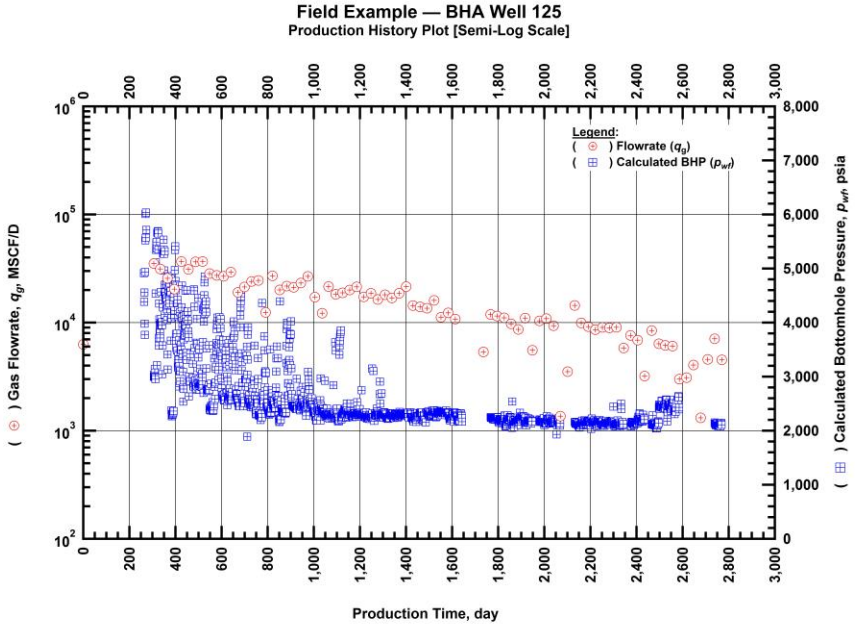

Fig. 140 — Semilog plot for BHA Well 125 — Production history plot of calculated bottomhole pressures and gas flowrates as a function of production time.

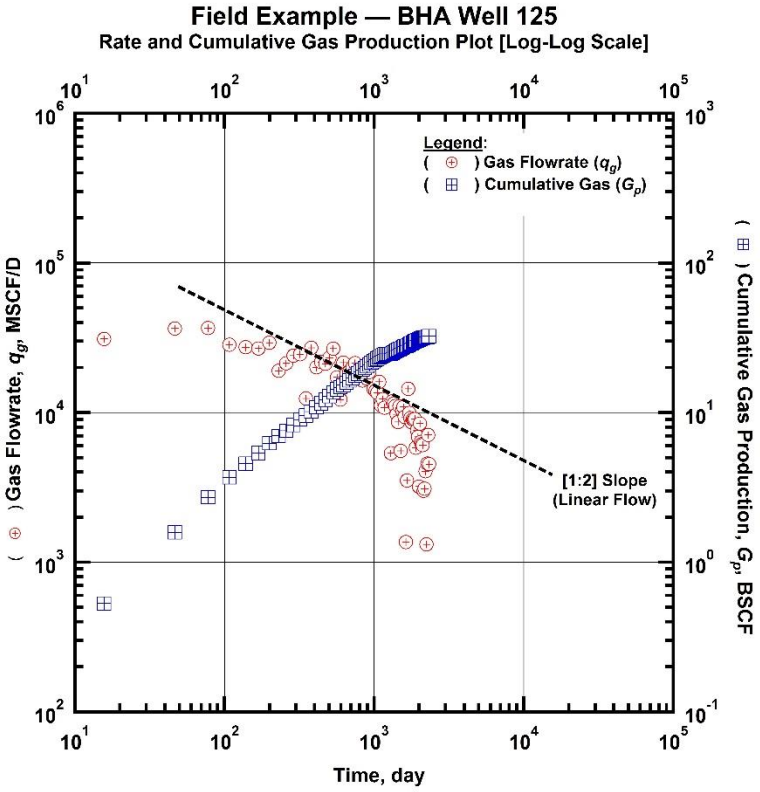

Fig. 141 — Log-Log plot for BHA Well 125 — Gas flowrate and cumulative gas production as a function of production time.

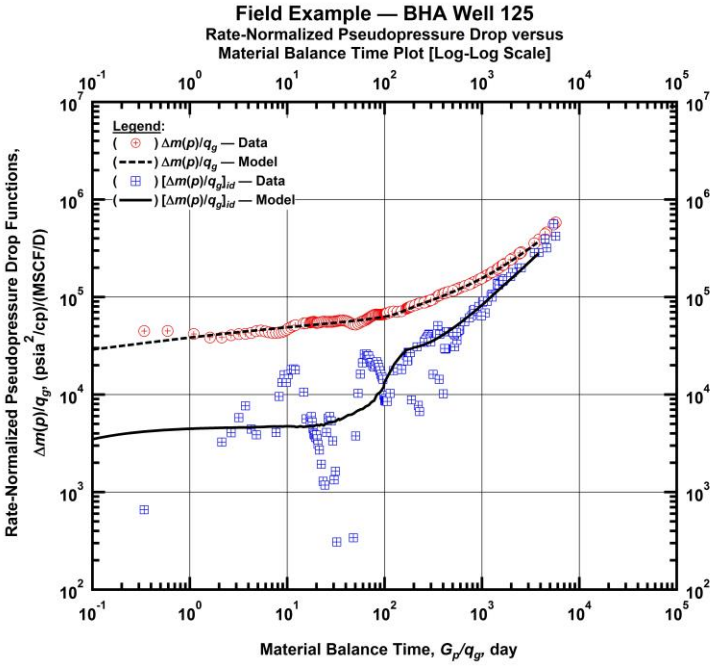

Fig. 142 — Log-Log plot for BHA Well 125 — Rate-normalized pseudopressure drop versus balance time ("Log-Log Plot").

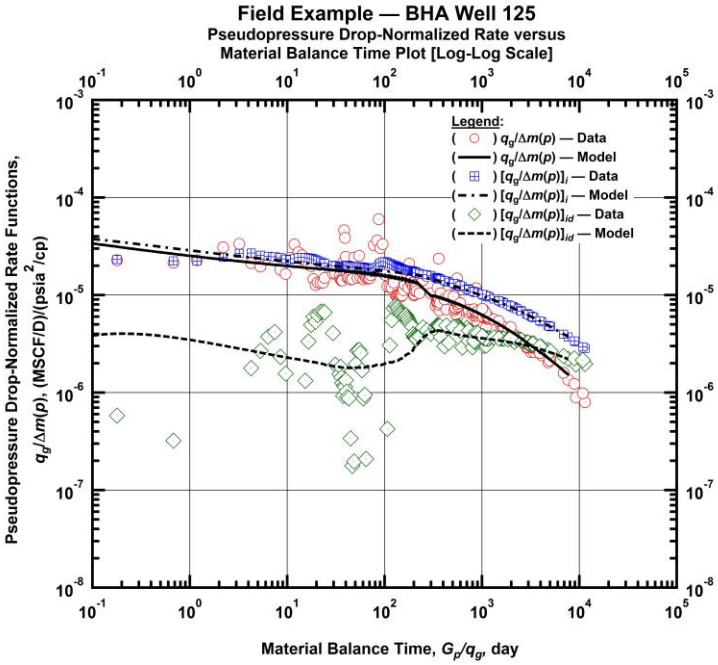

Fig. 143 — Log-Log plot for BHA Well 125 — Pseudopressure drop-normalized rate function versus material balance time ("Blasingame plot").

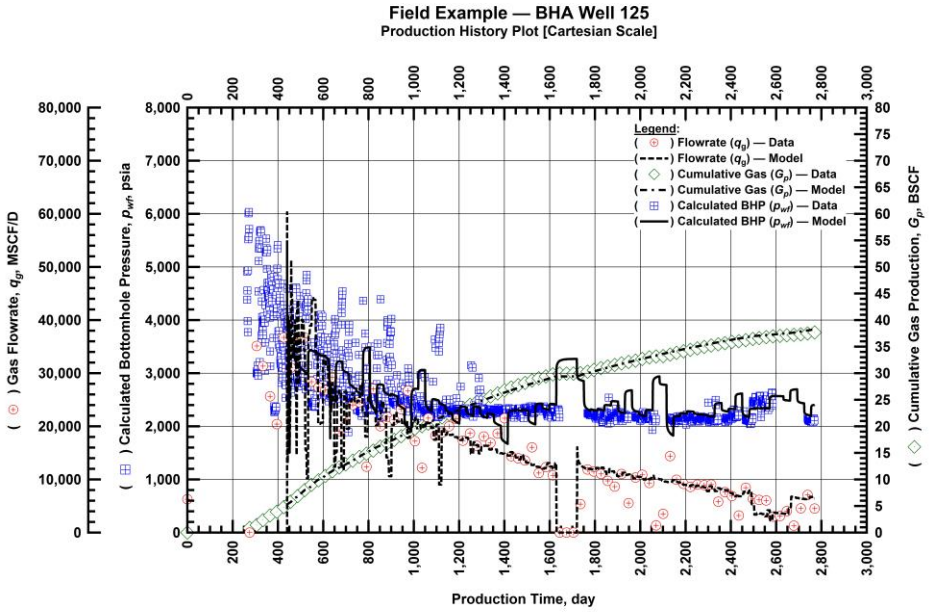

Fig. 144 — Cartesian plot for BHA Well 125 — production history and RTA history-match (gas flowrate, calculated bottomhole pressure, and cumulative gas production versus. production time).

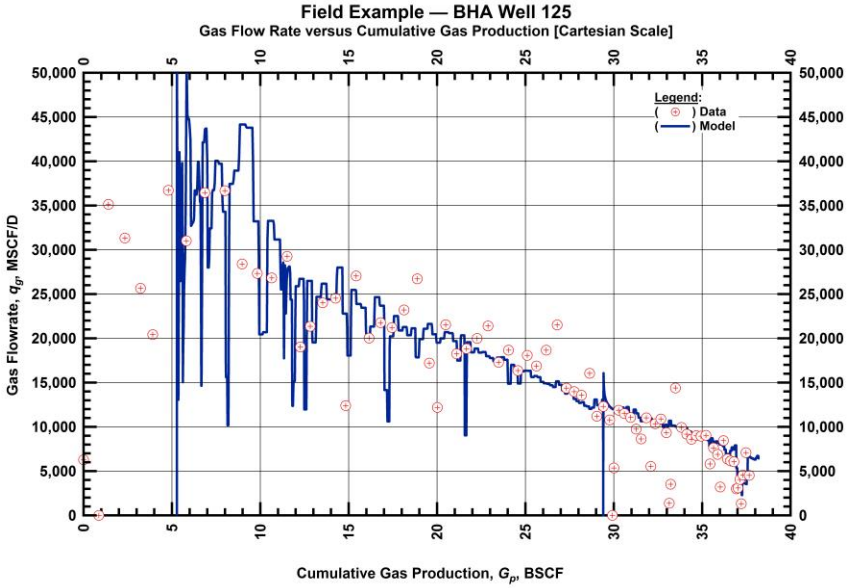

Fig. 145 — Cartesian plot for BHA Well 125 — historical and history-matched gas flowrate versus cumulative gas production.

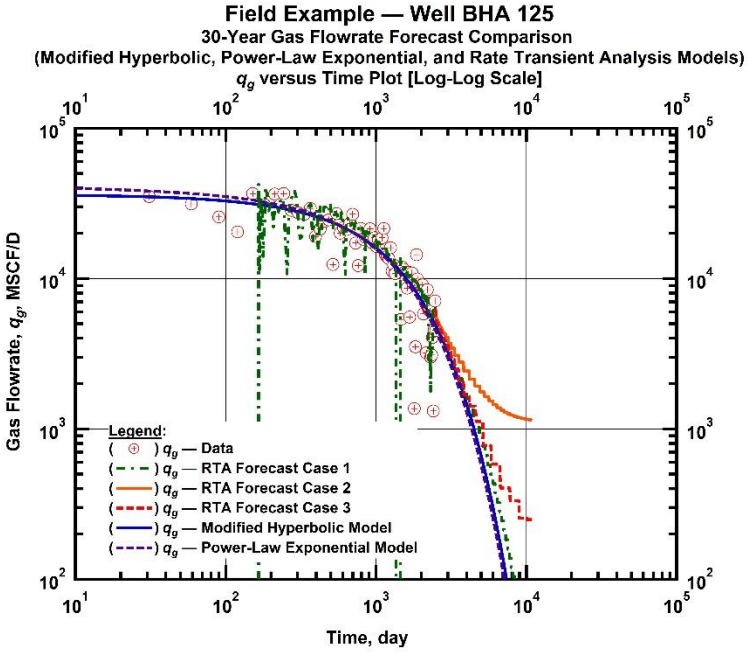

Fig. 146 — Log-Log plot for BHA Well 125 — Gas flowrate versus time for various RTA forecast cases (1, 2, 3) and Modified Hyperbolic and Power-Law Exponential time-rate models.

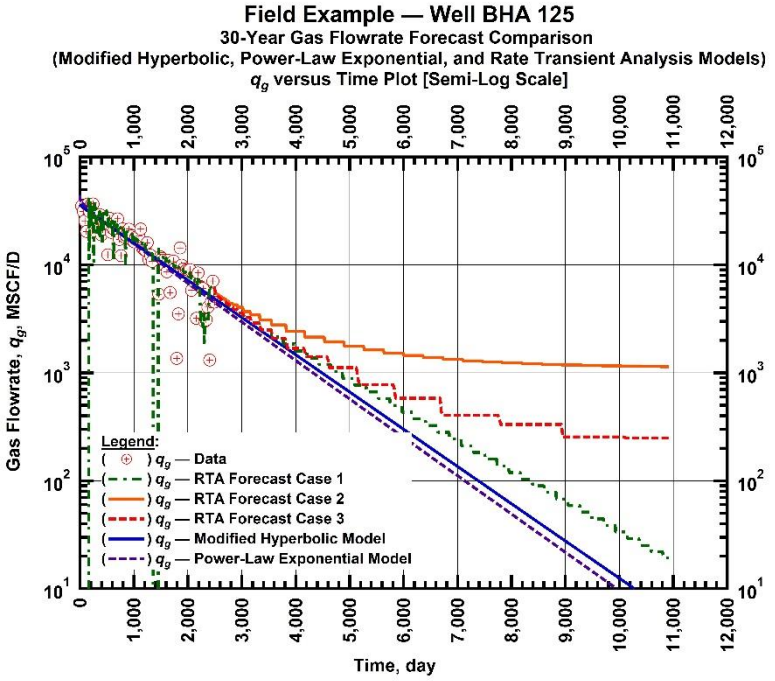

Fig. 147 — Semilog plot for BHA Well 125 — Gas flowrate versus time for various RTA forecast cases (1, 2, 3) and Modified Hyperbolic and Power-Law Exponential time-rate models.

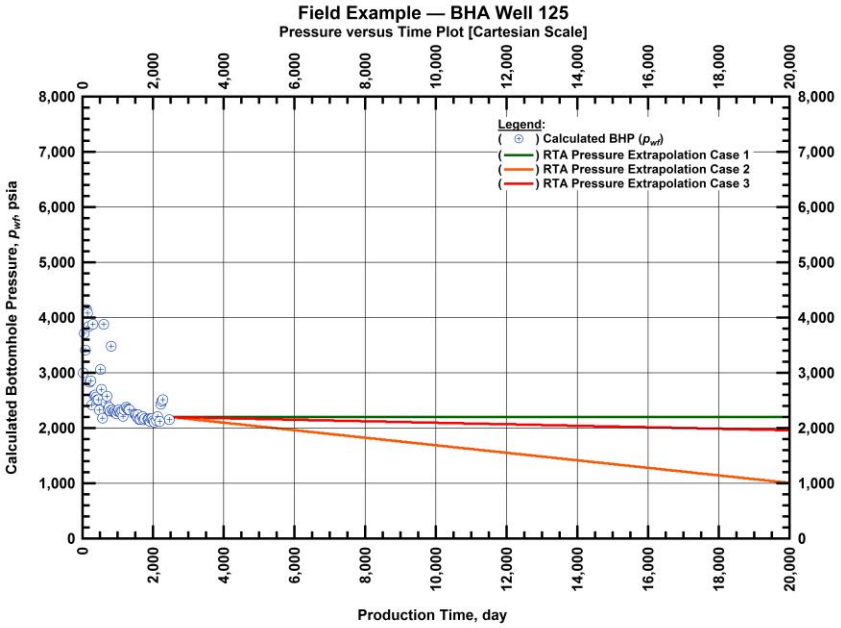

Fig. 148 — Cartesian plot for BHA Well 125 — historical and extrapolated bottomhole flowing pressures versus time (these pressure extrapolation scenarios are used for the RTA model).

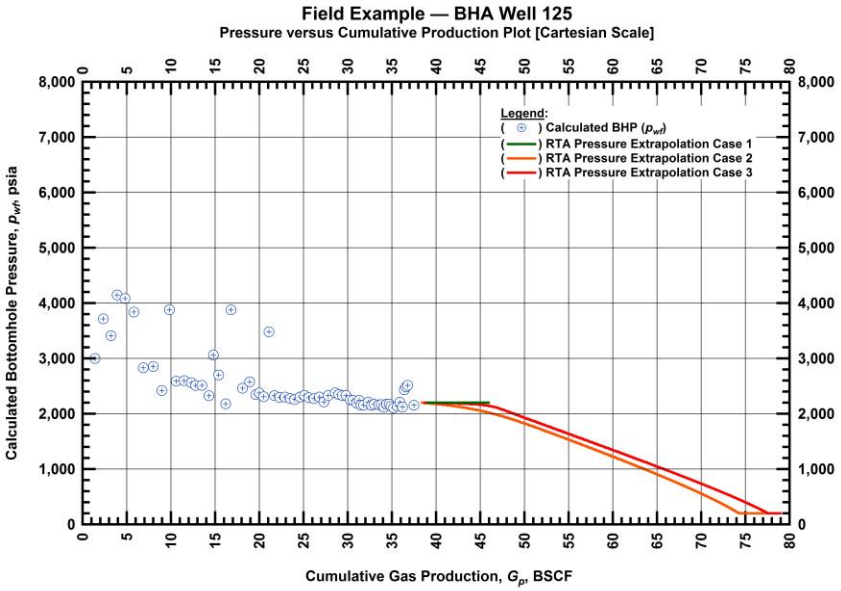

Fig. 149 — Cartesian plot for BHA Well 125 — historical and extrapolated bottomhole flowing pressures versus cumulative gas production (these pressure extrapolation scenarios are used for the RTA model).

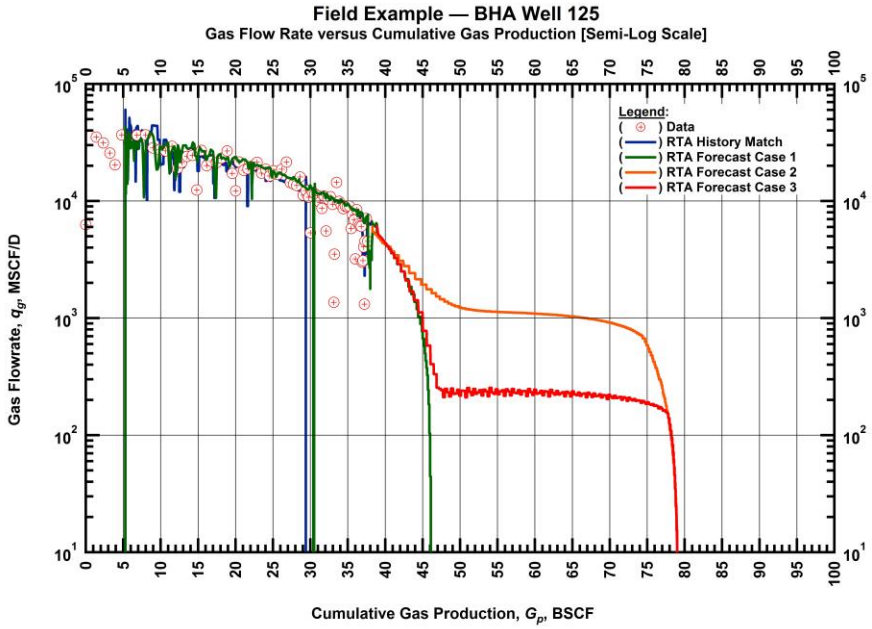

Fig. 150 — Semilog plot for BHA Well 125 — historical, history-matched, and forecasted gas flowrate versus cumulative gas production (various pressure extrapolation scenarios are prescribed (in time) for the RTA model).

Field Example — BHA Well 128

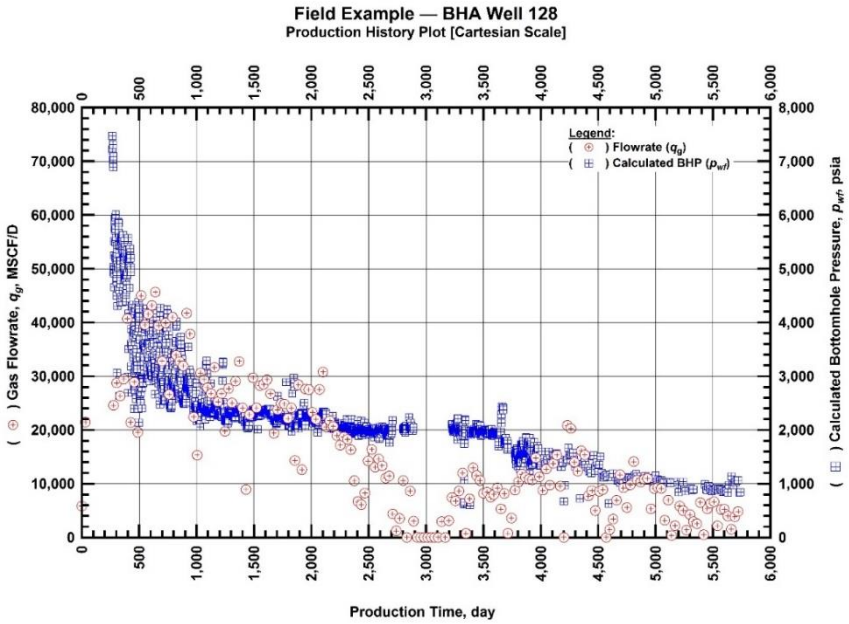

Fig. 151 — Cartesian plot for BHA Well 128 — Production history plot of calculated bottomhole pressures and gas flowrates as a function of production time.

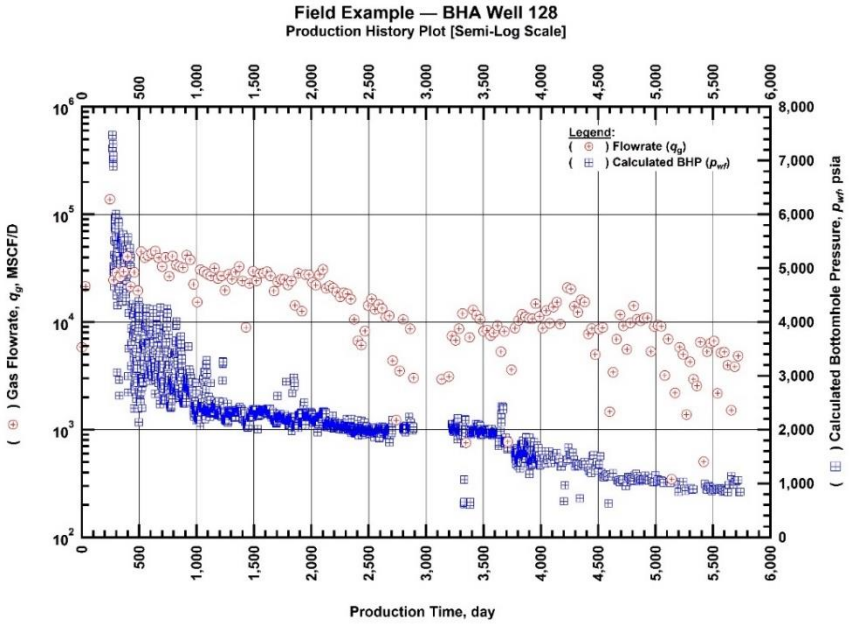

Fig. 152 — Semilog plot for BHA Well 128 — Production history plot of calculated bottomhole pressures and gas flowrates as a function of production time.

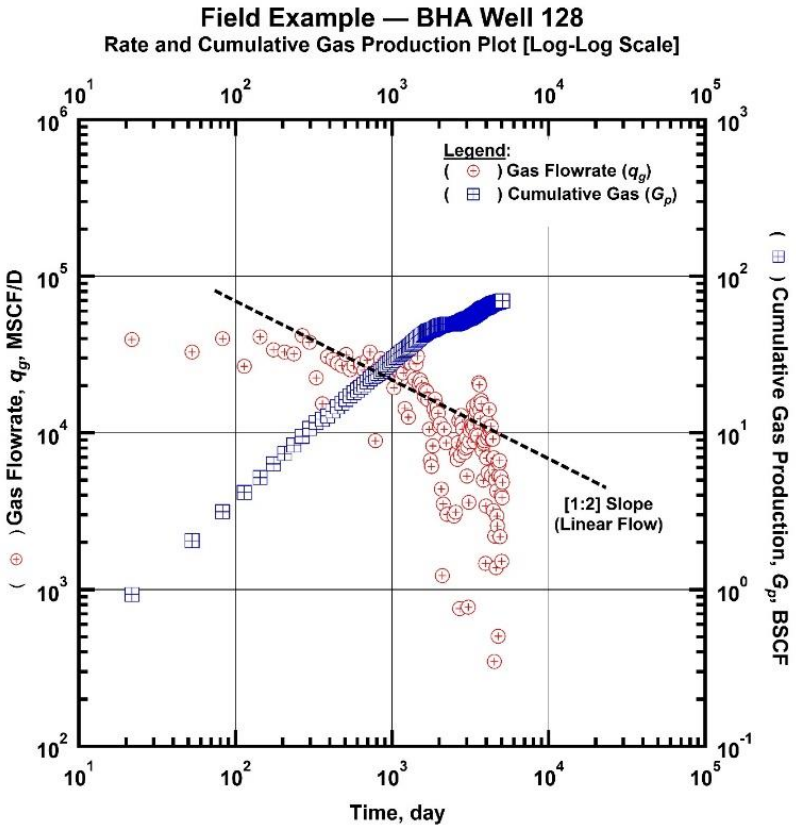

Fig. 153 — Log-Log plot for BHA Well 128 — Gas flowrate and cumulative gas production as a function of production time.

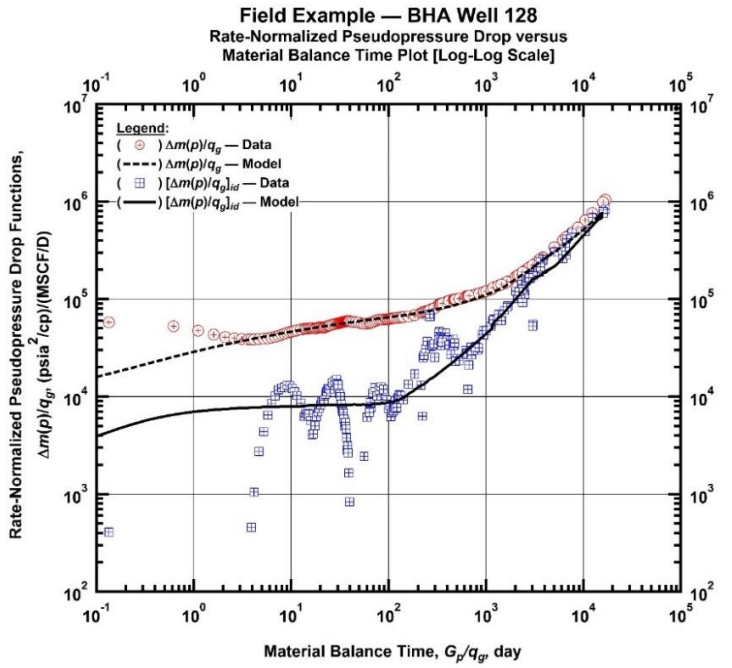

Fig. 154 — Log-Log plot for BHA Well 128 — Rate-normalized pseudopressure drop versus material balance time ("Log-Log Plot").

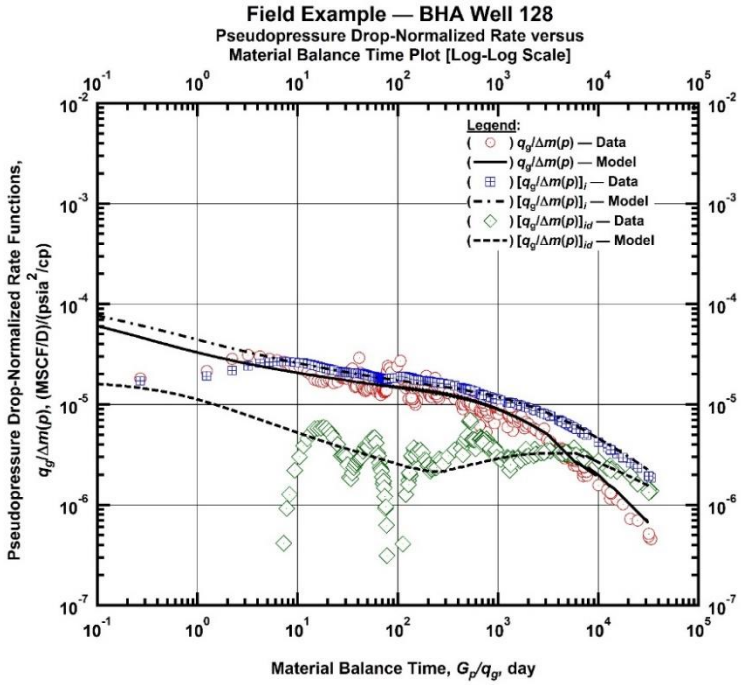

Fig. 155 — Log-Log plot for BHA Well 128 — Pseudopressure drop-normalized rate function versus material balance time ("Blasingame plot").

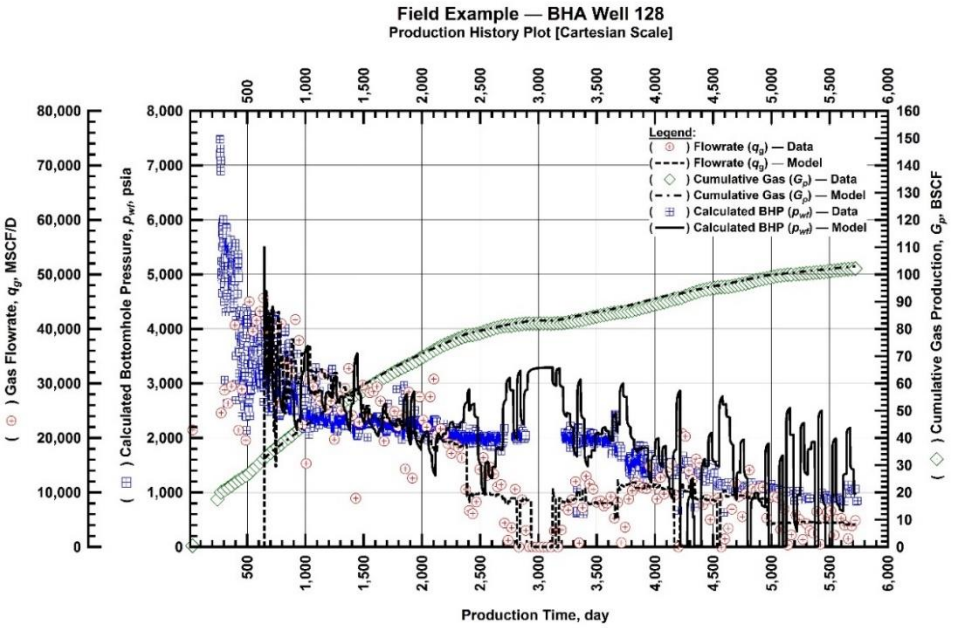

Fig. 156 — Cartesian plot for BHA Well 128 — production history and RTA history-match (gas flowrate, calculated bottomhole pressure, and cumulative gas production versus production time).

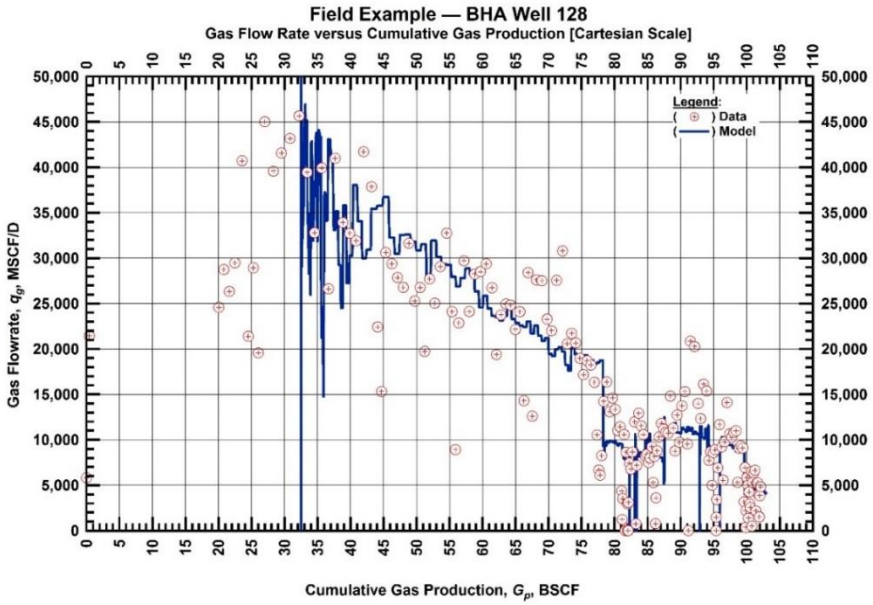

Fig. 157 — Cartesian plot for BHA Well 128 — historical and history-matched gas flowrate versus cumulative gas production.

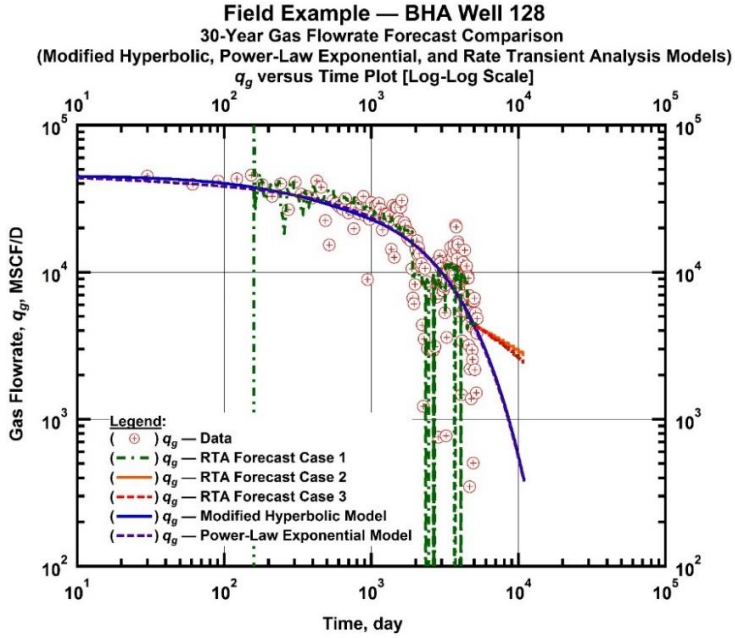

Fig. 158 — Log-Log plot for BHA Well 128 — Gas flowrate versus time for various RTA forecast cases (1, 2, 3) and Modified Hyperbolic and Power-Law Exponential time-rate models.

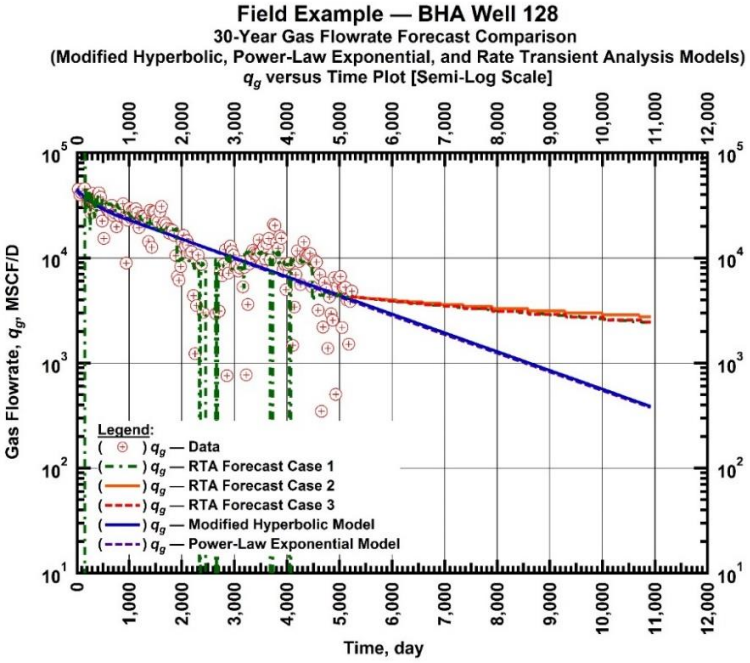

Fig. 159 — Semilog plot for BHA Well 128 — Gas flowrate versus time for various RTA forecast cases (1, 2, 3) and Modified Hyperbolic and Power-Law Exponential time-rate models.

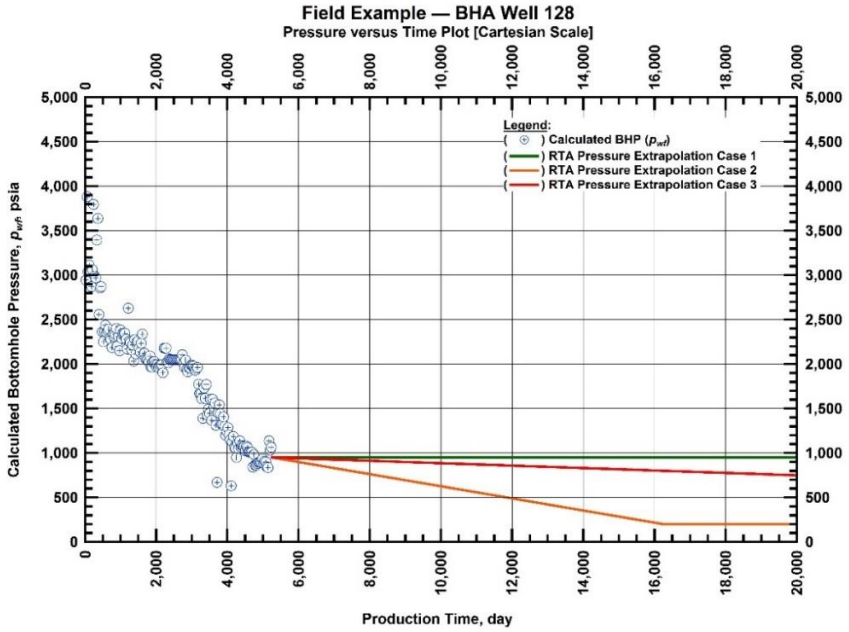

Fig. 160 — Cartesian plot for BHA Well 128 — historical and extrapolated bottomhole flowing pressures versus time (these pressure extrapolation scenarios are used for the RTA model).

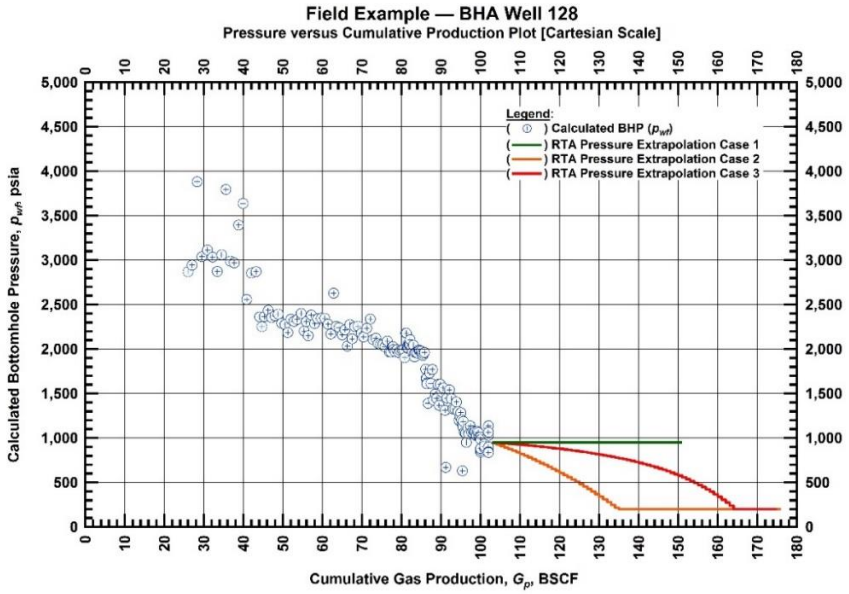

Fig. 161 — Cartesian plot for BHA Well 128 — historical and extrapolated bottomhole flowing pressures versus cumulative gas production (these pressure extrapolation scenarios are used for the RTA model).

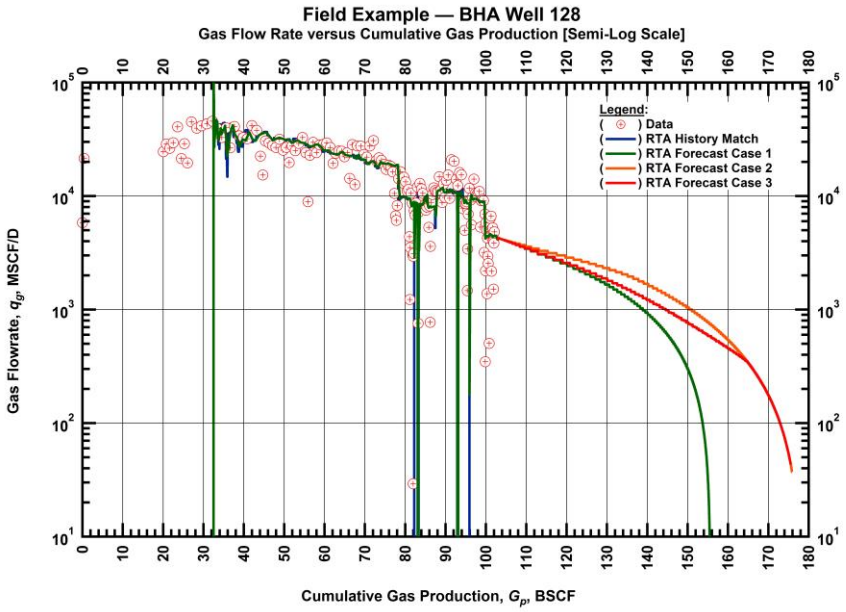

Fig. 162 — Semilog plot for BHA Well 128 — historical, history-matched, and forecasted gas flowrate versus cumulative gas production (various pressure extrapolation scenarios are prescribed (in time) for the RTA model).

Field Example — BHA Well 131

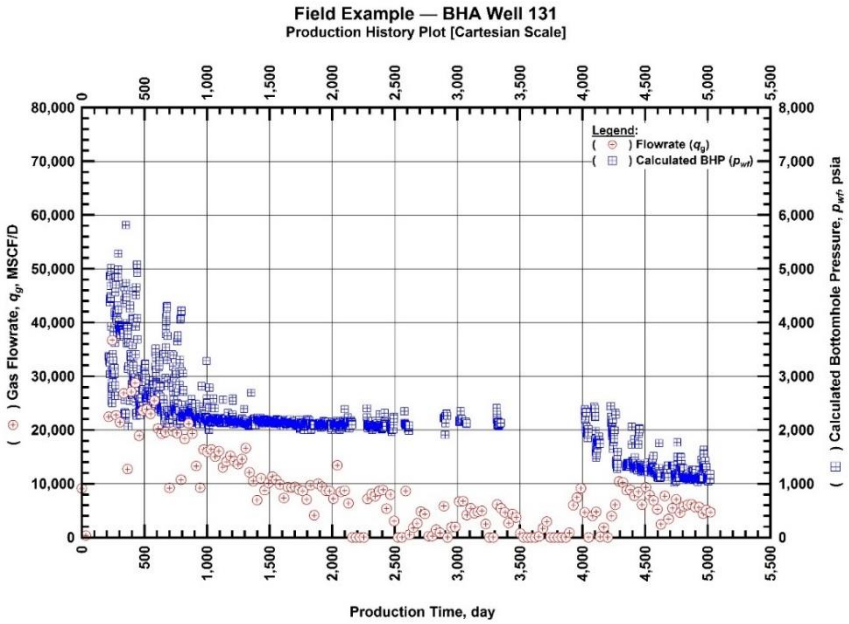

Fig. 163 — Cartesian plot for BHA Well 131 — Production history plot of calculated bottomhole pressures and gas flowrates as a function of production time.

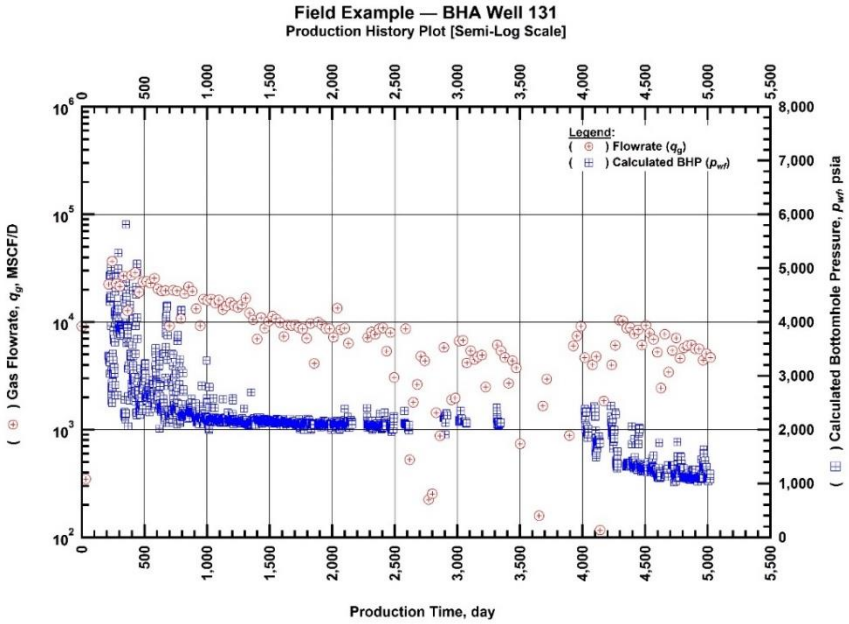

Fig. 164 — Semilog plot for BHA Well 131 — Production history plot of calculated bottomhole pressures and gas flowrates as a function of production time.

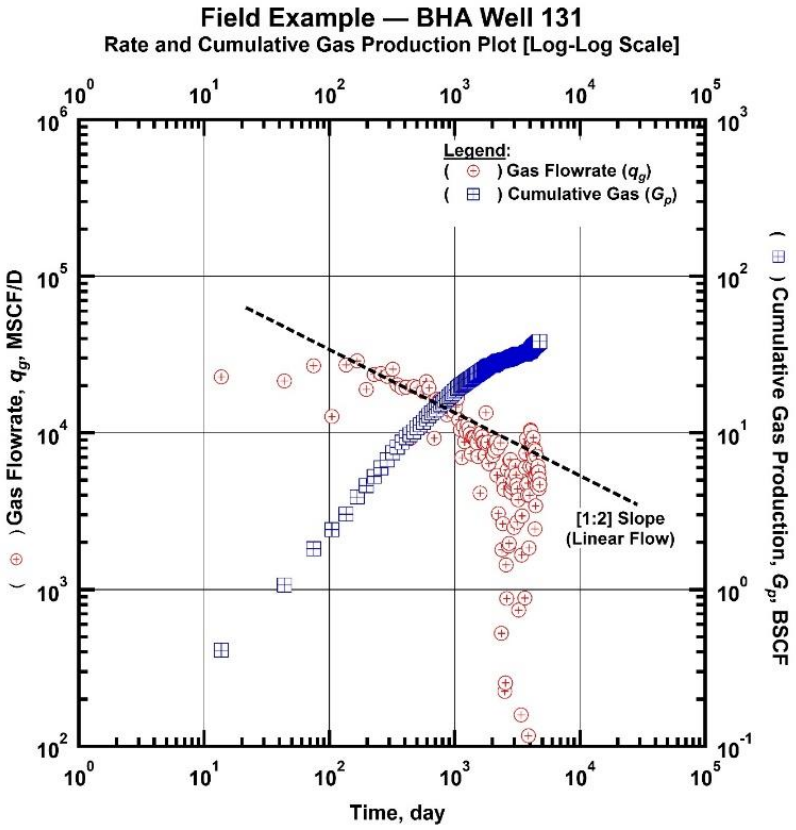

Fig. 165 — Log-Log plot for BHA Well 131 — Gas flowrate and cumulative gas production as a function of production time.

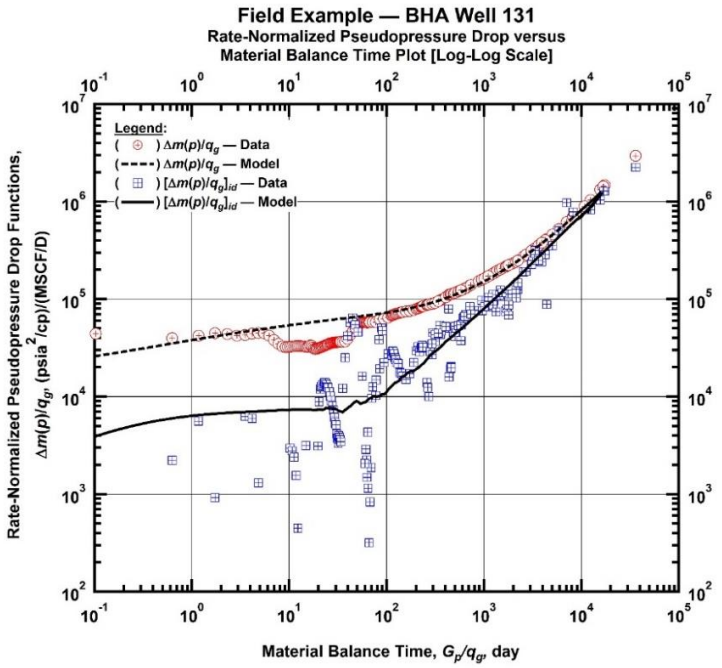

Fig. 166 — Log-Log plot for BHA Well 131 — Rate-normalized pseudopressure drop versus material balance time ("Log-Log Plot").

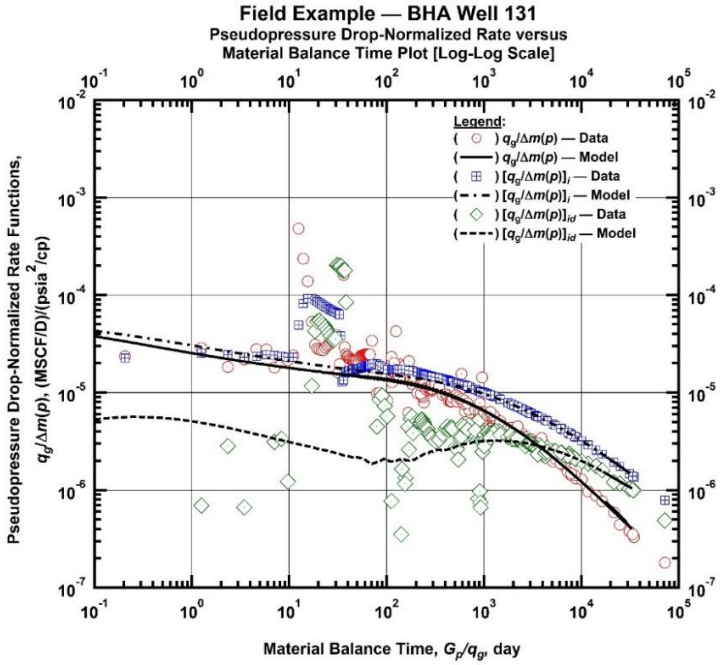

Fig. 167 — Log-Log plot for BHA Well 131 — Pseudopressure drop-normalized rate function versus material balance time ("Blasingame plot").

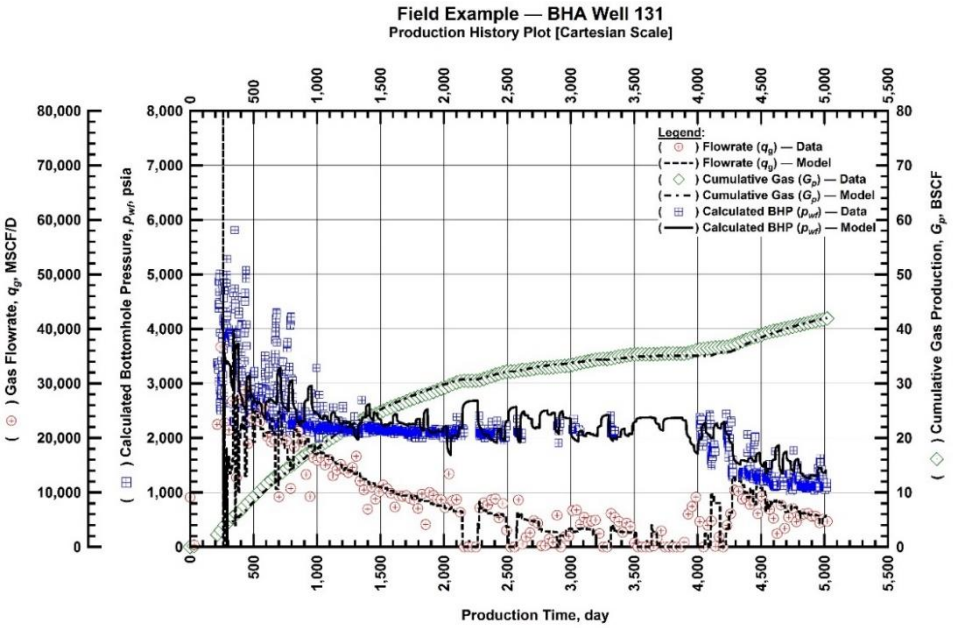

Fig. 168 — Cartesian plot for BHA Well 131 — production history and RTA history-match (gas flowrate, calculated bottomhole pressure, and cumulative gas production versus production time).

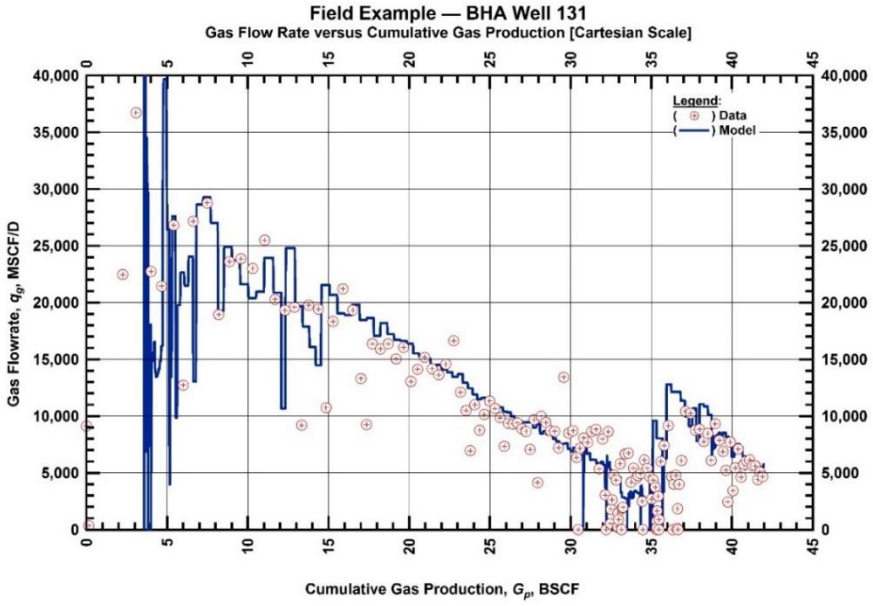

Fig. 169 — Cartesian plot for BHA Well 131 — historical and history-matched gas flowrate versus cumulative gas production.

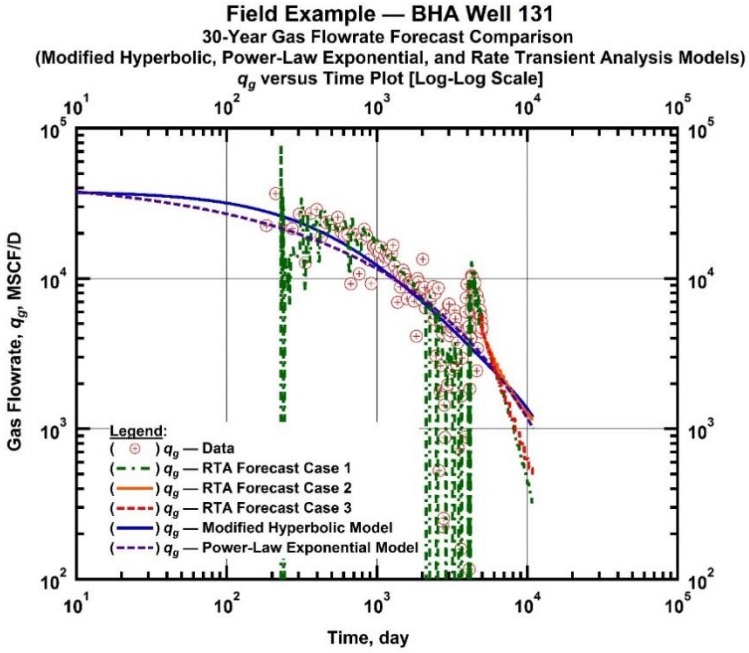

Fig. 170 — Log-Log plot for BHA Well 131 — Gas flowrate versus time for various RTA forecast cases (1, 2, 3) and Modified Hyperbolic and Power-Law Exponential time-rate models.

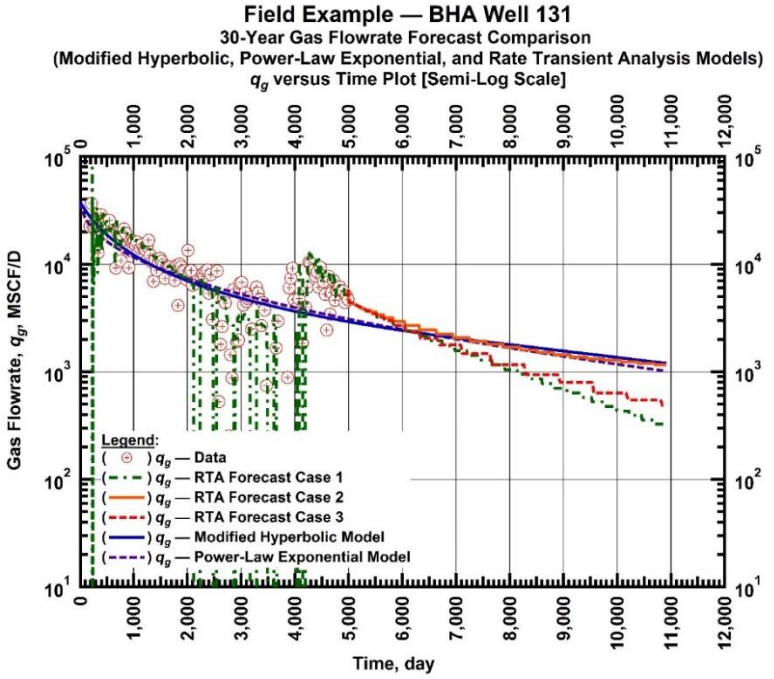

Fig. 171 — Semilog plot for BHA Well 131 — Gas flowrate versus time for various RTA forecast cases (1, 2, 3) and Modified Hyperbolic and Power-Law Exponential time-rate models.

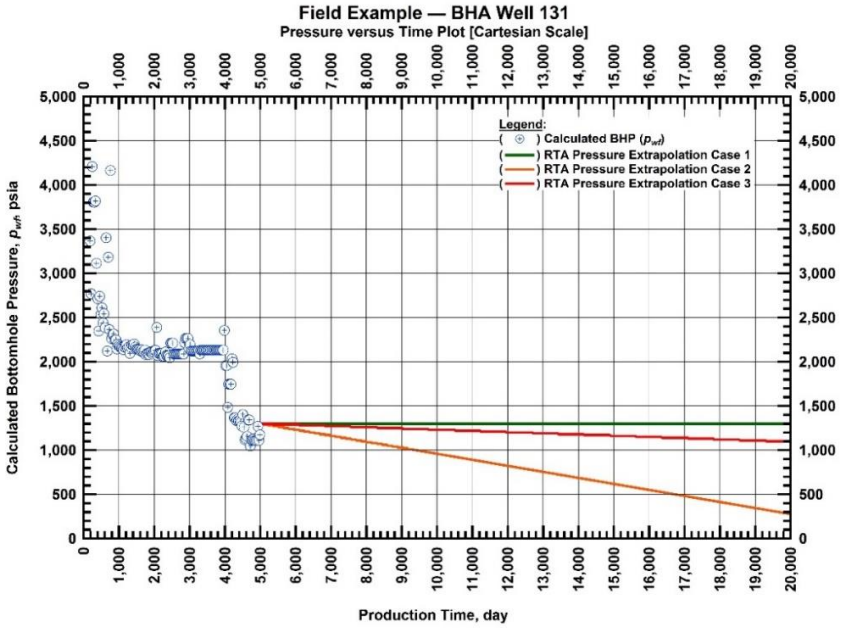

Fig. 172 — Cartesian plot for BHA Well 131 — historical and extrapolated bottomhole flowing pressures versus time (these pressure extrapolation scenarios are used for the RTA model).

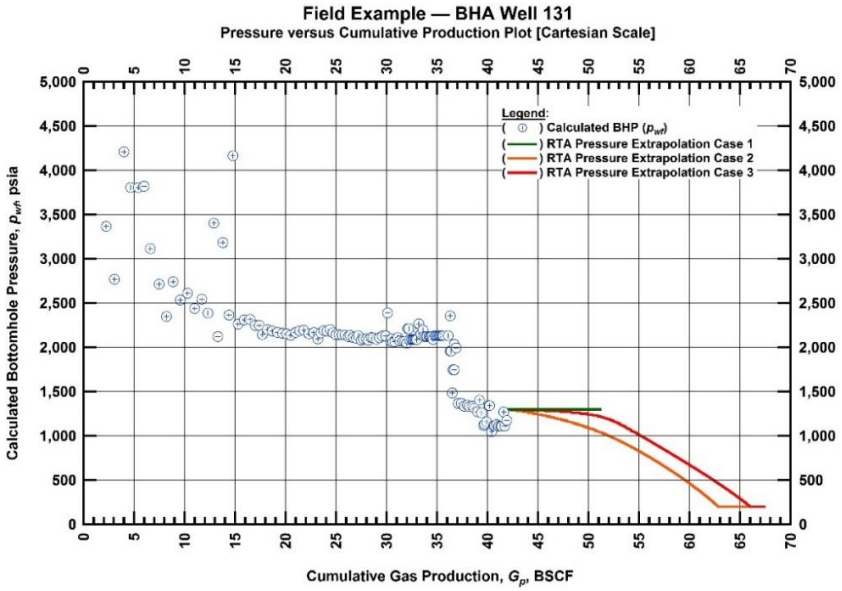

Fig. 173 — Cartesian plot for BHA Well 131 — historical and extrapolated bottomhole flowing pressures versus cumulative gas production (these pressure extrapolation scenarios are used for the RTA model).

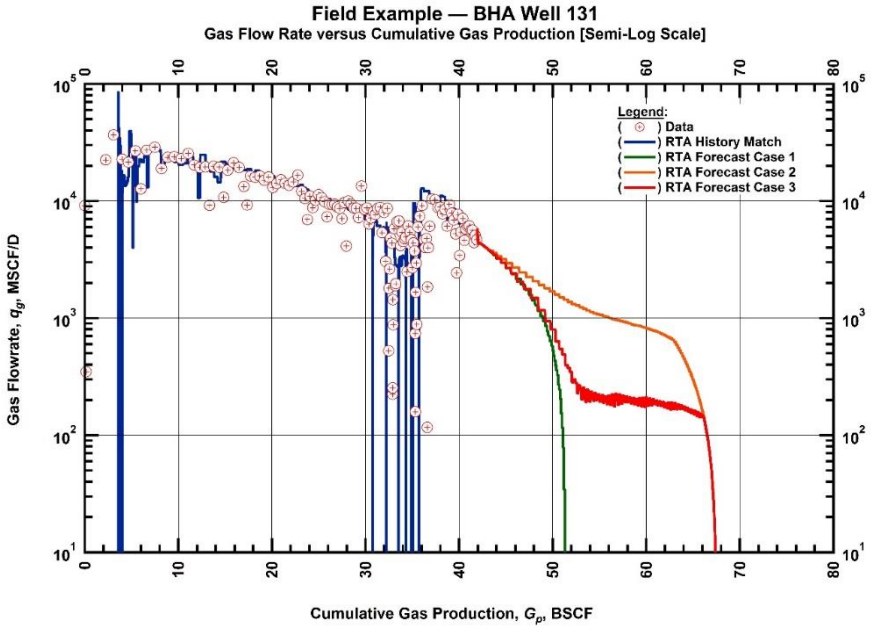

Fig. 174 — Semilog plot for BHA Well 131 — historical, history-matched, and forecasted gas flowrate versus cumulative gas production (various pressure extrapolation scenarios are prescribed (in time) for the RTA model).

Field Example — BHA Well 134

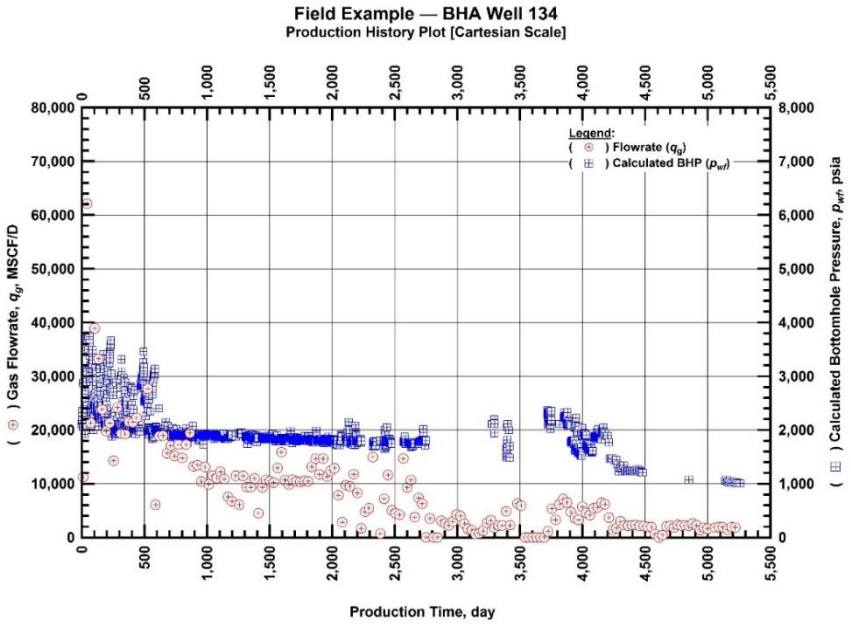

Fig. 175 — Cartesian plot for BHA Well 134 — Production history plot of calculated bottomhole pressures and gas flowrates as a function of production time.

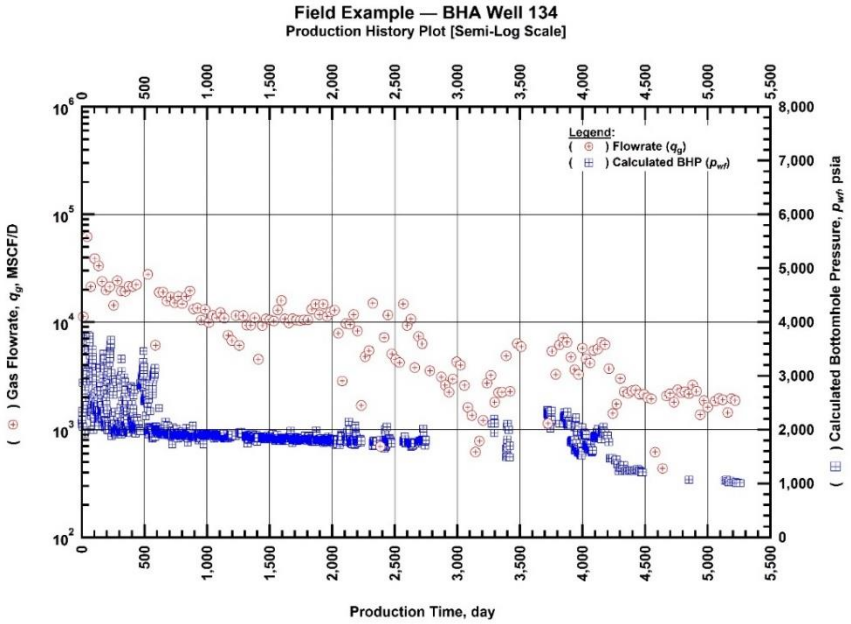

Fig. 176 — Semilog plot for BHA Well 134 — Production history plot of calculated bottomhole pressures and gas flowrates as a function of production time.

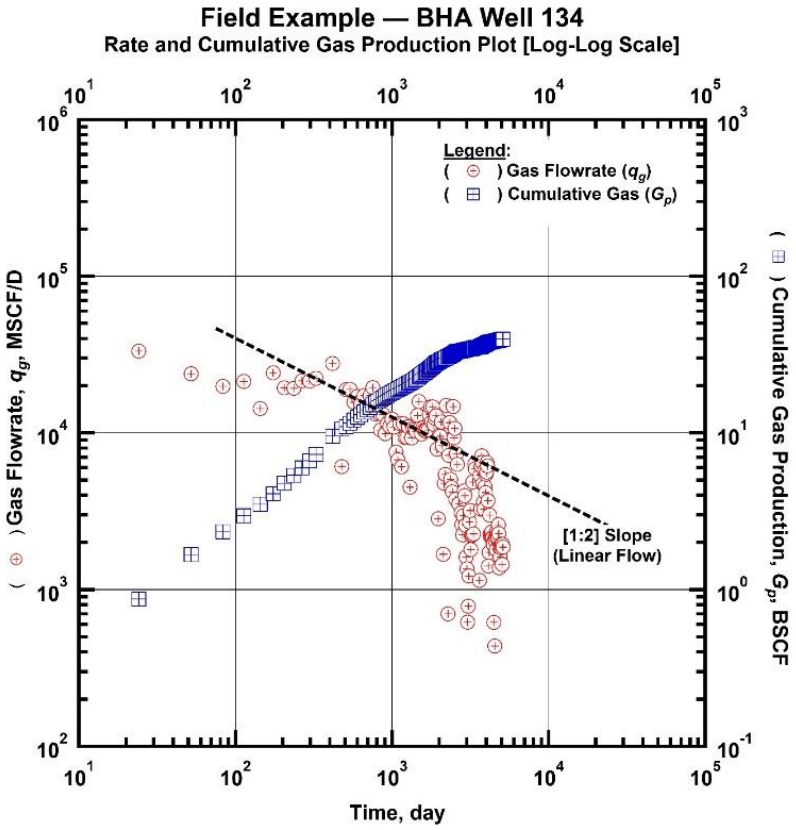

Fig. 177 — Log-Log plot for BHA Well 134 — Gas flowrate and cumulative gas production as a function of production time.

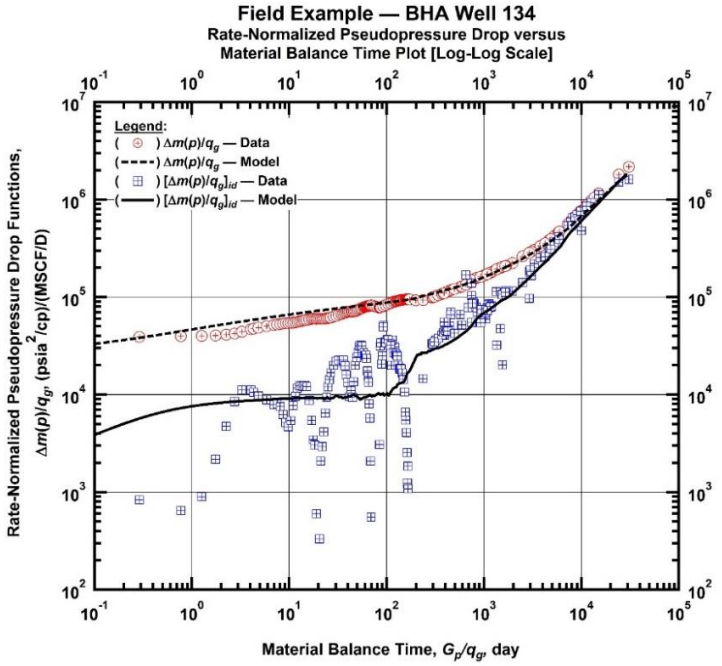

Fig. 178 — Log-Log plot for BHA Well 134 — Rate-normalized pseudopressure drop versus material balance time ("Log-Log Plot").

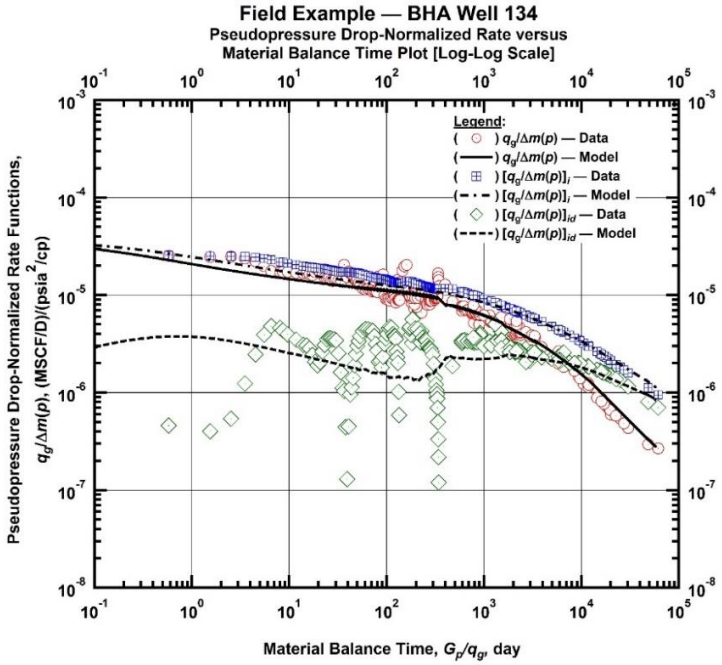

Fig. 179 — Log-Log plot for BHA Well 134 — Pseudopressure drop-normalized rate function versus material balance time ("Blasingame plot").

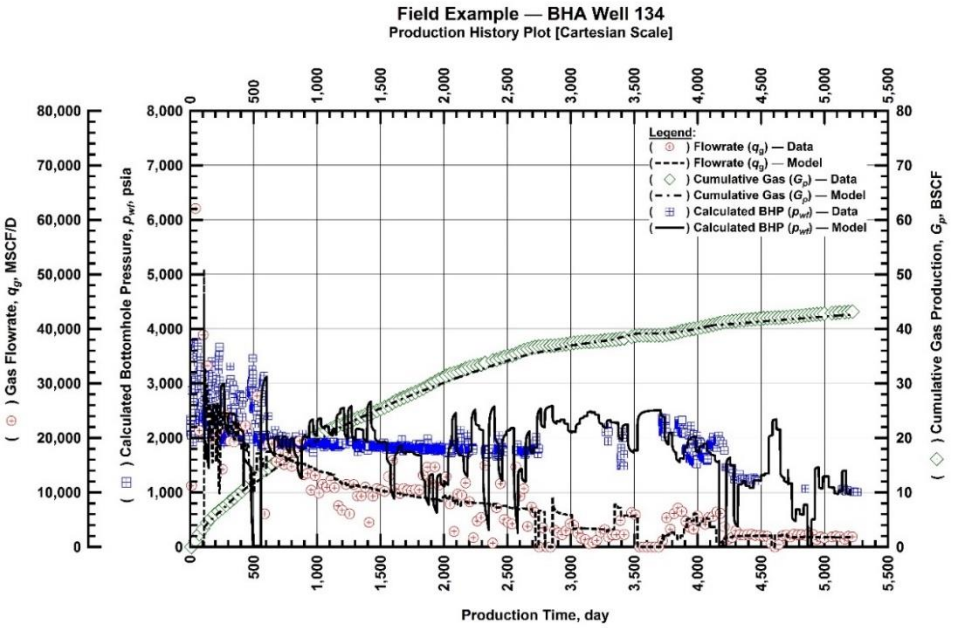

Fig. 180 — Cartesian plot for BHA Well 134 — production history and RTA history-match (gas flowrate, calculated bottomhole pressure, and cumulative gas production versus production time).

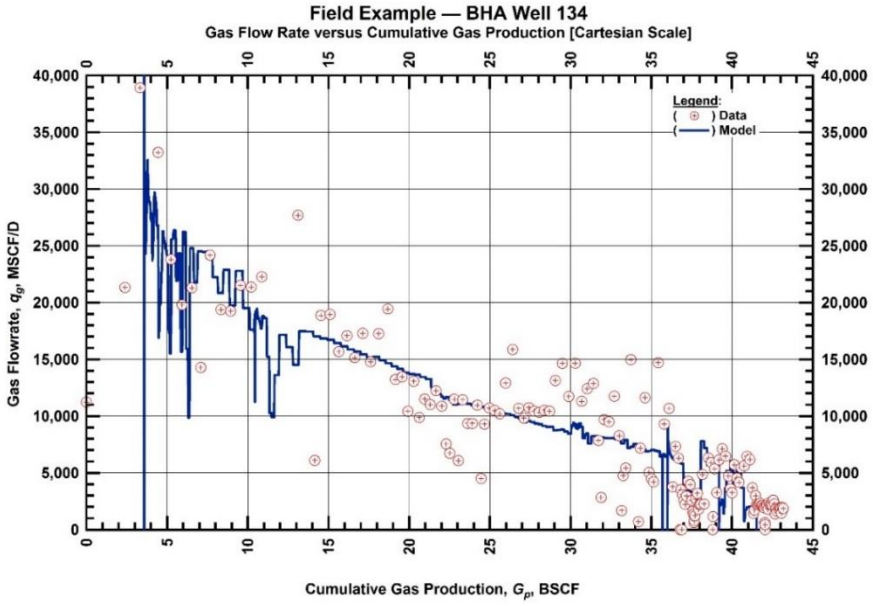

Fig. 181 — Cartesian plot for BHA Well 134 — historical and history-matched gas flowrate versus cumulative gas production.

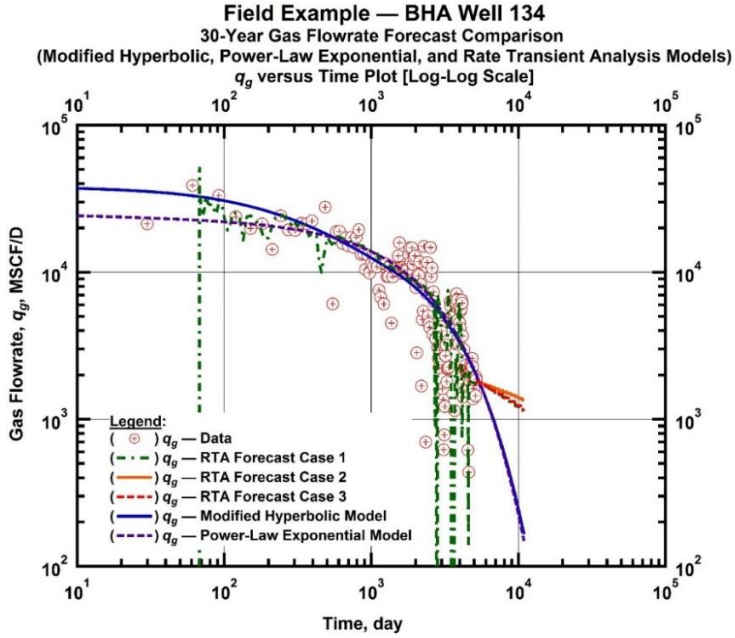

Fig. 182 — Log-Log plot for BHA Well 134 — Gas flowrate versus time for various RTA forecast cases (1, 2, 3) and Modified Hyperbolic and Power-Law Exponential time-rate models.

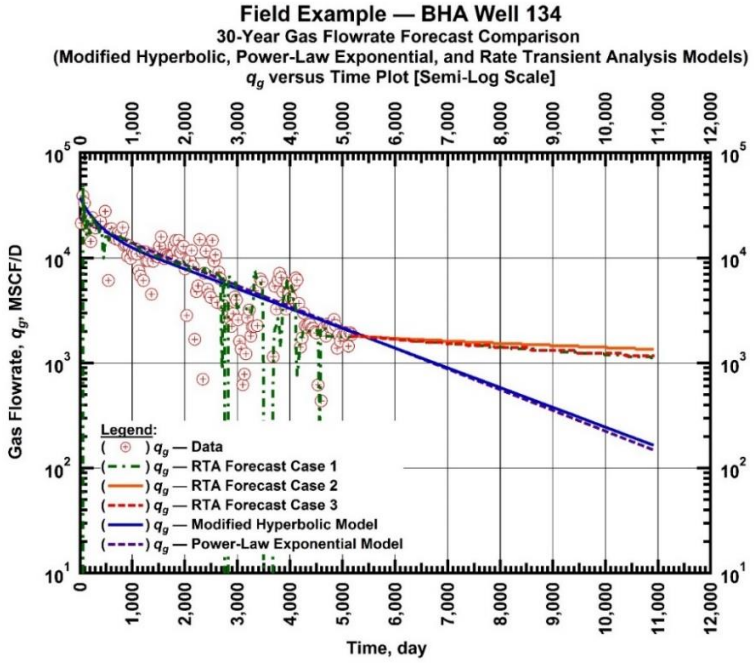

Fig. 183 — Semilog plot for BHA Well 134 — Gas flowrate versus time for various RTA forecast cases (1, 2, 3) and Modified Hyperbolic and Power-Law Exponential time-rate models.

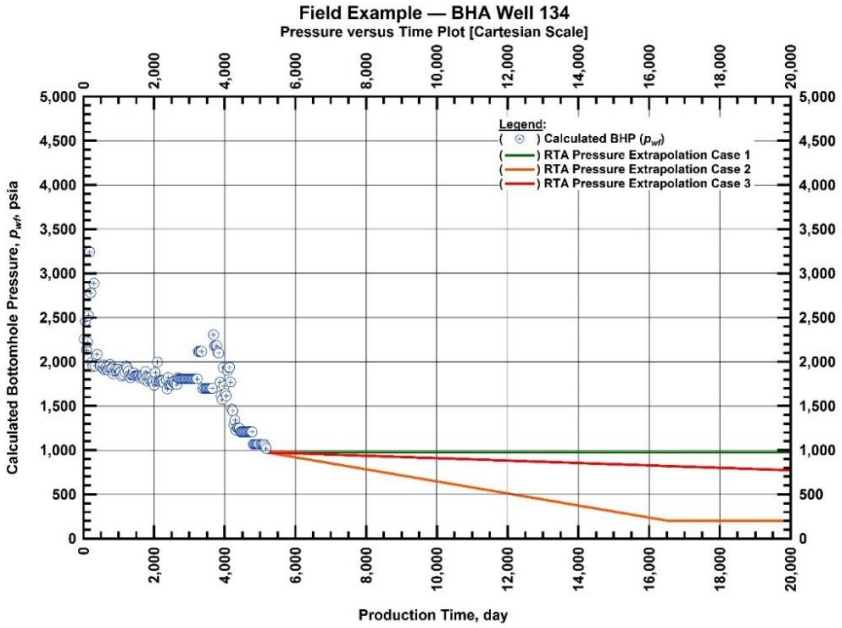

Fig. 184 — Cartesian plot for BHA Well 134 — historical and extrapolated bottomhole flowing pressures versus time (these pressure extrapolation scenarios are used for the RTA model).

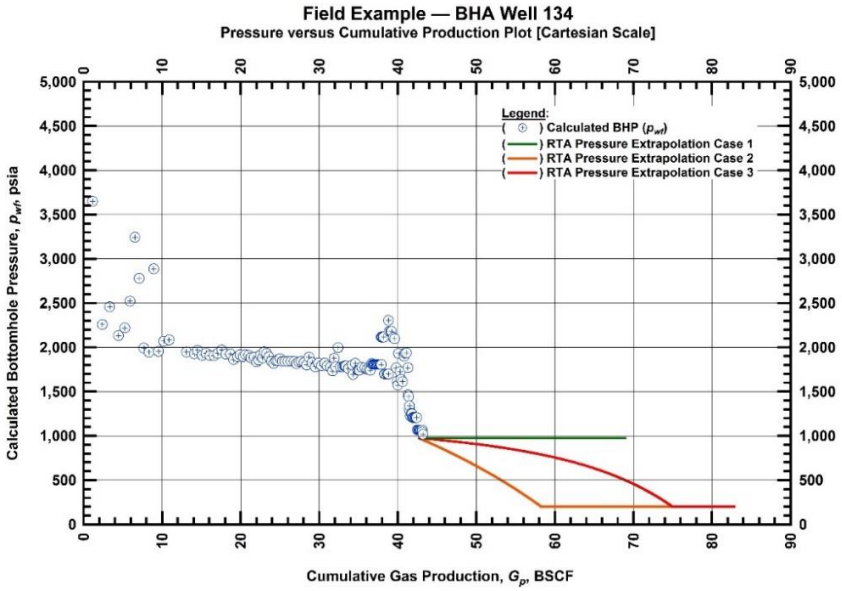

Fig. 185 — Cartesian plot for BHA Well 134 — historical and extrapolated bottomhole flowing pressures versus cumulative gas production (these pressure extrapolation scenarios are used for the RTA model).

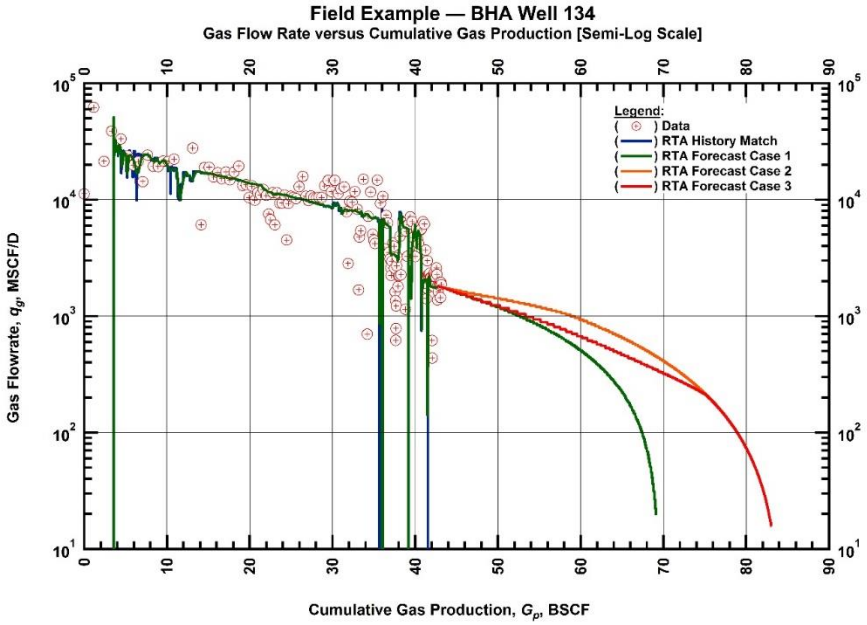

Fig. 186 — Semilog plot for BHA Well 134 — historical, history-matched, and forecasted gas flowrate versus cumulative gas production (various pressure extrapolation scenarios are prescribed (in time) for the RTA model).

APPENDIX B
FIELD EXAMPLE ANALYSES

This appendix contains a detailed analysis for the field example cases used in this study, with corresponding plots presented in **APPENDIX A**.

Field Example — BHA Well 090

BHA Well 090 has been producing for approximately 18 years, with flowing surface pressures first reported following the first year of production (**Figs. 55-56)**. Pressure and gas flowrate data appear to be well synchronized. Between 2003 and 2008 (or 1,500-3,160 days), surface pressures were constrained to calculated bottomhole pressures of approximately 2,000 psia. To enhance production, first-stage compression was initiated at ≈4,300 days, which followed an increase in gas production rates. Gas flowrates were further increased at ≈5,000 days after the addition of second-stage compression. However, there were no signs of improvement in the production performance following the addition of third-stage compression (≈5,700 days) and the gas flowrates decline significantly, producing at very low gas flowrates. We note that there is production instability at these very low flowrates, which could be have been caused by other factors (*e.g*. well integrity, liquid loading, etc.). In **Fig. 57**, we impose a straight-line of 1:2 slope and we can speculate that possible transient linear flow behavior exists between ≈150-4,000 days.

In **Figs. 58-59** we begin our "rate transient analysis" (or RTA). A good match of the model fit to the data trend is achieved using a vertical well model with a single fracture of high conductivity. However; similar to most wells, due to noise in early material balance time, the model match during these production periods is not particularly good. Based on our interpretation from **Figs. 58-59**, boundary-dominated flow appears to begin at ≈2,000 days material balance time.

In **Fig. 60**, we present the traditional "history match" plot of rate, cumulative production, and pressure as functions of time and in **Fig. 61** we present the gas flowrate versus cumulative production match as a further validation. An excellent model match is achieved, but we note that the pressure match fluctuates frequently (**Fig. 60**). This happens specifically at late times, where changes in the flowrate data are not reflected in the pressure data.

The Log-Log and semilog plots are presented in **Figs. 62-63** to compare the rate extrapolations generated from the rate transient analysis (RTA) model and the rate extrapolations generated from the two decline curve analysis (DCA) models (*i.e.*, the modified hyperbolic (MH) and the power-law exponential (PLE)). We note in this case (BHA Well 090) that the RTA predictions are consistently higher than the DCA extrapolations. The RTA model extrapolations are based on assumed extrapolated pressure histories presented in **Figs. 64-65**. Finally in **Fig. 66**, we note that decreasing the intake pressure to the assumed abandonment pressure of 200 psia predicts a 22 % increase in the cumulative gas production

Field Example — BHA Well 98

The analysis for BHA Well 098 begins by reviewing the production history plot (**Fig. 67**). The well has been producing for over 16 years. Between 2,000-3,500 days, the well appears to be producing under a surface production constraint. At approximately 4,100 days, we notice a decline in the reported pressures which coincides with the period in which first-stage compression commenced. We note that this resulted in slightly improved production flowrates, but production instability persisted. Beyond 5,500 days (or 2014) both well performance deteriorated and pressure data were no longer reported. Hence, this production period was removed from the analysis. We overlay a straight-line onto **Fig. 69** and estimate that possible transient linear flow occurs between 400 and 2,000 days.

We begin time-rate-pressure analysis and we present **Figs. 70-71**. An excellent overall model match of the dataset was achieved. In **Fig. 70** we find that the match of the raw data (red symbols) is very good even at early material balance times, however there exists a mismatch in the match of the calculated trends (blue symbols). From the "Log-Log" plot (**Fig. 70**) and the "Blasingame" plot (**Fig. 71**), we can interpret that boundary-dominated flow fully develops at 1,000 days material balance time.

In **Figs. 72-73** we examine the model match on the traditional production history plots and see that an excellent match was obtained for BHA Well 098. We note that we started our analysis at 620 days due to the suboptimal production performance of the well previously. We believe that the flowrates during this time period are not characteristic of the reservoir behavior.

In **Figs. 74-75** we present a semilog and a Log-Log plot for the production history comparison for both the rate extrapolations generated using DCA (2 cases) and rate extrapolations generated using RTA model (3 cases). We found that the RTA predictions are consistently higher than the DCA extrapolations. The RTA model extrapolations are based on assumed extrapolated pressure histories presented in **Figs. 76-77**.

Finally **Fig. 78** presents a comparison of the predicted production between the three generated RTA model based extrapolations. We note that decreasing the abandonment pressures (to 200 psia) results in 31% additional production.

Field Example — BHA Well 99

The initial analysis for BHA Well 99 begins by plotting the gas flowrates and calculated bottomhole pressures as a function of time on both Cartesian and semilog scales (**Figs. 79-80).** In reviewing these plots, we observe that the well has been producing for more than 17 years. Similar to other wells, the well appears to have started producing approximately one year after it was drilled. Between 1,500 and 3,500 days, the well produced against a set choke. After 2014 (or ≈5,500 days), surface pressures are not continuously reported and pressure and production data are therefore eliminated from the analysis. In **Fig. 81** we observe a possible "linear flow" trend exhibited by the flowrate data and speculate that transient linear flow behavior exists between ≈300-2,000 days.

For RTA we use the "diagnostic plots", "Log-Log" plot (**Fig. 82**) and the "Blasingame" plot (**Fig. 83**), to determine different flow regimes. We observe a good overall model fit to the rate data in the two auxiliary plots, and while the late material balance time data match is very good, this is not the case at early times due to the erratic nature of the data. Sensitivity of the auxiliary functions to noise is very apparent in the "Blasingame" plot, where though the data match appears to be good we can see that there is a very distinct mismatch between the model and the calculated functions in **Fig. 83**.

In **Fig. 84** we present the traditional "history match" plot of rate, cumulative production, and pressure as functions of time and in **Fig. 85** we present the gas flowrate versus cumulative production match as a further validation. A very good model match is achieved in the production history plot. Due to the behavior of the early time data, we begin the analysis at 665 days. We note that these matches required the use of "time-dependent skin" in order to capture the behavior exhibited during certain production periods. In **Fig. 85**, we confirm that in general there is an excellent match in the "rate-cumulative" plot.

We present the three rate extrapolations generated from the RTA models and the rate extrapolations generated from the two DCA models in **Figs. 86-87**. Each of the three RTA model extrapolations is based on the assumption of an extrapolated pressure history, where these pressure histories are presented in **Figs. 88-89.** We note that in this case (BHA Well 99), the RTA predictions are comparable to the DCA extrapolations, with PLE being the most conservative model.

As a final comparison, we present the RTA extrapolations on a semilog "rate-cumulative" plot in **Fig. 90**. Decreasing the intake pressure in the RTA cases from a constant 700 psia to the assumed abandonment pressure of 200 psia predicts a 14 % increase in production.

Field Example — BHA Well 103

The initial well analysis for BHA Well 103 begins by evaluating the production history plots (**Figs. 91-92)**. The well has been producing for more than 16 years, with flowing surface pressures reported one year after the well first produced (one month). In addition, surface pressures were no longer reported after 5,140 days, which coincides with a period of low and unstable production. Due to the absence of pressure data during the early and late production times of this well, we only considered data analysis for periods where both flowrates and pressures are reported. We continue to examine the production performance and note that at ≈3,900 days, there is an increase in gas flowrates after the installation of first-stage compression. Once surface pressures were further decreased with a second compressor, gas flowrates stabilized (at ≈5,500 days). We plot the gas flowrates and cumulative gas production versus time on a log-log scale (**Fig. 93)** and observe that possible transient linear flow behavior exists between ≈200-3,000 days.

We present the RTA model match against the data trends and we note that a good model match is obtained during late times in both the "Log-Log" plot (**Fig. 94**) and the "Blasingame" plot (**Fig. 95**). Specifically the ($q_g/\Delta m(p)$) raw data functions (red symbols) of the "Blasingame" plot **(Fig. 95)** appear to be well-behaved for the most part. However, the instability present in this data has led to poor performance of the auxiliary functions. Based on these plots boundary-dominated flow appears to begin at ≈4,000 days material balance time.

In **Figs. 96-97** we present the traditional "history match" plots. Using "time-dependent skin," a relatively good gas flowrate model match is achieved. Nevertheless, it was difficult to obtain a good pressure match since the data does not appear to be synchronous and flowrate data changes were not reflected in the pressure data. A clear example of this occurs is at 2,300 days, where despite a reported flowrate increase, pressures were held constant due to surface pressures produced against a set choke.

The Log-Log and semilog plots are presented in **Figs. 98-99** (respectively) to compare the two rate extrapolations generated from the RTA model and the three rate extrapolations generated from the DCA models. In **Figs. 100-101** we have pressure histories for each of the three RTA model extrapolations. From **Figs. 98-99**, we see that although the DCA models have a general good fit, at 4,100 days, operating conditions changed when the first stage compression commenced and DCA models were no longer applicable. This explains the significant difference between the start of the extrapolations of the RTA and DCA models. Therefore, the RTA extrapolation cases result in higher expected flowrates than the DCA models.

As a final comparison, we present the RTA extrapolations on a semilog "rate-cumulative" plot in **Fig. 102**, which helps us to understand the influence of the prescribed pressure extrapolation history on the gas recovery.

Field Example — BHA Well 116

BHA Well 116 produced for 16 years, with flowing surface pressures first reported after the first year of production (**Figs. 103-104).** In April 2009 (at 3,400 days), velocity strings were installed in BHA Well 116 to enhance the productivity of the well, and we note that the produced gas flowrates stabilized. In addition, production performance improved notably after installing first-stage compression at ≈3,800 days. With the addition of the second-stage of compression, there was no additional improvement in production (≈4,300 days). Despite the relatively consistent flowrates, surface pressures are not reported after ≈5,150 days (2014), with the exception for a few points in 2016. From **Fig. 105**, we can speculate that possible transient linear flow behavior exists between ≈200-3,000 days.

For RTA we use the "diagnostic plots", "Log-Log" plot (**Fig. 106**) and the "Blasingame" plot (**Fig. 107**), to determine different flow regimes. We note a good model match is achieved during late times, while it was difficult to match the early material balance data due to its erratic nature. Based on our interpretation from these plots, boundary-dominated flow is fully developed at ≈800 days material balance time.

In **Fig. 108** we present the traditional "history match" plot of rate, cumulative production, and pressure as functions of time and in **Fig. 109** we present the gas flowrate versus cumulative production match as a further validation. We note that we begin the analysis at 434 days due to the erratic nature of the production data. An excellent model match is achieved. We note that these matches require the use of "time-dependent skin" in order to capture the behavior exhibited during certain production periods. .

In **Figs. 110-111** we plot the three rate extrapolations generated from the RTA model and the two rate extrapolations generated from the DCA models on both semilog and Log-Log scales. In **Figs. 112-113** we present the extrapolated pressure history of each of the three RTA cases. From **Figs. 110-111**, we see that although the DCA models have a general good fit, at 4,100 days operating conditions changed when the first stage compression commenced and DCA models are no longer applicable. This explains the significant difference between the start of the extrapolations of the RTA and DCA models. RTA extrapolation cases will result in higher expected flowrates than DCA models.

As a final comparison, we present the RTA extrapolations on a semilog "rate-cumulative" plot in **Fig. 114**, which helps us to understand the influence of the prescribed pressure extrapolation history on the gas recovery. Decreasing the intake pressure in the RTA cases from a constant 1200 psia to the assumed abandonment pressure of 200 psia predicts a 24 % increase in production.

Field Example — BHA Well 119

We begin our well analysis by reviewing the production history plots on both Cartesian and semilog scales (**Figs. 115-116**). BHA Well 119 has been producing for approximately sixteen years. The well produced continuously until mid 2008 (at 3,100 days) when the well was shut-in for 5 months. Unlike many wells, beginning 2010 (after the start of compression in the field), the production performance in the well stabilized. The well continued to produce at very low declining rates since 2013. It appears however, that the pressure data was not reported between 5,000-5,500 or 5,600-5,800 days. In **Fig. 117** we plot the gas flow rate and cumulative gas production as a function of time on a log-log scale. We observe from this "orientation" plot that possible transient linear flow exists between 200-1,000 days, although such a conclusion cannot be made due to the erroneous nature of the data.

For RTA, from the two auxiliary plots **Figs. 118-119**, we observe that the model fits the rate data very well at late times. This is expected, since the late material balance time data is associated with the volume, while the early time match is not very good. Specific to the "Log-Log" plot (**Fig. 118**), we find that the minor fluctuations in the raw data results in exaggerated scattering of the auxiliary integral derivative function, which is very sensitive to data noise. Sensitivity of the auxiliary functions to noise is also very apparent in the "Blasingame" plot, where we can see that there is a very distinct mismatch between the model and the calculated functions in **Fig. 119**.

We then examine the model match to the data trends in the traditional "production history" plot (**Fig. 120**). We note that the overall match is excellent, with a few minor areas where the data does not appear synchronous. Due to the significant noise in the early time data, we begin our analysis at ~ 330 days. We notice that between 1,700 and 2,200 days, we were unable to match the rate data as the increase in rate data was not associated with a decline in pressures. This is also apparent in the in **Fig. 121**, where this period coincides with cumulative gas production of around 78-82 BSCF. The remainder of the match appears to be more or less well synchronized.

In **Figs. 122-123** , we provide a comparison between the generated rate extrapolations for the DCA and RTA models in log-log and semilog scales. We note that in this case both the RTA and DCA rate extrapolations are very similar. We find that there is an overlap between the RTA case 1 model extrapolation (where the assumed extrapolated pressure is equivalent to the last producing pressure) and the MH DCA model. This suggests that the MH extrapolation for this case is very representative. The pressure extrapolations for each of the three RTA cases are presented in **Figs. 124-125** as a function of both time and cumulative production.

In examining **Fig. 126**, we find that decreasing the intake pressure from a constant 900 psia to the assumed abandonment pressure of 200 psia predicts a 13 % increase in production.

Field Example — BHA Well 121

We begin analyzing BHA Well 121 by reviewing the production history plot **(Fig. 127 and Fig 128)**. BHA Well 121 has been producing for approximately 16 years. We observe that beginning 1,400 days, the well produced against a set surface pressure (calculated to a bottomhole pressure of 2,000 psia). The well stopped producing at ≈3,400 days for 7 months, in order to install velocity strings. In 2010 (≈3,200 days) first–stage compression was started in the field and we note that although we see a slight improvement in the production flowrates, the well did not sustain the improved performance despite the addition of the second-stage compression at 4,252 days. In **Fig. 129**, we speculate that transient linear flow behavior exists between ≈300-2,000 days.

We use **Figs. 130-131** for "rate transient analysis". We achieve a good model match against data trends using the vertical well with a single vertical fracture of high conductivity model. We note that the model match in the "Log-Log" plot during late times (beyond 800 days material balance time) is particularly good. Our interpretation from the "Log-Log" plot (**Fig. 130**) and the "Blasingame" plot **(Fig. 131**) is that boundary-dominated flow is fully developed at ≈2,000 days material balance time.

In **Fig. 132** we present the traditional "history match" plot of rate, cumulative production, and pressure as functions of time and in **Fig. 133** we present the gas flowrate versus cumulative production match as a further validation. An excellent model match is achieved. We note that these matches required the use of "time-dependent skin" in order to capture the behavior exhibited during certain production periods. As an example, due to the excessive noise in the pressure data at early times (<1,000 days), time-dependent skin was used to match the production rates for this period.

In **Figs. 134-135,** we present the Log-Log and semilog plots to compare the three rate extrapolations generated from the rate transient analysis (RTA) model and the rate extrapolations generated from the two decline curve analysis (DCA) models. We note that in this case (BHA Well 121) the RTA predictions are consistently higher than the DCA extrapolations, with PLE being most conservative model. We note that the three RTA model extrapolations are based on an extrapolated pressure history presented **in Figs. 136-137.**

As a final comparison, we present the RTA extrapolations on a semilog "rate-cumulative" plot in **Fig. 138**, which helps us to understand the influence of the prescribed pressure extrapolation history on the gas recovery. We find that decreasing the intake pressure in the RTA cases from a constant 1,200 psia to the assumed abandonment pressure of 200 psia predicts a 23 % increase in production.

Field Example — BHA Well 125

The initial analysis for BHA Well 125 begins by plotting the gas flowrates and calculated bottomhole pressures as a function of time on both Cartesian and semilog scales (**Figs. 139-140).** In reviewing these plots, we observe that the well has been producing for approximately 16 years and we note that the well did not produce for approximately one year after it was drilled. The well produced against a set choke pressure from 1,000 days until 2,400 days. The well's production declined significantly and it underwent an extended shut-in period at 2,800 days. The well was unable to recover its production performance and resulted in low and unstable flowrates. Due to these low flowrates, we were unable to accurately calculate the bottomhole pressures due to the limitation in Prosper and we therefore eliminated data beyond 2008 from our analysis. In **Fig. 141** we observe a possible "linear flow" trend exhibited by the flowrate data and speculate that transient linear flow behavior exists between ≈200-1,000 days.

We use the "diagnostic plots", "Log-Log" plot (**Fig. 142**) and the "Blasingame" plot (**Fig. 143**), for RTA to determine different flow regimes. The model fit is obtained by adjusting the reservoir properties and reservoir volume, where for the case of BHA Well 125, we chose a vertical well with a single vertical fracture of high conductivity. A good model match is achieved during late times. Based on these plots, we believe that boundary-dominated flow is fully developed at 600 days material balance time. The production history plots in **Figs 144-145** show that an excellent model match is achieved. We note that due to the nature of the early time data, we begin our analysis at ≈440 days.

In **Figs. 146-147**, we present the three rate extrapolations generated from the RTA models and the rate extrapolations generated from the two DCA models (*i.e.*, the modified hyperbolic (MH) and the power-law exponential (PLE)). Each of the three RTA model extrapolations is based on the assumption of an extrapolated pressure history, where these pressure histories are presented in **Fig. 148 -149**. We note that in this case (BHA Well 125), the RTA predictions are comparable to the DCA extrapolations, with RTA Case 1 being most comparable to the DCA extrapolations.

As a final comparison, we present the RTA extrapolations on a semilog "rate-cumulative" plot in **Fig. 150**. Decreasing the intake pressure in the RTA cases from a constant 2,200 psia to the assumed abandonment pressure of 200 psia predicts a 71 % increase in production.

Field Example — BHA Well 128

The well analysis begins by analyzing the production history plots (**Figs. 151-152).** BHA Well 128 has been producing for more than 16 years. We note that the production flowrates experienced a steep decline between 2,000 and 2,800 days, until the well stopped producing. The well remained shut in for approximately one year. At 3,800 days, first-stage compression resulted in an improved production performance. In **Fig. 153**, we plot the gas flowrates and cumulative gas production versus time on a log-log scale. We observe a possible "linear flow" trend exhibited by the flowrate data and speculate that transient linear flow behavior exists between ≈200-3,000 days.

The "Log-Log" plot (**Fig. 154**) and the "Blasingame" plot (**Fig. 155**) are used for the RTA analysis. A good overall model match is obtained for both of these plots. However, we notice that there is considerable noise in the early material balance time data. In **Fig. 156** we present the traditional "history match" plot of rate, cumulative production, and pressure as functions of time, and in **Fig. 157** we present the gas flowrate versus cumulative production match as a further validation. An excellent model match is achieved. We select 647 days as the start of the analysis selection period, due to the uncertainty of the allocated flowrate data at earlier times. We observe considerable fluctuations in the pressure model match due to changes in flowrate data with no corresponding changes in the pressure data.

We then compare the rate extrapolation generated using DCA versus those generated using RTA models in **Fig. 158 and Fig 159**. We find that each of the three forecasts obtained using RTA models are very similar, though they are obtained for different pressure extrapolations plotted in **Fig. 160 and Fig 161**. We observe that for BHA Well 128, DCA extrapolations are much more conservative than those obtained using RTA models.

Finally, in **Fig. 162** we present the expected recoveries from each of the three RTA extrapolations. We find that decreasing the intake pressure in the RTA cases from a constant 950 psia to the assumed abandonment pressure of 200 psia predicts a 23 % increase in production.

Field Example — BHA Well 131

The analysis for BHA Well 131 begins with the analysis of the production history plot (**Fig. 163**). The well has been producing for over 16 years, and we note that the well produced for three months prior to a five-month shut in in order to fracture the well. Between 600-2,500 days, the well appears to be producing under a surface production constraint. Between 2,600 to 4,000 days, substantial data filtration was done, resulting in production periods in which the surface pressures appear to be missing. These periods coincide with low and unstable well production. Despite the installation of first-stage compression at around 3,800 days, the well continued to have issues with its production. Unfortunately, the reason for the low well productivity is undocumented and could be due to operational issues or well integrity. By 2012 (4,300 days), the well started producing at increased and stabilized production rates. During this time, second stage compression had commenced and we note a corresponding decrease in pressures. Further data filtration was completed after 5,100 days due to the erratic behavior of the data. We next overlay a straight-line onto **Fig. 165** and we estimate that possible transient linear flow occurs between 200 to 1,000 days.

We then begin time-rate-pressure analysis and we present **Figs. 166-167**. The model match during early material balance times is not very good due to the erroneous nature of the data. However, based on the general trend of the data, we identified that this case is best modeled using a vertical well with a single vertical fracture of finite conductivity. From the "Log-Log" plot (**Fig. 166**) and the "Blasingame" plot (**Fig. 167**), we can interpret that boundary-dominated flow fully develops at 2,000 days material balance time. We examine the model match on the traditional production history plots (**Figs. 168-169**) and see that a very good model match is obtained for BHA Well 131.

In **Figs. 170-171** we present a semilog and a Log-Log plot for the production history comparison for both the rate extrapolations generated using DCA (2 cases) and rate extrapolations generated using RTA model (3 cases). We note that although both methods appear to fit the historical production of the well, the starting point for the rate extrapolations between the DCA and RTA methods differ significantly. This is attributed to the fact that DCA does not account for the operational changes that occur in the well and therefore did not account for the increase in the production rates that occurred at ≈4,100 days.

Finally **Fig. 174** presents a comparison of the predicted production between the three generated RTA model based extrapolations, where pressure profiles for each of these cases is presented in **Figs. 172-173**. We note that decreasing the abandonment pressures (to 200 psia) results in 31% additional production.

Field Example — BHA Well 134

We begin our analysis for BHA Well 134 by reviewing the production history plots (**Figs. 175-176**). The well has been producing for more than 14 years. The start of production coincides with the period in which the field surface pressures were constrained until around 2,700 days, after which production data have been filtered due to their erratic nature (2009). We also note that in BHA Well 134, production flowrates fluctuate frequently and there are a few shut-ins throughout the production period, which we believe could be attributed to liquid loading. This instability is seen until the end of 2011 (3,700 days), where a velocity string was installed in the well. The gas flowrate is initially improved, but the improvement diminishes a year later and production rates decline. In **Fig. 177**, we impose a straight-line trend on the gas flowrate data and speculate that transient linear flow behavior exists between ≈400-2,000 days.

A vertical well with a single vertical fracture of high conductivity model is the identified case using RTA. In **Figs. 178-179** we note a good match of the model against production data trends. In **Fig. 179** we observe some instability in the raw productivity index (red circle symbols), which leads to very poor performance of the auxiliary functions, specifically the "rate-integral derivative" function (green diamond symbols). Based on our interpretation from **Figs. 178-179**, boundary-dominated flow is fully developed at ≈2,000 days material balance time.

In the traditional "history match" plot of rate, cumulative production, and pressure as functions of time **(Fig. 180)** and the gas flowrate versus cumulative production match (**Fig. 181**), we see that the data is not very synchronous. While the overall model match is good, there are numerous fluctuations in the pressure match. Despite the use of "time-dependent skin", there are numerous periods in which changes in the rate data are not reflected in the pressure data.

Next, we analyze the log-log and semilog plots (respectively) to compare the rate extrapolations generated from the RTA model and the rate extrapolations generated from the two DCA models (**Fig. 182-183)**. We observe that the DCA models result in significantly more conservative predictions than the RTA models. Each of these three RTA model extrapolations is based on the assumption of an extrapolated pressure history, where these pressure histories are presented in **Fig. 184-185**.

As a final comparison, we present the RTA extrapolations on a semilog "rate-cumulative" plot in **Fig. 186**, which helps us to understand the influence of the prescribed pressure extrapolation history on the gas recovery. We note that decreasing the intake pressure to the assumed abandonment pressure of 200 psia predicts a 20 % increase in the cumulative gas production (**Fig. 186**).

APPENDIX C
CORRELATION PLOTS

This chapter contains the correlation plots constructed using the DCA (Modified Hyperbolic and Power-Law Exponential) and RTA results.

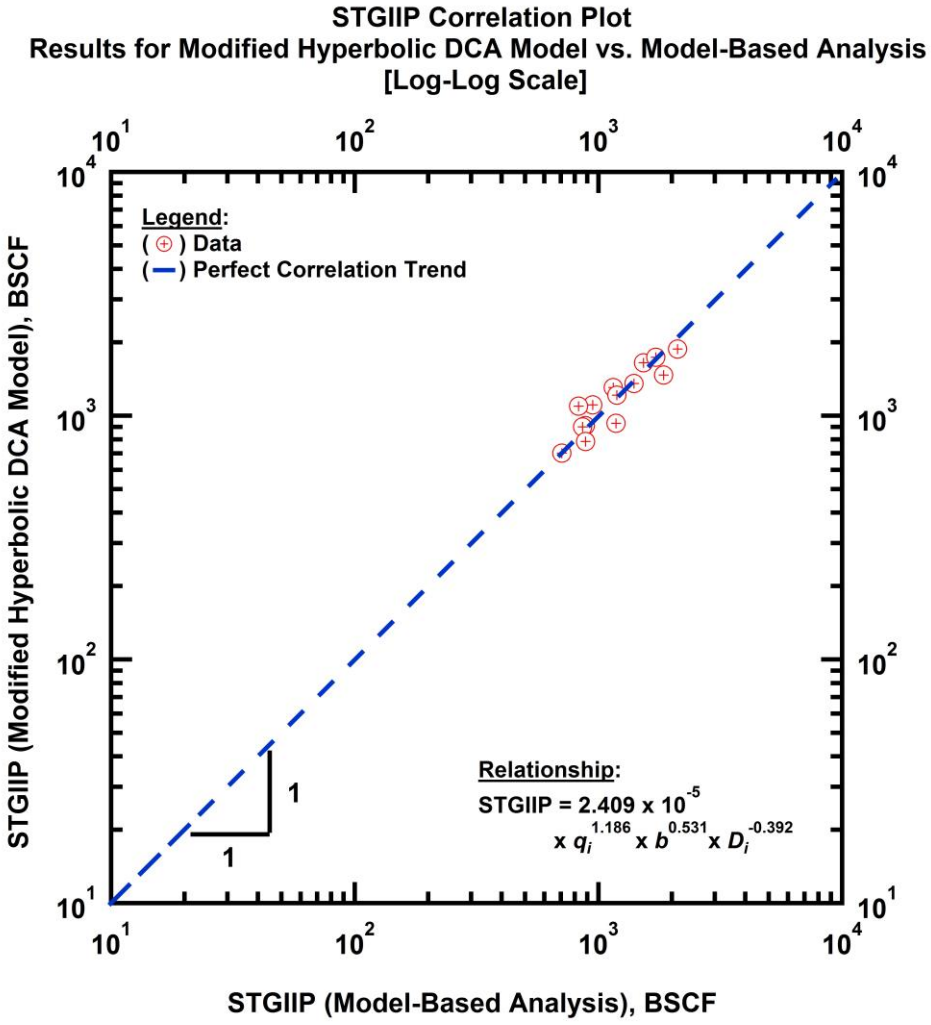

Fig. 187 — Correlation plot comparing STGIIP calculated using the Modified Hyperbolic DCA model parameters versus STGIIP estimated using Model-Based Analysis (RTA).

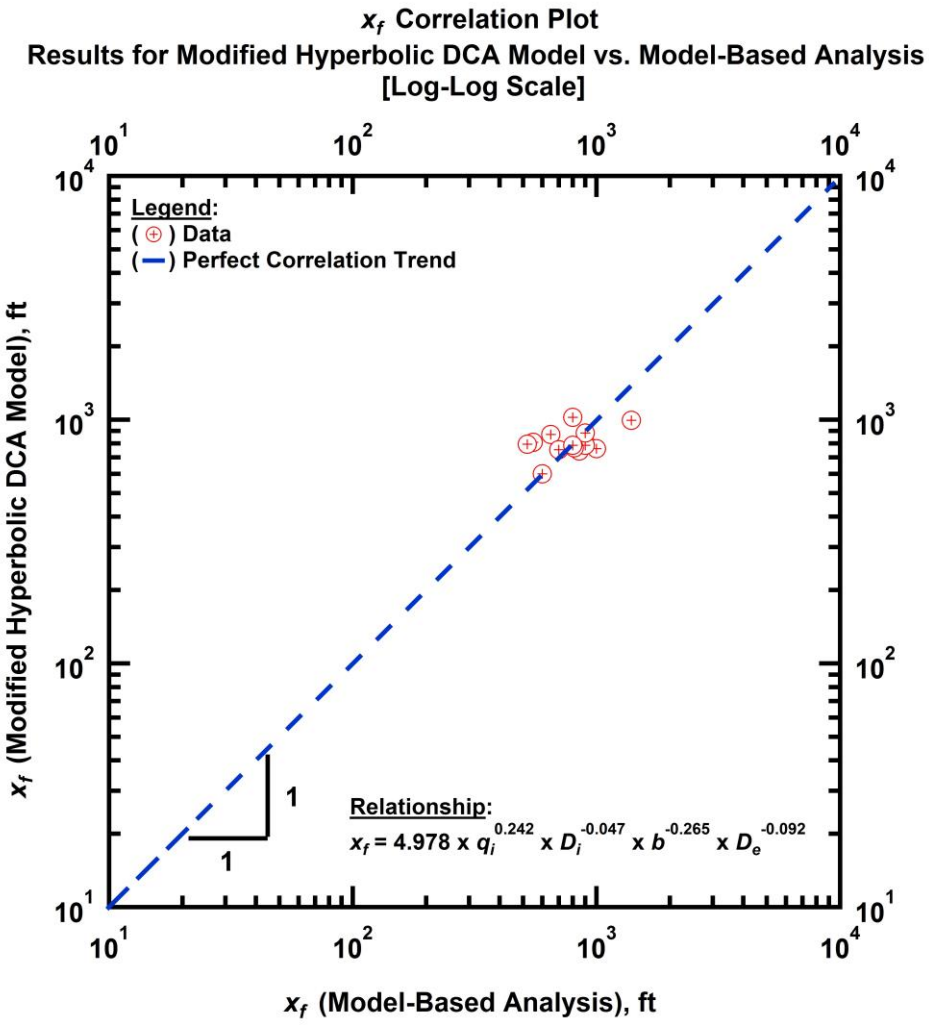

Fig. 188 — Correlation plot comparing x_f calculated using the Modified Hyperbolic DCA model parameters versus x_f estimated using Model-Based Analysis (RTA).

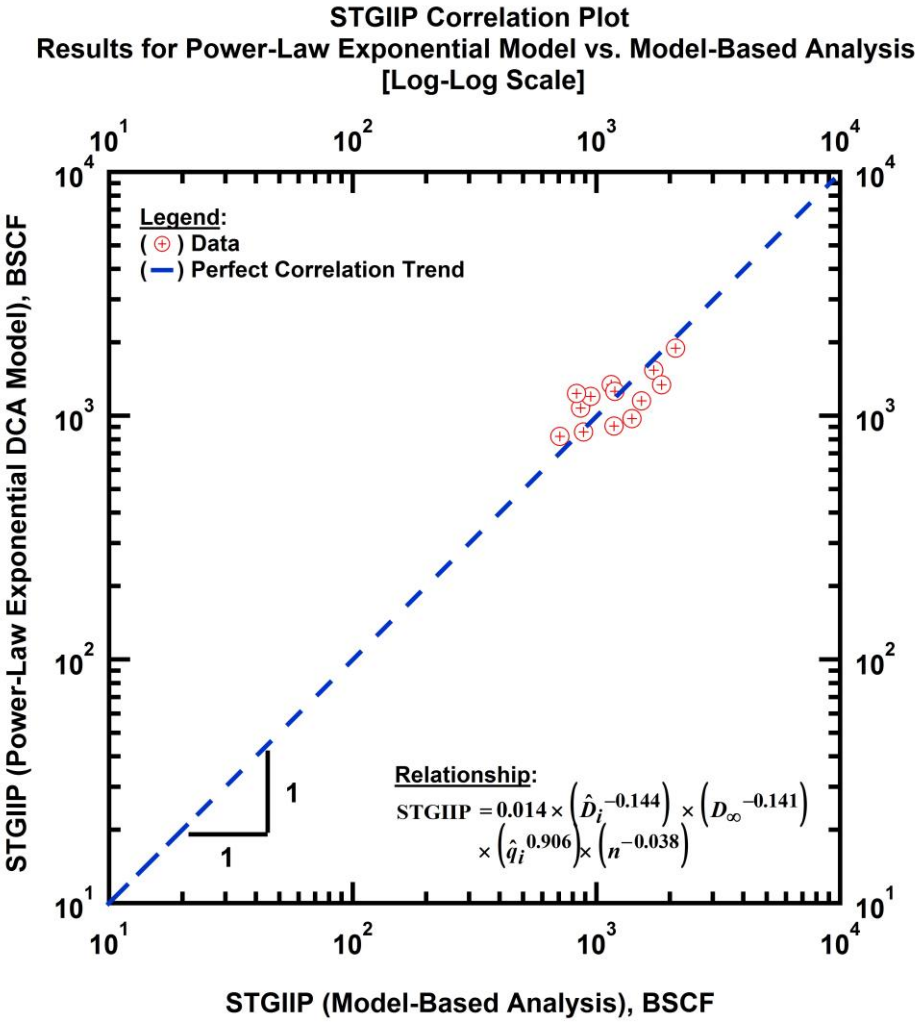

Fig. 189 — Correlation plot comparing STGIIP calculated using the Power-Law Exponential DCA model parameters versus STGIIP estimated using Model-Based Analysis (RTA)

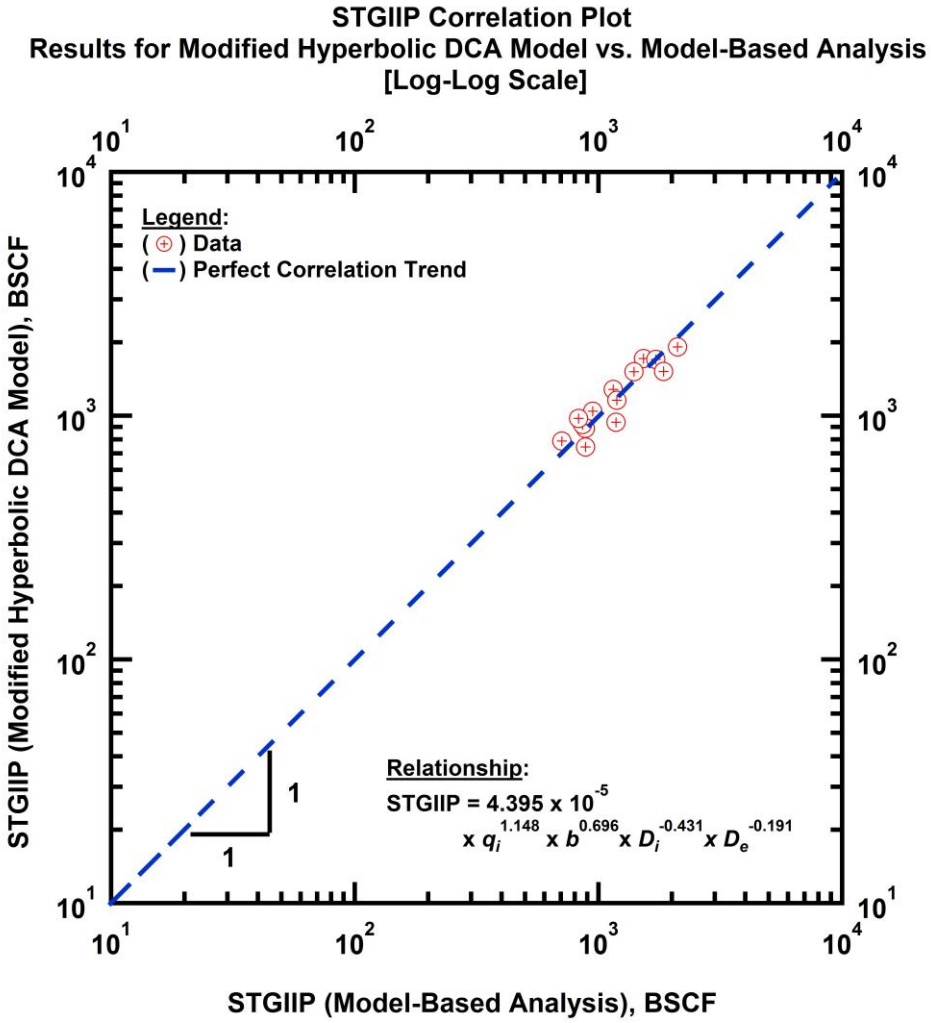

Fig. 190 — Correlation plot comparing STGIIP calculated using the Modified Hyperbolic DCA model parameters versus STGIIP estimated using Model-Based Analysis (RTA).

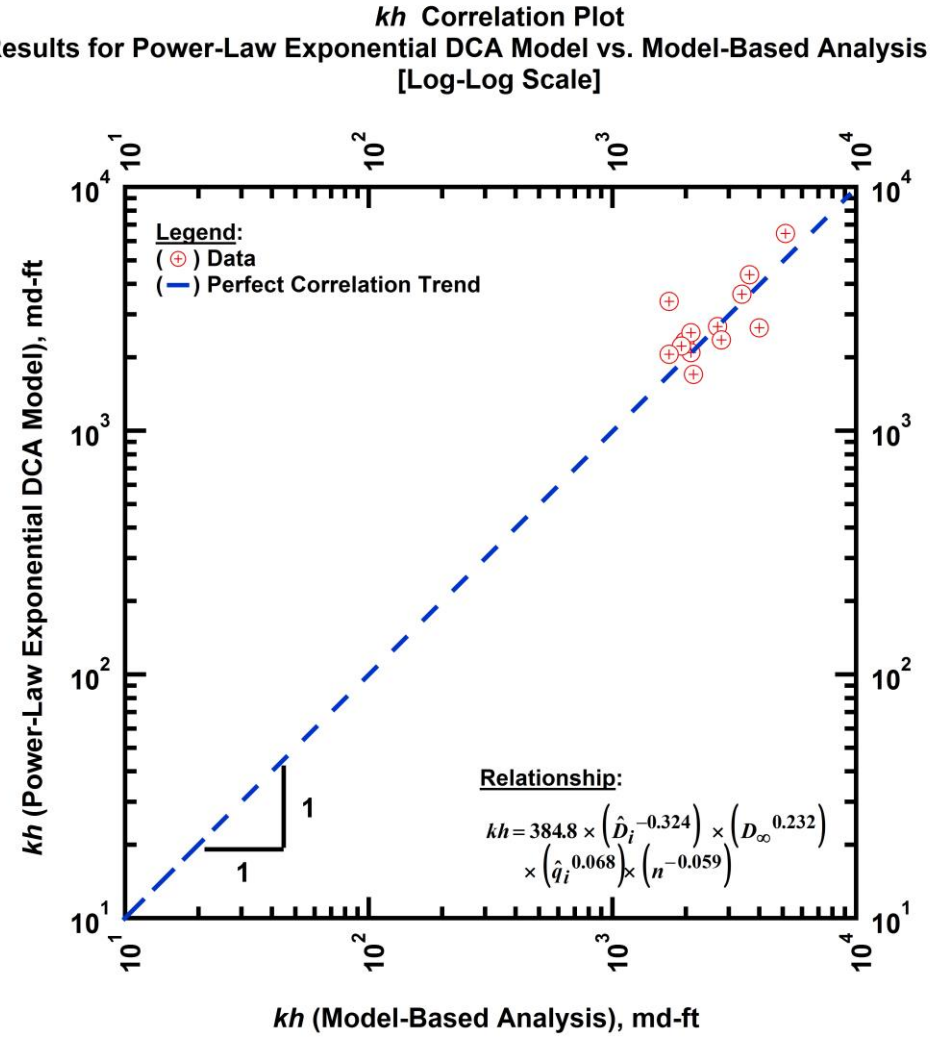

Fig. 191 — Correlation plot comparing *kh* calculated using the Power-Law Exponential DCA model parameters versus *kh* estimated using Model-Based Analysis (RTA).

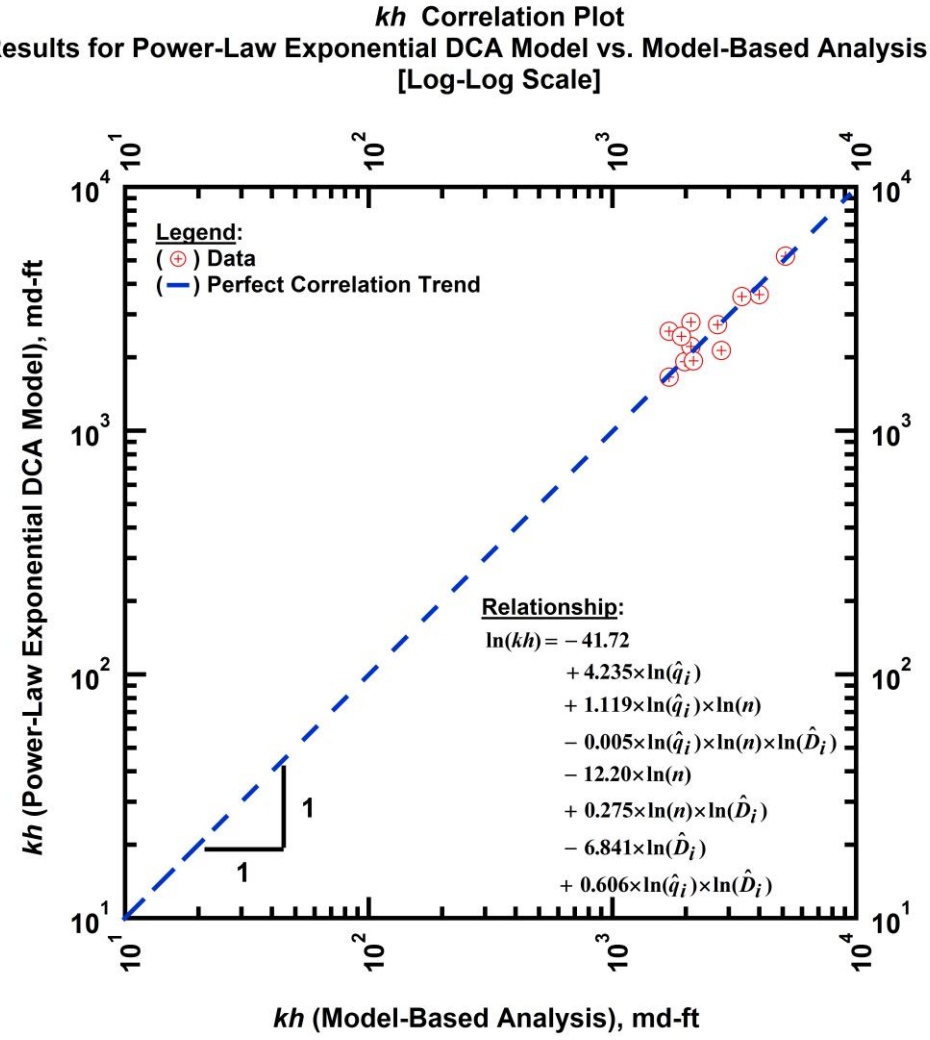

Fig. 192 — Correlation plot comparing *kh* calculated using the Modified Hyperbolic DCA model parameters versus *kh* estimated using Model-Based Analysis (RTA).

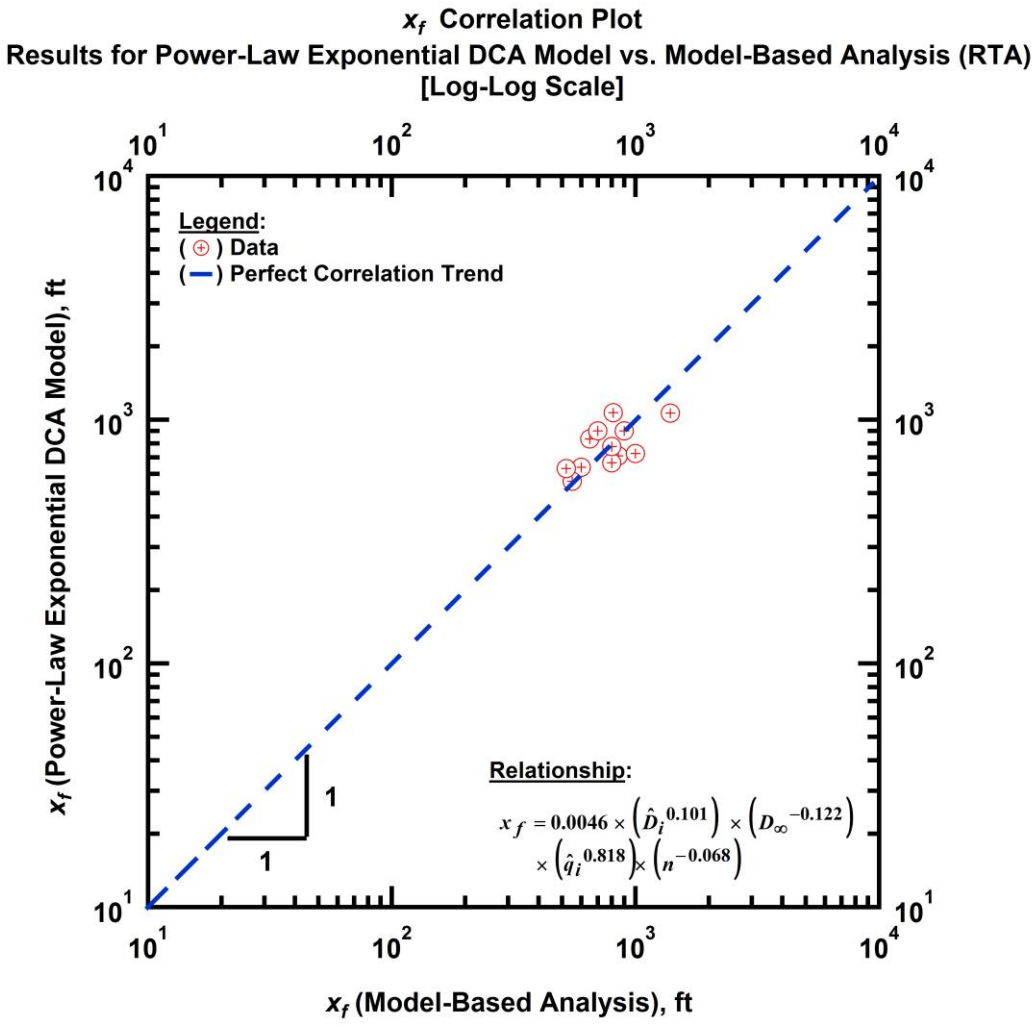

Fig. 193 — Correlation plot comparing x_f calculated using the Power-Law Exponential DCA model parameters versus x_f estimated using Model-Based Analysis (RTA).

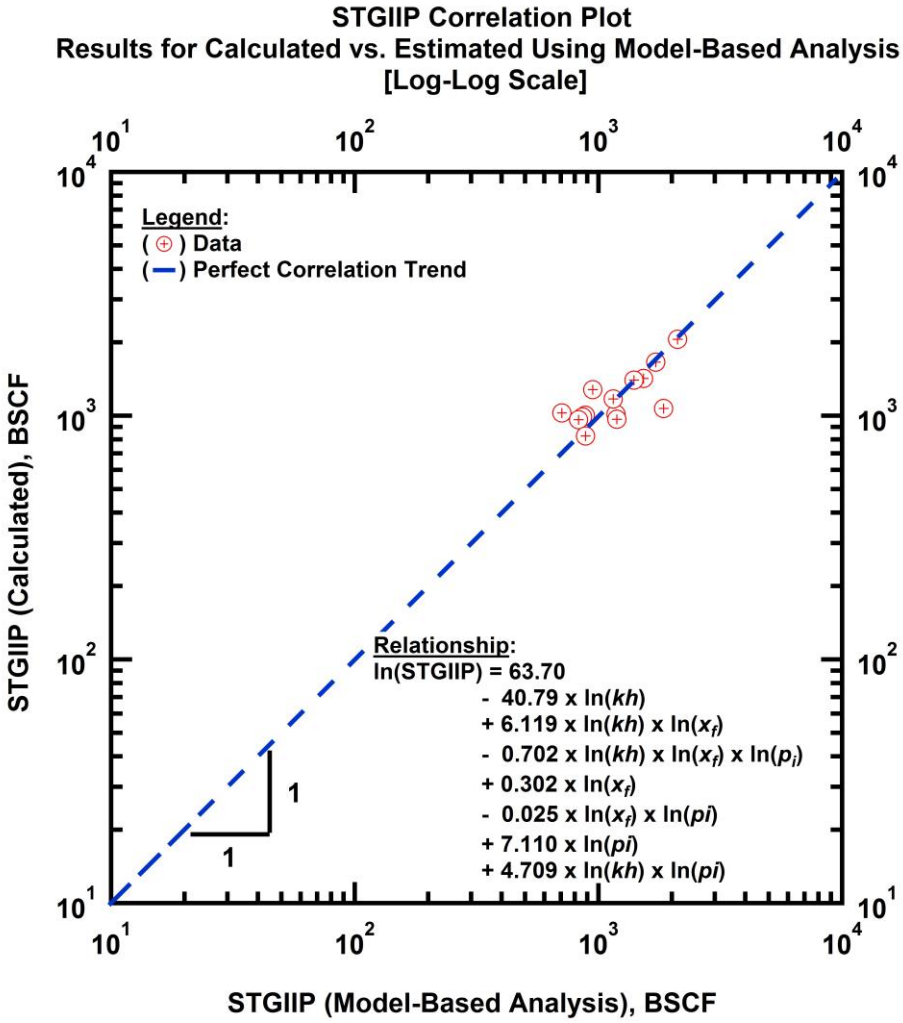

Fig. 194 — Calculated STGIIP versus estimated STGIIP from Model-Based Analysis (RTA).

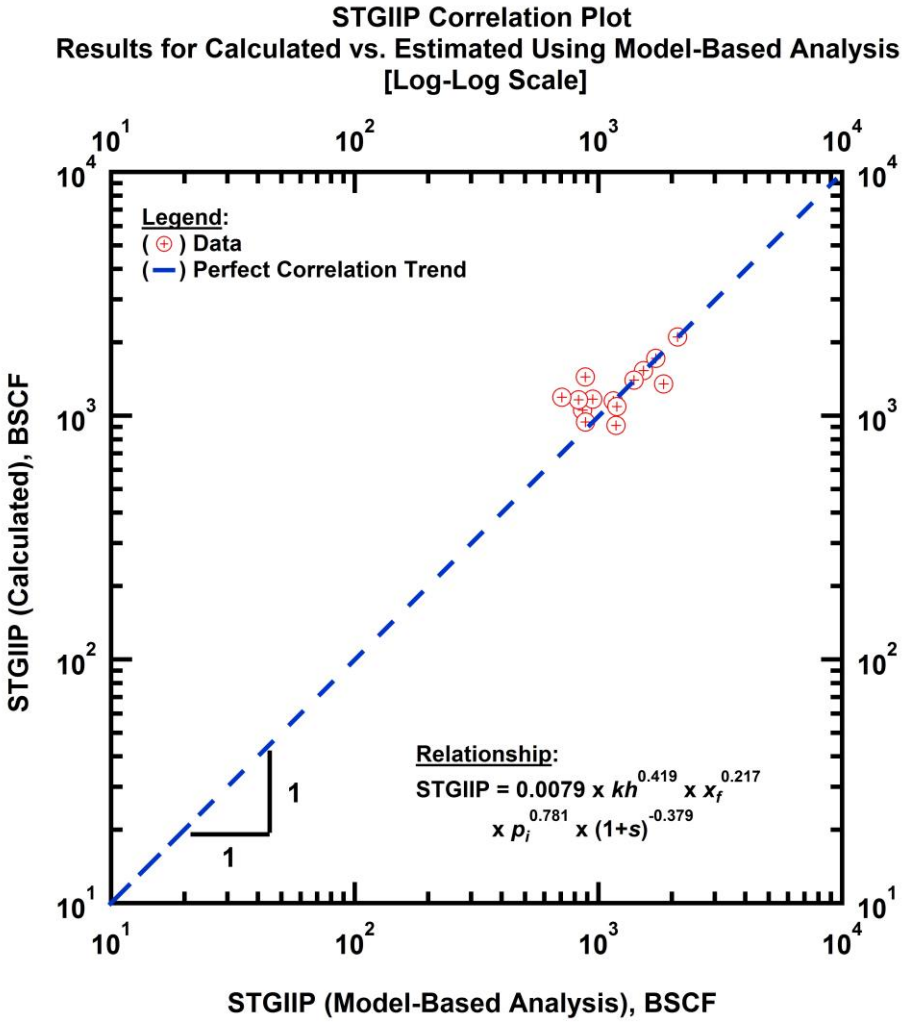

Fig. 195 — Calculated STGIIP versus estimated STGIIP from Model-Based Analysis (RTA).

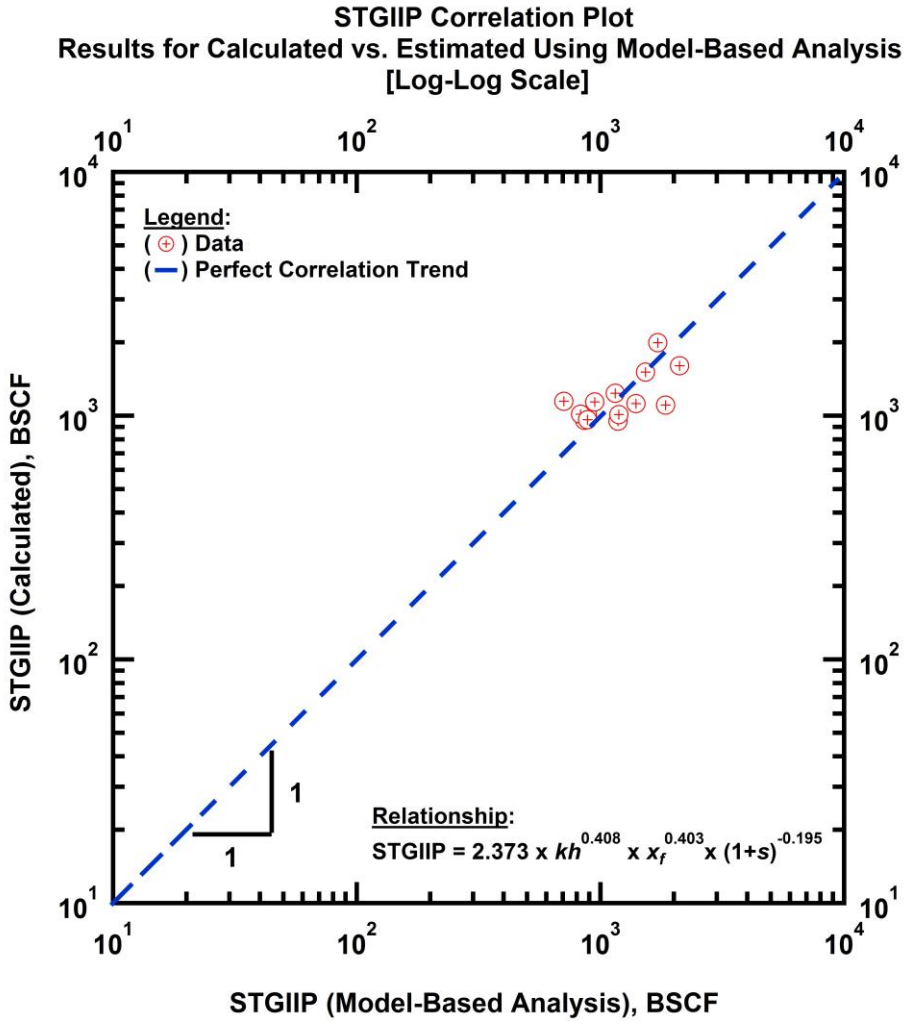

Fig. 196 — Calculated STGIIP versus estimated STGIIP from Model-Based Analysis (RTA).

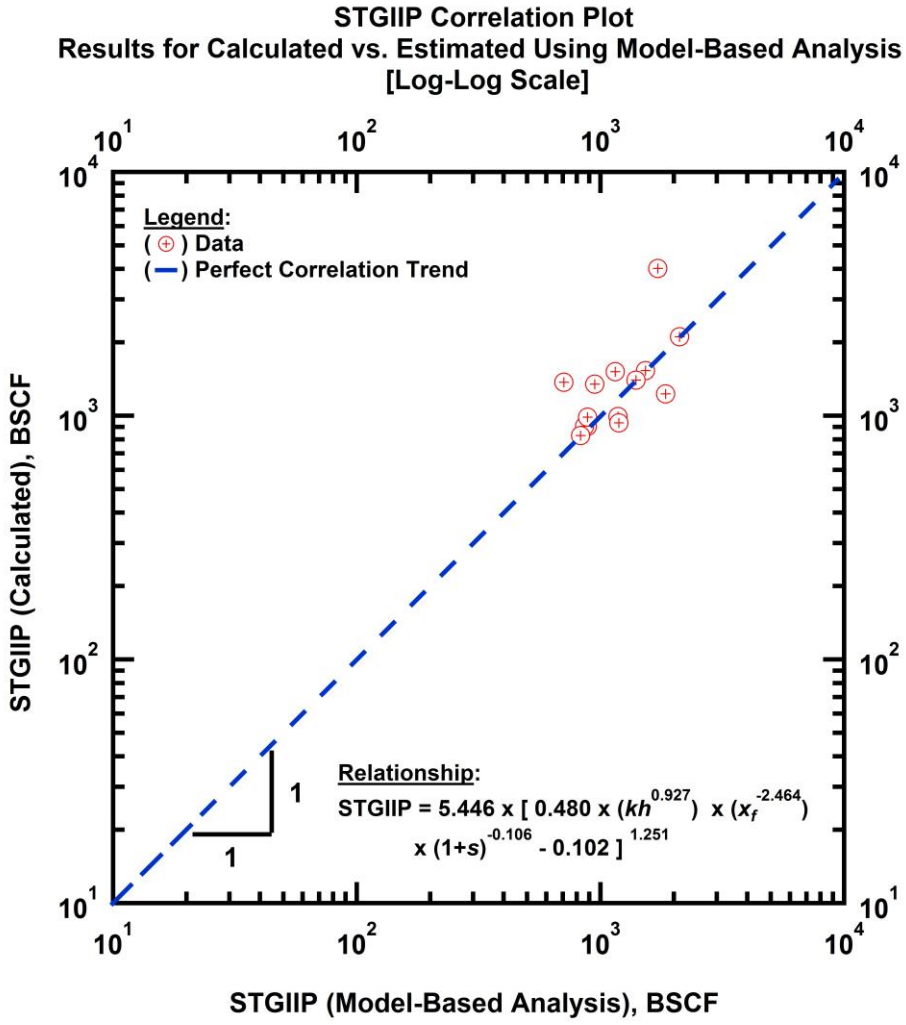

Fig. 197 — Calculated STGIIP versus estimated STGIIP from Model-Based Analysis (RTA).